



## **Deliverable 4.11 Calibrated water quantity and quality model for BSC, with impacts of scenarios. The hydrological model of the Black Sea**

<b>Title</b>	Deliverable 4.11 Calibrated water quantity and quality model for BSC, with impacts of scenarios. The hydrological model of the Black Sea
<b>Creator</b>	Karim Abbaspour, Elham Rouholahnejad
<b>Creation date</b>	01.03.2013
<b>Date of last revision</b>	14.03.2013
<b>Subject</b>	Water quantity and water quality of the Black Sea Basin
<b>Status</b>	Final
<b>Type</b>	Word document
<b>Description</b>	Data compiling, model building, model calibration, scenario analysis
<b>Contributing organizations</b>	Eawag, IHE, USRIEP, CEU
<b>Rights</b>	Public
<b>Identifier</b>	EnviroGRIDS_D4.11
<b>Language</b>	English
<b>Relation</b>	EnviroGRIDS_D4.3, EnviroGRIDS_D4.4, EnviroGRIDS_D4.5, EnviroGRIDS_D4.9, EnviroGRIDS_D4.11

## Abstract

The document contains an overview of the hydrological model of the Black Sea Basin. It contains information on input data, model building, model calibration, and uncertainty analysis. The hydrological model is coupled with water quality and crop yield as well.





## **Executive Summary**

The aim of D4.11 is to build a hydrological model of the Black Sea Basin (BSB) that computes all components of the water balance at subbasin level with monthly time steps. This high resolution model could then be used for more local analysis. We have integrated in this model water quality in terms of NO<sub>3</sub> concentration and crop yields for barley, corn, and wheat. Such an integrated model is a valuable tool for the analysis of landuse and climate change as well as various analyses with respect to droughts and other natural and manmade disasters.

The Black Sea Basin with an area of approximately 2,000,000 km<sup>2</sup> covers entirely or partially 23 countries. Of these, six countries are located in its coastal zone and 17 countries are closely linked with the sea via the rivers that flow into the sea. The program Soil and Water Assessment Tool (SWAT ver. 2009) (Arnold et al., 1998) was used to build the model in the ArcGIS ver. 9.3 environment. Initially, the region is divided into 12982 subbasins, which were further divided into 89202 HRUs (hydrologic response units) consisting of unique soil, landuse, and slope ranges.

Water resources is an important consideration in the BSB as population growth and water quality deterioration is taking its toll on the quantity of the freshwater availability per capita. An objective of this work is to estimate the water resources availability per capita and to estimate the impact of climate change on the water resources in the future.

Agriculture is an important sector in the Black Sea region. The region has relatively favorable land and water endowments. Currently, the agricultural productivity is low compared with its western European counterparts as well as the world average. The potential for increasing production is therefore considered to be high. However, the Sea is vulnerable to pressures from land-based pollution in its catchment areas (UNEP, 2005). Agriculture is one of the major sources of pollutions to the water bodies in the region, particularly to the Black Sea coastal ecosystems. The pollution was reduced during the 1990s following the collapse of the former Soviet Union. With the recovery of the agricultural production in the region in recent years, the pollution to the water bodies is likely to increase. In this work we will analyze the impact of climate change on the crop yield and the consequent impact on water quality of the region.



---

## **Contents**

<b>1 Introduction</b>	6
<b>2. Study area</b>	8
<b>3. SWAT model</b>	11
<b>4. Data availability and sources for modeling with SWAT</b>	13
- Black Sea boarder	16
- Digital Elevation Model	16
- Soil	17
- Landuse	18
- Climate	23
- River discharge and NO <sub>3</sub> concentration	26
- Point sources of pollution	26
- River network	31
- Agricultural management statistics	32
- Potential evapotranspiration	37
<b>5. Model setup</b>	38
<b>6. Model Calibration, parameterization, uncertainty analysis</b>	40
<b>7. Model results</b>	45
- Calibration/validation results	45
- Problems with large-scale modeling	53
1. Placement of outlets	53
2. Outlets downstream of a dam	54
3. Water management	58
<b>8. Some pertinent model results</b>	59
- Precipitation distribution	61
- Average temperature distribution	62
- Blue water	63
- Green water storage	66

**enviroGRIDS – FP7 European project**

Building Capacity for a Black Sea Catchment

Observation and Assessment supporting Sustainable Development



---

- Green water flow	68
- Water scarcity	70
- Yield barley	72
- Yield wheat	74
- Nitrate released into river from HRU	76
- Nitrate leached below the soil profile	77
- Nitrate transported by surface runoff into reach	78
- Nitrate contributed by HRU to groundwater into reach	79
- Temporal distribution of green water flow	80
- Temporal distribution of green water storage	82
- Temporal distribution of blue water	84
- Crop yield per country	86
<b>Appendix 1</b>	<b>88</b>
<b>Case Study 1</b>	<b>109</b>
<b>Case Study 2</b>	<b>133</b>
<b>Case Study 3</b>	<b>148</b>
<b>Case Study 4</b>	<b>158</b>
<b>Case Study 5</b>	<b>160</b>
<b>References</b>	<b>189</b>



## **1. Introduction**

The Black Sea Catchment (BSC) is internationally recognized for its ecologically unsustainable development and inadequate resource management leading to severe environmental, social and economical problems. The Black Sea is located between the continents of Europe and Asia. It is connected to the Atlantic Ocean via the Mediterranean Sea. The Black Sea Catchment with the total area of around 2 million km<sup>2</sup> is five times the surface of the Black Sea. It is located between 38° and 56° north latitude and 8° to 46° east longitude and includes entirely or partially 19 European and Asian countries. Some of Europe's longest and largest rivers flow into the Black Sea, including the Danube, the Dnieper, the Southern Bug, the Dniester and the Don. The area is inhabited by a total population of around 160 million people (BSEI, 2005). Areas of high precipitation (> 3000 mm y<sup>-1</sup>) are in the west, and areas of low precipitation (< 190 mm y<sup>-1</sup>) are in the north and east (Tockner et al., 2009).

The core environmental problem of the Danube River Basin can be described as “an ecologically unsustainable development and inadequate water resources management” (PCU 1999). The problems are caused by factors such as: inadequate management of wastewater/solid waste, ecological unsustainable industrial activities, inadequate land management and improper agricultural practices leading to pollution of surface/groundwater, eutrophication, and accelerated runoff /erosion. These factors have negative impacts on the quality of life, human health, biodiversity, economical welfare, and water availability.

The Black Sea itself is affected by severe environmental degradation. In 1995, it was rated as having the highest concern in five out of seven environmental categories, making it the worst of any of the European seas (Stanners and Boudreau, 1995). Some signs of recovery have been observed in the recent years, but eutrophication remains a severe problem. To help answering some of the above-stated problems, the EnviroGrids project (Building Capacity for the Black Sea Basin Observation and Assessment System Supporting Sustainable Development) was defined in the 7th European Framework. The project aims at building capacities in the Black Sea region on new international standards to gather, store, distribute, analyze, visualize and disseminate crucial information on past, present and future status of this region in order to assess its sustainability and vulnerability.

The EnviroGrids project also looks at the impacts of climate changes on selected societal benefit areas. The European Community is addressing the crucial problem of water quality and quantity by adopting the Water Framework Directive (CEC 2000) which promotes water management based on watersheds rather than administrative or political boundaries. In this framework, EnviroGrids performed a gap analysis to identify areas where most efforts are needed to reinforce existing observation systems in this



region. Then, spatially explicit scenarios of key drivers of changes such as climate, demography, and land cover were determined. These scenarios are analyzed using calibrated and validated hydrological model developed for the entire Black Sea Basin. The combined impacts of expected climatic, demographic, land cover, and hydrological changes were assessed and projected on Group on Earth Observation's (GEO, <http://www.earthobservations.org/>) societal benefit areas. Specific outcomes were analyzed and made accessible to both the expert and non-expert public through a state-of-the-art web interface providing advance warning to target audiences about risks.

As part of the EnviroGrids project, the general goal of WP4 is to build a hydrologic model of Black Sea Catchment. This model was then used to estimate all components of water resources at the sub-basin level on a monthly time step. We explicitly quantified river discharge, deep aquifer recharge, soil moisture, as well as actual and potential evapotranspiration for the very first time in this region. To bring the outputs of this model closer to the needs of water resources objectives we calculated blue water flow (river discharge plus deep aquifer discharge), green water flow (evapotranspiration), and green water storage (soil moisture). Furthermore, the hydrologic model was calibrated, validated, and sensitivity and uncertainty analysis were performed to assess the goodness of modeling results.

Calibration of large-scale models is data intensive, time consuming and not straight forward. Important issues to address are how to deal with the availability of input data, watershed parameterization, and uncertainties associated with input data accuracy and scarcity (especially rainfall), model uncertainty and parameter non-uniqueness. Therefore, one of the aims of this project is to find ways of properly quantifying all model uncertainties, identifying data gaps, and finding time-efficient ways of calibrating the hydrological model.

Once the BSC hydrologic model is calibrated, the impact of landuse and climate change will be evaluated. Climatic change is a worldwide concern that will affect many areas of human activities. The last report of the Intergovernmental Panel on Climate Change (IPCC 2007a, b, c) predicts important changes in the coming decades that will not only modify climate patterns in terms of temperature and rainfall, but will also drastically change freshwater resources qualitatively and quantitatively. Climate change is expected to lead to more floods or droughts in various regions, lowering drinking water quality and increasing the risk of water-borne diseases and irrigation problems. Such changes may trigger socio-economic crises across the globe that need to be addressed well in advance of the events in order to reduce the associated risks.

The results of this project provide useful information of current and future status of water in BSC to support decision makers to meet the challenges posed by water scarcity and climate change across the region as well as regional policies. The methodology that

was developed is fully transferable to other regions of the world in the future. The resulting tools and data will allow for the analysis of river basin pressures and their impacts on human and ecosystem well-being by local stakeholders and decision makers. These efforts will also help to identify and provide early warning to vulnerable populations and identify the efforts needed to adapt and to limit negative social, economic and environmental impacts in the future.

## 2. Study area

*Geography and vegetation:* Black Sea is an inland sea between Europe and Asia and its catchment (Fig. 1) with the total area of 2.3 million km<sup>2</sup> represents a very important water source for the region. The rivers of 23 European and Asian countries (Austria, Belarus, Bosnia, Bulgaria, Croatia, Czech Republic, Georgia, Germany, Hungary, Moldova, Montenegro, Romania, Russia, Serbia, Slovakia, Slovenia, Turkey and Ukraine, Italy, Switzerland, Poland, Albania and Macedonia) partially or fully drains to the Black Sea whereas the contribution of the last five countries is negligible. Some of Europe's longest and largest rivers flow into the Black Sea including the Danube, the Dnieper, the Dniester and the Don. The area is inhabited by a total population of around 160 million people (BSEI, 2005).



Fig. 1. Region of Black Sea Basin modeled in the project



The area is mountainous in the east and south, in the Caucasus and in Anatolia, and to the North West, with the Carpathians in the Ukraine and Romania. Most of the rest of the Black Sea's western and northern neighborhood is low lying. Mean annual air temperature shows a distinct north-south gradient from  $< -3^{\circ}\text{C}$  to  $> 15^{\circ}\text{C}$ . Precipitation pattern is characterized by a west-east gradient that is decreasing precipitation with distance from the Atlantic Ocean. Areas of high precipitation ( $> 3000\text{ mm y}^{-1}$ ) are in the west and areas of low precipitation ( $< 190\text{ mm y}^{-1}$ ) are in the north and east (Tockner et al., 2009).

The dominant land use in the basin is agriculture with 65 % of coverage according to MODIS Land Cover 2008 (Fig 3). 13 % of the general agricultural land class is declared as crop/natural vegetation which all considered as general agricultural land (AGRL). The region's natural ecosystems include forests in the west, south and east, steppes to the north, and Alpine ecosystems at higher altitudes in the Carpathians, in Anatolia and in the Caucasus.

*Water quality and quantity:* The Black Sea is a very isolated sea, and due to its geomorphologic structure and specific hydrochemical conditions, is vulnerable to pressures from land-based pollution in its catchment areas (UNEP, 2005). Eutrophication is one of the most serious problems facing the Black Sea and one of the key explanations for its environmental decline. More than 300 rivers flow into the Black and Azov Seas, including the second, the third and the fourth major European rivers, namely the Danube, Dnieper and Don. The estimated annual volume of river discharge entering the Black Sea fluctuates from 294 to 480 km<sup>3</sup> (Paleari et al., 2005). The greatest sources of diffuse pollution are related to agricultural activities, to households not connected to sewer systems and to atmospheric depositions. Inadequate land use and the excessive application of mineral and organic fertilizers result in high nutrient inputs into the rivers and ultimately into the Black Sea. The quantities of inorganic fertilizers used in those Black Sea states with transitional economies were drastically reduced in the 1990s. The high prices for fertilizers and pesticides and inability of the population to pay were major causes of reduced loads of discharges from diffuse pollution sources. With the recovery of the agricultural production in the region in recent years, the pollution to the water bodies is likely to increase.

Transboundary pollution effects (TPE) can be seen with respect to all economic sectors. In the municipal sector, major towns that are situated directly along the river systems and that discharge large amounts of untreated wastewater are often the cause of TPE. The downstream countries, as a consequence, face problems of limited use of water resources and risk for human health and biodiversity. In the industrial sector, TPE have been observed in the whole Danube Basin, and are more pronounced in the middle and



low sections. Agriculture activities also result in transboundary effects, which might primarily affect surface water, causing pollution and thereby presenting a threat to the health of the downstream water quality.

*Water and wastewater management:* The construction of dams for irrigation and power generation purposes has resulted in a substantial net decrease in the runoff to the Black Sea and the Sea of Azov. This, in turn, has caused a reduction in the freshwater and sediment inflow into these areas, with concomitant coastal erosion and changes in salinity. Danube river basin which is only one third of the Black Sea Catchment has about 600 major hydraulic structures (dams and weirs >15 m) including 156 hydropower dams that have been built along the Danube and in the catchments of its major tributaries, not including the countless smaller dams (Tockner 2009; Bloesch 2003; ICPDR 2005).

The population that is connected to water supply networks ranges from 95% in Bulgaria to 65% in Georgia, while the population that has access to sewerage system ranges from 86% in Russia to 52% in Romania (Paleari et al., 2005) whereas this is reported by Eurostat to be 90% in Germany and Austria and 30% in Romania. The lack of wastewater treatment facilities contributes to the poor quality of water resources in most Black Sea countries.

*Agriculture:* The Black Sea region has always been an important trade crossroad between Europe and Asia. The region is a unique combination of EU Member States and Non-member States. Sustainable agriculture in the region is a shared concern between the EU and the Black Sea region. The region is considered to have major potentials in agriculture and energy. Figure 3 demonstrates the share of agricultural land use among other land classes in the region. The region has relatively favorable land and water endowments. Wheat, barley and maize are the three major crops in the Black Sea countries (MARS). Currently, the agricultural productivity is low compared with its western European counterparts as well as the world average. The potential for increasing production is therefore considered to be high. It is expected that the region's agricultural production will increase in the coming years in the wake of the recent hike of the world food prices. Some projections have shown that the region has the potential to be a food exporter, especially to the Middle Eastern and North African countries (MENA).



### 3. SWAT model

SWAT is a basin-scale, continuous-time model that operates on a daily time step and is developed to predict the impact of land management practices on water, sediment, and agricultural chemical yields in large complex watersheds with varying soils, landuses, and management conditions. The program has been successfully used in a wide range of scales and environmental conditions from small catchments to continental level (Gassman et al., 2007). It performs plant growth processes as well as water quantity and water quality modeling. In this study, we used the ArcSWAT (Olivera et al., 2006) program, where ArcGIS (ver. 9.1) environment is used for project development.

In SWAT, a watershed is divided into multiple sub-watersheds, which are then further subdivided into HRUs that include homogeneous slope, landuse, and soil characteristics. Calculated flow, sediment yield, and nutrient loading obtained for each sub-basin are then routed through the river system.

The water in each HRU is stored in four storage volumes: snow, soil profile (0–2 m), shallow aquifer (typically 2–20 m), and deep aquifer. Surface runoff from daily rainfall is calculated using a modified SCS curve number method. Downward flow happens when water content exceeds field capacity for each layer. Percolation from the bottom of soil profile recharges the shallow aquifer. If the temperature in a particular layer is  $\leq 0^{\circ}\text{C}$ , no percolation is allowed from that layer. Groundwater flow contribution to total stream flow is estimated by routing a shallow aquifer storage component to the stream (Arnold and Allen, 1996).

Depending on data availability, potential evapotranspiration (PET) can be calculated using different approaches. In this study, potential evapotranspiration was calculated using the Hargreaves method, which only requires minimum and maximum temperature. The daily value of leaf area index (LAI) was applied to partition the PET into potential soil evaporation and potential plant transpiration. LAI and root development were estimated using the crop growth component of SWAT. This element indicates the relationship between vegetation and hydrologic budget (Faramarzi et al., 2009, 2010; Liu et al., 2008).

The crop growth component of SWAT, which is a simplified version of EPIC model, is capable of simulating a wide range of crop rotation, grassland/pasture systems, and trees. Harvest index ( $HI$ ) is the fraction of above-ground plant dry biomass that is removed as dry economic yield. Potential crop growth and yield are usually not achieved as they are inhibited by temperature, water, nitrogen and phosphorus stress factors. In the SWAT model the actual yield is calculated by multiplication of the actual aboveground biomass ( $bio_{act}$ ) and actual harvest index ( $HI_{act}$ ). In a given area,  $bio_{act}$  is affected by all management stress factors (water, fertilizer, and temperature), while



$HI_{act}$  is affected only by water stress factor. The latter can be calibrated to achieve a certain water-stress-limited yield. There are two options for irrigation and fertilization: user specified and automatic. Automatic irrigation can be used by triggering irrigation events according to a water stress threshold. Automatic fertilizer routine can be used to simulate fertilizer applications based on nitrogen stress. We selected automatic irrigation and fertilization option in this study because of the difficulty in obtaining irrigation and fertilization schedule data for different provinces. In the model we assumed an unlimited source for irrigation but controlled it through calibration of  $HI_{act}$ . This is a reasonable assumption as in most parts of Iran large amounts of water is extracted from deep aquifer or is transferred from other river basins for irrigation purpose. The fertilizer use in the model was limited to the available data at the provincial level and crop specific fertilizer use per year.

Plant growth is determined from leaf area development, light interception and conversion of intercepted light into biomass assuming a plant species-specific radiation use efficiency. Potential evapotranspiration (PET) in this study was simulated using Hargreaves method. Actual evapotranspiration (AET) was determined based on the methodology developed by Ritchie (1972). Leaf area index LAI and root development were simulated on daily time steps. The daily value of LAI was used to partition PET into potential soil evaporation and potential plant transpiration. A more detailed description of the model is given by Neitsch, et al. (2005).



#### 4. Data availability and sources for modeling with SWAT

Most of the data for building the hydrological-crop model came from freely available data on Internet and some from the project partners. In a previous report we stated the insufficiency of the data provided by the partners. It should be emphasized that data remains a main obstacle in watershed research in Europe. Although there are efforts in creating a European as well as a global data base in web servers such as GEO and INSPIRE, but as these databanks operate on voluntary basis, they are not yet adequate. A more serious effort needs to be done for collecting and unifying data format in Europe. In Table 1 we provide a list of the data require for a SWAT model.

**Table 1.** Data required by SWAT program.

Data name	Required information
<b>DEM map</b>	
<b>Landuse map</b>	
<b>Soil map</b>	<ul style="list-style-type: none"> <li>- Number of soil layers up to 10 may be specified</li> <li>- Soil Hydrologic group (A, B, C, or D) - Maximum rooting depth (mm)</li> <li>- Textural class of first soil layer</li> <li>- Depth from soil surface to bottom of each layer (mm)</li> <li>- Moist bulk density (g/cm<sup>3</sup>)</li> <li>- Available water capacity (mm H<sub>2</sub>O/mm soil)</li> <li>- Saturated hydraulic conductivity (mm/hr)</li> <li>- Organic carbon content (% soil weight)</li> <li>- Clay content (% soil weight)</li> <li>- Silt content (% soil weight)</li> <li>- Sand content (% soil weight)</li> <li>- Rock fragment content (% total weight)</li> <li>- Moist soil albedo</li> <li>- Soil erodibility factor, K, in USLE equation</li> </ul>
<b>River network map</b>	
<b>Climate data</b>	<ul style="list-style-type: none"> <li>- Daily precipitation (mm)</li> </ul>



	<ul style="list-style-type: none"> <li>- Dail Max temperature (degree C.)</li> <li>- Dail Min temperature (degree C.)</li> <li>- Location (lat, long, elevation) of the climate stations</li> <li>- Wind speed (m/s) (if available)</li> <li>- Relative humidity (if available)</li> <li>- Solar radiation (MJ7m2/day) (if available)</li> </ul>
<b>Reservoir operation information</b>	<ul style="list-style-type: none"> <li>- Month the reservoir became operational (0-12)</li> <li>- Reservoir surface area when the reservoir is filled to the emergency spillway (ha)</li> <li>- Volume of water needed to fill the reservoir to the emergency spillway (<math>10^4 \text{ m}^3</math>)</li> <li>- Reservoir surface area when the reservoir is filled to the principal spillway (ha)</li> <li>- Volume of water needed to fill the reservoir to the principal spillway (<math>10^4 \text{ m}^3</math>)</li> <li>- Initial reservoir volume.</li> <li>- Initial sediment concentration in the reservoir (<math>\text{mg L}^{-1}</math>)</li> <li>- Equilibrium sediment concentration in the reservoir (<math>\text{mg L}^{-1}</math>) -</li> <li>Hydraulic conductivity of the reservoir bottom (<math>\text{mm hr}^{-1}</math>)</li> <li>- Daily reservoir outflow (<math>\text{m}^3 \text{ s}^{-1}</math>).</li> </ul>
<b>Inlet</b>	<p>This has to do with water transfer into the watershed (if any)</p> <ul style="list-style-type: none"> <li>- Lat and long for any inlet to the watershed is required</li> <li>- daily data for any inlet (optional)</li> </ul>
<b>Agricultural management data</b>	<p>Currently, I have not too much information on agricultural management. This is essential for water quality modeling.</p> <ul style="list-style-type: none"> <li>- Planting and harvest dates</li> <li>- Fertilization information (when, where, how much)</li> <li>- Tillage operation (method, date)</li> <li>- Irrigation (source, date, amount)</li> <li>- Grazing</li> <li>- Tile drains (exits or not, if yes, at what depth)</li> <li>- Pesticide application</li> <li>- Crop rotation</li> </ul>

**enviroGRIDS – FP7 European project**

Building Capacity for a Black Sea Catchment

Observation and Assessment supporting Sustainable Development



<b>Water management</b>	<ul style="list-style-type: none"><li>- Water transfer information, water use from shallow and deep aquifer, river, and ponds</li></ul>
<b>River discharge data at hydrometric stations</b>	<p>We need this data for model calibration.</p> <ul style="list-style-type: none"><li>- Daily river discharge (<math>\text{m}^3 \text{s}^{-1}</math>)</li><li>- River water quality data (see below)</li><li>- lat and long of the stations</li><li>- The river names where the stations are located</li></ul>
<b>Crop yield data</b>	<ul style="list-style-type: none"><li>- Annual yield for major crops in the region</li></ul>
<b>Water quality at hydrometric stations (if water quality is required)</b>	<ul style="list-style-type: none"><li>- Sediment load transported by the river (daily, or monthly) (tn)</li><li>- River sediment concentration (<math>\text{mg l}^{-1}</math>)</li><li>- Nitrate load transported by the river (kg N)</li><li>- Phosphorus load transported by the river (Kg P)</li><li>- Dissolved oxygen transported by the river (kg <math>\text{O}_2</math>)</li><li>- Algal biomass transported by river (kg)</li><li>- Other chemicals such as: <math>\text{NH}_4</math>, <math>\text{NO}_2</math>, Mineral P, organic P, Organic N, CBOD are also considered by SWAT</li></ul>
<b>Point sources</b>	<ul style="list-style-type: none"><li>- Input from water treatment plants (quantity and quality of water, and Lat-Long location)</li><li>- Springs (quantity and quality, and Lat-Long location)</li></ul>

The following data was eventually used in the model:

### - Black Sea boarder



Fig. 2. Boarder of the Black Sea Basin used in the project  
Source: EnviroGrids web site (<http://www.envirogrids.net/>)

### - Digital Elevation Model (DEM)

DEM was obtained from SRTM (Jarvis. et al, 2008) 90 m resolution (Fig. 3).

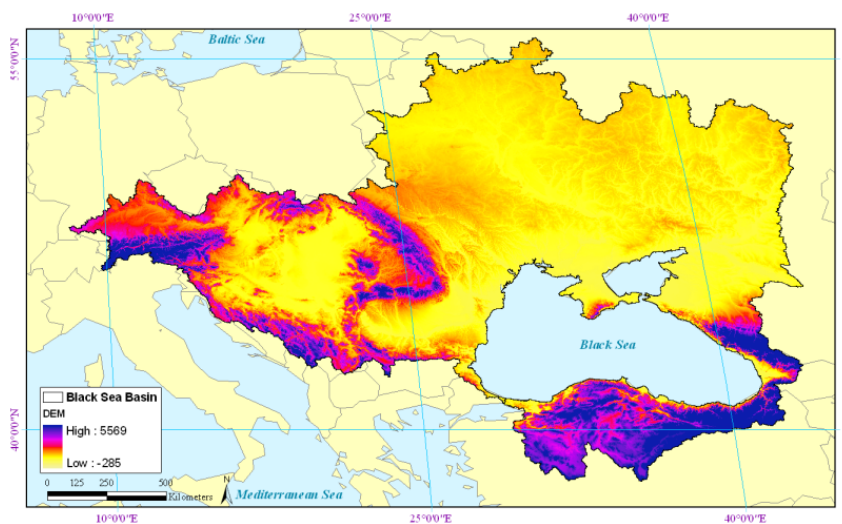
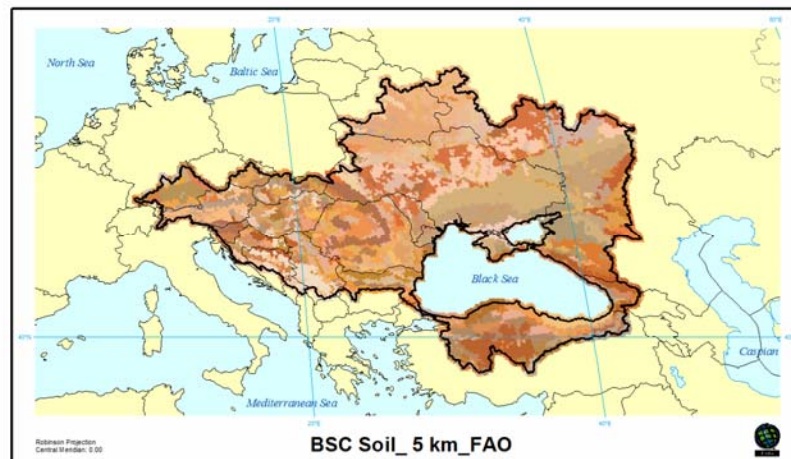


Fig. 3. Digital Elevation Model

## - Soil

The Soil data was obtained from the FAO-UNESCO global soil map (FAO, 1995), which provides data for 5000 soil types comprising two layers (0–30 cm and 30–100 cm depth) at a spatial resolution of 5 km. The database of this soil map was created by Schuol et al., in their Africa project (2008a) using pedotransfer files. Corrections were made to the soil map to cover the entire Black Sea (Fig. 4a,b).



**Fig. 4a.** Soil map of the Black Sea Basin

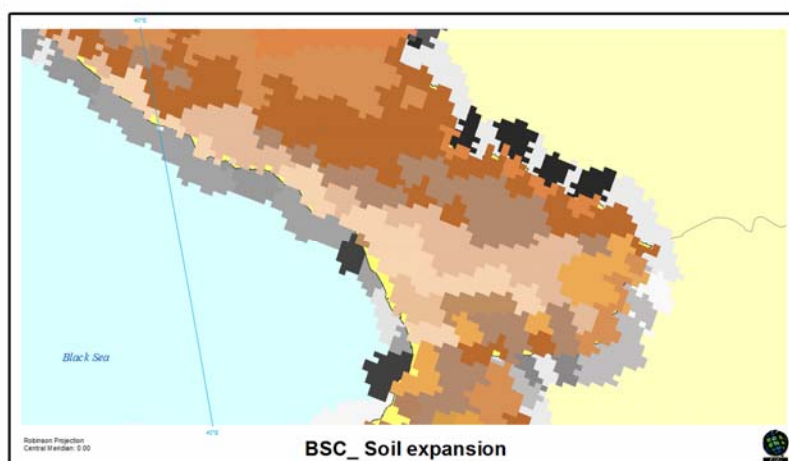


**Fig. 4b.** Areas where soil map was expanded to match the DEM

## - Landuse

- Four different landuse, database were tested in the region: (i) Global Landuse/Land Cover Characterization (GLCC) at 1 km spatial resolution from USGS (<http://landcover.usgs.gov/usgslandcover.php>) (Fig. 5a.), (ii) MODIS land cover with spatial resolution of 500 m (<http://earthdata.nasa.gov/data/standards-and-references/earth-data-science-disciplines/land/land-cover-land-use-change>) maintained by the NASA Land Processes Distributed Active Archive Center (LP DAAC) at the USGS/Earth Resources Observation and Science Center (EROS) (Fig. 5b), (iii) GlobCover with spatial resolution of 300 m by European Space Agency (ESA\_a) (<http://due.esrin.esa.int/globcover/>) (Fig. 5c), (iv) Global Corine at 300 m spatial resolution provided by European Space Agency (ESA\_b) (<http://www.eea.europa.eu/publications/CORO-landcover>) (Fig. 5d) The landuse datasets were used in four different SWAT models, each using one landuse type. The model response to various landuse maps with different resolution were compared looking at the simulated river discharges versus the observed discharges in each project. Result of this study showed that landuse resolution does not have a significant effect on river discharge simulation in BSC meaning that the choice of input landuse resolution could depend on the scale of watershed. However the model is sensitive to the combination of the various landuses with different resolution and from different sources. This could affect the simulation differently in other locations and needs to be further investigated.

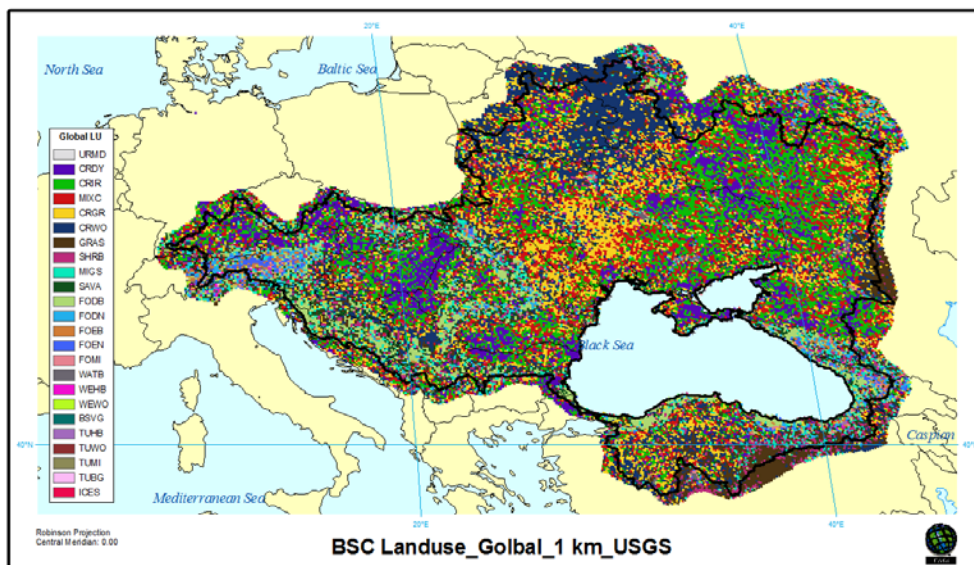


Fig. 5a. Global landuse map from USGS

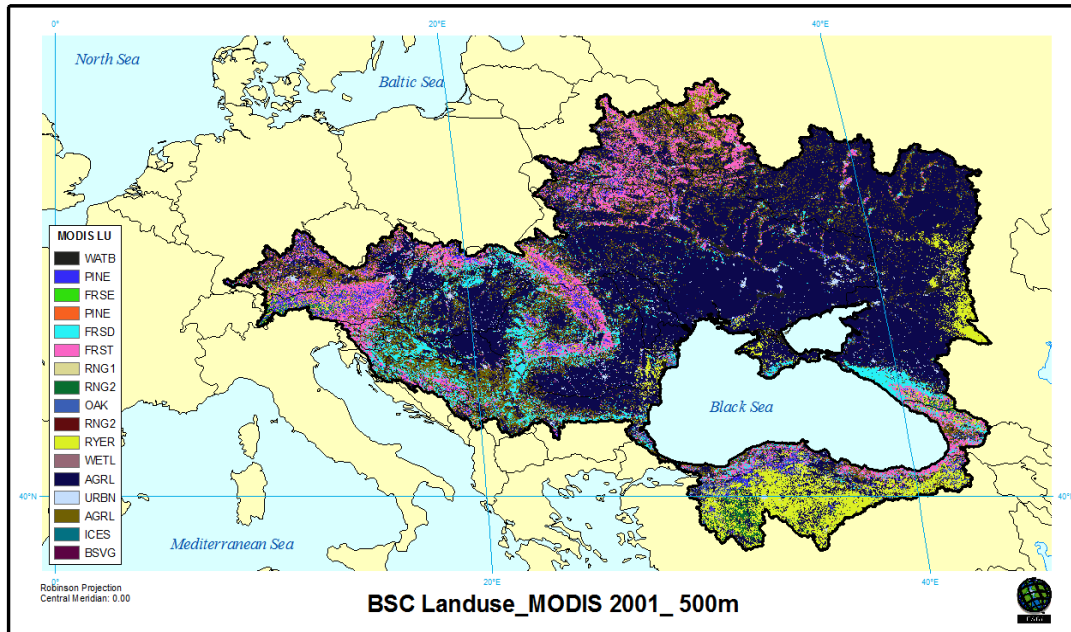


Fig. 5b. MODIS landuse map



Fig. 5c. Global Cover landuse map

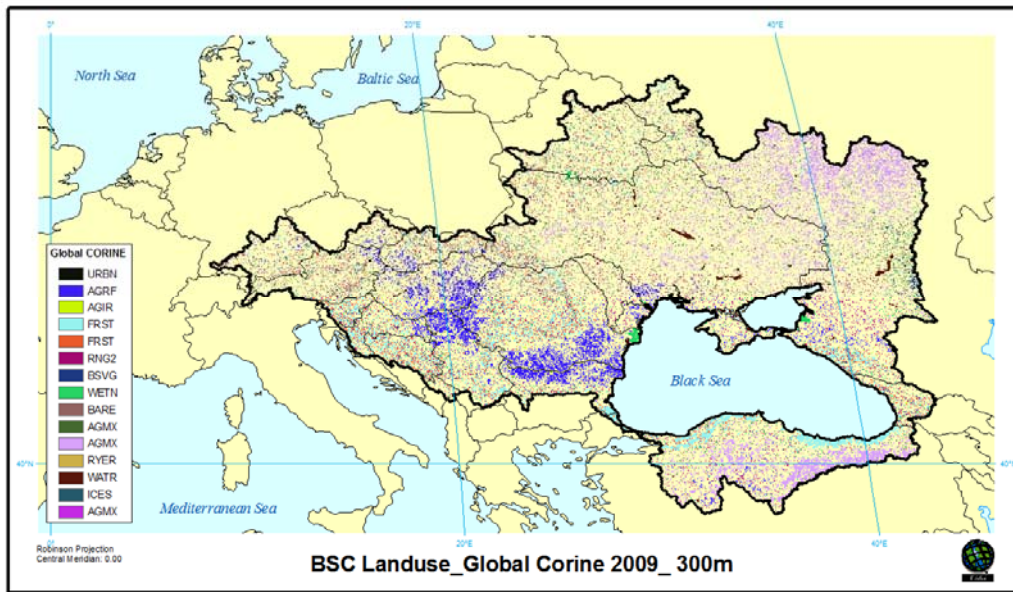
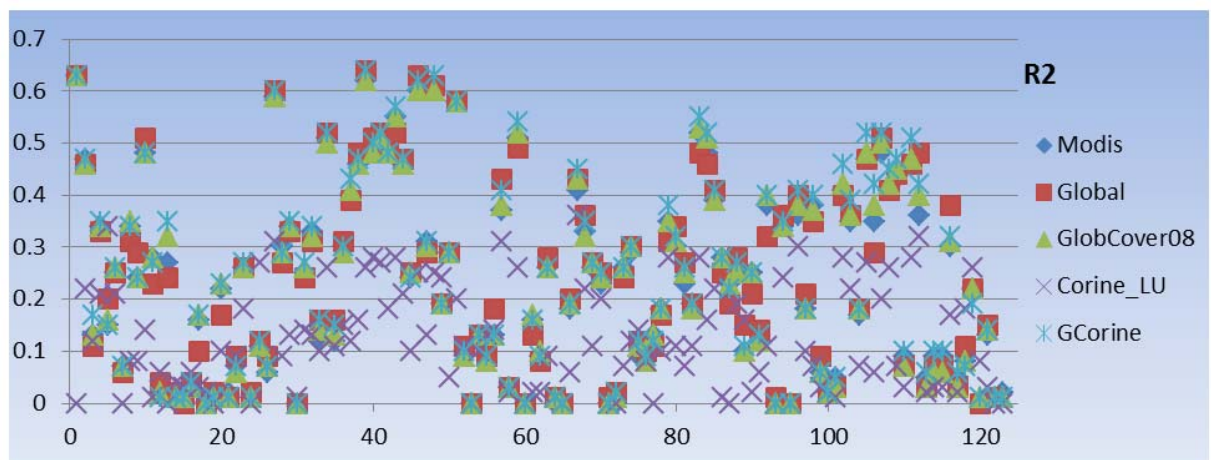
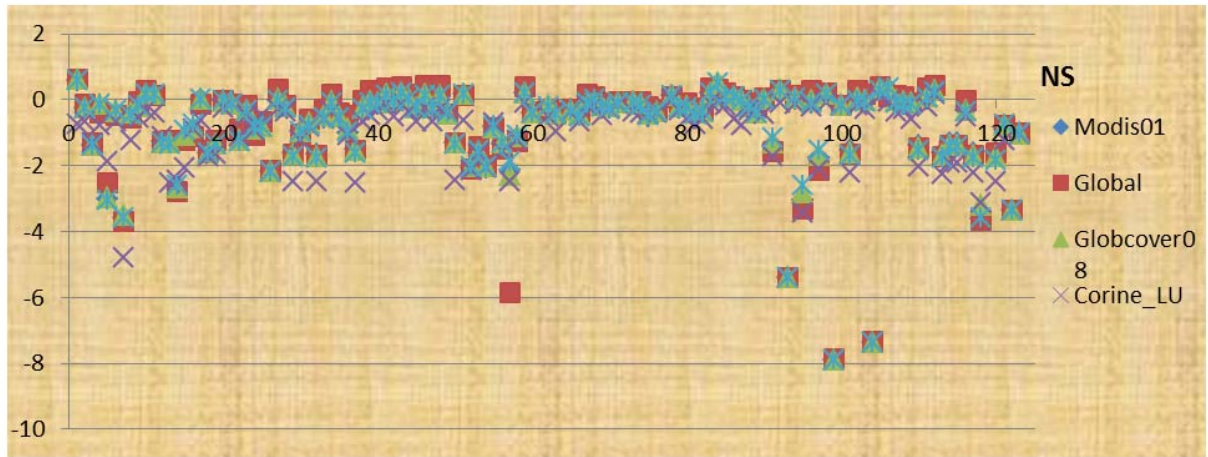


Fig. 5d. Global Corine Landuse map

MODIS land cover with spatial resolution of 500 m was chosen to be used in the final SWAT project of the BSB due to the relatively good results in the test phase as illustrated in Figs. 6a,b,c using  $R^2$ , NS, and  $bR^2$  statistics.



**Fig. 6a.** Comparing the performances of different landuse maps in terms of  $R^2$



**Fig. 6b.** Comparing the performances of different landuse maps in terms of NS

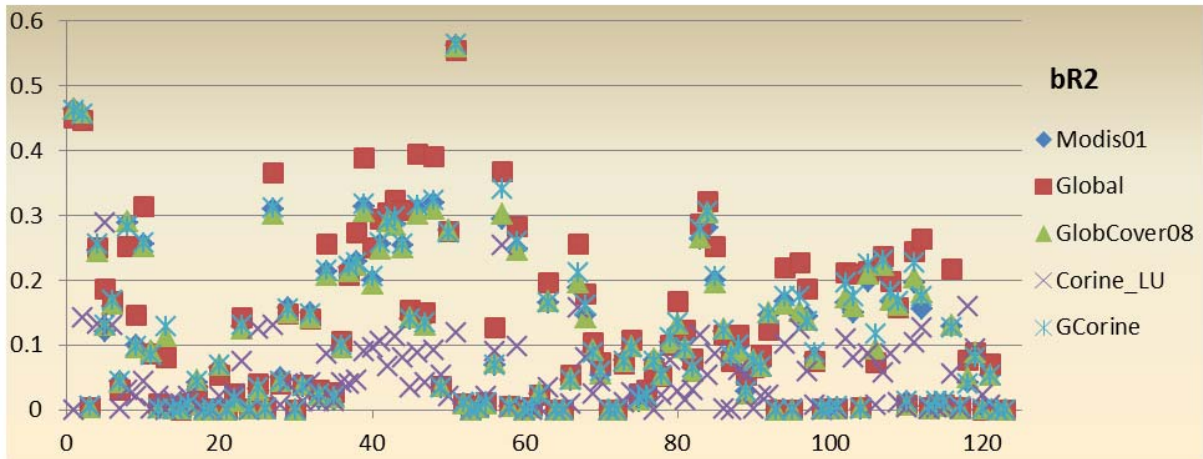


**Fig. 6a.** Comparing the performances of different landuse maps in terms of  $bR^2$

MODIS was also the basis of further analysis on landuse change studies in this region (Fig. 5b). Fourteen different landuse classes from the SWAT database were assigned to MODIS land cover classes to connect the landuse database with SWAT crop database (Fig. 7, Table 2). Subsequently each sub-basin was split into unique combinations of slope, landuse classes and soil types resulting in 89202 hydrologic Response Units (HRUs).

Modis Landuse, SWAT classification

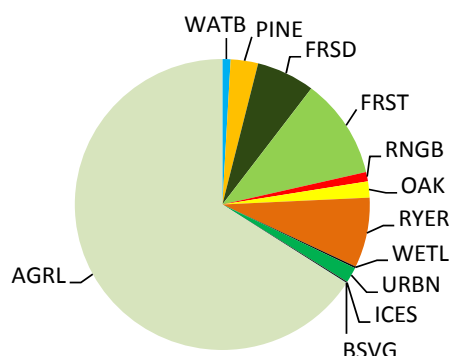


Fig. 7. Distribution of landuses in MODIS classification

Table 2. Modis landuse classes and the corresponding SWAT landuse classification and the percentage of the coverage in Black Sea Catchment

MODIS Classes	MODIS legend	Land cover	SWAT Classes	SWAT land cover legend
0	Water		WATB	WATER BODIES
1	Evergreen forest	needleleaf	PINE	Pine
2	Evergreen forest	broadleaf	FRSE	Forest evergreen
3	Deciduous Forest	needleleaf	PINE	Pine
4	Deciduous Forest	broadleaf	FRSD	Forest Deciduous
5	Mixed forests		FRST	MIXED FOREST
6	Closed Shrubland		RNG1	Range-Brush, modified for cold temperature and leaf area Index
7	Open Shrubland		RNG2	Range-Brush, modified for cold weather
8	Woody Savannas		OAK	Oak
9	Savannas		RNG2	Range-Brush, modified for cold weather
10	Grasslands		RYER	Russian wild rye
11	Permanent wetlands		WETL	Mixed WETLAND
12	Croplands		AGRL	Agricultural Land-Generic



13	Urban and build-up	URBN	Residential
14	Crops/natural vegetation	AGRL	Agricultural Land-Generic
15	Snow and ice	ICES	SNOW OR ICE
16	Baren or sparsely vegetated	BSVG	Baren or sparsely vegetated

### - Climate

The climate inputs consisted of daily data on precipitation, maximum and minimum temperature and are from two sources: i) Measured data ii) Gridded data. Measured climate data were mainly collected from the National Climatic Data Centre (NCDC) (<http://www.ncdc.noaa.gov>), the European Climate Assessment & Dataset (ECAD) (<http://eca.knmi.nl/>), Turkish ministry of Energy and Bulgarian Data Center for the period of 1970 to 2008. Only stations with < 20% missing data were included and the weather generator model of SWAT (Sharpley and Williams, 1990) was used to fill remaining gaps. Gridded data which is used in this study is from Climate Research Units (CRU) dataset at 0.5° resolution (Mitchell and Jones, 2005) (<http://www.cru.uea.ac.uk/data>). The performance of the CRU climate dataset versus measured climate data was tested by building up two SWAT projects of the BSB using CRU and Observed climate stations. The simulated discharge was compared against the observed using two statistical measures R<sup>2</sup> and NS coefficient. The simulated discharge were more promising in the project using CRU as shown in Table 3. The CRU data set was therefore selected as the final climate dataset to be used in modeling the hydrology of the BSB. The daily global solar radiation data (MJ m<sup>-2</sup> d<sup>-1</sup>) (Weedon et al., 2011) were obtained from 6110 cells or virtual stations at 0.5° resolution for the duration of 1960-2001. As SWAT only accepts 300 gauging stations, the number of stations reduced to 300. Both measured and CRU gridded data distributions are shown on Fig. 8a,b.

To capture the peaks of the river flows in melting seasons, the model allows the sub-basins to be split into a maximum of ten elevation bands. Snow cover and snow melt are simulated separately for each elevation band. In this study the sub-basins with the minimum altitude of 700 m and elevation discrepancy of 700 m were divided into 5 elevation bands. This way the model is able to assess the differences in snow cover and snow melt caused by orographic variation in precipitation and temperature. Precipitation and maximum and minimum temperature are calculated for each band as a function of the respective laps rate and the difference between the gauge elevation and the average elevation specified for the band in each sub-basin.



**Table 3.** Mean annual river discharges for a selection of European rivers based on four different climate datasets. The GRDC values are the observed annual average river discharges, all in  $\text{m}^3 \text{s}^{-1}$

River	Station Name	GRDC	Climate database			
			ECAD	CRU	NCAR	Observed
Volga	Volgograd	8141	5570	6924	5951	7465
Danube	Ceatal Izmail	6415	3243	5244	4724	4204
Pechora	Oksino	4444	1849	2396	2330	2277
North. Dvina	Ust-Pinega	3331	1419	1597	1470	1705
Rhine	Lobith	2229	1725	2065	2110	1589
Rhone	Beaucairw	1709	1735	1808	1707	1364
Sava	Sremska M.	1563	411	1078	881	973
Po	Pontelagoscuero	1514	1108	1589	1424	1210
Dnepr	Dnepr P.P	1492	1987	2182	1811	2421
Vistula	Tczew	1042	462	715	620	846
Loire	Montjean	838	761	948	909	831
Tisza	Senta	784	445	469	448	435
Inn	Passau-Ingling	737	493	723	510	367
Elbe	Neu-Darchau	708	327	516	495	500
Garonne	Mas-d'Agenais	606	343	451	422	605
Aare	Untersiggenthal	561	405	515	528	299
Duero	Regua	545	454	573	645	626
Oder	Gozdowice	530	181	391	345	365
Angermaelven	Sollefteae	503	144	190	215	239
Luleaelven	Boden	501	291	297	328	229
Ebro	Tortosa	485	678	469	509	250
Tiber	Roma	231	128	114	115	182
Guadalquivir	Sevilla	207	219	226	244	204
Siret	Lungoci	198	36	119	115	136
Maros	Mako	173	9	95	86	85
Olt	Stoenesti	161	21	62	67	47
Szamos	Satu Mare	126	41	63	81	54
Trent	Colwick	85	67	65	59	61
Thames	Teddington	82	37	47	72	36
<b>Root Mean Square Error</b>			<b>5500</b>	<b>3360</b>	<b>4100</b>	<b>3900</b>

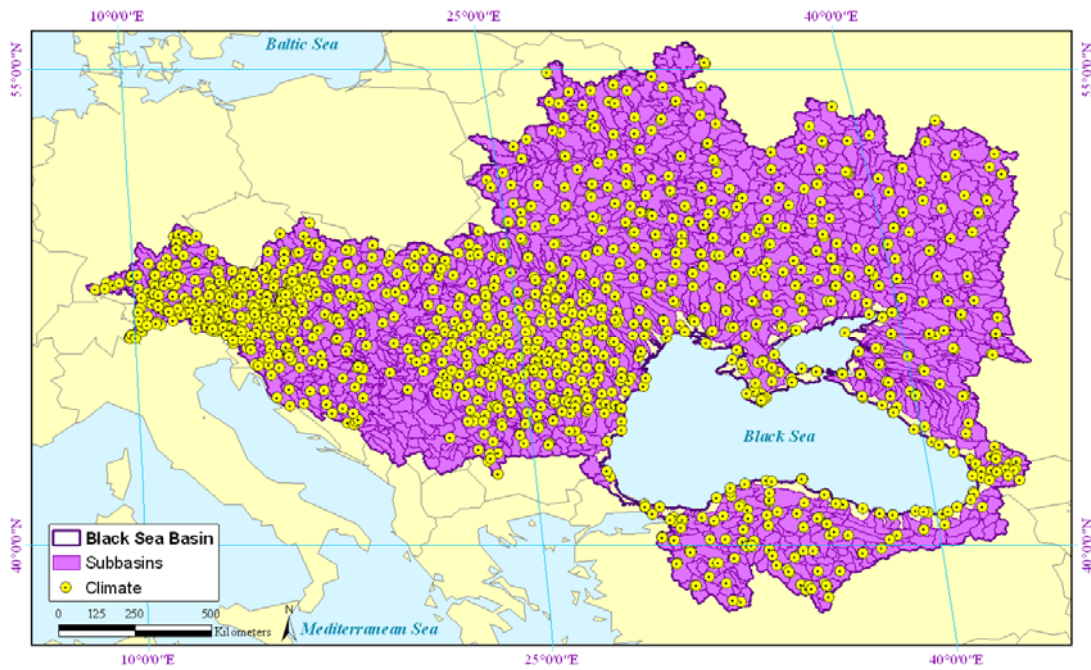


Fig. 8a. Distribution of climate stations in the Black Sea Basin

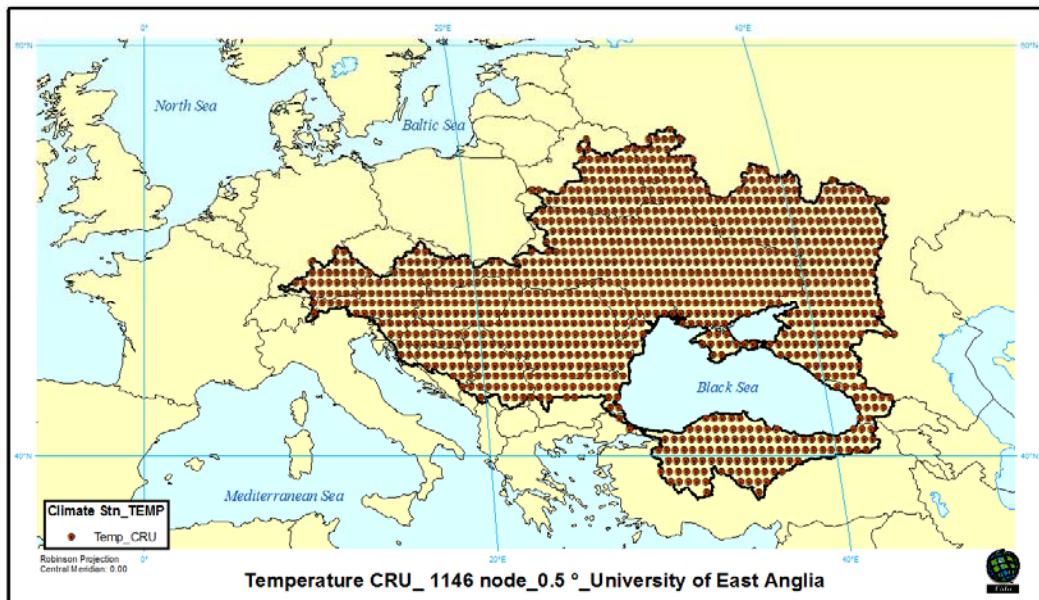


Fig. 8b. Distribution of climate stations based on the gridded CRU data

## - River Discharge and NO<sub>3</sub> concentration

Monthly river discharge data were obtained from Global Runoff Data Center (GRDC) and some from the project partners in Romania, Bulgaria, and Turkey for the period 1970–2008. Only data with < 20% of missing data and minimum length of 5 years were included in calibration-validation process. That led to 79 discharge stations in total. Monthly data on nitrate concentration in rivers were taken from 30 observation stations from ICPDR (<http://www.icpdr.org/main/>). The station distributions are shown in the following Figure (9) along with CRU climate stations.

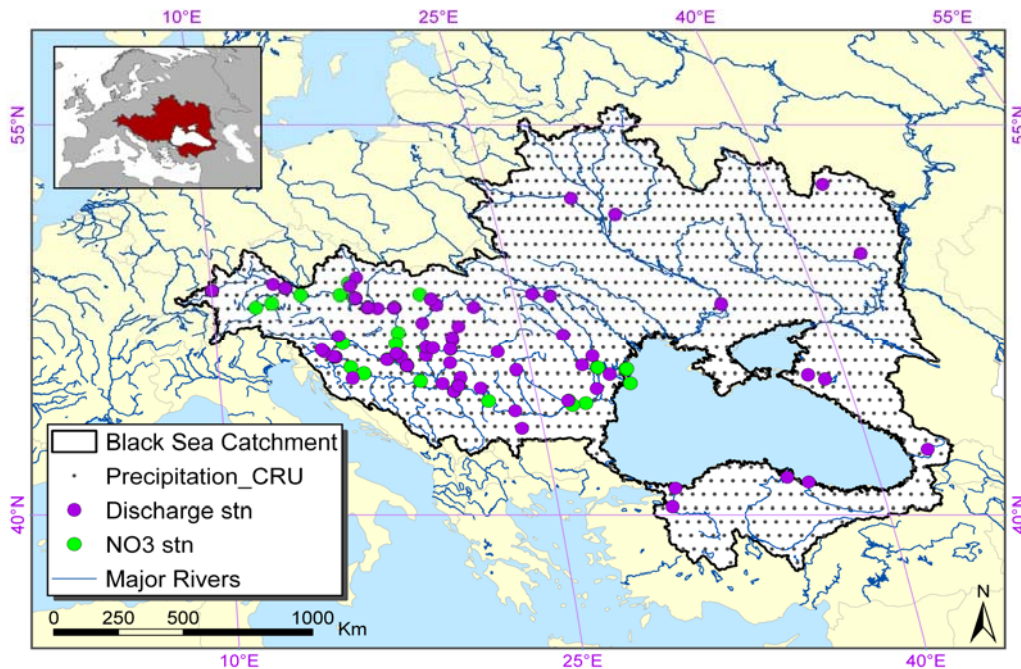


Fig. 9. Distribution of measured discharge and water quality stations

## - Point sources of pollution

To account for loadings of nutrients to stream network from sources not associated with land area, point sources loads were defined for every sub-basin in the catchment (Fig. 10). SWAT allows adding daily or average daily loadings from point sources to the main channel network. As the most common anthropogenic point source is sewage, the nutrient loads of each sub-basin was calculated based on the population of that sub-basin (Fig. 11), the percentage of population connected to wastewater treatment plant

and the average rate of nitrogen per population equivalent. These loads are then routed through the channel network along with the loadings generated by land areas.

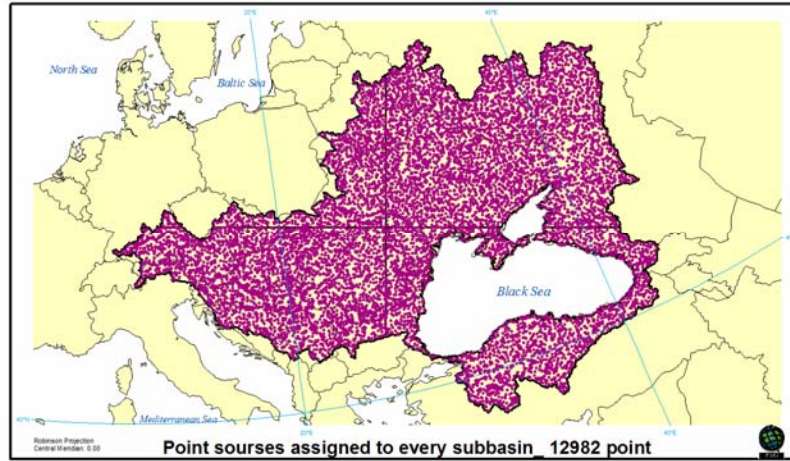


Fig. 10. Distribution of point source stations

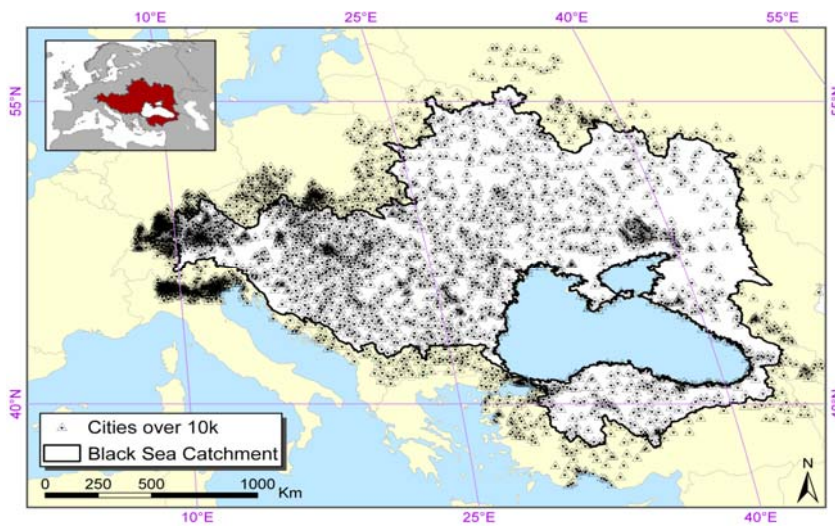


Fig. 11. Distribution of cities with population greater than 10,000



Population percentage connected to sewage treatment was derived from Eurostat for the period of 2000 to 2009 (Table 4). This share was above 80% in approximately half of the EU countries for which data was available (mixed reference years), rising to 95% in Germany. At the other end of the range, less than one in two households were connected to urban wastewater treatment in Bulgaria and Romania. As the data was not available for all countries we assumed that: Moldova, Ukraine, Russia, Belarus, Georgia have the same rates as Bulgaria has. Serbia, Bosnia, Montenegro was assumed to be in the same situation as Slovenia is. Albania, Italy, Macedonia, Poland and Switzerland are deleted from the pool because of their small shares in the BSB.

**Table 4.** Percent population connected to waste water treatment system

Country	2000	2001	2002	2003	2004	2005	2006	2007	2008	2009
<b>Austria</b>	85	86	86	89	89	89	92	92	93	93
<b>Belarus</b>	37	38	39	40	40	41	41	42	44	45
<b>Bosnia</b>	23	25	25	26	34	37	52	51	52	52
<b>Bulgaria</b>	37	38	39	40	40	41	41	42	44	45
<b>Croatia</b>	9	9	9	9	15	28	28	29	29	29
<b>Czech</b>	64	65	70	71	71	73	74	75	76	76
<b>Georgia</b>	37	38	39	40	40	41	41	42	44	45
<b>Germany</b>	93	93	93	93	94	94	94	95	95	95
<b>Hungary</b>	46	50	57	57	57	54	57	57	57	57
<b>Moldova</b>	37	38	39	40	40	41	41	42	44	45
<b>Montenegro</b>	23	25	25	26	34	37	52	51	52	52
<b>Romania</b>	27	27	27	27	27	27	28	28	29	29
<b>Russia</b>	37	38	39	40	40	41	41	42	44	45
<b>Serbia</b>	23	25	25	26	34	37	52	51	52	52
<b>Slovakia</b>	51	51	52	53	54	55	55	57	57	57
<b>Slovenia</b>	23	25	25	26	34	37	52	51	52	52
<b>Turkey</b>	26	27	28	30	36	36	42	46	46	46
<b>Ukraine</b>	37	38	39	40	40	41	41	42	44	45



As the available data period was shorter than the simulation requirements, the values from 1970 to 2000 were assumed to be constant and equal to year 2000 except for population. In terms of treatment levels, tertiary wastewater treatment was most common (again mixed reference periods) in Germany, Austria and Italy where at least four in every five persons were connected to this type of wastewater treatment. In contrast, no more than 1% of the population was connected to tertiary wastewater treatment in Romania and Bulgaria. We assumed the treatment efficiency to be 80% in all cases. The 20% pollution from the effluent of wastewater treatment plant along with untreated wastewater are assumed to be directly loaded in surface waters and hence considered as the point sources of each sub-basin.

The regional population was calculated based on the population map in year 2005 (World Bank, <http://data.worldbank.org/indicator/SP.POP.TOTL>) and extrapolated to other years based on the national population growth rate provided by World Bank Zessner et al, 2005 investigated the emissions of nutrient from municipal point sources based on detailed evaluation of data from 76 municipal wastewater treatment plants and calculation of discharge of N from households into wastewater in Austria. The results of this investigation show that the N and P loads are  $1.5 \text{ g P (pe.day)}^{-1}$  and  $8.8 \text{ g N (pe.day)}^{-1}$  as average values for municipal wastewater (contributions from households and industry) where pe is population equivalent to count for industrial releases (Zessner et al, 2005). The relation between inhabitants and actual pe-loading varies in a way that 80% of the treatment plants lie in the range 0.4 to 0.9. The average value that can be assumed as standard values for estimations of the pe-loading is 0.63 (Zessner et al, 2005).

$$Load_{NO_3} = POP_t * \left[ \left( 1 - S_{rate} * N / PE \right) + \left( (1 - T_{Eff}) * S_{rate} * N / PE \right) \right] \quad (1)$$

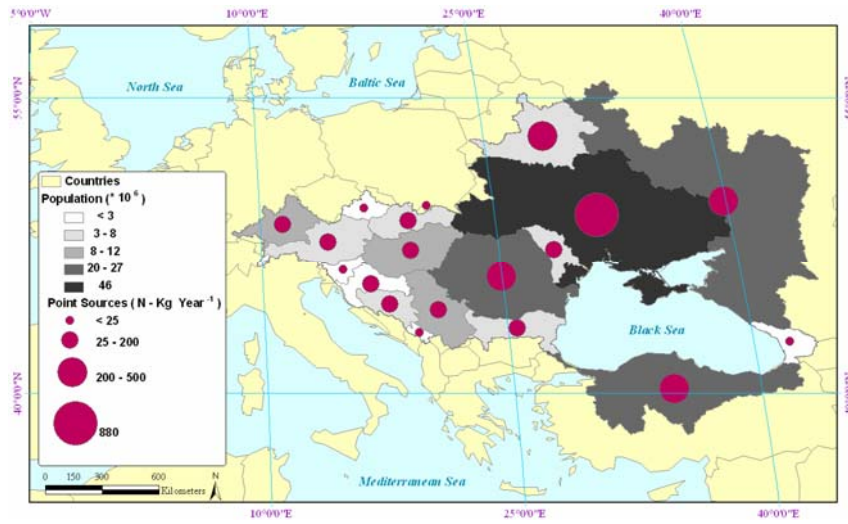
Where  $Load_{NO_3}$  is the nutrient loads to river in each sub-basin ( $\text{g day}^{-1}$ ),  $T_{eff}$  is the wastewater treatment efficiency and considered to be 0.8,  $N$  is the average input of nitrogen from household to wastewater and considered to be 8.8 (g),  $S_{rate}$  is percentage of the population connected to any kind of sewage treatment and presented in Table 4 for different countries, pe is population equivalent, and assumed to be 0.63 in BSB.

Figure 12 shows the contribution of BSB countries in point source pollution released to surface waters.

**enviroGRIDS – FP7 European project**

Building Capacity for a Black Sea Catchment

Observation and Assessment supporting Sustainable Development



**Fig. 12.** Distribution of point source pollution from different countries

## - River network

The river dataset from European catchments and rivers network system (Ecrins) was used to produce the river network and consequently the subbasin configuration of the Black Sea Basin. The following Figure shows the Ecrins as well as the river network created by ArcSWAT (Figs. 13a,b).

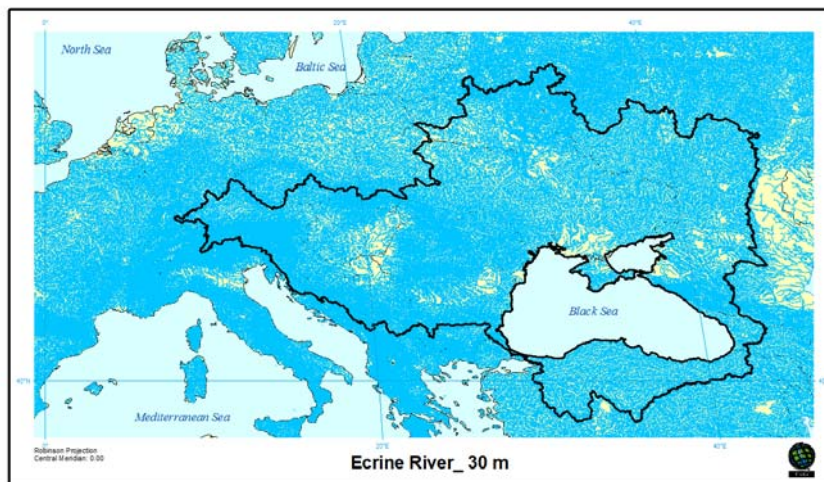


Fig. 13a. The Ecrine river network in the Black Sea Basin

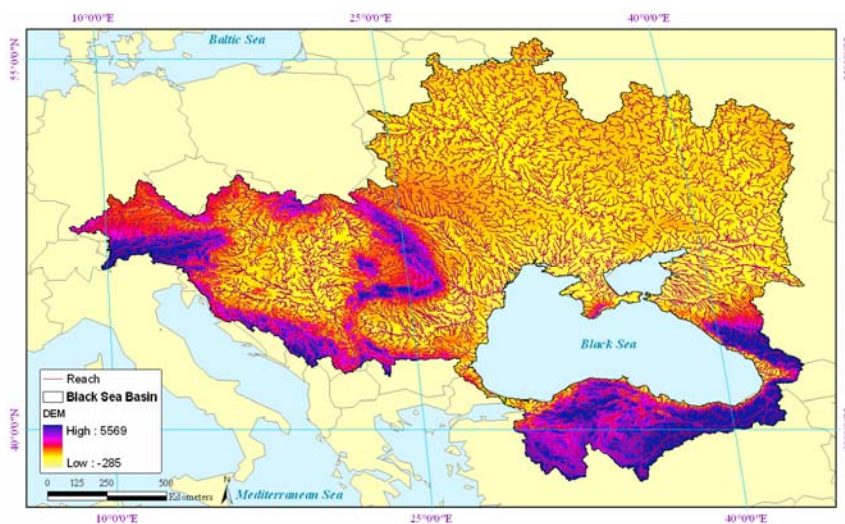


Fig. 13b. River network created by the SWAT model

## - Agricultural management statistics

Growing area, start and end month of the cropping periods in the countries of BSB was derived from MIRCA2000, global monthly irrigated and rain-fed crop areas around the year 2000, at a spatial resolution of 5 arc min (Portmann et al, 2010). The data set covers all major food crops as well as cotton. It represents multi-cropping systems and maximizes consistency with census-based national and subnational statistics. Identical agricultural classes were defined in all countries of BSB so that desired management could be applied at national level. Subsequently the agricultural areas were subdivided proportional to the cropping areas of irrigated/rain-fed, winter/spring types for wheat, maize and barely as the three major crops in the region. However there is a large discrepancy between the two databases (MODIS landuse and MIRCA2000) which made the cropping management a challenging task in this region. In most of the cases the MODIS land cover declares larger agricultural areas than MIRCA2000. As it was the only available agricultural management data in such a large scale, we proceeded using the database making some simplification. Though we anticipate that may lead in larger uncertainty in crop yields prediction in the region (Conceptual model uncertainties). Crop yield data originates from McGill University (Monfreda et al., 2008) in NetCDF and ArcGIS ASCII format at 5 minute resolution and was used to calculate per sub-basin crop yields for maize, barley and wheat (Figs. 14a,b,c).

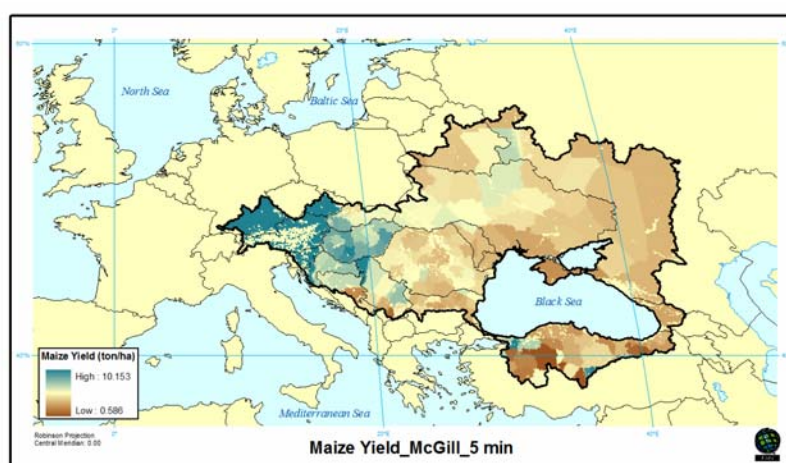


Fig. 14a. Reported maize yield used to calibrate the crop component of the model

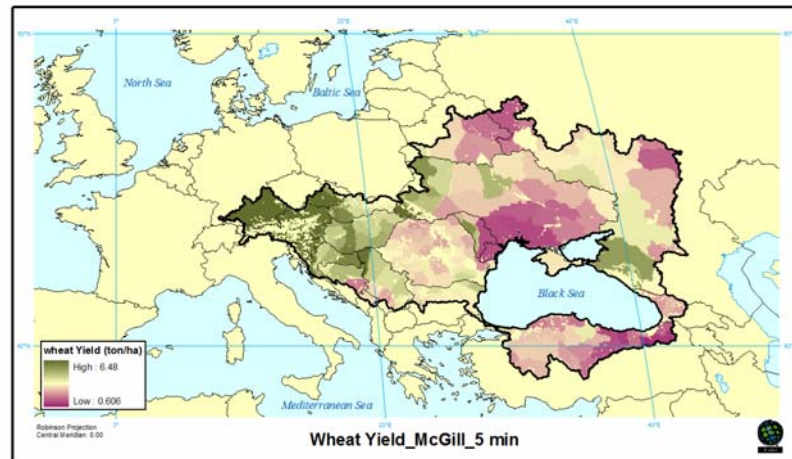


Fig. 14b. Reported wheat yield used to calibrate the crop component of the model

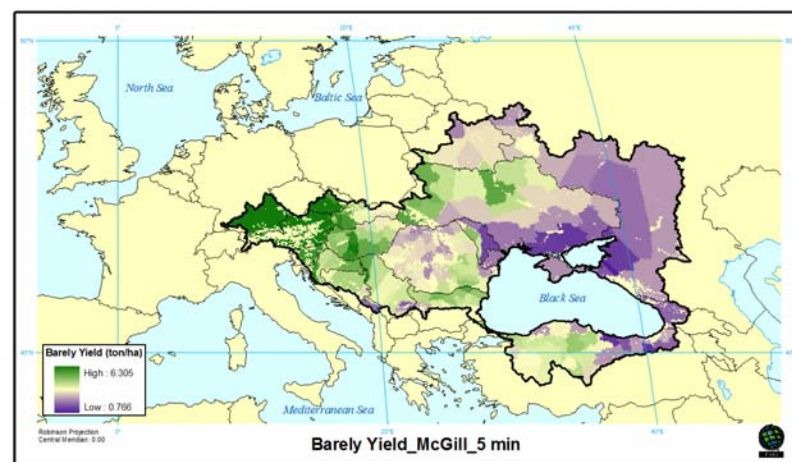


Fig. 14c. Reported barley yield used to calibrate the crop component of the model

The three major crops, maize, wheat and barley, were allocated to agricultural lands, based on MODIS landuse map, proportional to their contribution in each country's harvested areas as MIRACA2000 reported (Figs. 15a,b,c). Twenty five different management plans were designed based on the crop type, cropping dates, winter or summer crops, irrigated or rain-fed applications (Figs. 16a,b). Plant-nutrient deficit automatic fertilization scheduling was employed and the annual maximum application

amount was set to  $300 \text{ kg N ha}^{-1}$ . Elemental nitrogen and elemental phosphors were selected as the main fertilizer in BSB.

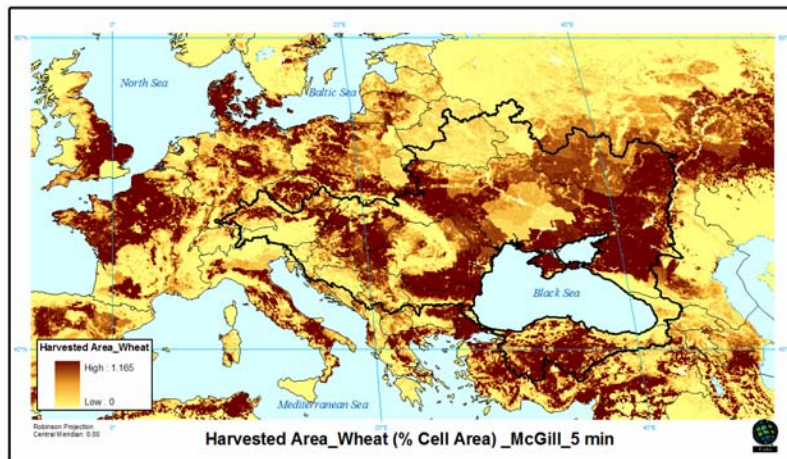


Fig. 15a. Harvested area of wheat used to assign wheat growing region in the model

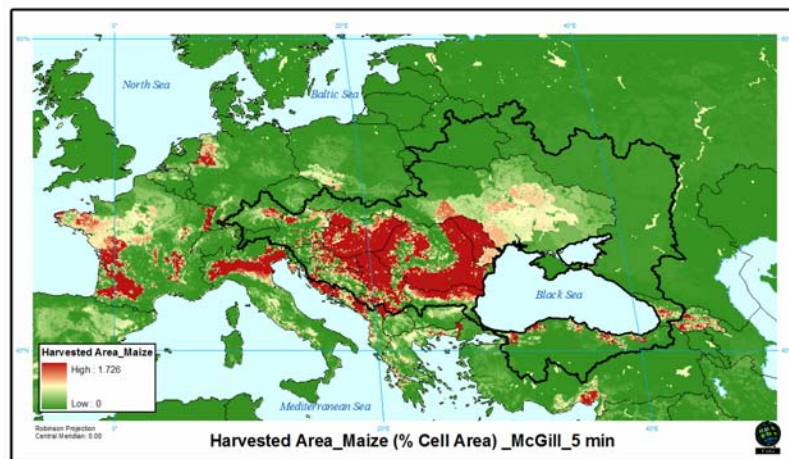
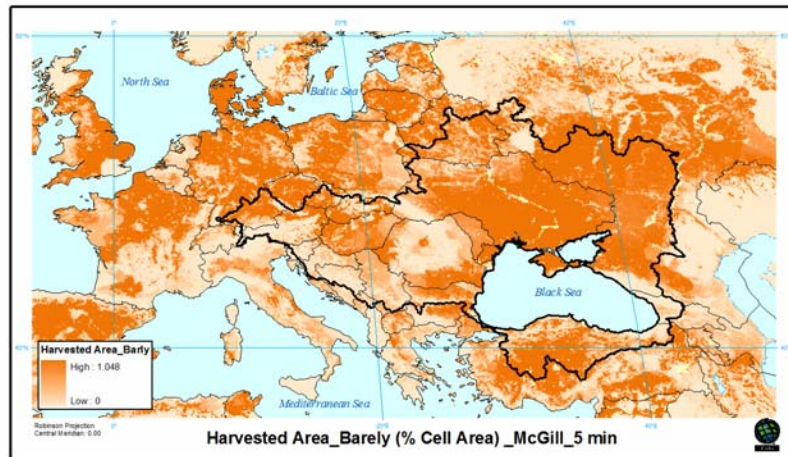


Fig. 15b. Harvested area of maize used to assign maize growing region in the model



**Fig. 15c.** Harvested area of barely used to assign barely growing region in the model

The nitrogen stress threshold, which is a fraction of potential plant growth, was set to 0.95 which ensures that there is almost no reduction of plant growth due to nutrient stress. Any time actual plant growth falls below this threshold fraction due to nitrogen stress, the model will automatically apply fertilizer to the HRU. The nitrogen stress factor is calculated by dividing the growth of the plant undergoing nitrogen stress by the growth of the plant if there was no nitrogen stress. The application efficiency was set to 1.3 to allow the model to apply fertilizer to meet harvest removal plus an extra amount to make up for nitrogen losses due to surface runoff/leaching. Fraction of fertilizer applied to top 10 mm of soil is 0.8. Irrigation was based on plant-water-stressed automatic scheduling, and withdrawn from outside sources so that the model will add water to the soil until its field capacity.

The automatic irrigation option is triggered by plant water demand. Water stress threshold which is a fraction of plant growth is assumed to be 0.95 to ensure that there is no reduction of plant growth due to water stress. Any time the actual plant growth falls below this threshold fraction due to water stress, the model will automatically apply water to the HRU. The major crops heat units to reach maturity are set to 1000, 1200, and 1400 for wheat, barley and maize respectively. Remaining crop parameters and parameters for non-crop land covers, originate from SWAT default database (Neitsche et al., 2005). Parameters sensitive to model outputs were subsequently calibrated to the local conditions.



		IRRIGATED crops								
country code		WHEAT			MAIZE			Barly		
country cc	country name	WWIRR	%	Start_en	SMIRR	%	Start_en	WbalRR	%	Start_end
1	Russia									
2	Albania	WW02	1	11_6	SM02	3	4_9			
3	Bosnia & Herzegovina									
4	Croatia									
5	Italy	WW05	1	11_5	SM05	18	4_9			
6	Macedonia									
7	Bulgaria									
8	Georgia	WW08	1	11_6						
9	Turkey	WW09	5	11_5	SM09	1	6_10	WB09	1	12_4
10	Austria									
11	Czech Republic									
12	Hungary									
13	Poland									
14	Slovakia				SM14	1	4_9			
15	Slovenia									
16	Germany									
17	Switzerland				SM17	1	5_10			
18	Belarus									
19	Moldova	WW19	1	11_6	SM19	3	5_10			
20	Romania	WW20	1	11_6	SM20	1	5_10			
21	Ukraine									
22	Montenegro									
23	Serbia									

		RAINFED Crops														
country code		WHEAT						BARLY								
country cod	country name	SWRF	%	SBart_e	WWRF	%	SBart_e	SMRF	%	SBart_e	SBRF	%	SBart_e	WBRF	%	SBart_end
1	Russia				WW24	15	9_8	SM24	3	5_10				WB24	7	9_8
2	Albania				WW25	5	11_7	SM25	1	4_9						
3	Bosnia & Herzegovina				WW26	4	11_6	SM26	10	4_9				WB26	1	11_5
4	Croatia				WW27	8	11_6	SM27	15	4_9				WB27	1	11_5
5	Italy	SW28	4	5_8	WW28	32	10_7	SM28	12	4_9	SB28	1	5_8	WB28	5	12_6
6	Macedonia				WW29	6	11_7	SM29	2	4_9				WB29	2	11_6
7	Bulgaria				WW30	15	10_7	SM30	6	5_10				WB30	4	11_5
8	Georgia	SW31	1	7_10	WW31	5	9_8	SM31	11	4_8				WB31	2	3_6
9	Turkey				WW32	37	10_7	SM32	2	6_10				WB32	15	11_6
10	Austria	SW33	1	5_8	WW33	12	11_6	SM33	12	4_9	SB33	6	5_8	WB33	4	11_5
11	Czech Republic	SW34	2	5_8	WW34	14	11_6	SM34	5	5_9	SB34	6	5_8	WB34	3	11_5
12	Hungary	SW35	1	5_8	WW35	15	10_7	SM35	19	5_10	SB35	3	5_8	WB35	2	11_5
13	Poland	SW36	6	5_8	WW36	19	10_8	SM36	3	5_10	SB36	10	5_8	WB36	2	10_7
14	Slovakia	SW37	1	5_8	WW37	17	10_8	SM37	11	4_9	SB37	9	5_8	WB37	1	11_5
15	Slovenia				WW38	6	10_8	SM38	12	4_9				WB38	1	11_5
16	Germany				WW39	13	10_8	SM39	7	5_10	SB39	3	5_9	WB39	7	10_7
17	Switzerland	SW40	2	5_8	WW40	35	11_6	SM40	24	5_10	SB40	11	5_8	WB40	7	11_5
18	Belarus	SW41	1	5_8	WW41	3	11_6	SM41	3	5_10	SB41	6	5_9	WB41	1	9_8
19	Moldova				WW42	12	9_8	SM42	15	5_10	SB42	1	5_8	WB42	2	11_5
20	Romania				WW43	14	10_8	SM43	21	5_10	SB43	1	5_8	WB43	2	11_5
21	Ukraine				WW44	13	9_8	SM44	7	5_10	SB44	3	5_9	WB44	6	11_5
22	Montenegro				WW45	8	10_8	SM45	15	4_9				WB45	1	11_5
23	Serbia				WW46	10	10_8	SM46	18	4_9	SB46	1	5_8	WB46	1	11_5

Fig. 16. Twenty five different management plans were designed based on the crop type, cropping dates, winter or summer crops, irrigated or rain-fed applications



## - Potential evapotranspiration

In this study, potential evapotranspiration (PET) was estimated using the Hargreaves method (Hargreaves et al., 1985) while actual evapotranspiration (ET) was estimated based on Ritchie (Ritchie, 1972). The daily value of leaf area index was used to partition between evaporation and transpiration. The simulation period was 1970–2006, considering 3 years as the warm-up period. Daily time step of model run and monthly output was chosen. SWAT 2009 was run on a laptop with a 64 bit operating system, 4 CPUs, 8 GB of RAM and 2.7 GHz processors. It took 42 hours to have a run of 37 years of simulation. Table 5 summarizes the data sources.

**Table 5.** Data description and sources used in the European SWAT project

Data type	Resolution	Source
Digital Elevation Model (DEM)	90 m aggregated to 700 m	SRTM [Jarvis. et al, 2008] <a href="http://www2.jpl.nasa.gov/srtm/">http://www2.jpl.nasa.gov/srtm/</a>
Soil	5 km	FAO-UNESCO global soil map (FAO, 1995) <a href="http://www.fao.org/nr/land/soils/digital-soil-map-of-the-world/en/">http://www.fao.org/nr/land/soils/digital-soil-map-of-the-world/en/</a>
Landuse	300 m	GlobCover European Space Agency (ESA_a) Global Corine: ( <a href="http://dup.esrin.esa.int/ionia/globcorine/products.asp">http://dup.esrin.esa.int/ionia/globcorine/products.asp</a> ), CORINE:( <a href="http://www.eea.europa.eu/data-and-maps/data/corine-land-cover-2000-raster">http://www.eea.europa.eu/data-and-maps/data/corine-land-cover-2000-raster</a> ).
River network dataset		European catchments and Rivers network System (Ecrins) , <a href="http://projects.eionet.europa.eu/ecrins">http://projects.eionet.europa.eu/ecrins</a>
Climate		- Measured data, NCDC (200?) - ECAD 0.25°-gridded data - CRU 0.5°-gridded [Mitchell and Jones, 2005] - NCDC , <a href="http://www.climate.gov/#dataServices/dataLibrary">http://www.climate.gov/#dataServices/dataLibrary</a> ECAD <a href="http://eca.knmi.nl/dailydata/predefinedseries.php">http://eca.knmi.nl/dailydata/predefinedseries.php</a>
River discharge		Global Runoff Data Center (GRDC) GRDC ( <a href="http://grdc.bafg.de">http://grdc.bafg.de</a> )
Crop yield	Wheat, maize	(McGill, <a href="http://www.geog.mcgill.ca/landuse/pub/Data/175crops2000/NetCDF/">http://www.geog.mcgill.ca/landuse/pub/Data/175crops2000/NetCDF/</a> ), MARS <a href="http://mars.jrc.ec.europa.eu/mars/Projects/GLOBCAST">http://mars.jrc.ec.europa.eu/mars/Projects/GLOBCAST</a>
Agricultural management	Plating, harvesting dates, irrigation, fertilization	FAO Statistics <a href="http://faostat.fao.org/site/339/default.aspx">http://faostat.fao.org/site/339/default.aspx</a>
Point source pollution		Eurostat for the period of 2000 to 2009



Population		2005 (source, Rosi) Eurostat: population connected to wastewater treatment ( <a href="http://epp.eurostat.ec.europa.eu/statistics_explained/index.php/Water_statistics">http://epp.eurostat.ec.europa.eu/statistics_explained/index.php/Water_statistics</a> ).
Population growth rate		World bank population rate ( <a href="http://data.worldbank.org/indicator/SP.POP.GROW">http://data.worldbank.org/indicator/SP.POP.GROW</a> ) World Bank [1].

## 5. Model setup

The Arc-SWAT interface (Olivera et al., 2006) with ArcGIS (version 9.3) was used in project set up and analysis. Black Sea Catchment Digital Elevation Database at 90 m spatial resolution extracted from SRTM (Jarvis et al., 2008) along with river network dataset from European catchments and rivers network system (Ecrins) was employed to derive slope and drainage network and to divide the 2.3 million km<sup>2</sup> catchment of Black Sea into smaller sub-basins. A river network dataset was superimposed onto the DEM to define the location of the river network. This feature is most useful where DEM does not provide enough detail to allow the interface to accurately predict the location of the stream network. However, if the river network is in conflict with DEM, it may affect the resulting flow direction adversely. In addition, lines crossing the edge of DEM can affect the flow direction. It seems that mapping the flow at a very early stage is inevitable in large-scale modeling to make sure the rivers are flowing to the right place. The Ecrins river map was corrected in many areas where there was a mismatch with DEM. River flow directions were also modified manually in the Black Sea Catchment SWAT project where needed. In addition, flow directions in lowland areas close to the Black sea coast line were also manually guided to the sea (Figs. 17a,b,c).

The sub-basins were delineated with a 100 km<sup>2</sup> threshold yielding 12982 sub-basins. This was the smallest threshold possible to be able to handle the project on a 64 bit machine with 2.7 GHz processors, 4 cores and Windows7 as an operating system.

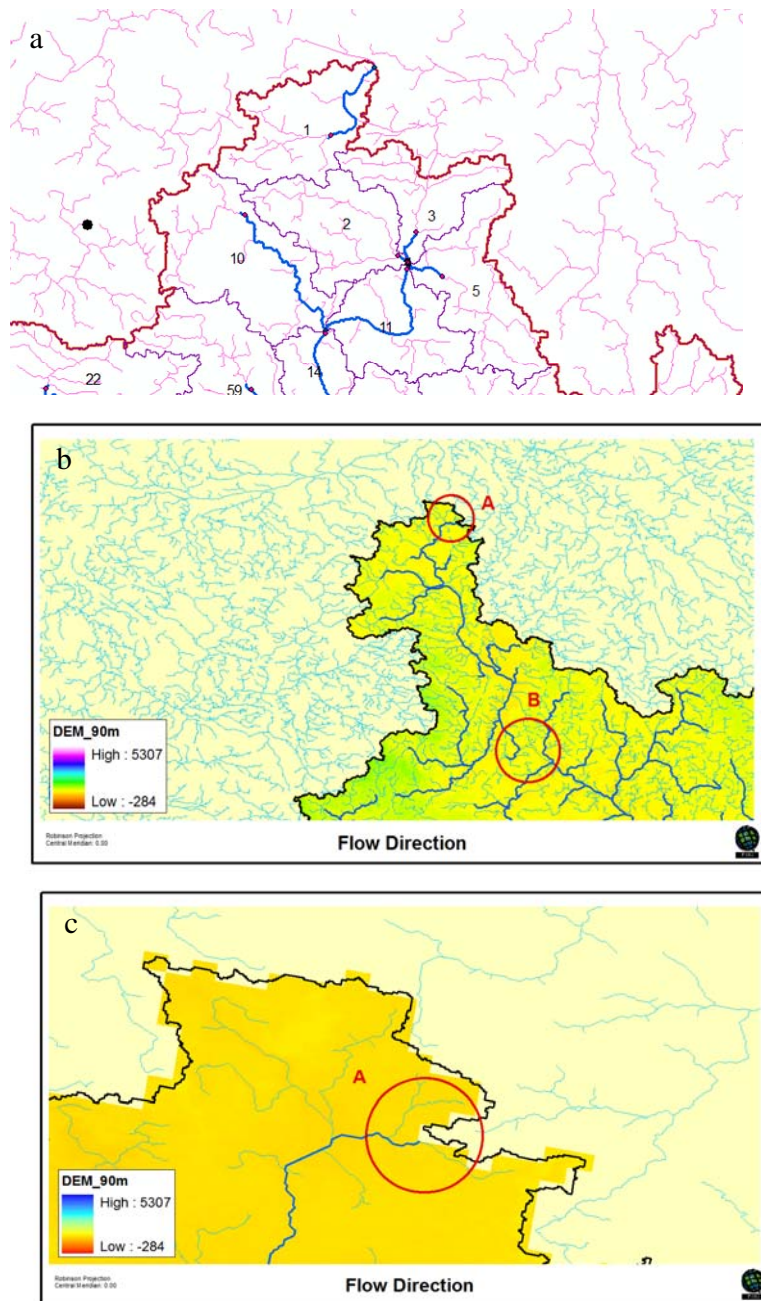


**Fig. 17.** Example of rivers crossing the DEM (a), being disconnected (b), and not connecting to the DEM



## 6. Model calibration, parameterization, and uncertainty analysis

The parallel processing routine linked to SUFI-2 (Rouhalnejad et al., 2012) in the SWAT-CUP software (Abbaspour, 2011) was used for preliminary calibration of the BSB model. Final runs were made in the Grid system developed by the Romanian partners (Gorgan et al., 2012). The program SUFI-2 program and the SWAT-CUP software package were upgraded to allow parallel processing, which was then developed by a private company. Appendix I contains the publication on this subject and more detail about calibration and parallel processing. A summary is provided below.

The SUFI-2 algorithm maps all uncertainties (parameter, conceptual model, input, etc.) on the parameter ranges and tries to capture most of the measured data within the 95% prediction uncertainty (95PPU) of the model. The 95PPU is calculated at the 2.5% and 97.5% levels of the cumulative distribution of an output variable obtained through Latin hypercube sampling. The goodness of fit and the degree to which the calibrated model accounts for the uncertainties are assessed by two indices: “P-factor” and “R-factor”. The P-factor is the fraction of measured data bracketed by the 95PPU band and varies from 0 to 1, where 1 indicates 100% bracketing of the measured data within model prediction uncertainty. The R-factor on the other hand is the average width of the 95PPU band divided by the standard deviation of the measured variable. A value less or around than 1 is desirable for this parameter (Abbaspour et al., 2004, 2007). These two indices are used to judge the strength of the calibration. A larger P-factor can be achieved at the expense of a larger R-factor. Hence, often a balance must be reached between the two. When acceptable values of R-factor and P-factor are reached, then the parameter uncertainties are the calibrated parameter ranges. SUFI-2 allows usage of different objective functions such as  $R^2$  or Nash-Sutcliff Efficiency (NS), and  $bR^2$ . In this study we used  $bR^2$  for discharge and nitrate load. The objective function is defined as:

$$\phi = \begin{cases} |b|R^2 & \text{for } |b| \leq 1 \\ |b|^{-1}R^2 & \text{for } |b| > 1 \end{cases}, \quad (2)$$

where  $R^2$  is the coefficient of determination and  $b$  is the slope of the regression line between the measured and predicted variables. The objective function containing two variables (e.g., river discharge and nitrate load) at multiple sites was formulated as:



$$\Theta = \frac{1}{w_{v1} + w_{v2}} \left[ \frac{w_{v1}}{\sum_{i=1}^{n_1} w_i} \sum_{i=1}^{n_1} w_i \phi_i + \frac{w_{v2}}{\sum_{i=1}^{n_2} w_i} \sum_{i=1}^{n_2} w_i \phi_i \right], \quad (3)$$

where  $w_{v1}$  and  $w_{v2}$  are weights of the two variables,  $n_1$  and  $n_2$  are the number of discharge and nitrate stations, respectively, and  $w_i$ 's are the weights of variables at each station. The function  $\phi$ , and consequently  $\Theta$  varies between 0 and 1. In this form, the objective function, unlike for example NS, which may range from  $-\infty$  to 1, is not dominated by any one or a few badly simulated stations (Abbaspour et al., 2011). For crop yield, which was calibrated after calibrating the model for discharge and nitrate, we used MSE (mean square errors) as the objective function (Abbaspour et al., 2011):

$$\phi_3 = \frac{1}{n_3} \sum_{i=1}^{n_3} (Y_i^o - Y_i^s)^2, \quad (4)$$

where  $n_3$  is the number of sites with wheat, barley, and corn yield data,  $Y^o$  ( $\text{t ha}^{-1}$ ) is the observed yield, and  $Y^s$  ( $\text{t ha}^{-1}$ ) is the simulated yield.

To calibrate the model we used the following general approach:

- 1) Create the model with our best estimates of model parameters based on the available data. There are always more than one data set (e.g., soil, landuse, climate, etc.) available for a region. For Europe we were in possession of four different landuse maps, two different soil maps, and four different sets of climate data as explained in the section on database above. Hence, initially several models were built and ran without any calibration (here one referred to as the default model) with different databases. The model results were compared with observations (discharge and nitrate) and the best overall performing database was selected for further analysis.
- 2) The default model was run with the best (landuse, soil, and climate) datasets and the observation versus simulation results plotted with the help of SWAT-CUP. Based on the model performance at each outlet station, parameters of the upstream subbasins were parameterized using the guidelines summarized in Table 6. This procedure results in regionalization of parameters.
- 3) Based on step 2, ranges are then assigned to parameters of significance to hydrology and nitrate subjectively. Experience of the analyst is a great asset in defining these ranges keeping in mind that in nested outlets, for example, increasing overland flow (by increasing CN2) will have an impact on downstream discharge whose CN2 must increase less in order to meet a peak deficit in the downstream outlet.



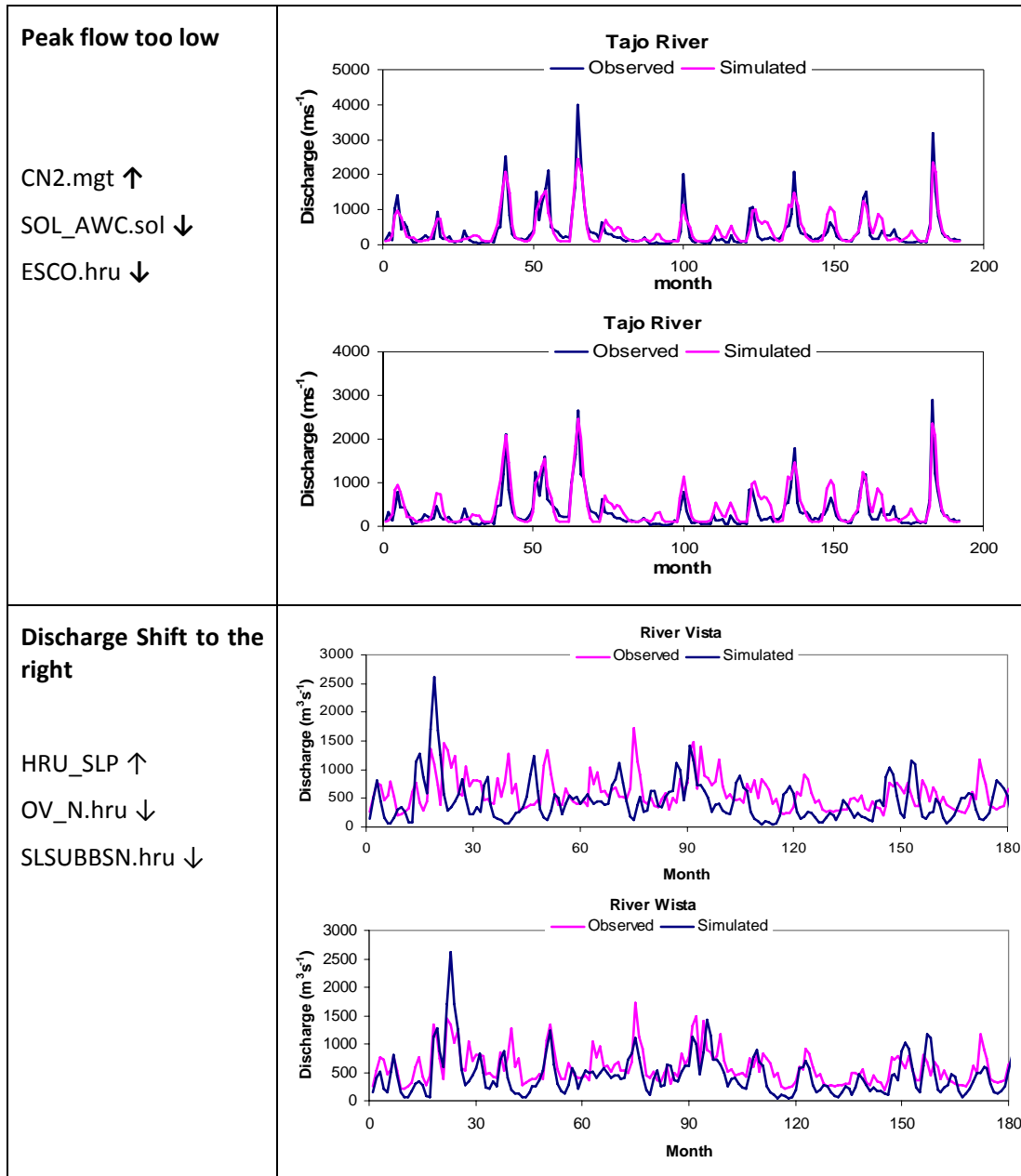
4) Once the model is parameterized and the ranges are assigned, the model is run some 200-1000 times, depending on the number of parameters, speed of the simulation, and the system capabilities. Great time saving could be achieved in parallel processing option of SWAT-CUP is invoked.

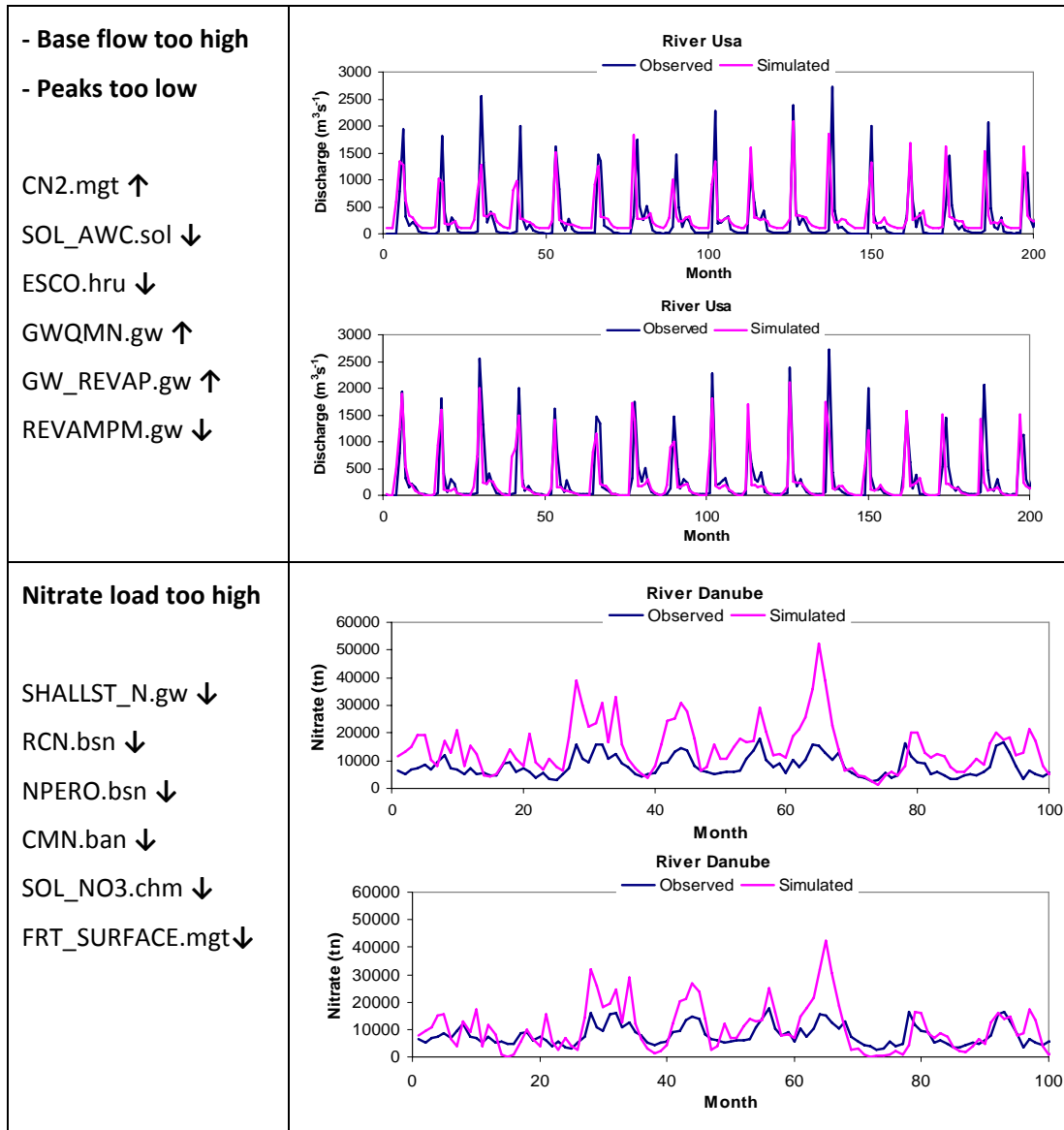
5) After all simulations are complete, the post processing option in SWAT-CUP calculates the objective function and the 95PPU for each observed variables in the objective function. New parameter ranges are then suggested for another set of iteration, which modifies the previous ranges focusing more on the best parameter set of the previous simulation.

6) The new parameters ranges could be modified by the user using Table 2. Another iteration is then performed. The procedure continues until satisfactory results are reached or no further improvements are seen in the objective function. Normally, two to four iterations are sufficient for a satisfactory result. More detailed information could be found in Abbaspour et al., (2004, 2007) and Rouholahnejad et al., (2012).

**Table 6.** Rules for parameterization

Simulated condition	Before (top) and after (below) parameter adjustment
<p><b>- Base flow too low</b></p> <p><b>-Evapotranspiration too high</b></p> <p>GWQMN.gw ↓</p> <p>GW_REVAP.gw ↓</p> <p>REVAMPM.gw ↑</p>	





## 7. Model Results

To avoid repetition, we present some model results here, mostly pictorially, and refer to the article by Rouholahjejad et al. (2013) for more discussion. This article is in preparation and will be submitted to the Journal of Hydrology.

A large amount of time was spent on input data formatting and corrections in the DEM, river map, landuses, and climate data. In the following we present some output maps, figures and tables.

### Calibration/validation results

The overall calibration results are shown in Fig. 18 below. The results are expressed in terms of the objective function value  $br^2$  as discussed above. Most of the discharge data came from the Danube River Basin. The general fit of the discharge stations with some minor exceptions are quite good.

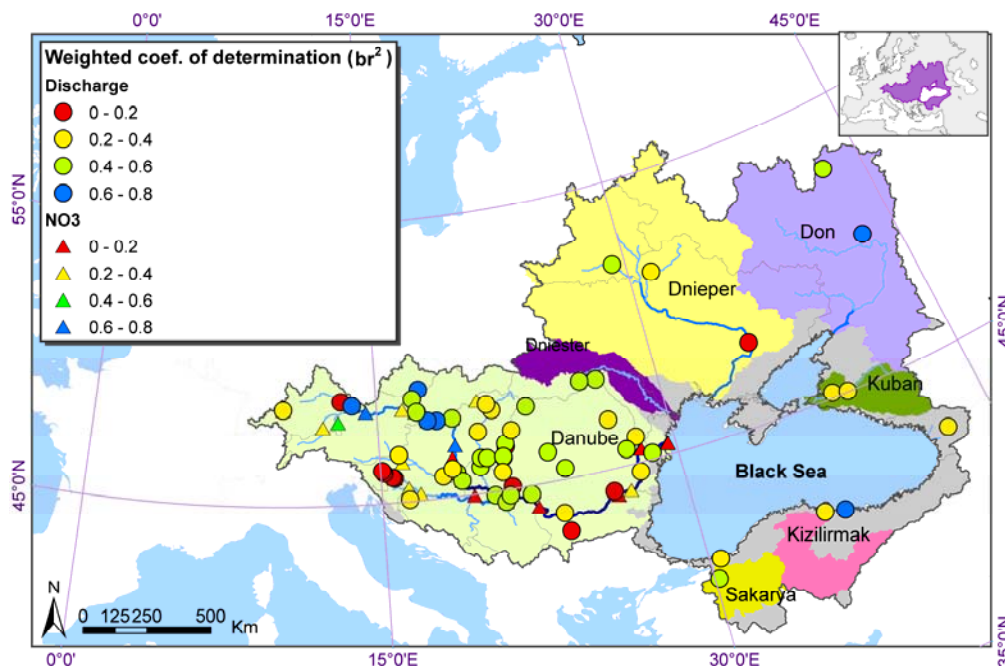
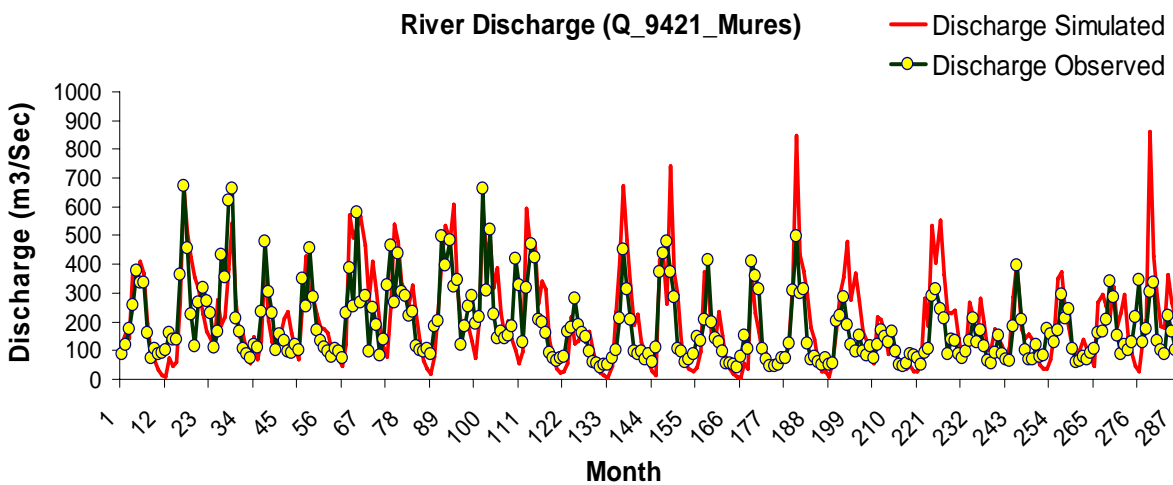
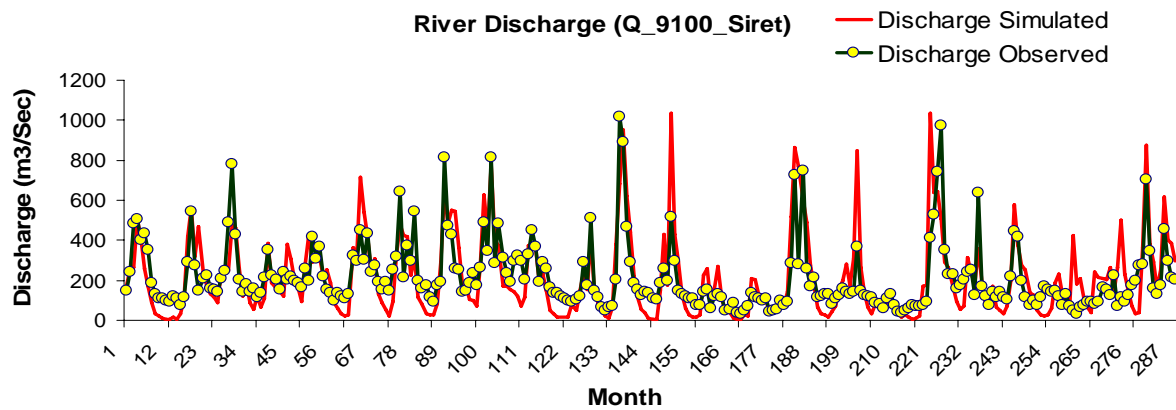
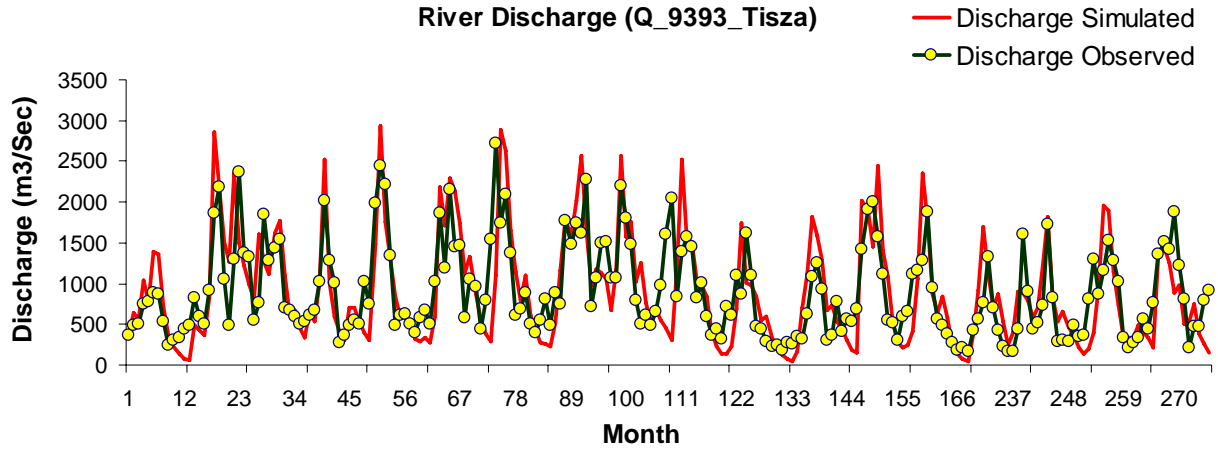


Fig. 18. Calibration results at discharge and nitrate stations

Examples of time series discharges on some famous rivers are shown in Figs. 19a-d.



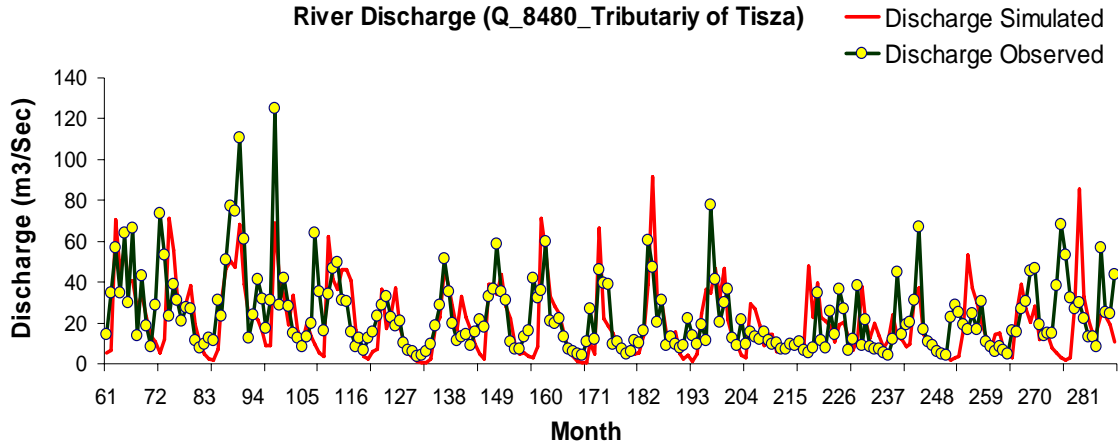
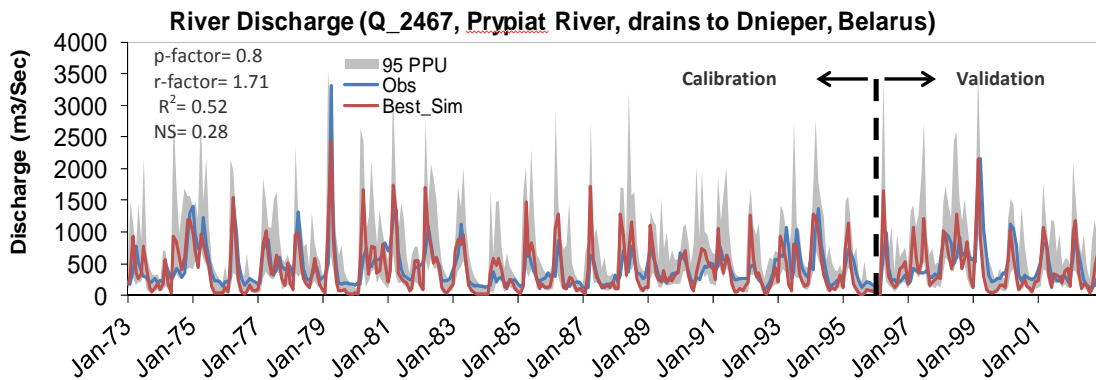


Fig. 19. Calibration results at different discharge stations

For the validation period, the model produced the same sort of results as the calibration as illustrated in the following examples (Fig. 20 a,b). Uncertainty analysis is shown in the shaded region where the discharge uncertainties are relatively small indicating high model prediction reliability.



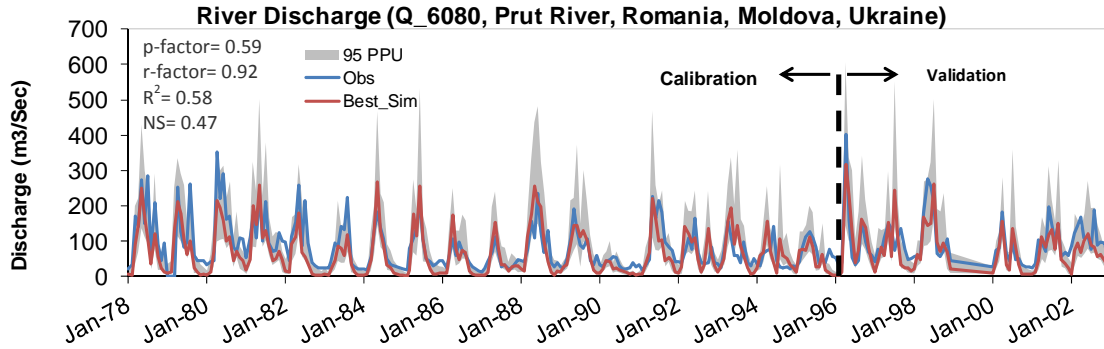
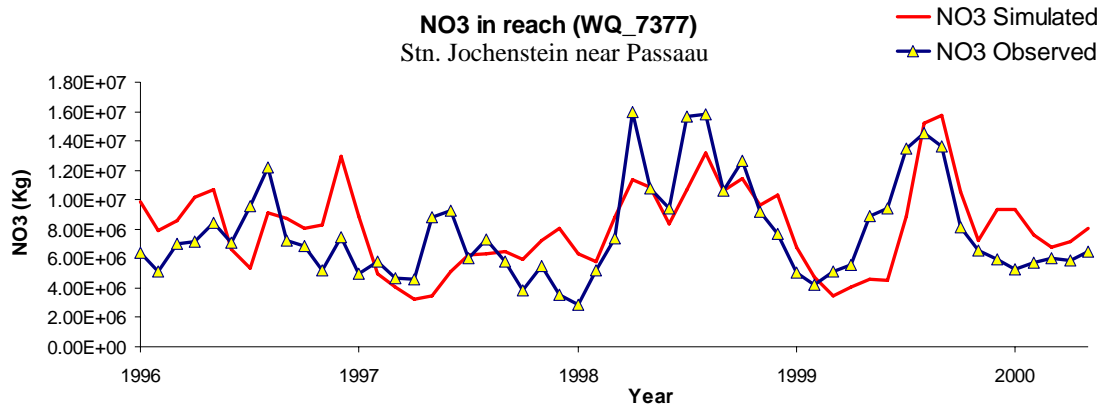


Fig. 20. Calibration and validation results for two selected station. The shaded region if the 95% prediction uncertainty

Water quality was analyzed in terms of nitrate concentration in the river. It is clear that point and diffuse sources play an important role in determining nitrate concentration, but also wetlands and deltas have a big impact. The goodness of fit in the stations not affected by wetlands or deltas indicates a good estimation of point and diffused sources of nitrogen. In fact, given the complexity of the region studies we are surprised that the program could to such as excellent extent simulate both the average quantity as well as the dynamics of the nitrate concentration (Figs. 21 a-c)



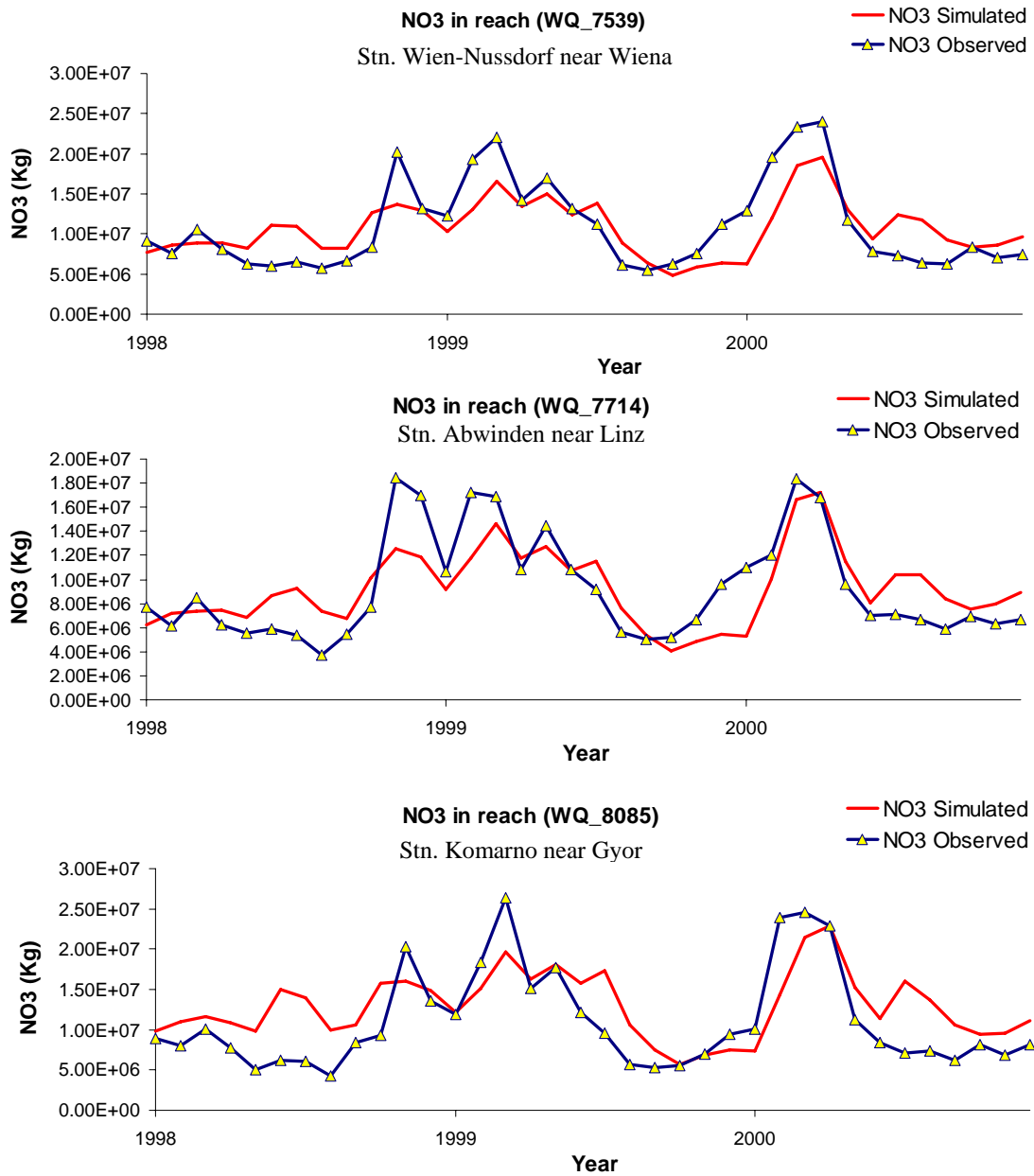
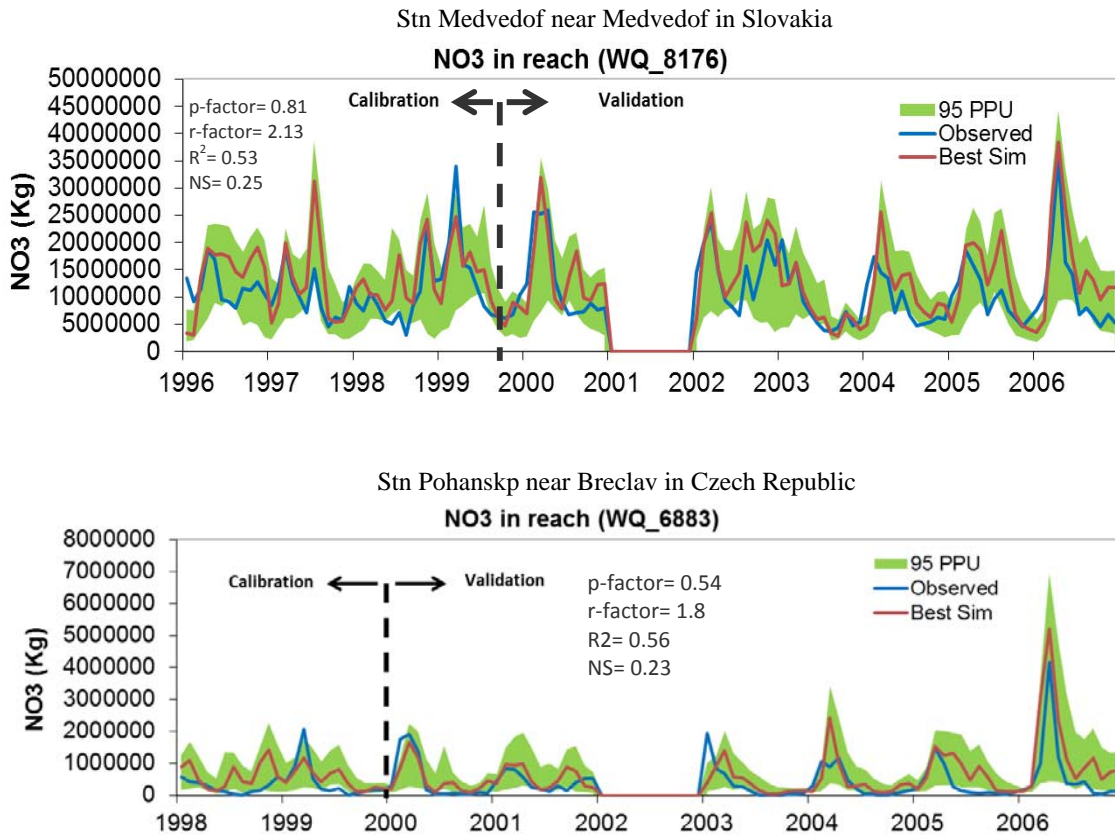


Fig. 21. Calibration results for different nitrate stations

Validation and uncertainty of the nitrate is shown in Figs. 21 a,b. The uncertainty of the nitrate as oppose to discharge is larger due to uncertainty in diffuse and point sources.



**Fig. 21.** Calibration and validation results for two selected stations. The shaded region is the model's 95% prediction uncertainty

General flow path of large rivers in terms of volume of water and nitrate are indicated in Figs. 22 a,b. Using such figures we were able to analyze and remove any anomalies in the river system such as disconnected rivers that caused flow in the wrong direction.

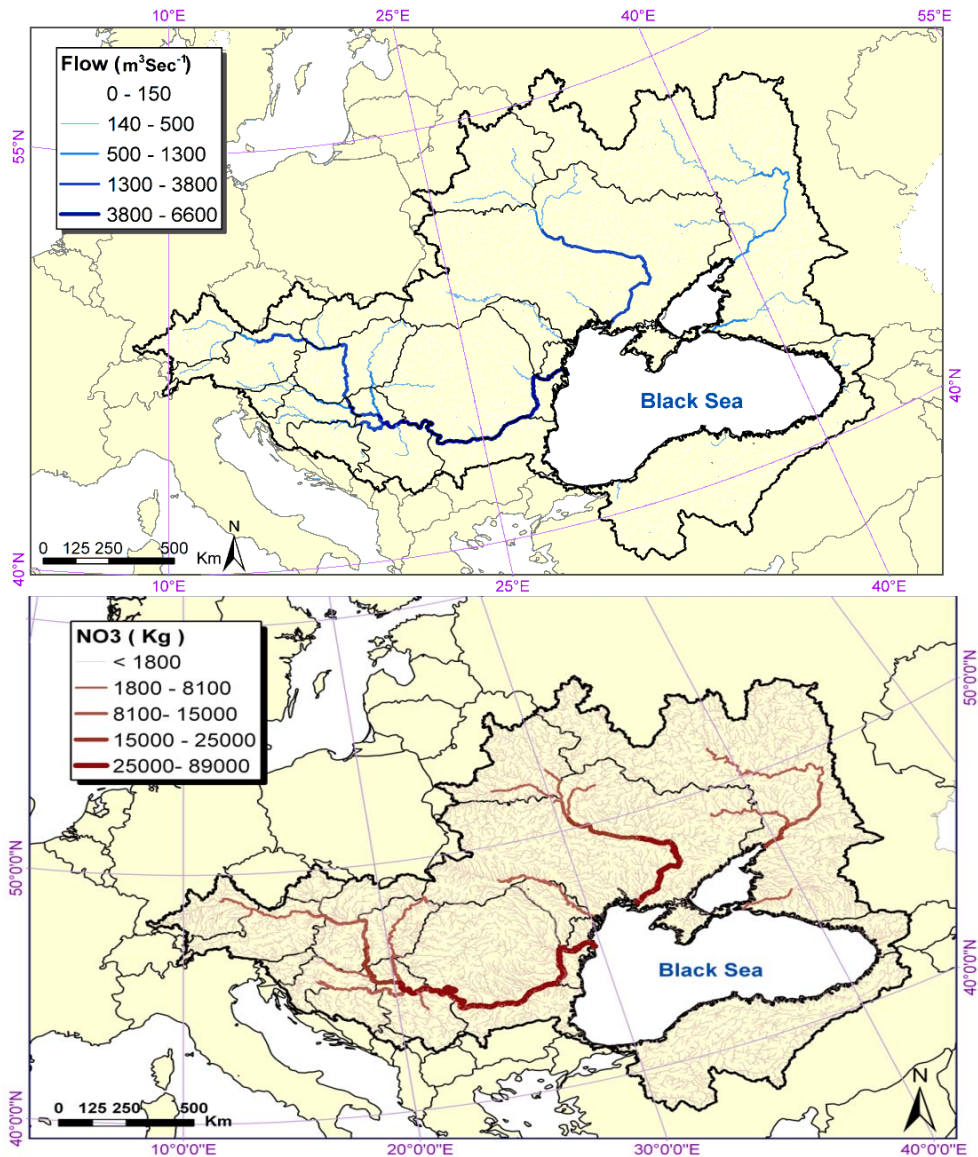
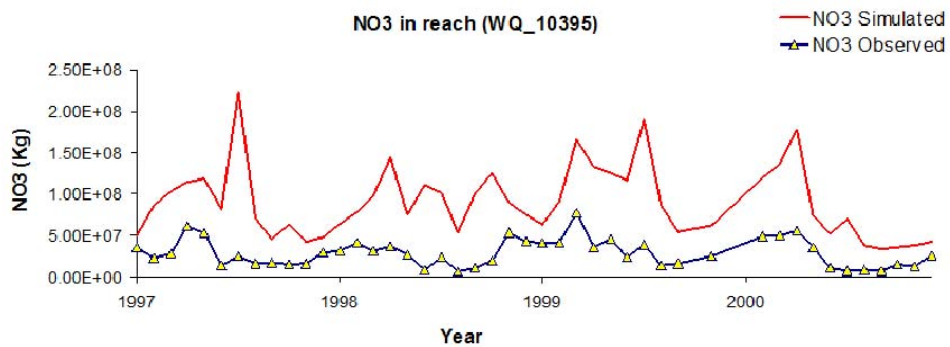
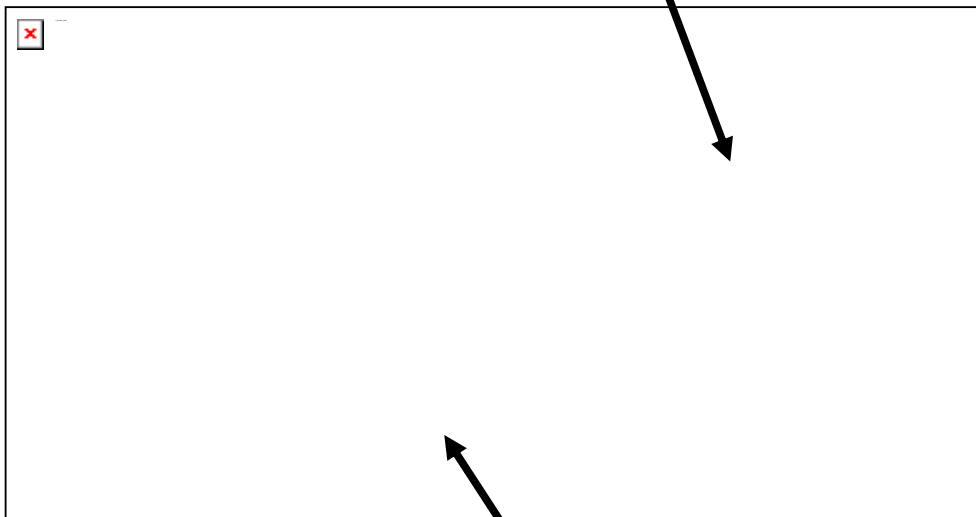
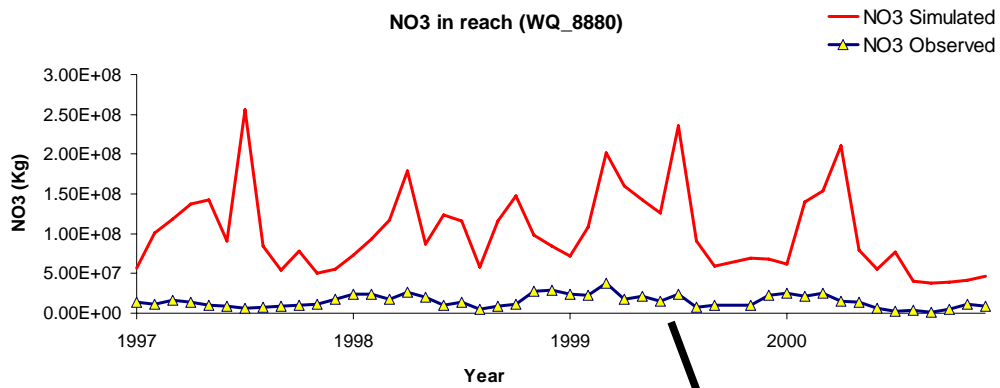


Fig. 22. General direction and magnitude of flow and nitrate loads in large rivers

Fig. 23 illustrates the point we made above about nitrate in the wetland and deltas. It is clearly seen that the model overestimates the observation as the concentration of the  $NO_3$  in the Danube dilutes greatly as it enters the delta.



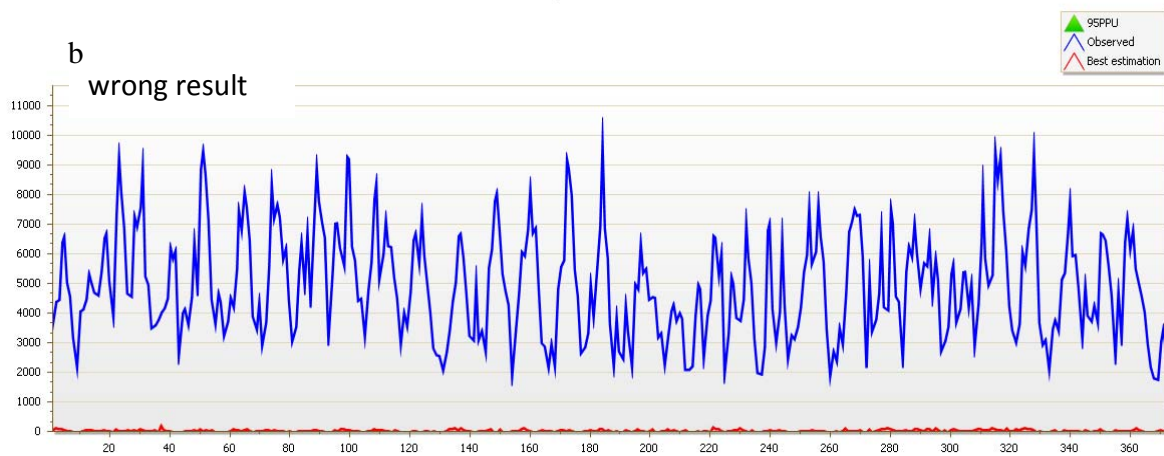
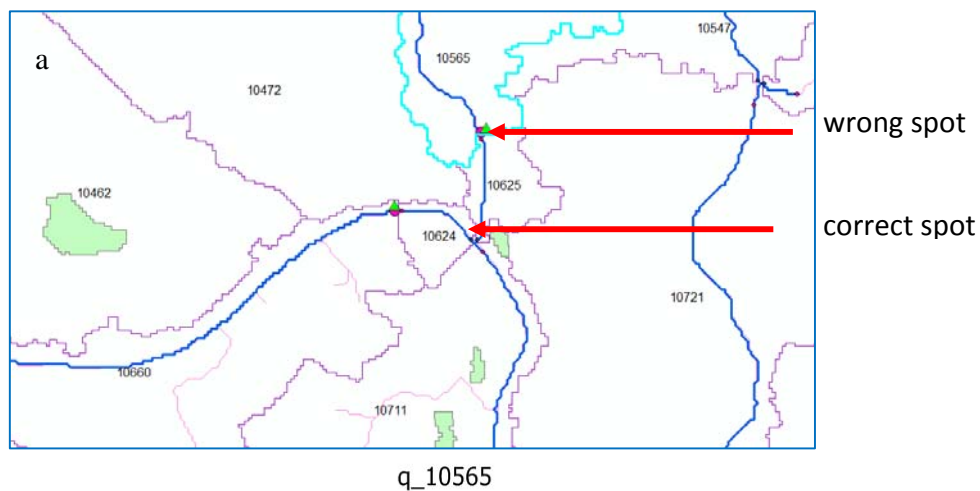
**Fig 23.** Nitrate loads at two locations in the Danube Delta. As the rivers flow into the Delta, the concentration of nitrate decreases, hence observations are much lower than what mode predicts

### Problems with large-scale modeling

In the following section we discuss other reasons why a model may produce bad results. In large-scale watershed modeling a careful analysis of these situations can greatly help the calibration process.

#### 1- Placement of the outlets

SWAT uses the coordinates of the outlet stations and connects the outlets to the nearest river. If the coordinates are wrong or not accurate enough, then the outlet will be attached to the wrong river. This situation causes the biggest headache for model calibration and it takes much tedious work to put the outlet on its proper spot. This is illustrated in Figs. 24 a-c.



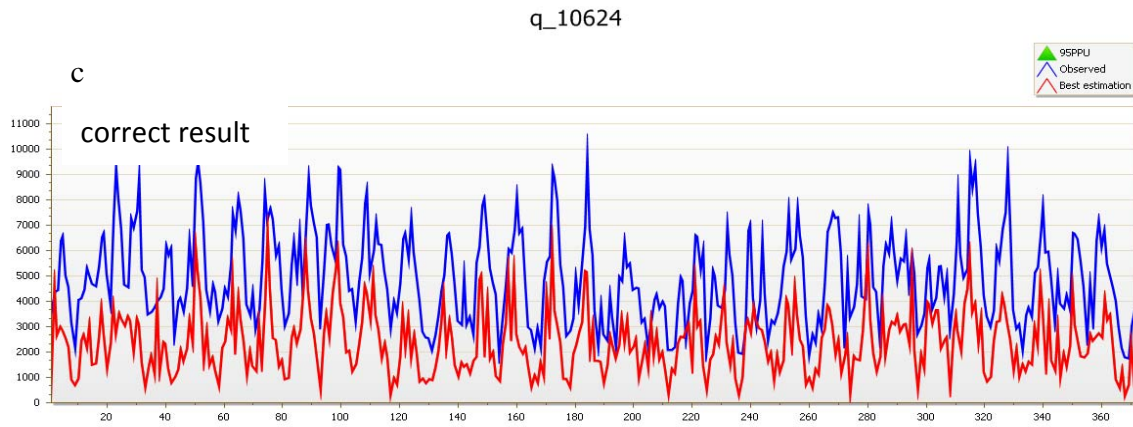


**Fig. 24.** The wrong coordinates of the discharge station caused SWAT to place it on the wrong river (a). The results indicated that the location was incorrect (b). Upon correction, much better results were obtained

## 2- Outlet is downstream of a dam

In another case an outlet may be downstream of a dam or reservoir. In such a case the flow is fully controlled by the dam or reservoir operation and cannot be modeled by SWAT unless the dam or reservoir management is known. The visualization tool in the SWAT-CUP software is an essential tool for such investigations as seen the Figs 25 a,b, 26 a,b, and 27 a,b.



**Fig. 25.** The Bing map in SWAT-CUP was used to visualize the location of the outlets. This graph shows the outlet was downstream of a dam, hence, its hydrology governed by dam operation.

This types of outlets cannot be modeled in SWAT unless dam's daily operation is known

q\_8136

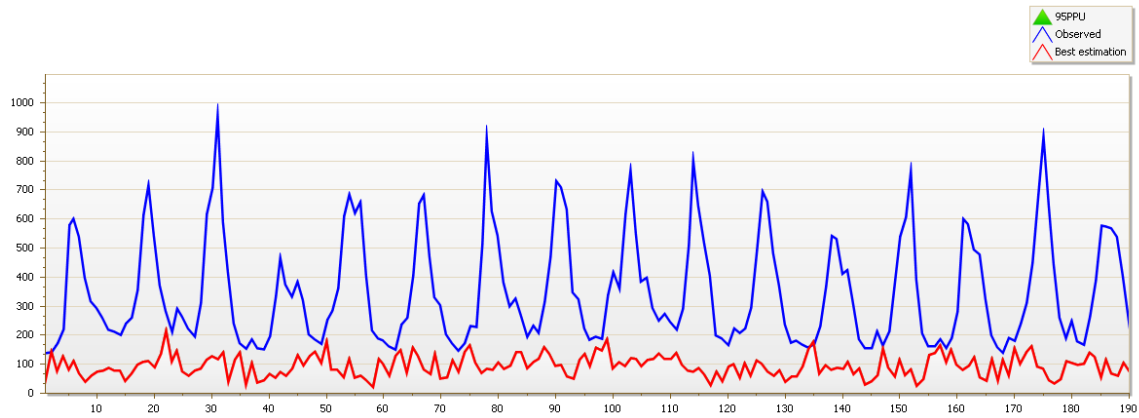


**Fig. 26.** The Bing map in SWAT-CUP was used to visualize the location of the outlets. This graph shows the outlet was downstream of a dam, hence, its hydrology governed by dam operation. This types of outlets cannot be modeled in SWAT unless dam's daily operation in known

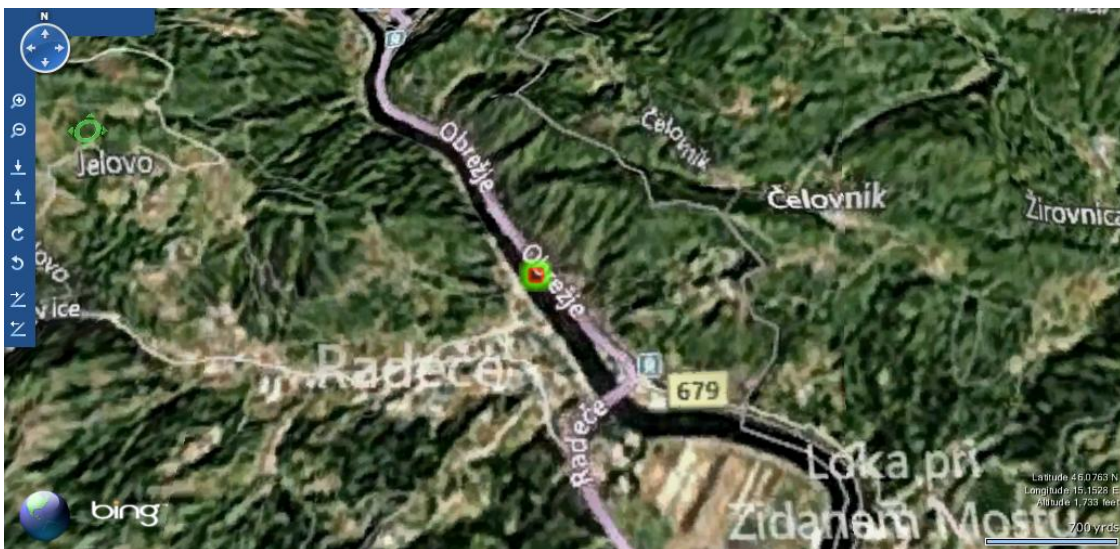
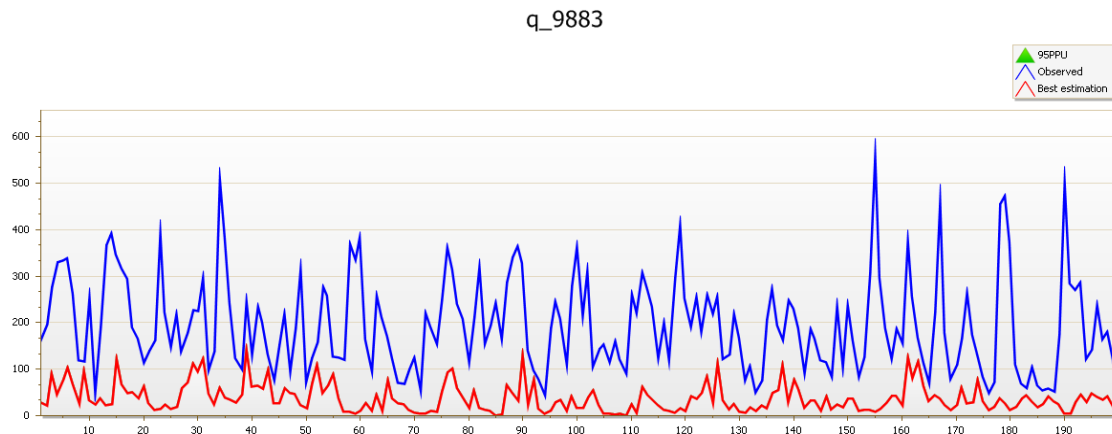


**Fig. 27.** The Bing map in SWAT-CUP was used to visualize the location of the outlets. This graph shows the outlet was downstream of a dam, hence, its hydrology governed by dam operation.

This types of outlets cannot be modeled in SWAT unless dam's daily operation in known

### 3- Water management

There are regions of high water management such as intensive agricultural and/or industrial areas. Near these areas where water allocation and water use is not known SWAT will have a hard time capturing the dynamics of water flow as shown in Fig. 28a,b..

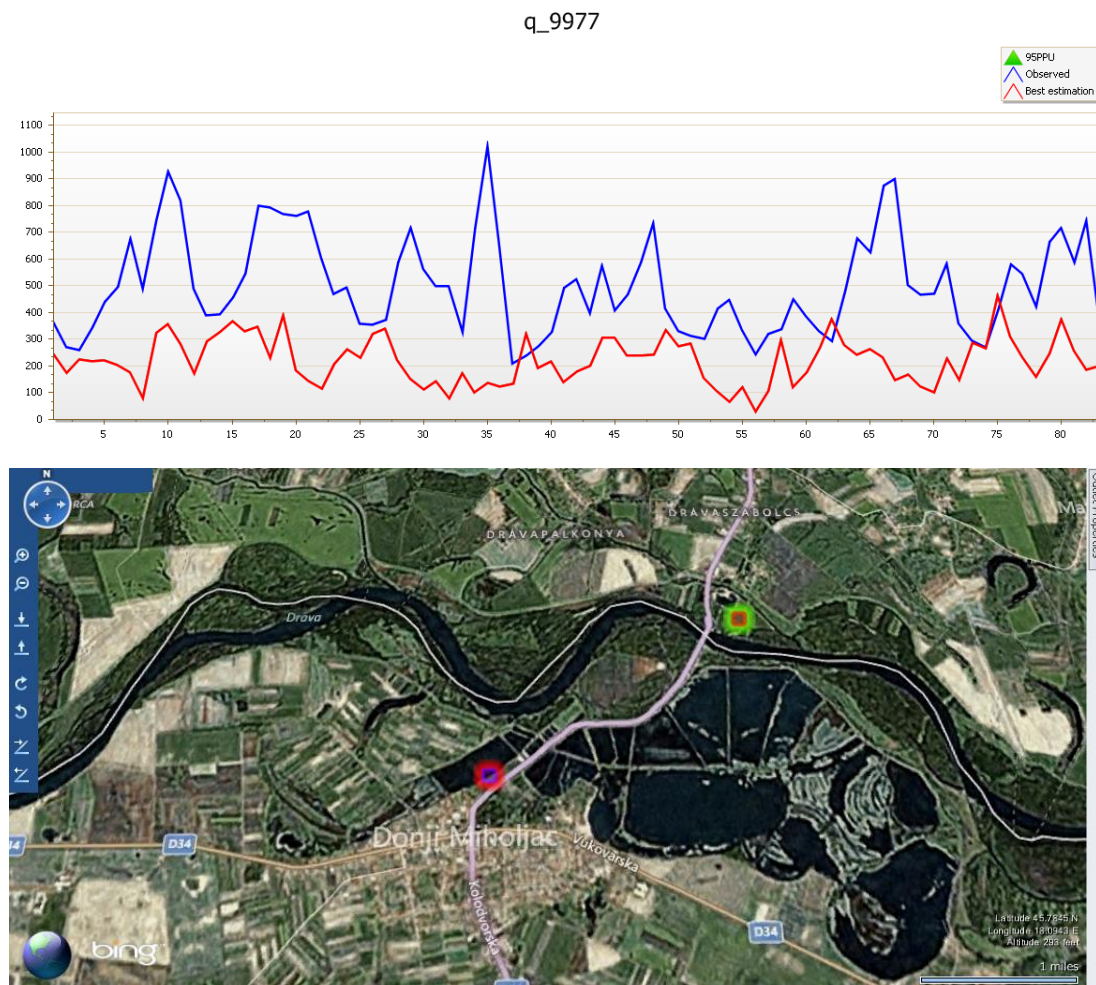


**Fig. 28.** When outlets are located in highly managed areas, then it is quite difficult for a hydrological model to capture the dynamics of the flow due to water transfer, water abstraction, etc.



## **8. Some pertinent model results**

SWAT produces a large amount of outputs. For management purposes and policy decisions, these outputs must be tailored to the needs of the decision makers compatible with the decision being made. What is missing in many projects, especially the EU projects, is the interaction of the modelers and the analysts with the policy makers as a project ends. The role of the analyst is to provide the decision makers with needed information. We refer to these as the “high-value” information as illustrated in Fig. 29. These Figure called the “cycle of decision making” highlights different components of decision making and the role of data, analyst, and the decision maker.

The cycle begins with raw data, which are processed into a model-usable format. The data are then fed to the model(s), and the model simulates the so-called “high-value” information (e.g., using rainfall to calculate river discharge). The high-value information could be of different types such as physical, social, environmental, economical, etc. The integration of this information is often conducted by a decision support system, or by local experts who are familiar with the local socio-economic situation. This integration leads to actual “knowledge” about the site which is then converted into policy formulation and implementation. At the end, a data gap analysis shows the shortcoming of the existing databases. The illustration also emphasizes the role of data in the whole cycle. Poor data quality leads to poor high-value information and eventually leads to poor decisions, and good quality data may lead to good high-value information and eventually good policies.

Based on the illustration in Figure xxx, we see that the role of modeling group is to provide high-value information to the local experts and stakeholders, who will then use their local understanding to integrate the information into the knowledge of the system to formulate policies. Hence, we emphasize that initially a meeting between the modeling group and the local experts is necessary to understand the needs of the local stakeholders and the end users. This could be more strongly emphasized in the future EU projects that include policy analyses.

What we provide as the output of our modeling work are the high-value information that could be used by the local experts, stakeholders, and policy makers. The outputs could be presented in many different formats and spatial and temporal scales. It would be up to the policy makers to express their wishes as to the form and type of information they require. Our general feeling is that EU projects lack this follow up session, which decreases the impact of the projects, or does not realize fully the project impact.

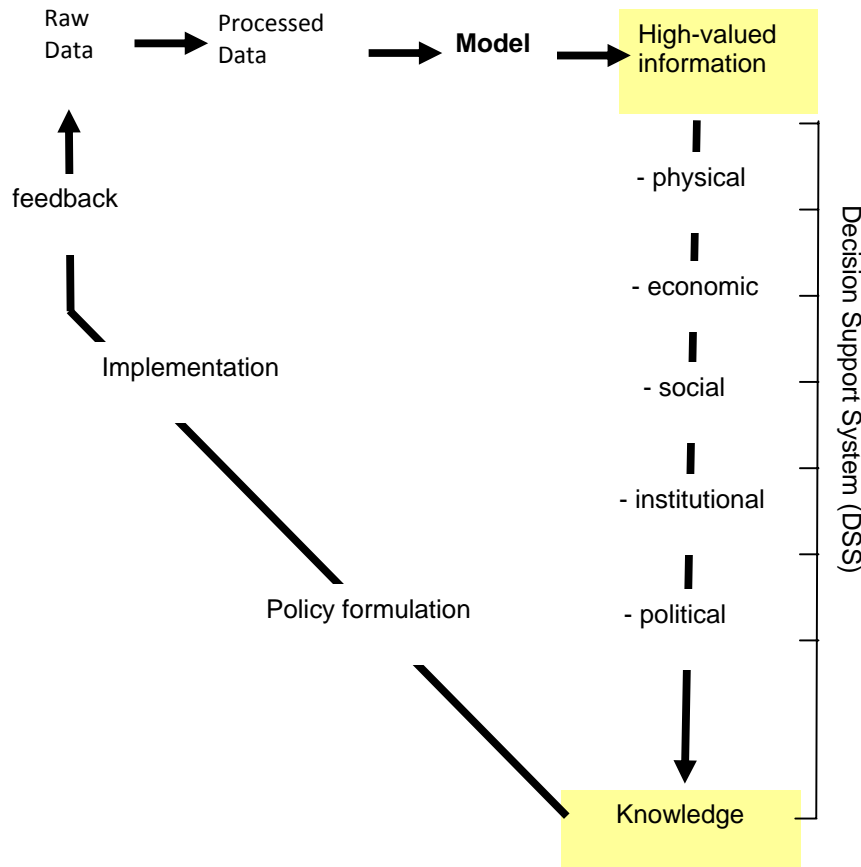


**Fig. 29.** Schematic of the cycle of decision making. The role of models are identifies as providing “high-value” information using basic data. The integration of the high-value information provides knowledge of the system, which is used in decision making and policy formulation

**Fig. 30.** Long-term average (1973-2006) subbasin-based distribution of precipitation across the BSB. The Figure shows country boundaries as well. It is evident that the rainfall distribution is quite uneven in the BSB. This Figure is a processed subbasin-based rainfall distribution. SWAT assigns station data to the nearest subbasins. Hence, station data is transformed into average subbasin data. Five elevation bands were considered in each subbasin and the rainfall was corrected based on elevation. A rainfall lapse rate of 1 mm/km was considered.

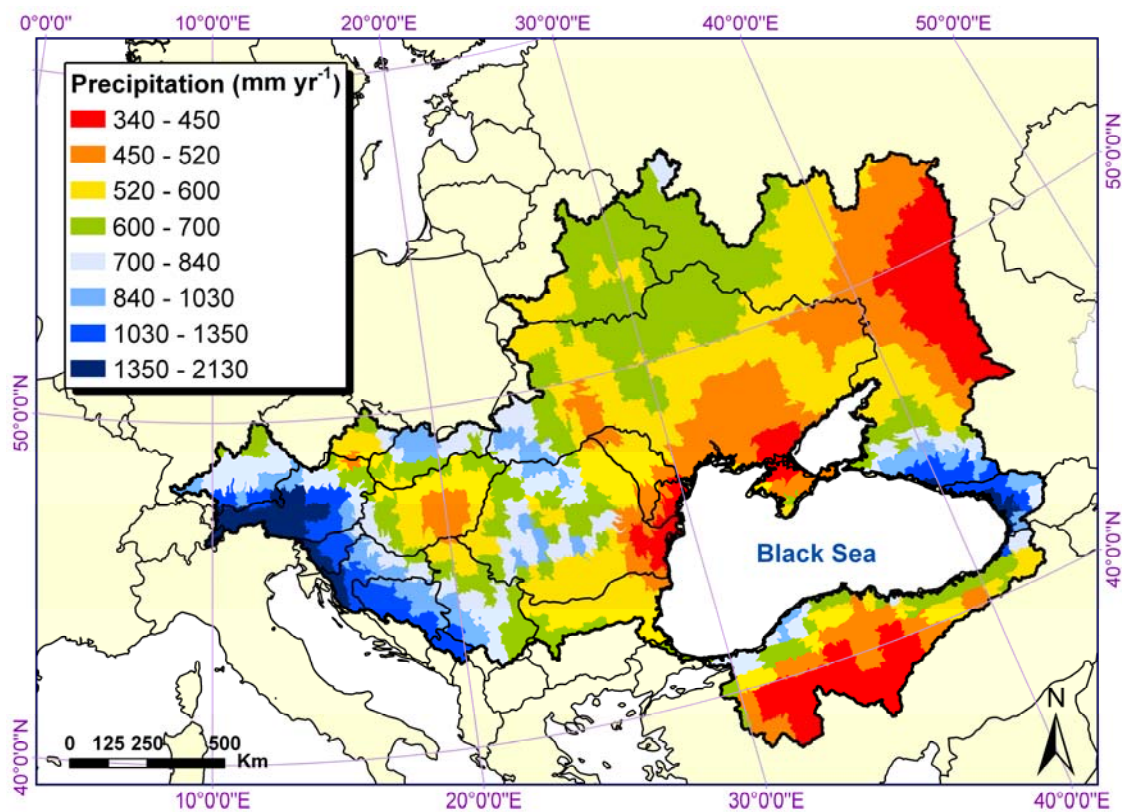


**Fig. 31.** Long-term average (1973-2006) subbasin-based distribution of average temperature across the BSB. The Figure shows country boundaries as well. It is evident that the temperature distribution is also quite uneven in the BSB. This Figure is a processed subbasin-based average temperature distribution. SWAT assigns station data to the nearest subbasins. Hence, station data is transformed into average subbasin data. Five elevation bands were considered in each subbasin and the temperature was corrected based on elevation. A temperature lapse rate of  $-6^{\circ}\text{C}/\text{km}$  was considered.

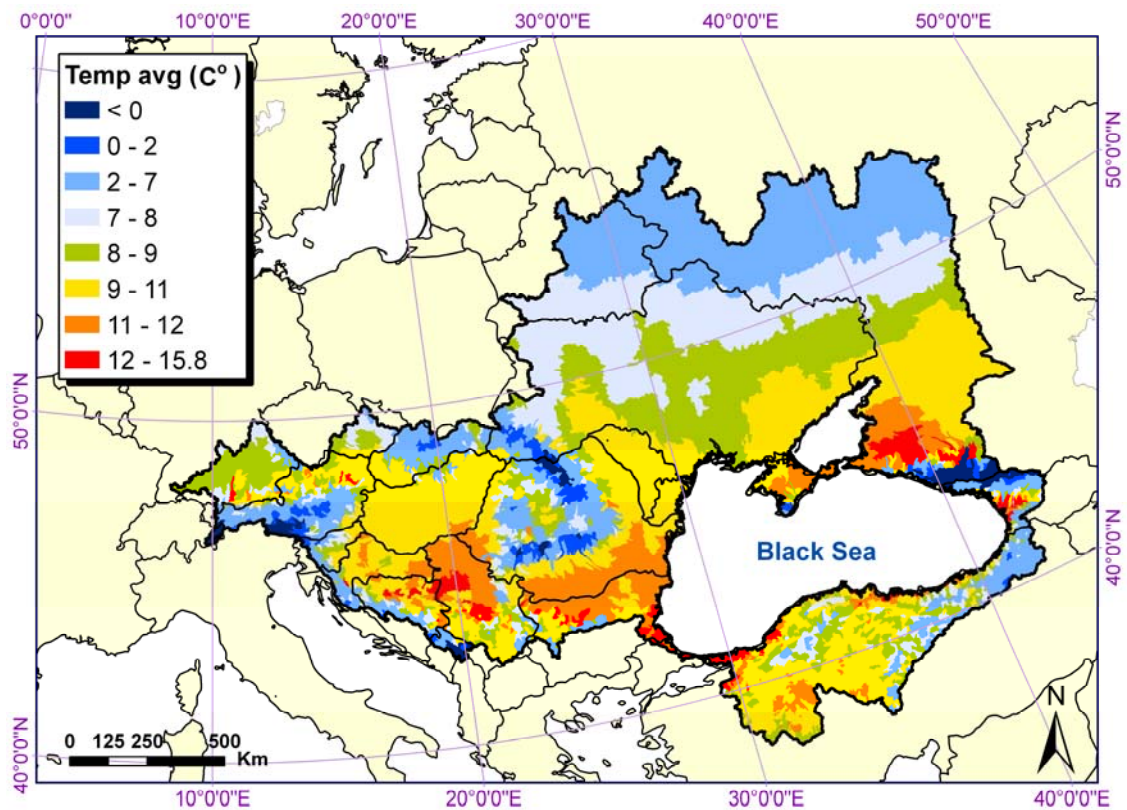


**Fig. 32.** Long-term average (1973-2006) subbasin-based distribution of lower and upper 95% prediction uncertainty (95PPU) of the blue water resources across the BSB. 95PPU highlights model prediction uncertainty. In other words, all values within the range of 95PPU are acceptable results. Comparison of the two graphs highlights the model prediction uncertainty and the importance of expressing these uncertainties. Based on the available data, the model uncertainty includes the uncertainty in the data, in the model, and in the year to year variability of the climate and the changes in the landuse.

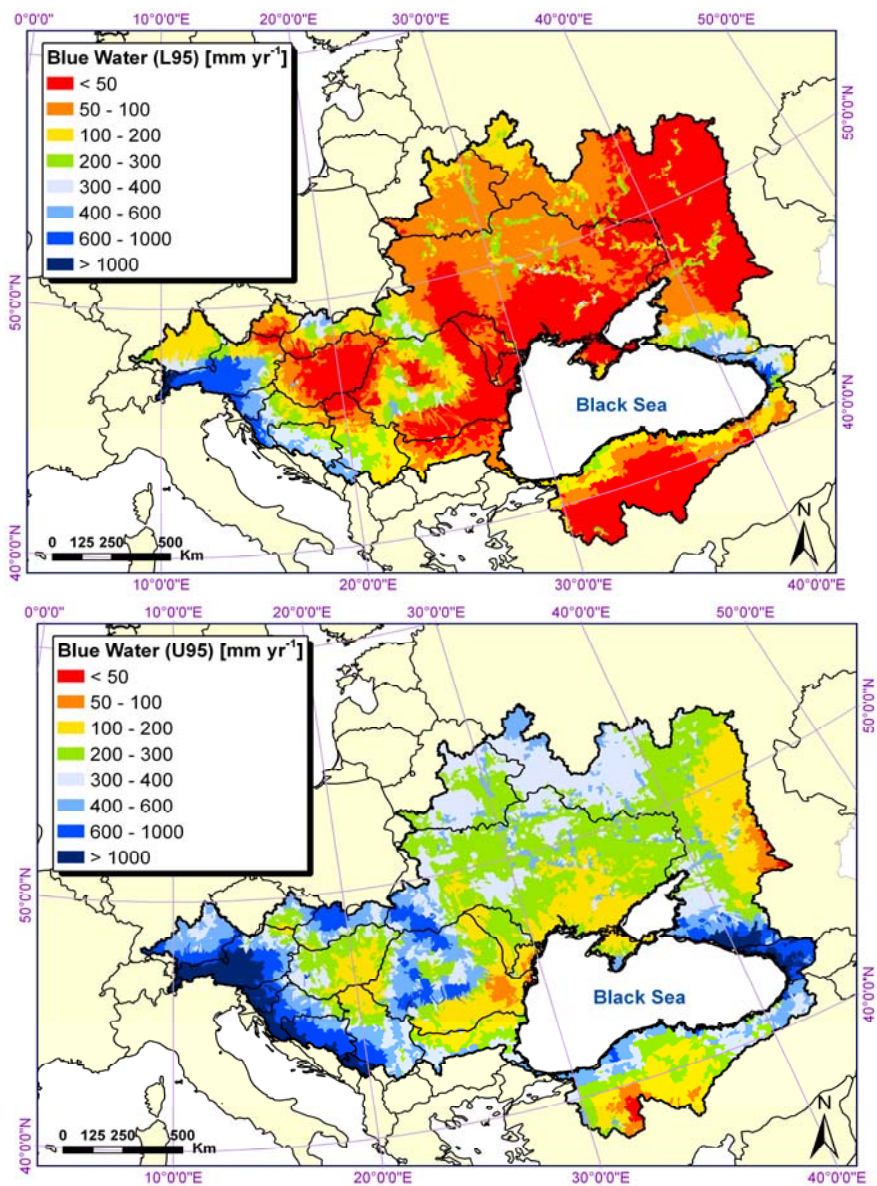


**Fig. 33.** Long-term average (1973-2006) subbasin-based distribution of the blue water resources at the 50% probability level across the BSB. This graph indicates the most probable values of the blue water across the region. The Figure below shows the coefficient of variation CV of the blue water resources. The CV figure indicates the reliability of the blue water resources from year to year. Larger CV values indicate greater year to year variability of the resource. Table xxx summarizes blue water flow in Black Sea countries.

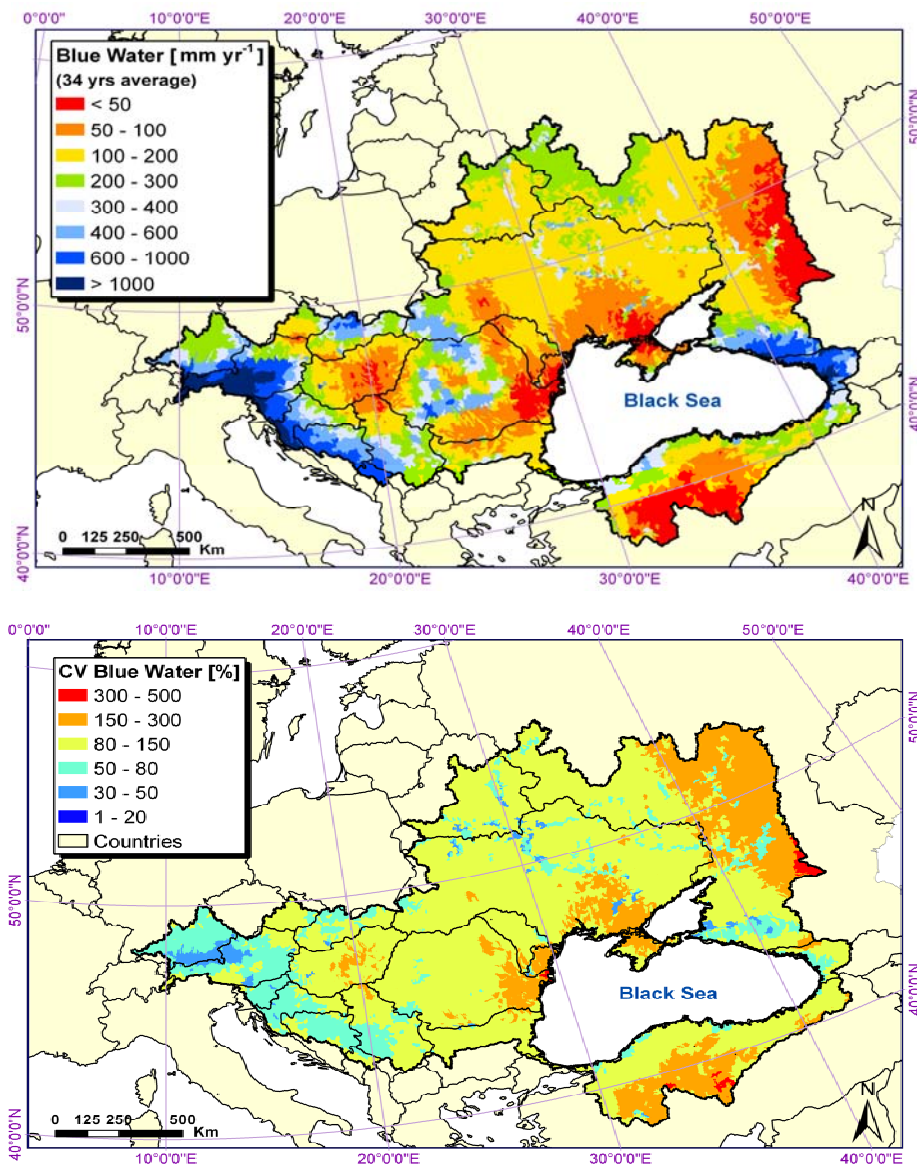




**Table 7.** Quantity of blue water flow in Black Sea countries. Values are given at the 2.5% probability level (lower bound), 97.5% probability level (upper bound) and the 50% probability level in terms of  $\text{mm yr}^{-1}$  and  $\text{m}^3$  per capita  $\text{yr}^{-1}$ .

Country	BW_L95ppu ( $\text{mm yr}^{-1}$ )	BW_U95ppu ( $\text{mm yr}^{-1}$ )	BW_M95pu ( $\text{mm yr}^{-1}$ )	BW_L95ppu ( $\text{m}^3 \text{capita}^{-1} \text{yr}^{-1}$ )	BW_U95ppu ( $\text{m}^3 \text{capita}^{-1} \text{yr}^{-1}$ )	BW_M95ppu ( $\text{m}^3 \text{capita}^{-1} \text{yr}^{-1}$ )
Austria	260	579	420	2886	6417	4662
Belarus	137	342	241	4535	11362	8002
Bosnia	232	550	397	3908	9262	6696
Bulgaria	67	192	124	<u>1556</u>	4458	2887
Croatia	162	394	281	3121	7602	5423
Czech	74	294	173	2159	8635	5092
Georgia	574	1203	895	19365	40597	30197
Germany	198	509	355	7372	18957	13229
Hungary	41	225	112	<u>398</u>	2166	<u>1077</u>
Moldova	60	238	138	<u>489</u>	1934	<u>1125</u>
Montenegro	443	1129	799	17184	43792	30967
Romania	87	242	161	<u>950</u>	2653	<u>1762</u>
Serbia	117	305	211	<u>1378</u>	3596	2481
Slovakia	124	378	246	<u>1179</u>	3601	2345
Slovenia	421	841	646	4278	8549	6558
Turkey	57	242	140	<u>1670</u>	7085	4096
Ukraine	134	308	219	1764	4061	2889
Russia	94	285	183	7117	21679	13891

**Fig. 34.** Long-term average (1973-2006) subbasin-based distribution of lower and upper 95% prediction uncertainty (95PPU) of the green water storage across the BSB. 95PPU highlights model prediction uncertainty. In other words, all values within the range of 95PPU are acceptable results. Comparison of the two graphs highlights the model prediction uncertainty and the importance of expressing these uncertainties. Based on the available data, the model uncertainty includes the uncertainty in the data, in the model, and in the year to year variability of the climate and the changes in the landuse.

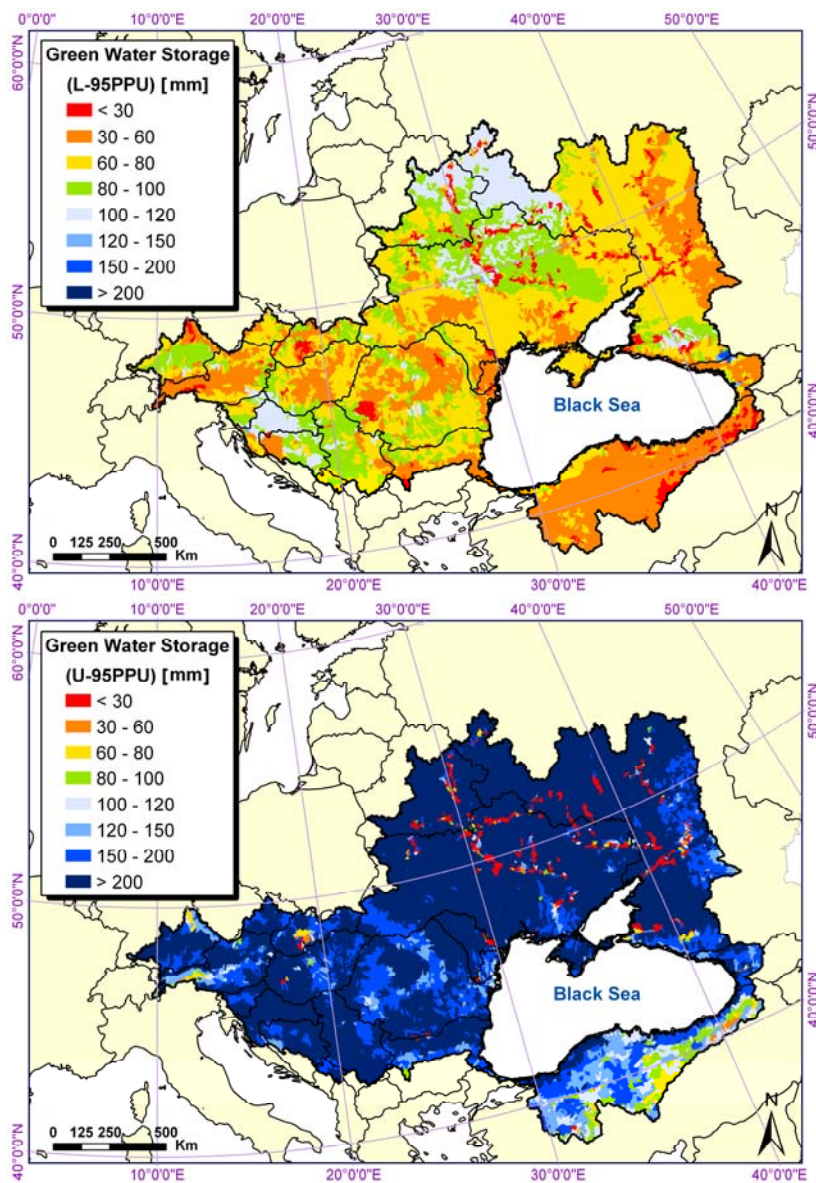


**Fig. 35.** Long-term average (1973-2006) subbasin-based distribution of the green water resources at the 50% probability level across the BSB. This graph indicates the most probable values of the green water across the region. The Figure below shows the coefficient of variation CV of the green water resources. The CV figure indicates the reliability of the green water resources from year to year. Larger CV values indicate greater year to year variability of the resource.

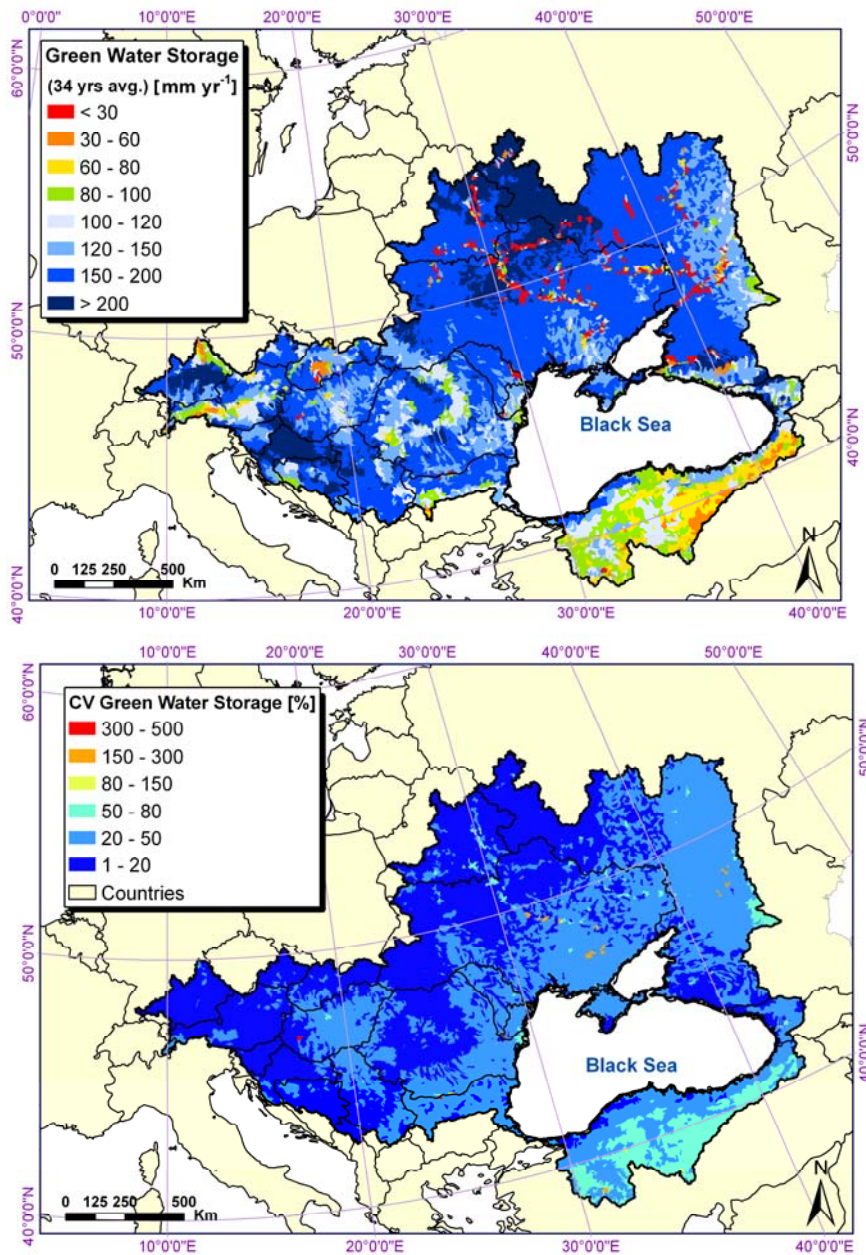


**Fig. 36.** Long-term average (1973-2006) subbasin-based distribution of lower and upper 95% prediction uncertainty (95PPU) of the green water flow across the BSB. 95PPU highlights model prediction uncertainty. In other words, all values within the range of 95PPU are acceptable results. Comparison of the two graphs highlights the model prediction uncertainty and the importance of expressing these uncertainties. Based on the available data, the model uncertainty includes the uncertainty in the data, in the model, and in the year to year variability of the climate and the changes in the landuse.

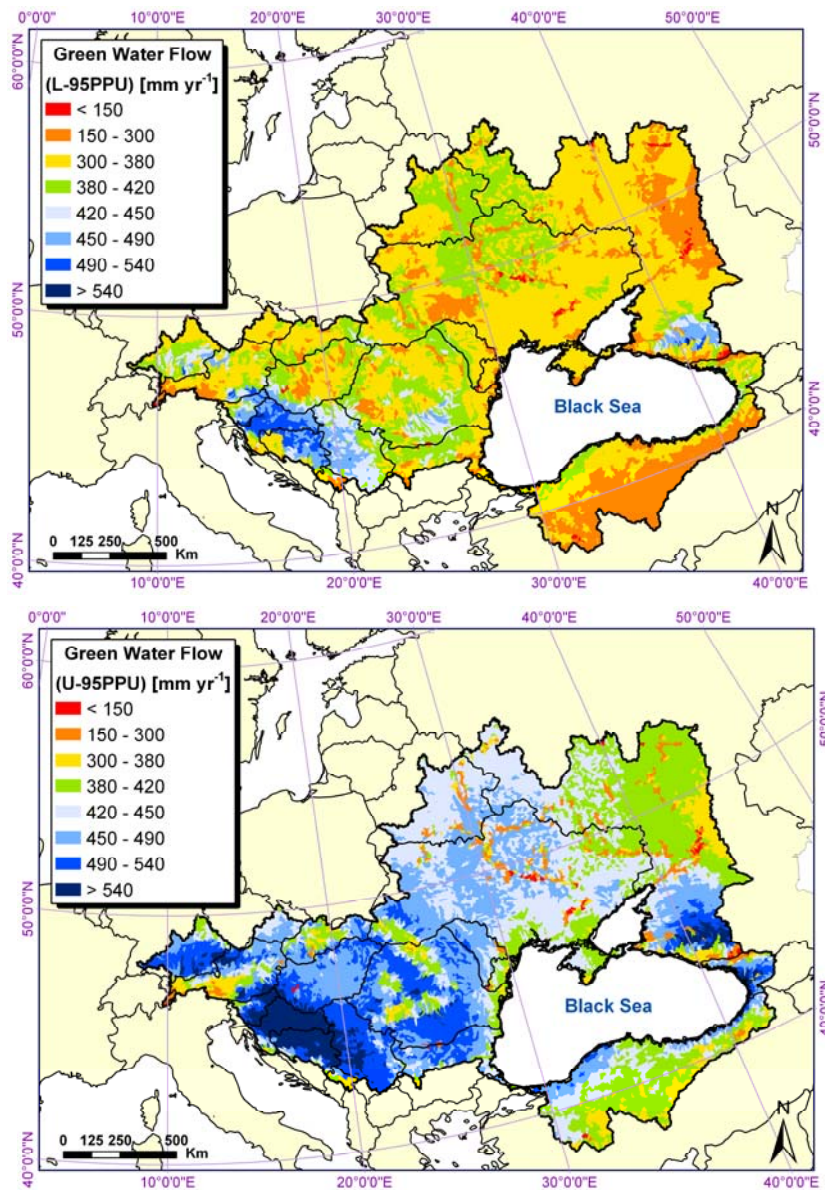


**Fig. 37.** Long-term average (1973-2006) subbasin-based distribution of the green water flow (actual evapotranspiration) at the 50% probability level across the BSB. This graph indicates the most probable values of the green water across the region. The Figure below shows the coefficient of variation CV of the green water flow. The CV figure indicates the reliability of the green water flow from year to year. Larger CV values indicate greater year to year variability of the resource.

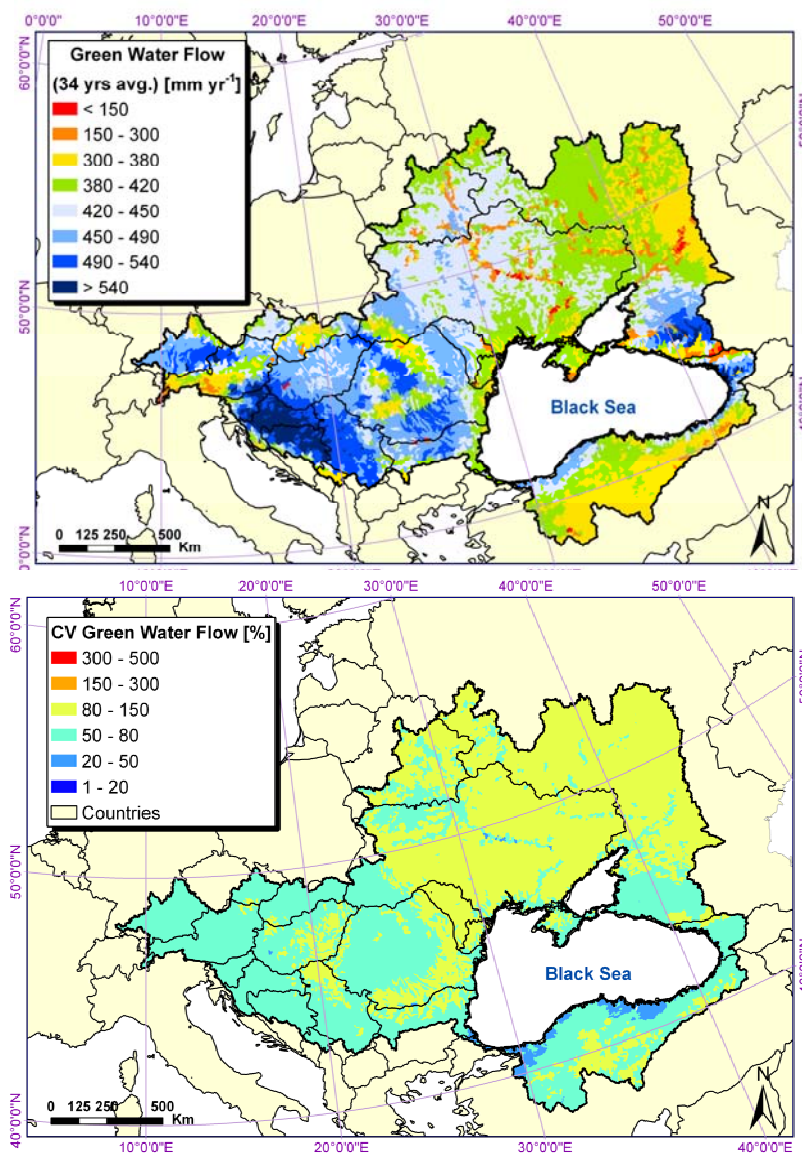


**Fig. 38.** Long-term average (1973-2006) subbasin-based distribution of water scarcity or blue water per capita. The figure shows lower and upper 95% prediction uncertainty (95PPU) of water scarcity across the BSB. The 95PPU range highlights model prediction uncertainty. In other words, all values within the range of 95PPU are acceptable results. Comparison of the two graphs highlights the model prediction uncertainty and the importance of expressing these uncertainties. Based on the available data, the model uncertainty includes the uncertainty in the data, in the model, and in the year to year variability of the climate and the changes in the landuse. Regions with water scarcity at the upper uncertainty bond are really water scarce, and vice versa regions that do not have water scarcity at the lower bond can be considered as not having water scarcity with confidence.

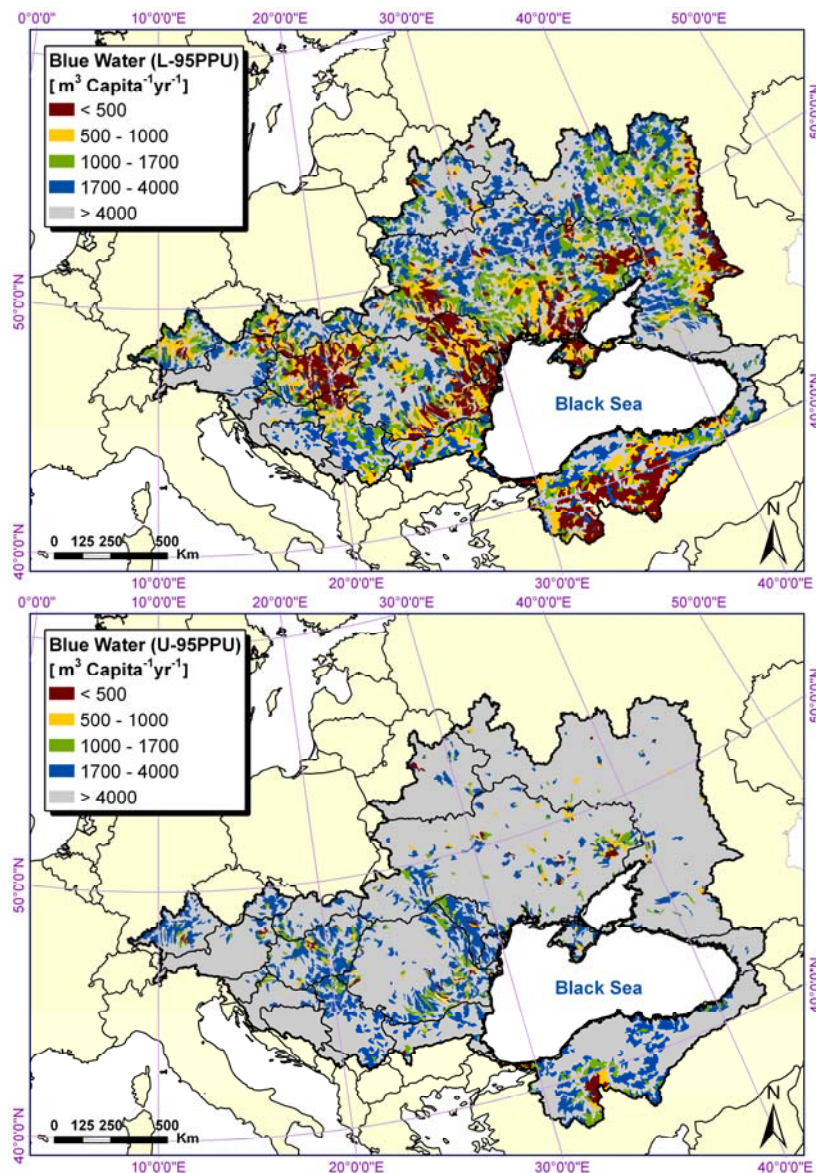


**Fig. 39.** Long-term average (1973-2006) subbasin-based distribution of water scarcity at the 50% probability level across the BSB. This graph indicates the most probable values of the water scarcity across the region.

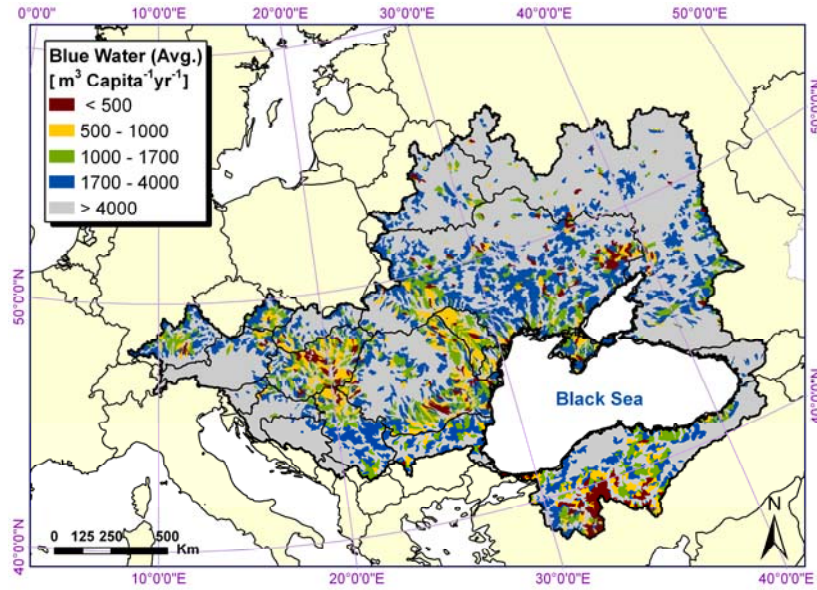


**Fig. 40.** Long-term average (1973-2006) subbasin-based distribution of barley yield. The figure shows lower and upper 95% prediction uncertainty (95PPU) of barley across the BSB. The 95PPU range highlights model prediction uncertainty. In other words, all values within the range of 95PPU are acceptable results. Comparison of the two graphs highlights the model prediction uncertainty and the importance of expressing these uncertainties. Based on the available data, the model uncertainty includes the uncertainty in the data, in the model, and in the year to year variability of the climate and the changes in the landuse.

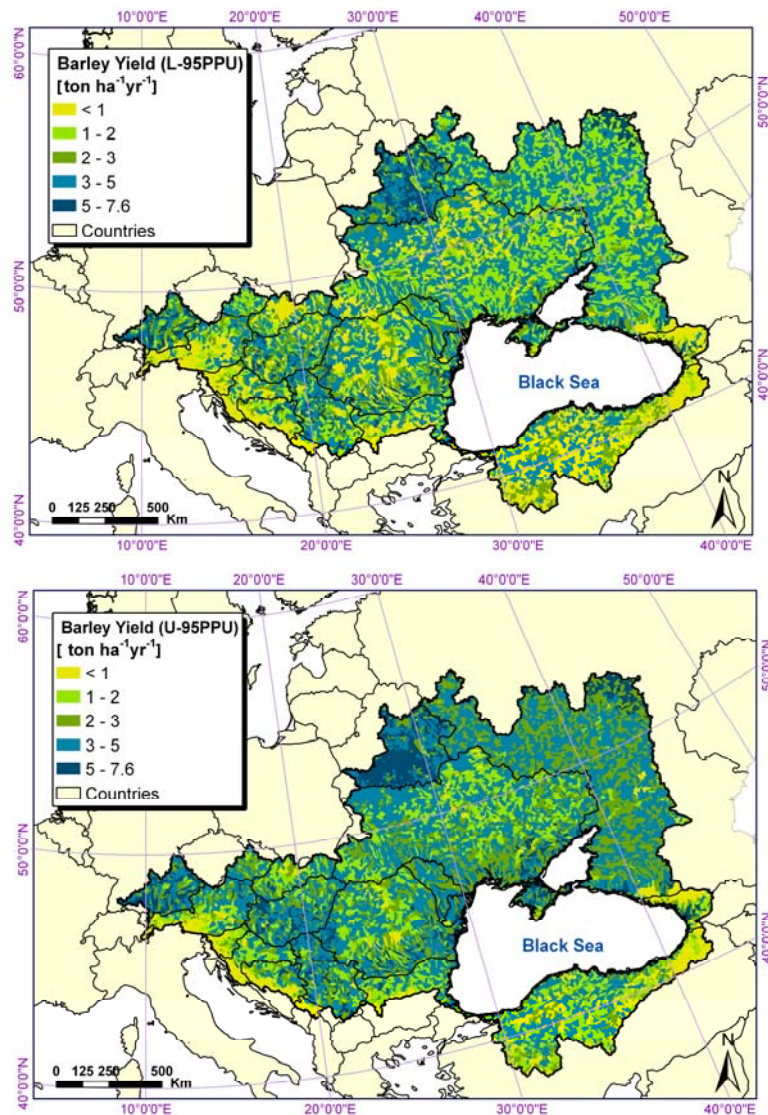


**Fig. 41.** Long-term average (1973-2006) subbasin-based distribution of barley yield at the 50% probability level across the BSB. This graph indicates the most probable values of the barley yield across the region. The lower Figure shows the coefficient of variation CV of the barley. The CV figure indicates the reliability of the yield from year to year. Larger CV values indicate greater year to year variability of the yield.

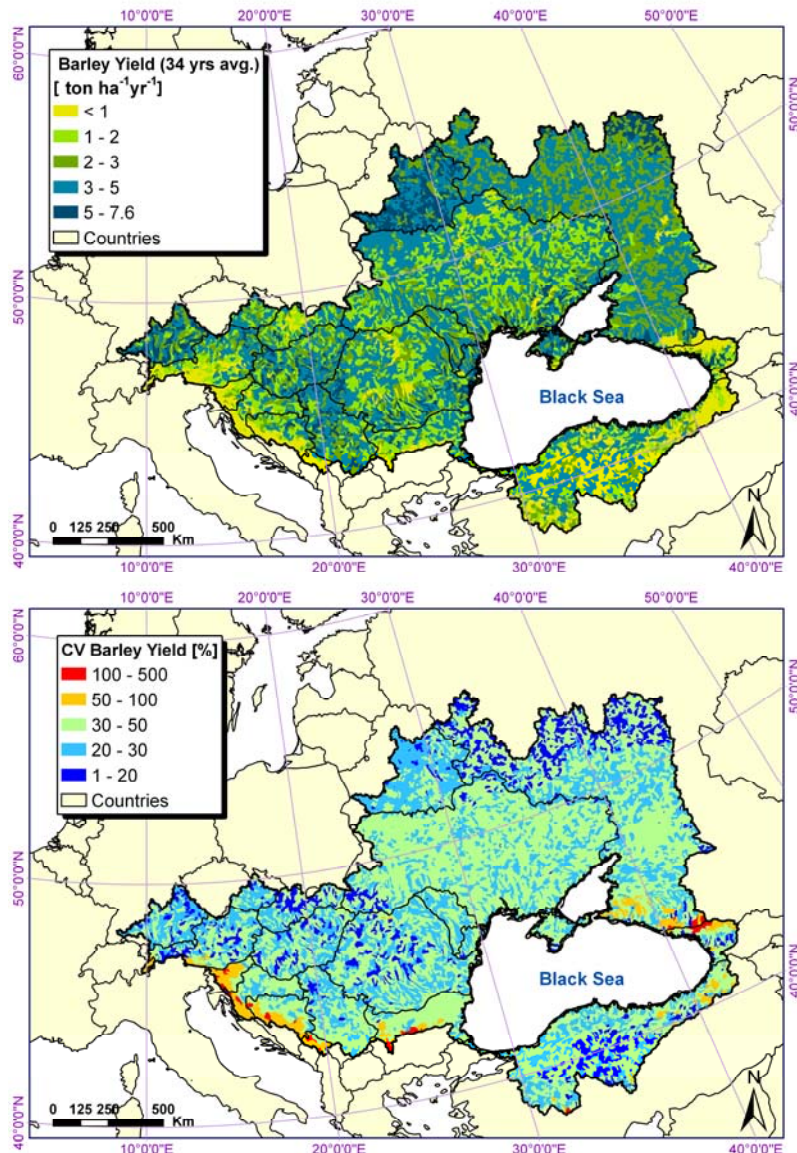


**Fig. 42.** Long-term average (1973-2006) subbasin-based distribution of wheat yield at the 50% probability level across the BSB. This graph indicates the most probable values of the wheat yield across the region. The lower Figure shows the coefficient of variation CV of the wheat. The CV figure indicates the reliability of the yield from year to year. Larger CV values indicate greater year to year variability of the yield.

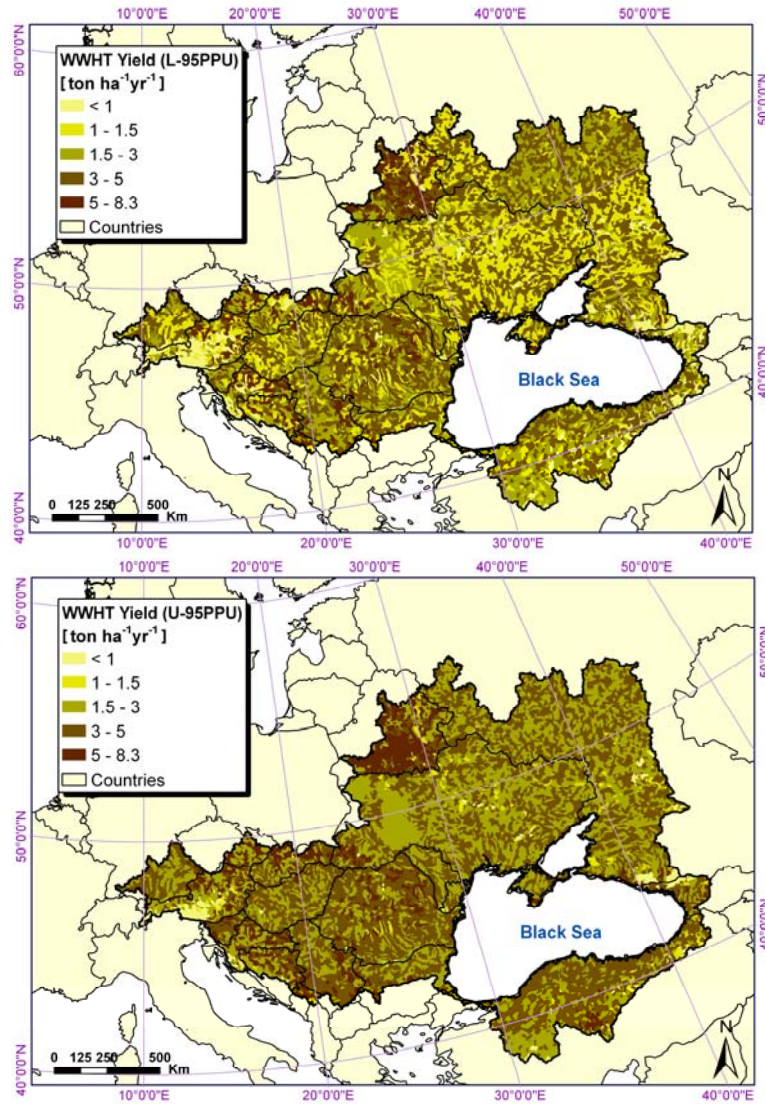


**Fig. 43.** Long-term average (1973-2006) subbasin-based distribution of wheat yield at the 50% probability level across the BSB. This graph indicates the most probable values of the wheat yield across the region. The lower Figure shows the coefficient of variation CV of the wheat. The CV figure indicates the reliability of the yield from year to year. Larger CV values indicate greater year to year variability of the yield.

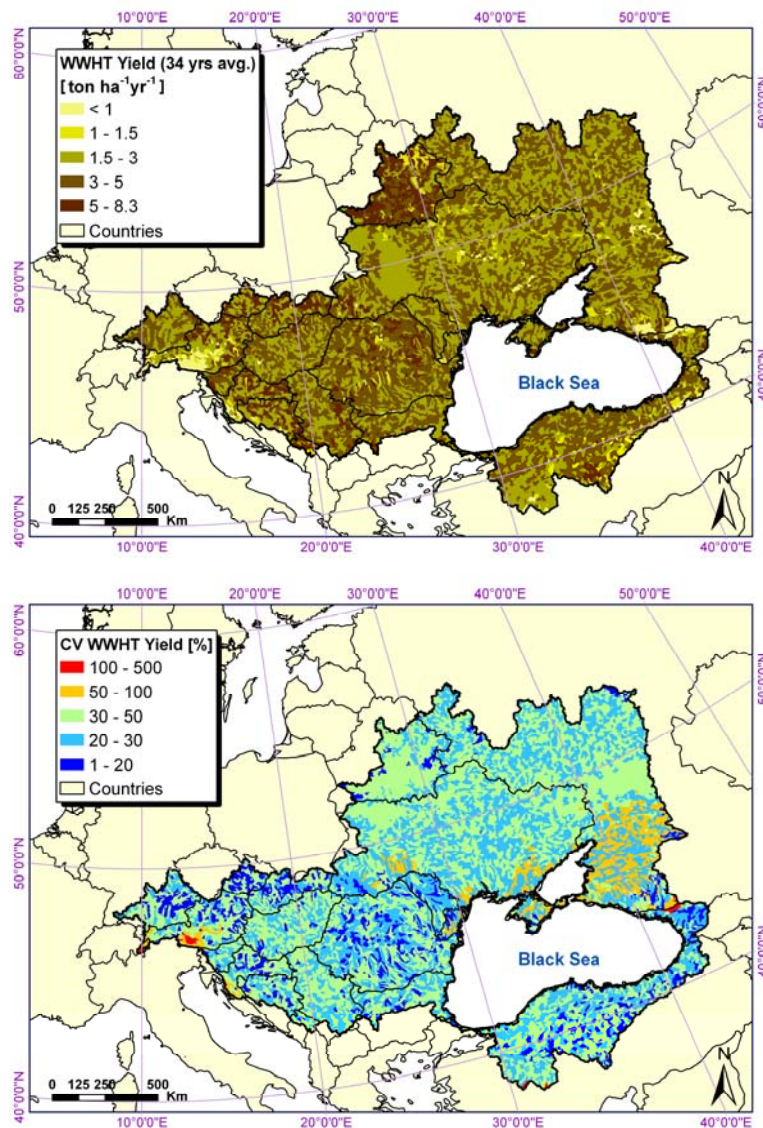


**Fig. 44.** Long-term average (1973-2006) subbasin-based distribution of nitrate released into river from HRU at the 50% probability level across the BSB. This graph indicates the most probable values of the nitrate released into river from HRU across the region.

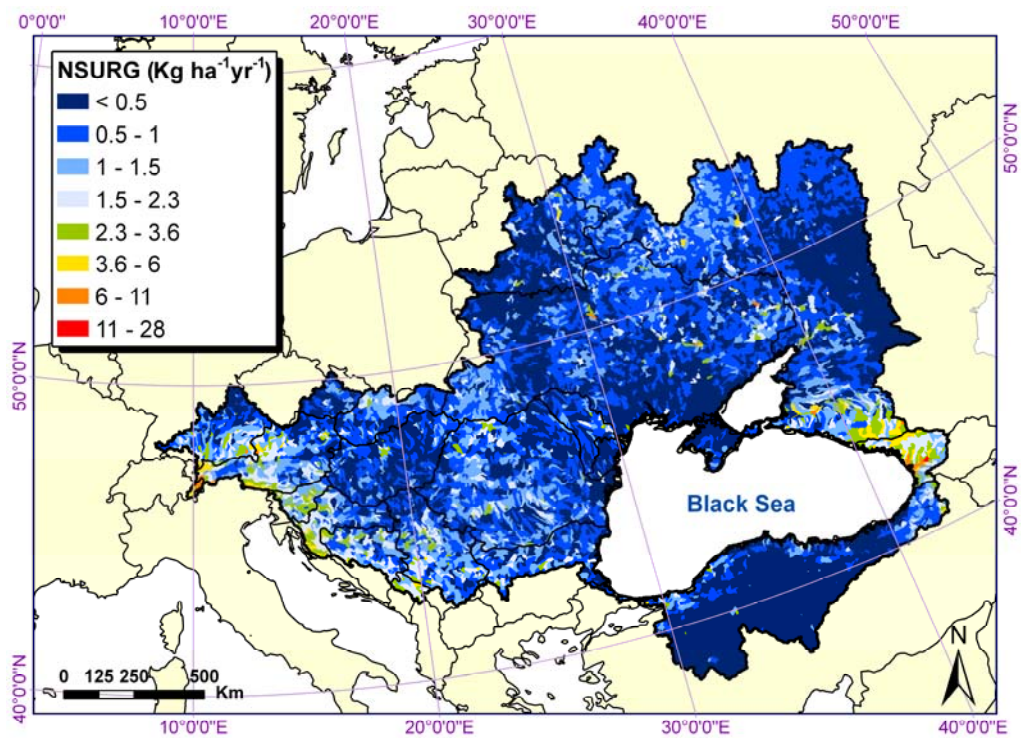


**Fig. 45.** Long-term average (1973-2006) subbasin-based distribution of Nitrate leached below the soil profile HRU at the 50% probability level across the BSB. This graph indicates the most probable values of the Nitrate leached below the soil profile from HRU across the region.

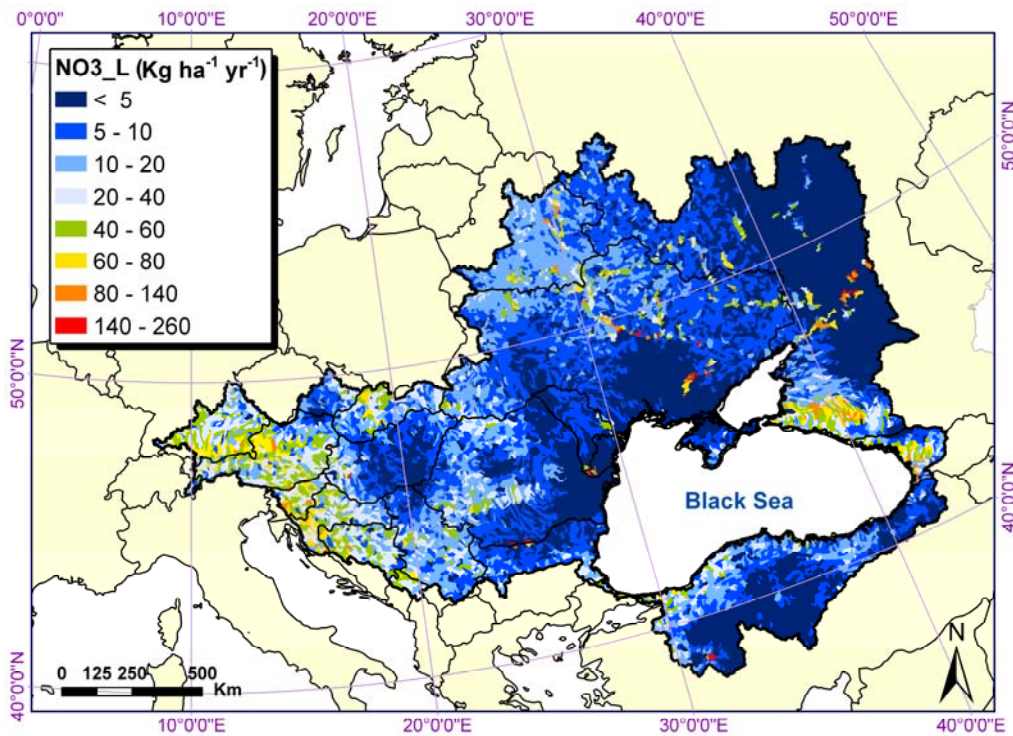


**Fig. 46.** Long-term average (1973-2006) subbasin-based distribution of nitrate transported by surface runoff into reach from HRU at the 50% probability level across the BSB. This graph indicates the most probable values of the nitrate transported by surface runoff into reach from HRU across the region.

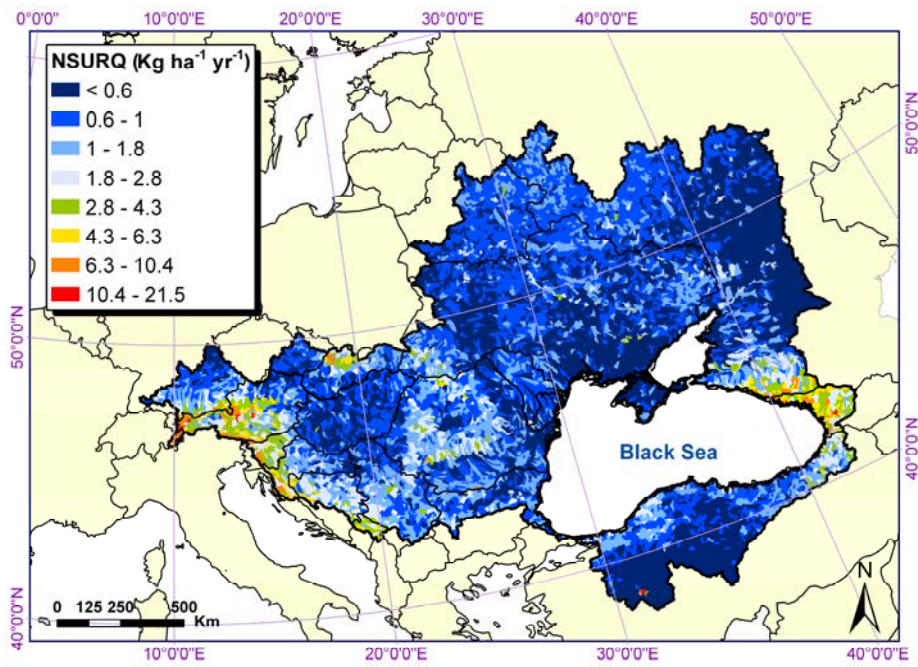
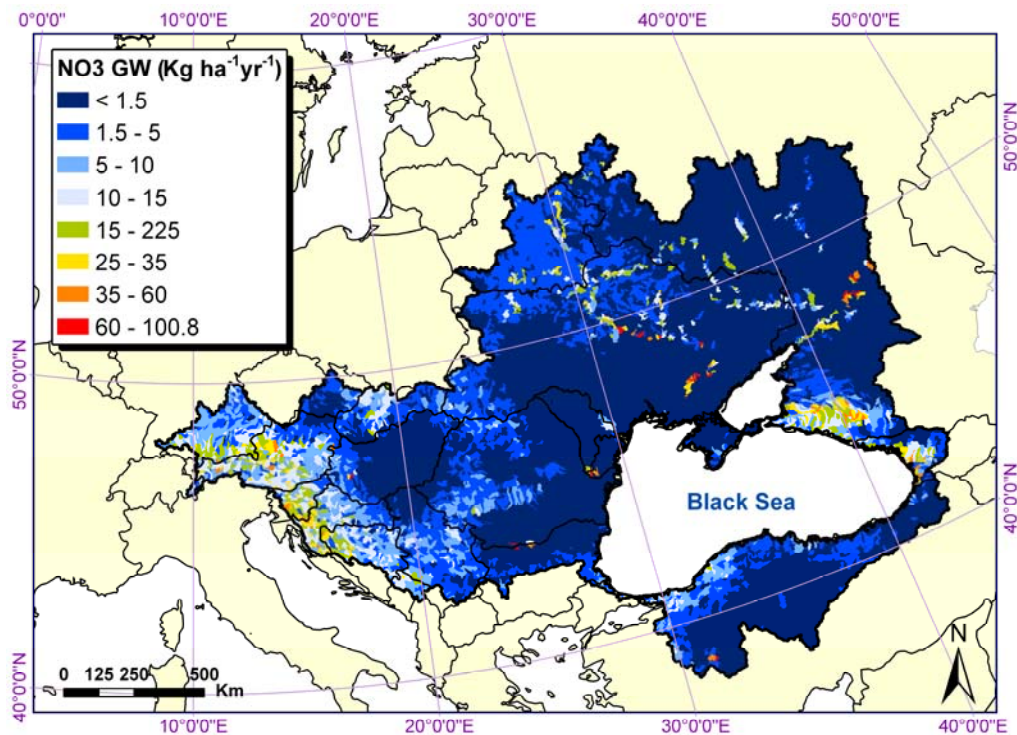
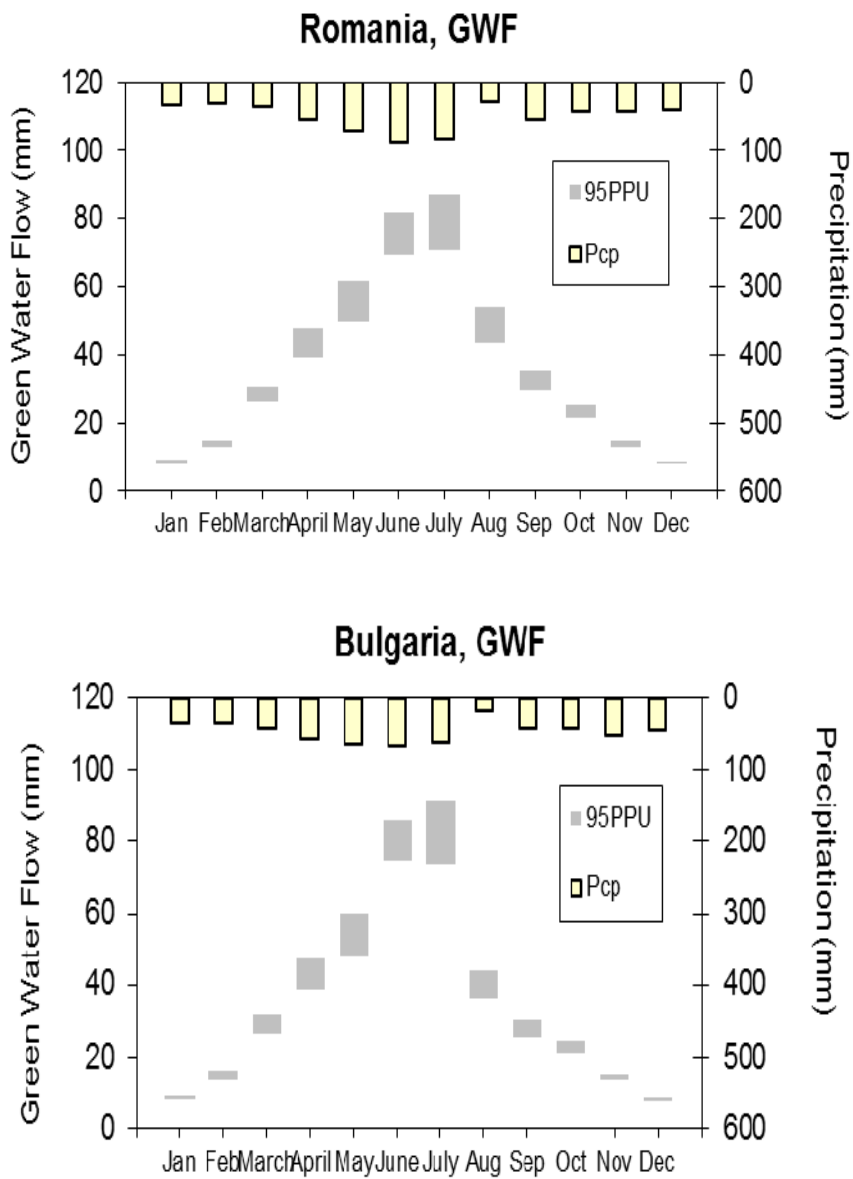


**Fig. 47.** Long-term average (1973-2006) subbasin-based distribution of nitrate contributed by HRU to groundwater into reach from HRU at the 50% probability level across the BSB. This graph indicates the most probable values of the nitrate contributed by HRU to groundwater from HRU across the region.



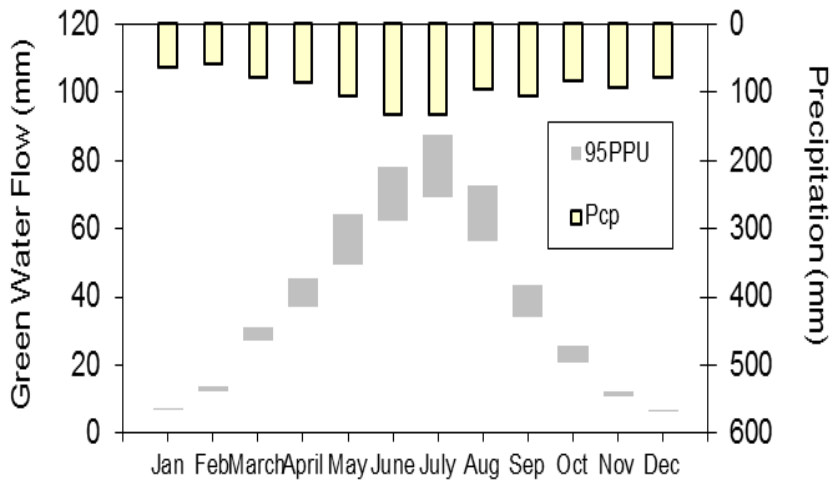
Time series data for some selected variables and countries are shown in the following Figures.

**Fig. 48.** Temporal distribution of actual evapotranspiration or green water flow of selected countries





### Austria, GWF



### Turkey, GWF

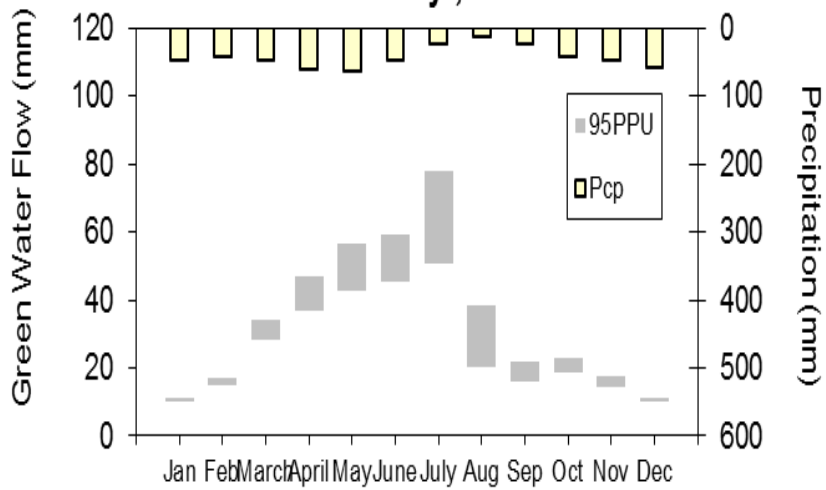
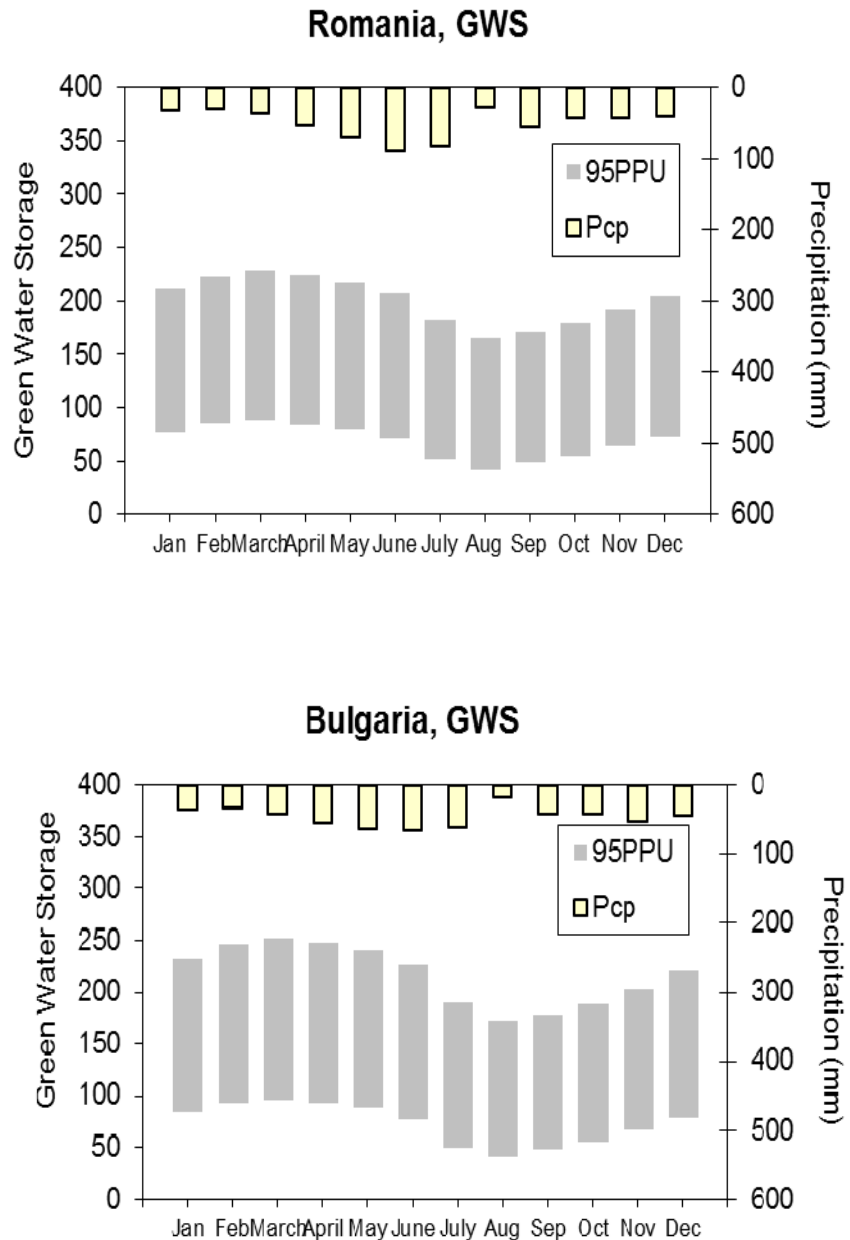
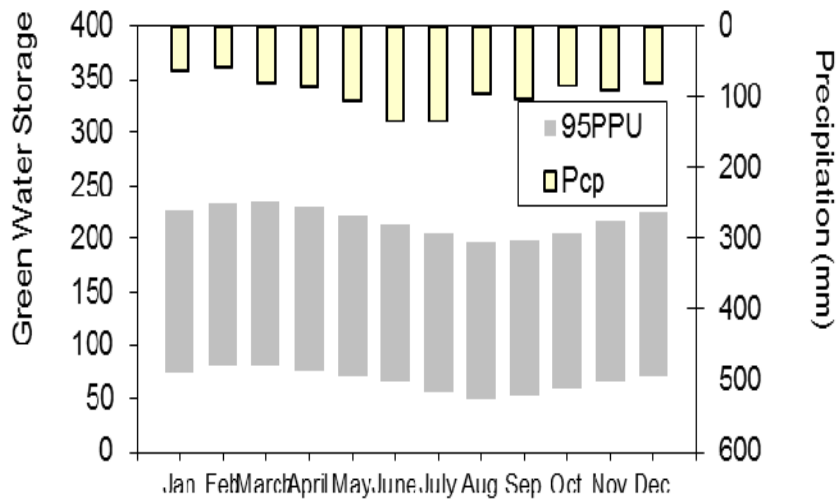


**Fig. 49.** Temporal distribution of soil moisture or green water storage. This shows the potential for green agriculture or rainfed agriculture. The large uncertainty distribution is due to both year to year climate variability and model uncertainty.





### Austria, GWS



### Turkey, GWS

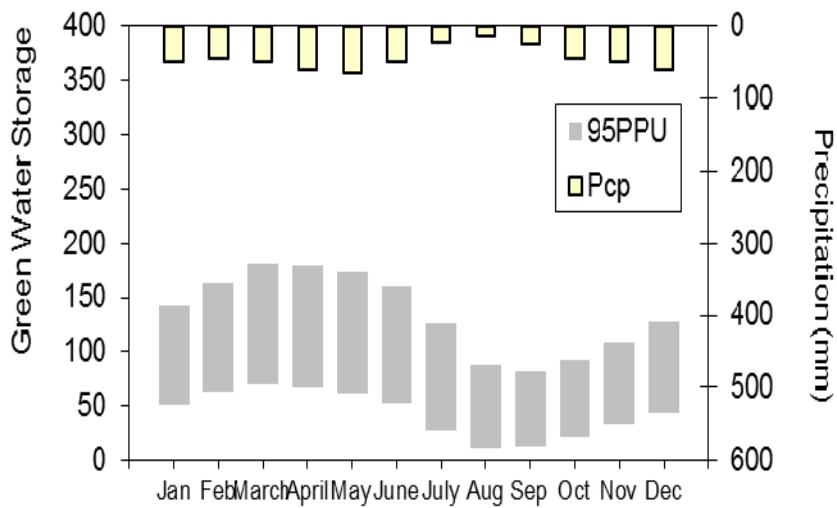
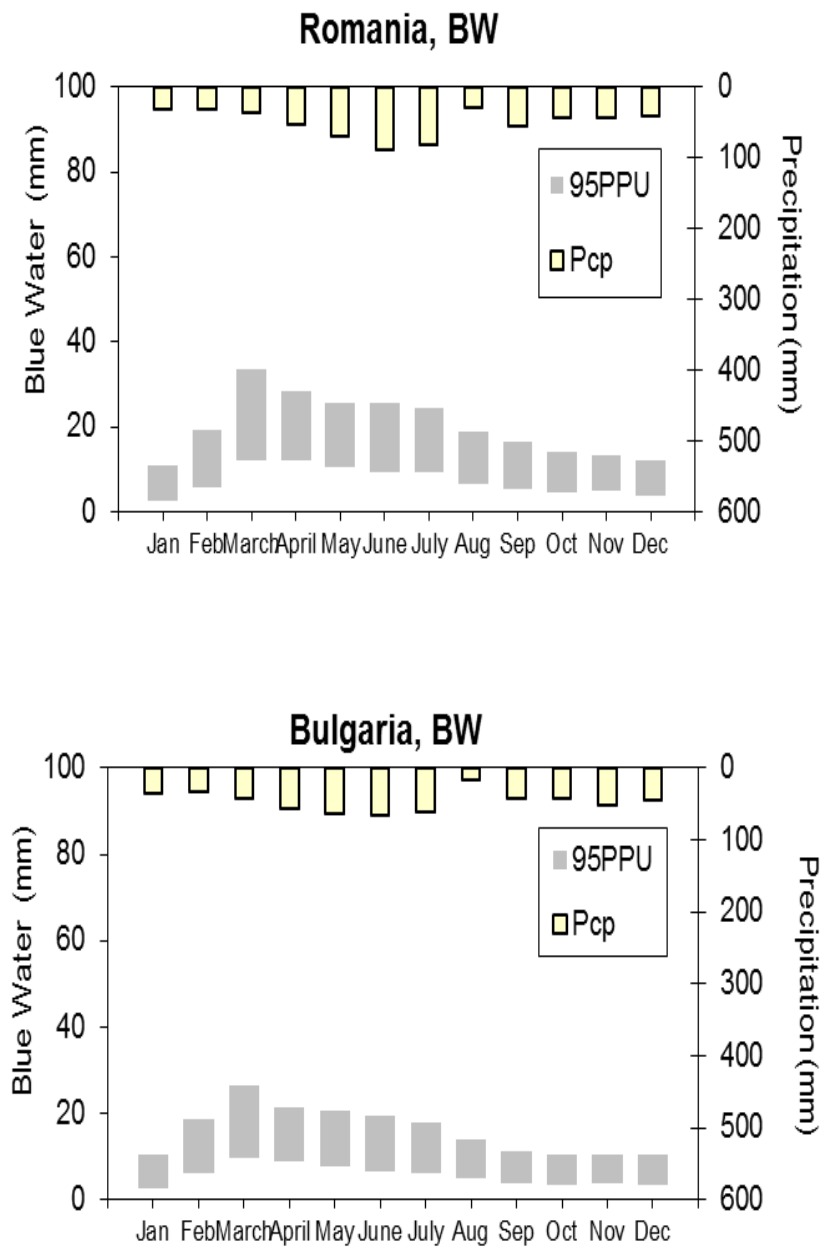
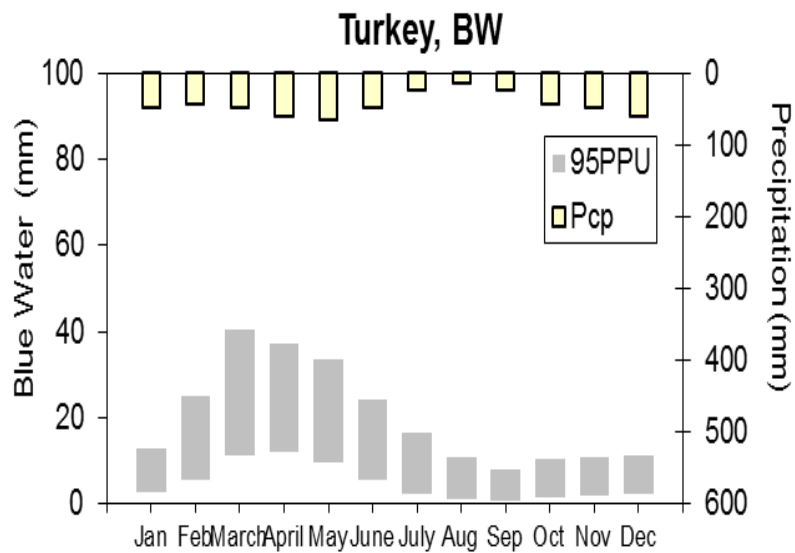
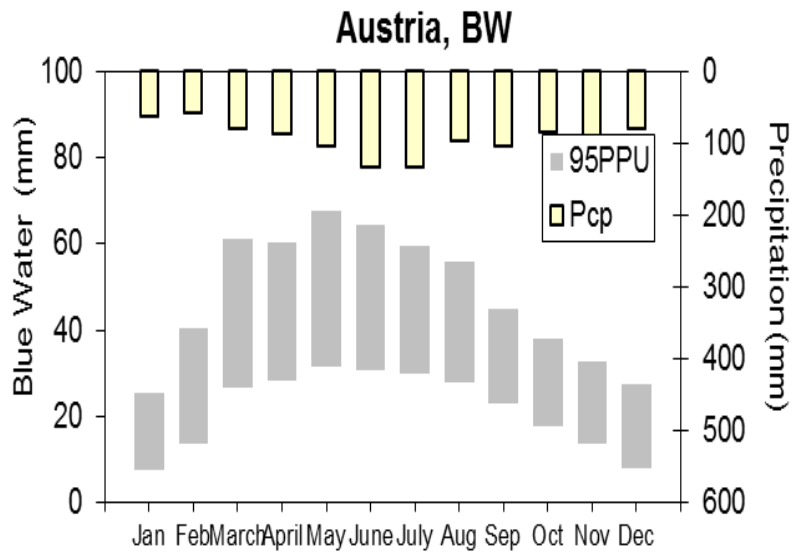


Fig. 50. Temporal distribution of blue water resources for some selected countries.

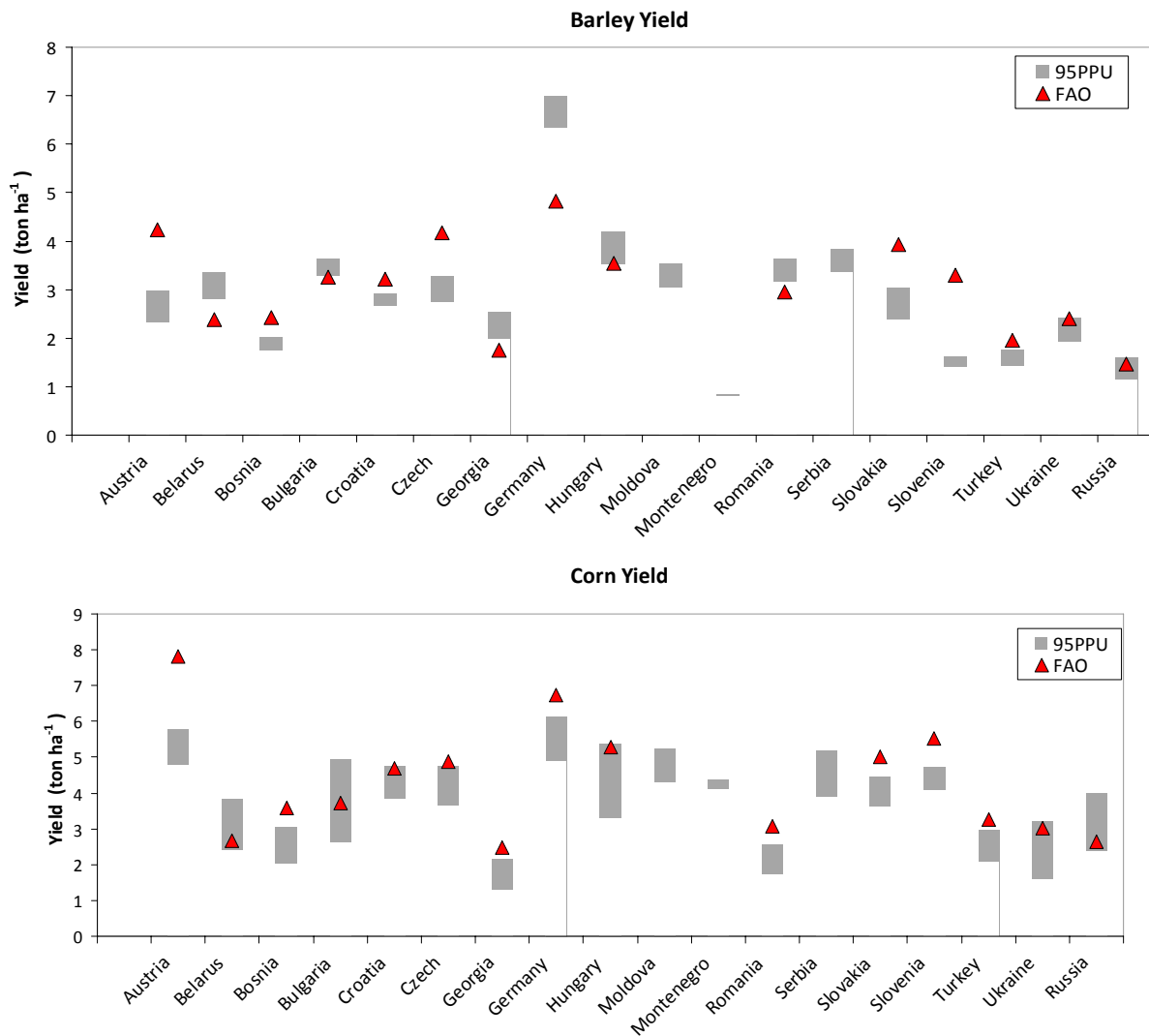






### Crop Yield

Crop yields were simulated for 3 major crops of barley, maize, and wheat. In general, it is very difficult to calibrate crop yields because of lack of information with respect to crop management such as fertilizer and irrigation inputs and nutrient status of the soil, etc., as well as natural disasters such as frost, drought, pest, etc. For this reason we compare the long-term average measured and simulated values. The model's simulated values compare relatively well with the simulated one although there are discrepancies. A much better database of agricultural management is needed such as local planting and harvest dates and types or varieties used to improve the simulation.



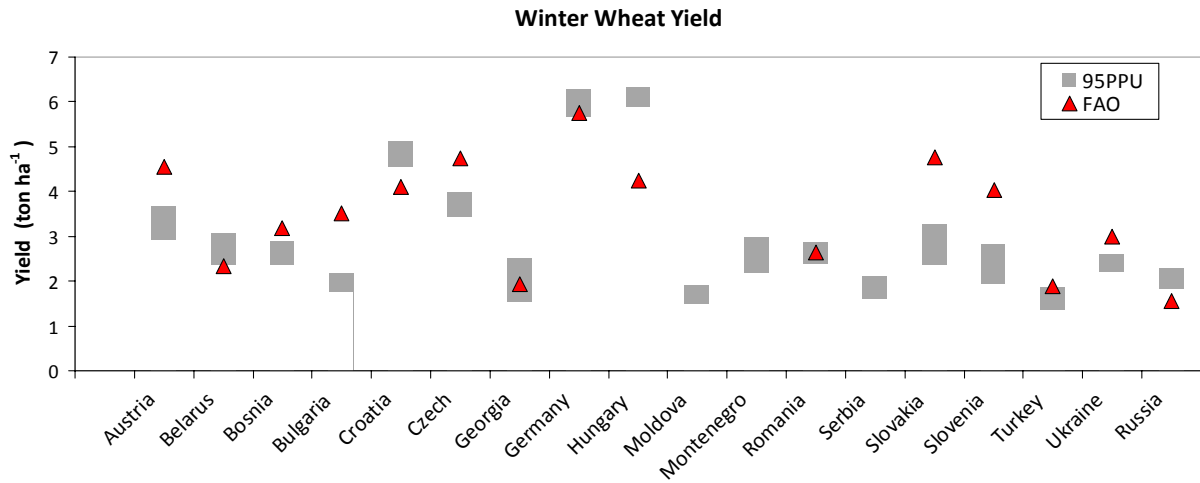


Fig. 51. Barley, corn, and wheat yield prediction (shaded bars) as compared to FAO data



## Appendix I

### **A Parallelization Framework for Calibration of hydrological Models**

E. Rouholahnejad<sup>a,\*</sup>, K.C. Abbaspour<sup>a</sup>, M. Vejdani<sup>b</sup>, R. Srinivasan<sup>c</sup>, R. Schulin<sup>d</sup>, A. Lehmann<sup>e</sup>

<sup>a</sup> Eawag, Swiss Federal Institute of Aquatic Science and Technology, Ueberlandstrasse 133, CH-8600 Duebendorf, Switzerland

<sup>b</sup> Neprash Technology, 1625 Sundew Pl, Coquitlam, B.C., V3E 2Y4, Canada

<sup>c</sup> Spatial Sciences Laboratory, Texas A&M University, Texas Agricultural, Experimental Station, College Station, Texas, USA

<sup>d</sup> ETH Zürich Institute of Terrestrial Ecosystem, Universitätstr. 16, 8092 Zürich, Switzerland

<sup>e</sup> University of Geneva, Climatic Change and Climate Impacts, 7 Route de Drize, CH-1227 Carouge, Switzerland

Corresponding author:

E. Rouholahnejad

Eawag, Ueberlandstrasse 133, 8600 Duebendorf, Switzerland

Tel: +41 58 765 5012

Fax: +41 58 765 5375

Email: [elham.rouholahnejad@eawag.ch](mailto:elham.rouholahnejad@eawag.ch)



## **Abstract**

Large-scale hydrologic models are being used more and more in watershed management and decision making. Sometimes rapid modeling and analysis is needed to deal with emergency environmental disasters. However, time is often a major impediment in the calibration and application of these models. To overcome this, most projects are run with fewer simulations, resulting in less-than-optimum solutions. In recent years, running time-consuming projects on gridded networks or clouds in Linux systems has become more and more prevalent. But this technology, aside from being tedious to use, has not yet become fully available for common usage in research, teaching, and small to medium-size applications. In this paper we explain a methodology where a parallel processing scheme is constructed to work in the Windows platform. We have parallelized the calibration of the SWAT (Soil and Water Assessment Tool) hydrological model, where one could submit many simultaneous jobs taking advantage of the capabilities of modern PC and laptops. This offers a powerful alternative to the use of grid or cloud computing. Parallel processing is implemented in SWAT-CUP (SWAT Calibration and Uncertainty Procedures) using the optimization program SUFI2 (Sequential Uncertainty Fitting ver. 2). We tested the program with large, medium, and small-size hydrologic models on several computer systems, including PCs, laptops, and servers with up to 24 CPUs. The performance was judged by calculating speedup, efficiency, and CPU usage. In each case, the parallelized version performed much faster than the non-parallelized version, resulting in substantial time saving in model calibration.

**KEYWORDS:** Parallel processing, SWAT-CUP, SUFI2, Hydrologic models

### **1.1.1 Software availability**

Software:

SWAT-CUP

Developer:

Karim C. Abbaspour

Eawag, Ueberlandstr 133, 8600 Duebendorf, Switzerland

[abbaspour@eawag.ch](mailto:abbaspour@eawag.ch)

Operating system requirements:

Windows XP or higher

Linux version of the SWAT-CUP package is also available without the interface

**enviroGRIDS – FP7 European project**

Building Capacity for a Black Sea Catchment

Observation and Assessment supporting Sustainable Development



---

Language:

C++ and C#

Size:

125 MB zipped version

Availability:

- SWAT-CUP with 5 different optimization routines is available free of charge and can be downloaded from:

<http://www.eawag.ch/forschung/siam/software/swat/index>



## 1. Introduction

Advances in GIS technology and interfacing of hydrological programs with advanced GIS systems allow the construction of high resolution large-scale models. However, the execution time of these models can be rather long, not allowing proper model calibration and uncertainty analysis. For this reason, in the last few years, the use of distributed computing in the form of grid and cloud computing has become increasingly prevalent. Distributed hydrologic models are especially difficult to calibrate because of reasons such as time constraints, difficulties in parameterization, non-uniqueness (having more than one acceptable solution), uncertainties in the conceptual model, and model inputs. In this paper we address the problem of computation time and describe a system where an optimization algorithm, SUFI2, is used in a parallel processing scheme to run on Windows-based computers. The parallel processing scheme developed here utilizes the existing capabilities of the available systems and is ideal for performing hydrologic model calibration and uncertainty analysis.

Distributed computing is an extension of the object-oriented programming concept of abstraction ([Sundaram, 2010](#)). Abstraction removes the complex working details from visibility. All that is visible is an interface which receives inputs and provides outputs. How these outputs are computed is completely hidden. Grid and cloud computing and parallel processing belong to the family of distributed computing. Currently, two different ways are pursued in parallelizing hydrological models. One is parallelization of the code itself to be run as parallel threads (Neal et al., 2010; Li et al., 2011), and another is to submit model runs with different parameters to different CPUs (or GPUs) on the same or different computers (Lecca, 2011; Sing et al., 2011; Kalayanapu et al., 2011). Jobs submitted to a network of computers are run on grid and cloud. Below is a brief definition of these systems and their advantages and disadvantages.

A *grid network* is a computer network consisting of a number of computers connected in a grid topology. Some advantages of grid computing are: there is no need to buy expensive symmetric multiprocessing (SMP) servers for applications that can be split up and distributed to less powerful servers; much more efficient use of idle resources is made; grid environments are much more modular and don't have single points of failure; and jobs can be executed in parallel, speeding up the performance (Fernandez-Quiruelas, et al., 2011; Vassilios, 2008).

Some disadvantages of the grid are: memory intensive applications that can't take advantage of message passing interface (MPI) may not be able to take advantage of the grid system; a fast connection between computer resources (gigabit Ethernet at a minimum) is needed in intense MPI applications; some applications may need to be tweaked to take full advantage of a new model; licensing across many servers may make it prohibitively expensive for some applications; and political challenges associated with



sharing resources across different administration domains may also prohibit the use of grids for many users (Taylor et al., 2004).

*Cloud computing* is Internet-based computing whereby shared resources, software, and information are provided to computers and other devices on demand, like the electricity grid. Similar to grid computing, some of the advantages offered by cloud computing are: lower computer costs, improved performance with less use of computer memory, virtually unlimited storage capacity, increased data reliability, universal document access, and easier group collaboration. There are also a number of disadvantages associated with cloud computing, which include: requiring a constant high-speed Internet connection, and not getting an instantaneous connection if the cloud servers are busy. It is the opinion of some experts that security may be a disadvantage of the cloud (Miller, 2009). Theoretically, data stored in the cloud should be safe because it is replicated across multiple machines. But in the case of missing data, there is no physical or local backup (unless data is methodically downloaded).

*Parallel processing* or *parallel computing* is the ability to carry out multiple operations or tasks simultaneously. In parallel processing more than one CPU or processor core is used to execute a program or multiple computational threads. Parallel processing makes programs run faster because there are more CPUs or cores running it. In practice, it is often difficult to divide a program in such a way that separate CPUs can execute different portions without interfering with each other. Older computers have just one CPU, but newer computers have multi-core processor chips and many CPUs. With single-CPU, or single-core computers, it is also possible to perform parallel processing by connecting the computers in a network. However, this type of parallel processing requires very sophisticated distributed processing software. The main advantages of the system we have developed is that: it does not have the disadvantages of the grid and cloud; but it has all the advantages of using a PC. These include: the user being in full control of the job being processed; the job can be stopped and restarted at any time; a PC is much simpler to use, not needing grid or cloud certificate and permission. For very large models, a powerful computer (e.g., 24-48 CPUs with >16 GB RAM) is, however, needed to take full advantage of parallel processing. With the advancement of new technologies, this is now available at a reasonable cost.

In the current paper we describe and test a parallel processing software that allows calibration of the hydrologic simulator Soil Water Assessment Tool (SWAT) (Arnold et al., 1998), which is linked to five different optimization schemes in the SWAT-CUP software package (Figure 1). SWAT-CUP is a standalone program that links to SWAT's output text files set. Theoretically, any other model or optimization algorithm could be added to this package. Currently, however, the program SWAT is linked with the Generalized Likelihood Uncertainty Estimation (GLUE) (Beven and Binley, 1992), Sequential Uncertainty Fitting (SUF12) (Abbaspour et al., 2004; 2007), Parameter

Solution (ParaSol) (Van Griensven and Meixner, 2006), Markov chain Monte Carlo (MCMC) (e.g., Kuczera and Parent, 1998; Marshall et al., 2004; Vrugt et al., 2003), and Particle Swarm Optimization (PSO) (Kennedy and Eberhart, 1995). The parallel processing currently only supports SUFI2, which lends itself easily to parallelization as the program runs with independent parameter sets. Support for PSO is under development.

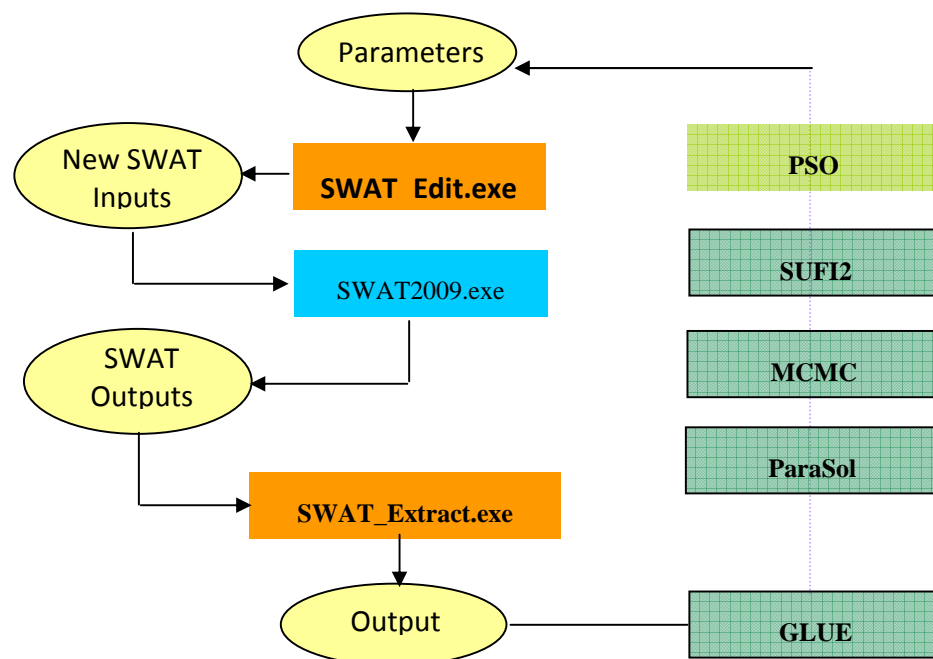


Figure 1. Structure of the SWAT-CUP and its linkage to five optimization algorithms.

The objective of this paper is to describe the SUFI2 parallel processing algorithm as implemented in the SWAT-CUP. We compare the computation time of parallel SUFI2 by applying it to a small, a medium, and a large size SWAT project using different computer systems. This study is designed to investigate parallel processing issues not to perform a meaningful calibration task. Finally, we summarize the performance of the parallelization and the gains in time obtained by parallel processing.



## **2. Materials and Methods**

### *2.1 The hydrologic simulator (SWAT)*

SWAT is a process-based, river basin-scale, semi-distributed hydrologic model. The program has been developed to predict the impact of land management on water, sediment, and agricultural chemical yield in large, complex watersheds. SWAT is an integrated model including components such as weather, hydrology, soil, nutrients, pesticides, land management, bacteria and pathogens. The model is a computationally efficient simulator of hydrology and water quality at various scales which has been used in many international applications (Arnold and Allen, 1996; Abbaspour *et al.*, 2007; Yang *et al.*, 2007; Schuol *et al.*, 2008a, b). It includes procedures to describe how CO<sub>2</sub> concentration, precipitation, temperature, and humidity affect plant growth. It also simulates evapotranspiration, snow and runoff generation, and is used to investigate climate change impacts [Abbaspour *et al.*, 2009; Eckhardt and Ulbrich, 2003; Fontaine *et al.*, 2001].

SWAT is a continuous simulation model which operates on a daily time step. In SWAT the spatial heterogeneity of the watershed is taken into account, considering information from the Digitized Elevation Model, soils, and landuse GIS data. Spatial parameterization of the SWAT model is performed by dividing the watershed into sub-basins based on topography. These are further subdivided into hydrologic response units (HRU) based on soil and landuse characteristics. These data and related parameters are stored in text files. A high resolution project could easily result in thousands of input files, which would make it challenging to reconfigure or update model parameters. All SWAT's text input and output files reside in the TxtInOut directory. Initially, SWAT-CUP copies these files to a BACKUP directory, which remain unchanged throughout the calibration process.

### *2.2. SUFI2 Optimization Program*

In Figure 2 a schematic diagram of the coupling between SUFI2 and SWAT is illustrated. Initially, a Latin hypercube (McKay *et al.*, 1979) procedure draws samples from the spaces defined by user-supplied parameter ranges. This is the pre-processing stage executed by a batch file *SUFI2\_pre.bat*, which runs the program *SUFI2\_LH\_sample.exe*. The parameter sets thus sampled are independent and for this reason parallel runs could be executed. Theoretically, all samples could be run at once, hence an entire iteration would require only the time that it takes to make one model run.

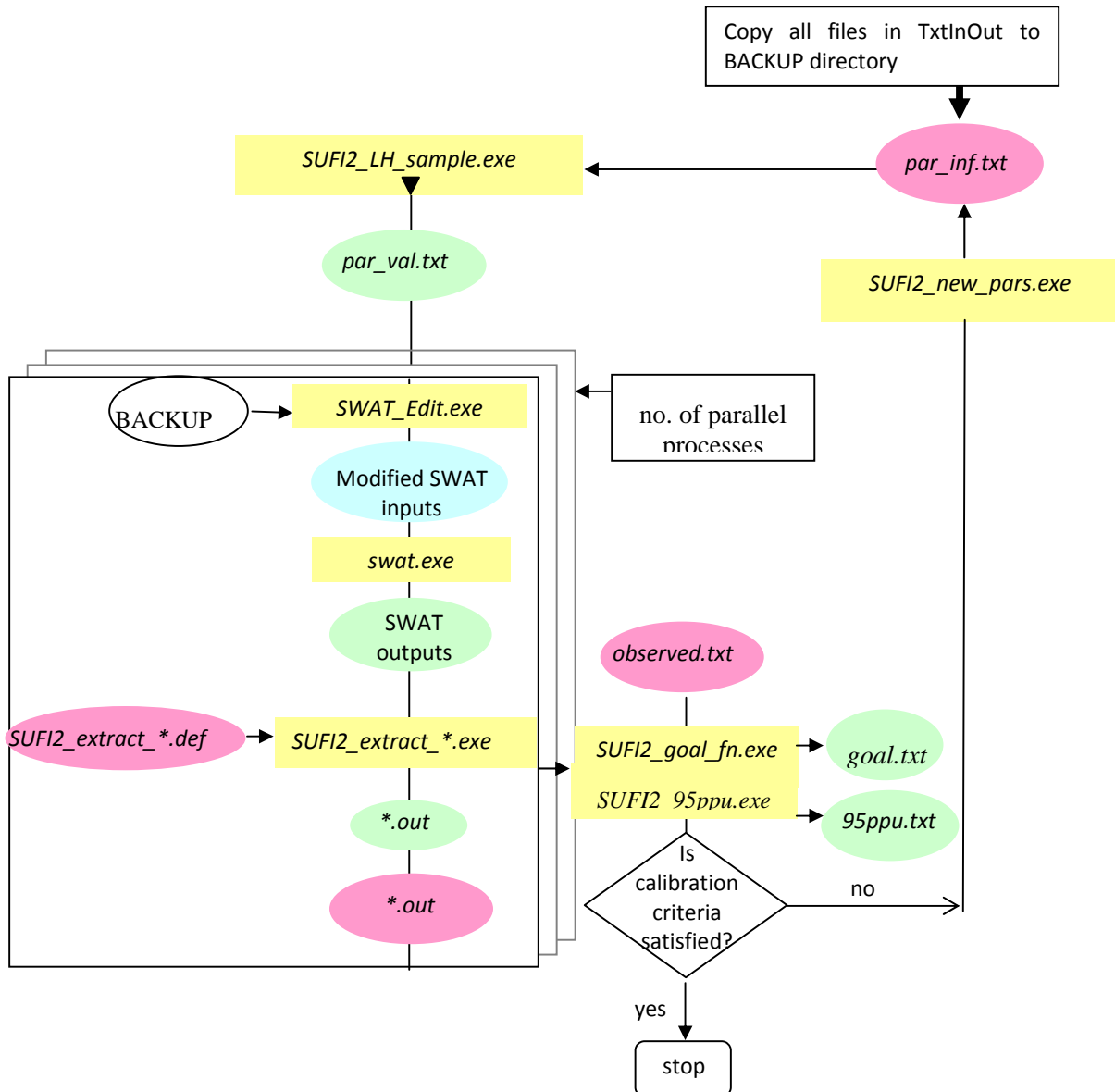


Figure 2. Schematic coupling of SWAT, and SUFI2. The entire algorithm is run by three batch files: *SUFI2\_pre.bat*, which runs the *SUFI2\_LH\_sample.exe*; *SUFI2\_run.bat*, which runs *SWAT\_Edit.exe*, *swat2009.exe*, and *SUFI2\_extract\_\*.exe* files, and *SUFI2\_post.bat*, which executes the *SUFI2\_goal\_fn.exe*, *SUFI2\_95PPU.exe*, and *SUFI2\_new\_pars.exe* programs. The symbol \* stands for rch, hru, and sub files.



After pre-processing, another batch file, *SUFI2\_run.bat*, executes the *SWAT\_Edit.exe* program, which copies a set of sampled parameters from *par\_val.txt* in their appropriate locations in the SWAT input files. Model parameterization is based on the physical characteristics of the parameters as described in the formulation below:

$x_{\text{<parname>.<ext>}_{\text{<hydrogrp>}_{\text{<soltext>}_{\text{<landuse>}_{\text{<subbsn>}_{\text{<slope>}}$

where  $x_{\text{}}$  is a code to indicate the type of changes to be applied to a parameter,  $\text{<parname>}$  is a SWAT parameter name,  $\text{<ext>}$  is the SWAT file extension,  $\text{<hydrogrp>}$  is the soil hydrological group,  $\text{<soltext>}$  is soil texture,  $\text{<landuse>}$  is the name of the landuse category,  $\text{<subbsn>}$  is the subbasin number, and  $\text{<slope>}$  is the slope of an HRU.

Any combination of the above factors can be used to describe a parameter. If the change is made globally, the identifiers  $\text{<hydrogrp>}$ ,  $\text{<soltext>}$ ,  $\text{<landuse>}$ ,  $\text{<subbsn>}$ , and  $\text{<slope>}$  are omitted. Table 1 shows examples of parameterization in different SWAT files.

**Table 1**

Examples of parameterization in SWAT-CUP \*

Parameter identifiers	Description
$r_{\text{SOL\_K}(1).\text{sol}}_{\text{FSL\_PAST}}_{1-3}$	Example of a parameter in .sol file. K of layer 1 of subbasin 1,2, and 3 with HRUs containing soil texture FSL and landuse PAST will be modified
$v_{\text{HEAT\_UNITS}}\{\text{rotation no,operation no}\}.\text{mgt}$	Example a parameter in .mgt file. Management parameters are subject to operation/rotation. Here, heat unit is modified for a certain rotation and operation
$v_{\text{PLTNFR}(1)\{3\}}.\text{CROP.DAT}$	Example of a parameter in crop.dat file. Nitrogen uptake parameter #1 for crop number 3 is modified
$v_{\text{precipitation}}(\quad)\{1977001-1977361,1978001-1978365,1979003\}.\text{pcp}$	Example of data in a precipitation file. ( ) means all stations from day 1 to day 361 in 1977, and from day 1 to day 365 in 1978, and day 3 in 1979 are modified

\*  $r_{\text{}}$  indicates relative change,  $v_{\text{}}$  indicates value change, SOL\_K is soil hydraulic conductivity, HEAT\_UNITS is the total heat units required for crops to reach maturity,



PLTNFR is crop's nitrogen uptake parameter, precipitation is the mm of daily precipitation.

The encoding scheme allows the parameters to be kept regionally constant to modify a prior spatial pattern, or be changed globally. This gives the analyst greater freedom in depicting the spatial complexity of a distributed parameter. By using this flexibility, a calibration process can be started with a small number of parameters that only modify a given spatial pattern, with more complexity and regional resolution added in a stepwise learning process.

Next, the SWAT model is executed, and the outputs of interest are extracted from SWAT output files (*output.rch*, *output.hru*, *output.sub*). In the last step, post-processing begins, where *SUF12\_post.bat* executes a number of programs, which are briefly described below.

First, *SUF12\_goal\_fn.exe* calculates the objective function. SUF12 allows seven different functions including summation and multiplicative forms of mean square error,  $r^2$ , Chi square, Nash-Sutcliffe, weighted  $r^2$ , and ranked sum of square error aimed at fitting the frequency distributions. Each formulation may lead to a different result; hence, the final parameter ranges are always *conditioned* on the objective function used. The use of a "multi-objective" formulation (Duan et al. 2003; Gupta et al., 1998) where different variables are included in the objective function reduces the non-uniqueness problem. An option is now included in SWAT-CUP where variables from different SWAT output files can be included in the objective function. Furthermore, As SUF12 is iterative; we also found advantages when different objective functions were used in different iterations.

Second, *SUF12\_95ppu.exe* is executed to calculate the 95% prediction uncertainty. SUF12 describes parameter uncertainty by means of a multivariate uniform distribution in a parameter hypercube, while the output uncertainty is quantified by the 95% prediction uncertainty band (95PPU). SUF12 maps uncertainties on the parameters in the hydrological model by bracketing all measurements in the 95PPU while minimizing the thickness of the uncertainty band (Fig. 3) (Abbaspour et al., 2007). Although disaggregation of the errors into their source components is quite desirable, deconvolution of the interacting errors both in the simulated and measured signals is quite difficult, particularly in nonlinear models.

Third, *SUF12\_new\_pars.exe* runs, which calculates updated parameters for the next iteration. For this step, the users must define physically meaningful absolute minimum and maximum ranges for the parameters being optimized. There is no theoretical basis for excluding any one particular distribution. However, because of the lack of information, we assume that all parameters are uniformly distributed within a region bounded by minimum and maximum values. Because the absolute parameter ranges

play a constraining role, they should be as large as possible, yet physically meaningful. Parameter ranges should be based on ranges measured in the watershed and the field under study when possible. SWAT-CUP reads a file called *Absolute\_SWAT\_Values.txt* where the absolute ranges of all parameters are listed. These ranges can be set by the user. When these data are lacking, then the suggested values from the SWAT database could be used. The absolute parameter ranges in the SWAT database are mostly based on professional judgment and the experimental values taken from the literature (Winchell et al., 2010). Updated parameters are then calculated as:

$$b'_{j,\min} = b_{j,\text{lower}} - \text{Max}\left(\frac{(b_{j,\text{lower}} - b_{j,\min})}{2}, \frac{(b_{j,\text{max}} - b_{j,\text{upper}})}{2}\right) \quad j = 1, \dots, p \quad (1)$$

$$b'_{j,\text{max}} = b_{j,\text{upper}} + \text{Max}\left(\frac{(b_{j,\text{lower}} - b_{j,\min})}{2}, \frac{(b_{j,\text{max}} - b_{j,\text{upper}})}{2}\right) \quad j = 1, \dots, p \quad (2)$$

where  $b'$  indicate updated values,  $b_{j,\text{lower}}$  and  $b_{j,\text{upper}}$  are calculated using the best parameter values of the current iteration as well as the confidence intervals around them,  $b_{j,\min}$  and  $b_{j,\text{max}}$  are the absolute parameter ranges, and  $p$  is the number of parameters. The above formulation, while producing narrower parameter ranges for the subsequent iteration; ensure that the updated parameter ranges are always centered on the best estimates of the current iteration. In the formulation of (1) and (2), the uncertainty in the sensitive parameters decrease faster than those of the insensitive parameters due to the inclusion of the confidence interval that is larger for less sensitive parameters.

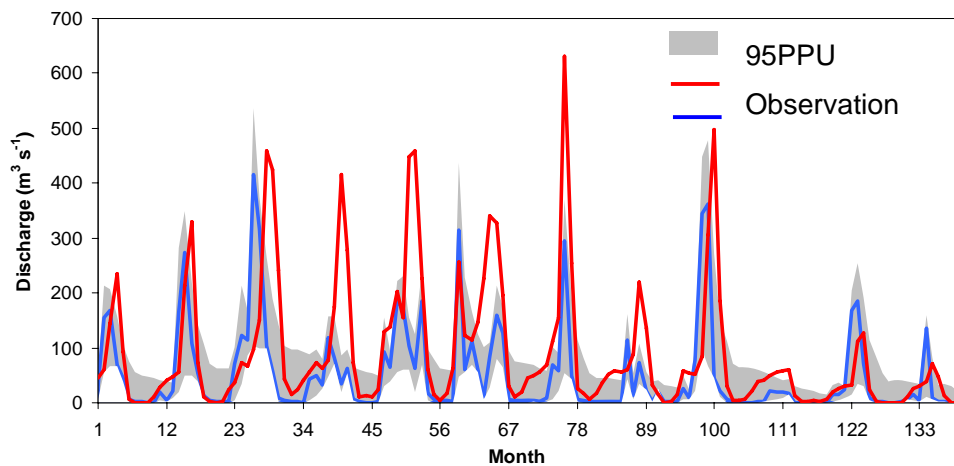


Figure 3. Example of a local (one-at-a-time) sensitivity analysis showing the effect of relative changes in CN2 on discharge.



After updating, the process repeats until a satisfactory value for the objective function or model evaluation parameters, *P-factor* and *R-factor*, are achieved. These indices are explained below.

### 2.3 Goodness of fit in SUFI2

As the simulation result is expressed by the 95PPU band, it cannot be compared with observation signals using the traditional indices such as  $r^2$ , Nash-Sutcliffe (*NS*) or mean square error (*MSE*). For this reason we used two measures referred to as the *P-factor* and the *R-factor* (Abbaspour et al., 2004, 2007). The *P-factor* is the percentage of the measured data bracketed by the 95PPU. This index provides a measure of the model's ability to capture uncertainties. As all the "true" processes are reflected in the measurements, the degree to which the 95PPU does not bracket the measured data, the predictions are in error. Ideally, *P-factor* should have a value of 1, indicating 100% bracketing of the measured data, hence capturing or accounting for all the correct processes. The *R-factor*, on the other hand, is a measure of the quality of calibration and indicates the thickness of the 95PPU. It is calculated as the average distance between the upper and the lower 95PPU divided by the standard deviation of the observed data:

$$R - factor = \frac{\frac{1}{m} \sum_{i=1}^m (X_{s,97.5\%} - X_{s,2.5\%})_i}{\sigma_{obs}} \quad (1)$$

where  $X_{s,97.5\%}$  and  $X_{s,2.5\%}$  represent the upper and lower boundary of the 95PPU for a simulated variable  $X_s$ , and  $\sigma_{obs}$  is the standard deviation of the measured data. *R-factor* should ideally be near zero, hence coinciding with the measured data.

The goodness of calibration and prediction uncertainty is judged on the basis of the closeness of the *P-factor* to 1 (i.e., all observations bracketed by the prediction uncertainty) and the *R-factor* to 0 (i.e., measured and simulated values coinciding). The combination of these two indices together indicates the strength of model calibration and uncertainty assessment as these are intimately linked.

### 2.4. Parallel Processing setup

The structure of parallel SUFI2 is also schematically shown in Figure 2. Although the parallelization is mostly hidden from the user, different processors are involved. The program initially calculates the number of parallel processes that can be submitted to a system by optimizing the number of CPUs against the required RAM to run a certain project.



Although the SUFI2 program has the potential to execute model tasks in parallel, using the full processing capacity of a computer was challenging. There are several hardware components which affect file read and write speed including CPU, RAM, and the hard disk. It was important to minimize communication to the hard disk by utilizing the RAM. All attempts were made to speed up the runs while using less memory by changing the SUFI2 algorithm, primarily in the following two areas:

*1- Changes in the SWAT-edit.exe program:* SWAT-edit is a program that incorporates updated calibration parameters into SWAT input files. Initially, the files in the BACKUP directory are cached, and held static during the calibration process. All relative changes in the parameters are made with respect to their initial values. The number of SWAT input/output files can vary from tens to hundreds of thousands of files, depending on the project, but each file is only a few KB in size. We took advantage of this characteristic and changed SWAT\_edit so that it loads a number of input files on the system's RAM, makes the necessary changes using the cached BACKUP files and writes them to the hard disc. Then it deletes them from the RAM to load the next set of files. This reduces memory usage by up to 90%.

*2- Changes in the SWAT-CUP:* SWAT-CUP functions were split to apply simultaneously on several nodes or parallel jobs. The number of nodes can be the same or fewer than the number of CPUs. Depending on the project size and the available RAM of the system, the program calculates the maximum number of jobs that can be submitted to the system. For example, to have 48 simulations on a machine with 8 processors, 8 nodes can be made, each conducting 6 simulations if the RAM allows. The parallel processing program does not allow the number of nodes to exceed a certain limit if there is a lack of memory. Hence, having a large system RAM ( $\geq 16$  GB) is an advantage.

The changes in the SWAT-CUP package include: a) changes in user interface to make the parallel option available to users, b) showing the status of each parallel node while the program is running, c) preventing system freezing by giving priorities to other jobs being simultaneously executed, and d) disallowing SWAT-CUP sub-processes to continue running in the background when the program is stopped for any reason. When the program is finished, or stopped unexpectedly, all systems resources are restored.

As parallel SUFI2 is being executed, the user sees the following tasks being performed:

*1- Collect and delete unused files.* These are cached files and files in the *ParallelProcessing* directory left over from previous runs in case of program failure or crash. It is necessary to delete these files to clear the RAM and establish the conditions necessary for step 4 below. This step is mostly used when a parallel processing job has already been run in the same directory.

*2- Collect source files.* It counts the number of files in the project directory.



3- *Validate memory usage.* It calculates the number of parallel processes that can be run on the system. In estimating the number of parallel processes, we consider the available RAM of the system, the amount of system cache memory per file, reserve memory for the system's other operations, and SWAT-edit memory usage. SWAT\_edit checks that total parallel processing memory usage plus protected free memory for other operations on the system are less than the available memory. If this constraint is not fulfilled, the program reduces the maximum number of parallel processes.

4- *Synchronize files.* The program copies the necessary files to each parallel folder from the project folder (these files are pre-fetched so the copy operation is done quite fast) and makes them available for each node to read from the corresponding folder.

5- *Collect BACKUP files.* The program enumerates BACKUP files to make the condition ready for pre-fetching all the files in this directory to make them ready for faster read operation by parallel nodes. In this parallel version of SWAT-Edit there is no need to copy the BACKUP directory in every parallel process directory. All the parallel processors will read from the same BACKUP files.

After finishing the program set up, the simulations are divided between different processors and run in a synchronized manner along each other.

After the parallel runs are finished, parallel processing clean up starts to work by collecting output files from each parallel processing directory and concatenating them in the SUFI2.OUT of the main project directories. Then all unused files are deleted, and the RAM which was used during the parallel process, including the RAM which was used by caching the BACKUP files are released.

Now all is done with the parallel section. The rest is post processing, which is done in the same way as the single calibration run by executing *SUFI2\_post.exe*.

### *2.5. Case studies and computer systems*

To demonstrate the functionality of parallel SUFI2, we evaluated the program with six benchmarks, including three hydrological models tested on six different systems. We used one server, three personal computers, and two laptops. Table 2 has a summary of the attributes of these systems. For hydrological models, we built large, medium, and small projects using the SWAT2009 program. The period of simulation for all runs was set to 5 years.

The large-size project is the Danube River Basin, which covers an area of 801,093 km<sup>2</sup>. Danube is Europe's second longest river, flows for a distance of 2,826 km and enters the Black Sea east of Izmail (Ukraine) and Tulcea (Romania). We simulate the Danube river basin using SWAT, where we divide the region into 1,224 smaller subbasins taking into



account elevation, soil, landuse and climatic information. This resulted in 69,875 HRUs. Running the calibration program SUFI2, 48 simulations took approximately 2 days to run on the server without using the parallel option. The medium-size project is the Alberta project that covers an area of 661,185 km<sup>2</sup>. The region is divided into 938 subbasins for a total of 2,689 HRUs. The small-size project (Test project) is a small test example in the SWAT program with only 4 subbasins and 75 files. It should be mentioned that calibration of the hydrological models is not the focus of this study and we only tried to focus on the speed of the calibration process.

### 2.6. Performance measures

There are two performance measures that are commonly used to evaluate the performance of parallel computation: *speedup* and *efficiency* (Houstis et al., 1997, Mateos et al., 2010). Speedup for  $n$  parallel sessions is defined as the computed time of the task when only one processor is used to the computing time when  $n$  processors are used. The efficiency of a parallel system of  $n$  processor is defined as the ratio of actual speedup to ideal speedup, where the ideal speed up is equal to the number of processors.

## 3. Results and Discussion

Parallel SUFI2 was tested on different computers using three different projects. Calibration speedup, designed system efficiency, and peak CPU usage of each system versus the number of processors is shown in Figures 4, 5 and 6, respectively.

Figures 4a and 4b show the speedup of the Danube, the Alberta, and the Test project on machines with 24 and 8 processors, respectively. In the system with 24 CPUs, the speedup of parallel SUFI2 follows closely the ideal speedup up to 8 processors. As the number of the processors increases, the gap between the parallel SUFI2 and the ideal performance grows. As the number of jobs increases, the communication of each CPU with the hard disk increases. The loss of speed is, hence, mostly due to hard disk limitation. The use of Redundant Array of Independent Disks (RAID) or Solid State Drive (SSD) should improve the performance. If the number of parallel jobs is set to 24, then in the Danube project (24 x 69,875) files are simultaneously read and written to the hard disk. For this reason, as the number of parallel processes increases, the speedup decreases for large projects. Hence, Danube shows a smaller speedup than the Alberta or Test project for 24 CPUs (Figure 4a).



**Table 2**

Description of the 6 computer systems used to test the parallel Sufi2.

<p><b>Server 1</b> 24 CPUs Processors: Intel(R) Xeon(R) CPU <a href="#">L5640@2.27GHz</a> (2 processor) RAM = 24.0 GB System type = 64-bit OS Windows 7</p>	<p><b>PC 1</b> 8 CPUs Process: Intel(R) Core(TM) i7 CPU <a href="#">860@2.8 GHz</a> RAM = 16.0 GB System type = 64-bit OS Windows 7</p>
<p><b>PC 2</b> 2 CPUs Processor: Intel(R) Core(TM) 2 Duo CPU <a href="#">E8600@3.3GHz</a> RAM = 3.46 GB System type = 32-bit OS Windows XP</p>	<p><b>PC 3</b> 2 CPUs Processor: Intel(R) Pentium(R) D CPU 3.01 GHz RAM = 1.00 GB System type = 32-bit OS Windows XP</p>
<p><b>Laptop 1</b> 2 CPUs Processor: Intel(R) Core(TM) 2 Duo CPU <a href="#">T960000 @ 2.80 GHz</a> RAM = 3.0 GB System type = 32-bit OS Windows XP</p>	<p><b>Laptop 2</b> 2 CPUs Processor: Intel(R) Core(TM) 2 Duo CPU <a href="#">P8700 @ 2.53 GHz</a> RAM = 4.0 GB System type = 64-bit OS Windows 7</p>

Figures 4 (c,d,e,f) shows the speedup of running the same projects on 2 PCs with weaker capabilities than PC 1, and two laptops with only 2 CPUs. Because the machines only have 2 processors, we could only submit up to 2 parallel jobs. The speedup achieved using parallel SUFI2 is around 1.9 with 2 processors. This compares quite well to the ideal speedup, indicating that the running time was halved. The small deviations in different machines and projects have to do with the initial state of the computers. For the best result the computers should be re-started before each run to release the remaining occupied memories from previous computer use. It should be noted that the Danube project is missing from Figures 4 c,d,e. This is because the memory limitation, as the size of the project was too large for these machines to run two parallel processes.



Figure 5 illustrates the efficiency of parallel SUFI2. In general, the efficiency of a parallel system is less than unity because of the system overhead such as the resolution of conflicting demands between shared resources, the communication time between processors, and the inability to keep every processor fully busy. For the ideal case, when the number of processors allocated to a particular task increases, a higher speedup (reduction in computing time) can usually be obtained. The efficiency therefore decreases for the above reasons and the fact that the processors can not be fully utilized. For small requests, such as the Test case in this study, the overhead introduced by the initial model set up is not compensated because the number of processors is too small. This can be seen in Figure 5a, which shows that for very small jobs the server becomes more efficient as the number of processors increase.

Figure 6 shows the peak CPU usage. In Server 1 and PC 1 a non-parallelized program used little of the CPU capacities. As the number of parallel jobs increases, more CPUs are used. In each machine, as the number of parallel jobs equals the number of CPUs, 100% of the CPU is used.

A few recommendations should be followed when running SUFI2 in parallel mode. 1) Do not run multiple SWAT-CUP projects on a single system using the parallel process. 2) It is recommended to restart the computers before starting the parallel calibration project to access the full memory available on the computer although the program itself will clean up the unused files related to the SWAT-CUP project. As the number of parameters increase, SWAT\_edit requires more RAM to cache the files. 3) No other memory consuming programs along the parallel SWAT-CUP should be run simultaneously. 4) The number of simulations should be (but not absolutely necessary) a multiple of the number of parallel processing jobs. 5) It is very important to switch off any antivirus program during the parallel program run or exclude the corresponding directory from the virus scan. The antivirus scan decreases the speed of parallel SUFI2 substantially.

#### **4. Conclusion**

In this paper, we presented parallel SUFI2, a framework that automatically and transparently parallelizes the SUFI2 optimization program for higher performance calibration purposes. Performance results with both small and large size projects show that parallel SUFI2 achieves good speedup and reasonable scalability in most cases.

Although the parallel SUFI2 is designed to be used on any system, larger time savings can be achieved with multiple CPUs and larger RAM memory. Note that the emphasis of this research was not on achieving the highest possible speedup and that our current implementation is an early proof-of-concept prototype that does not contain

## **enviroGRIDS – FP7 European project**

Building Capacity for a Black Sea Catchment

Observation and Assessment supporting Sustainable Development



---

optimization or refinement. Computations based on GPU technology hold the promise of achieving greater speed ups in execution of hydrologic models (Kalyanapu, et al., 2011; Singh, et al., 2011). However, we show that parallel SUFI2 is able to achieve reasonable speedup on real-world computation-intensive calibration applications, while significantly exceeding the performance of non parallelized packages.

### **Acknowledgments**

This project has been funded by the European Commission's Seventh Research Framework through the enviroGRIDS project (Grant Agreement n 226740).

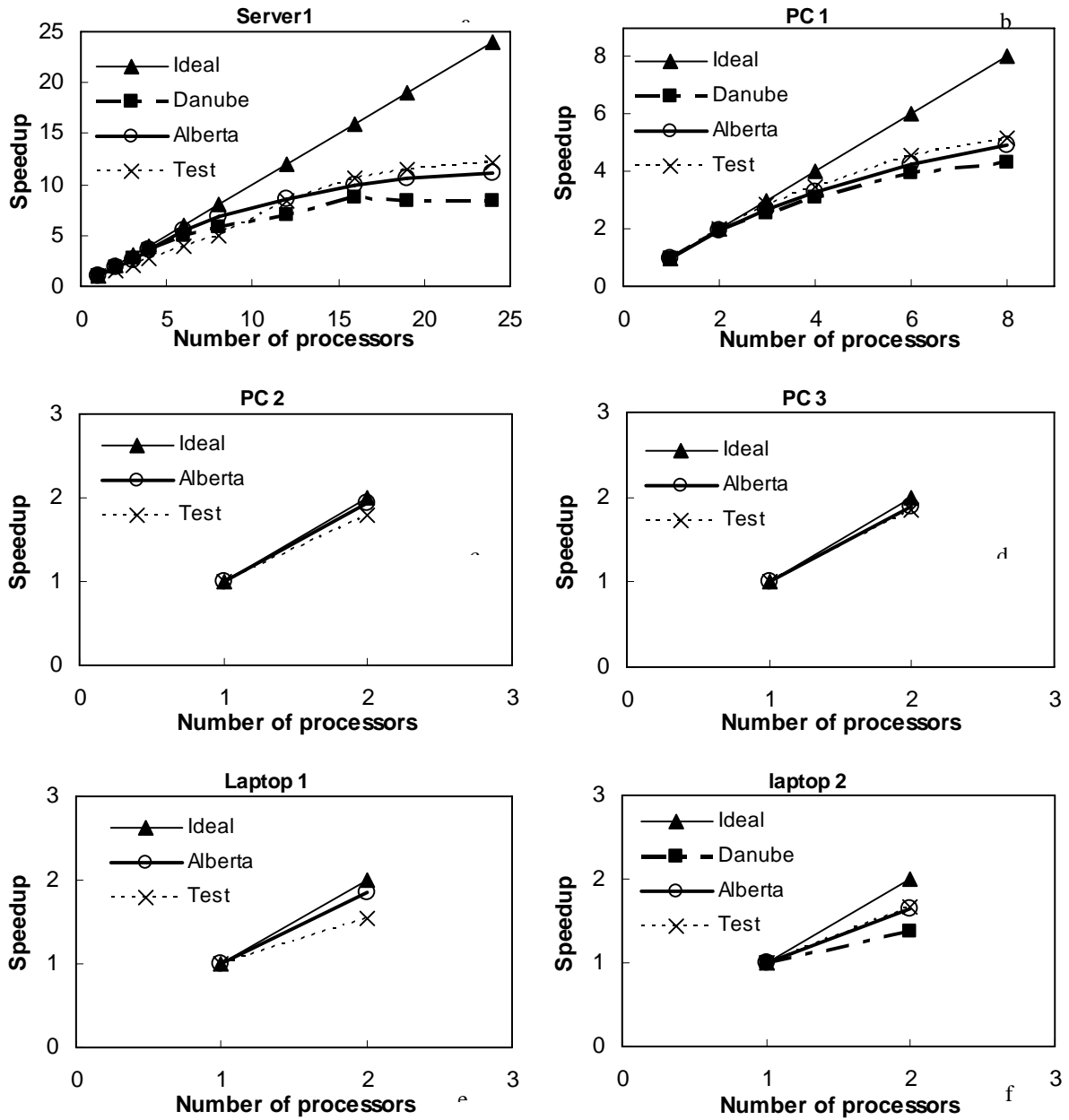


Figure 4. The 95PPU graph in the SWAT-CUP interface. Also shown are the observed signal and the best simulation. The 95PPU is given for every variable considered in the objective function.

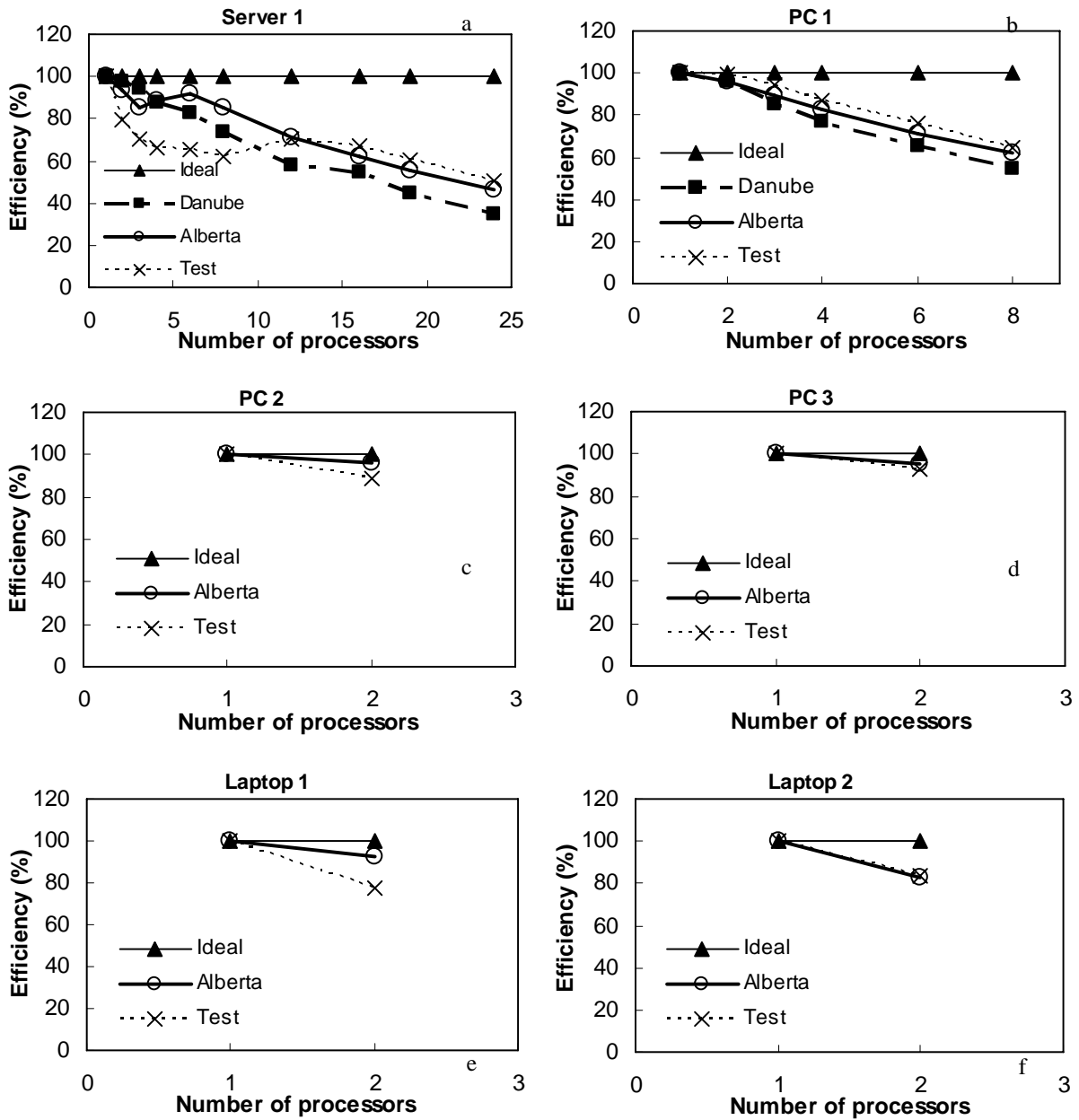


Figure 5. The speedup achieved for different computer systems and SWAT projects. Number of processors on the horizontal axis indicates the number of parallel jobs submitted. The Figure shows that most projects could be run 10 times faster with about 16 processors. Note that PC 2, PC 3, and Laptop 1 could not handle the size of the Danube project for two parallel runs.

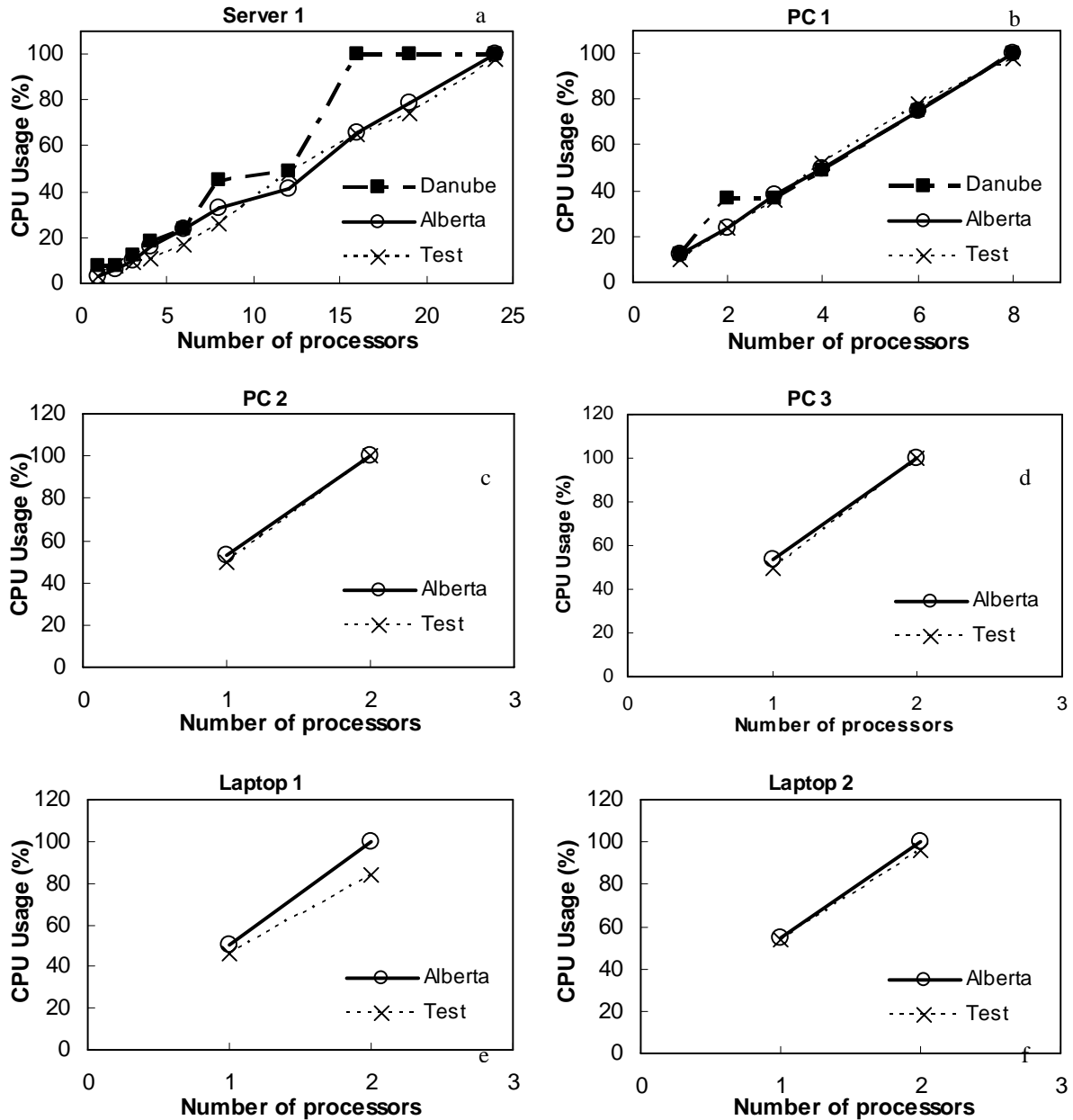


Figure 6. Percentage efficiency calculated for different computer systems and SWAT projects. The decrease in efficiency is a function of the size of the project and the characteristics of the hard disk.



---

## **Case Study 1**

### **Don River Basin**

#### **Hydrological modeling and remote sensing analysis for the**

---

## **1. Introduction**

### **1.1 Objectives of study**

The overall objective of this study was to make use of remote sensing products to support better understanding of the hydrology of the upper Don catchment. The SWAT model developed for the Upper Don River Catchment by Central European University (CEU) has been used as a case study for application of remote sensing study.

The specific objectives of the study were;

- Generate remote products of ET and snow cover
- Analysis of the products to support understanding of the catchment hydrology
- Prepare the products to enable their application in SWAT Model calibration and validation
- Setup a SWAT model of the catchment and use the remote sensing products to calibrate it

### **1.2 Description of the Upper Don River Basin**

The Azov is a sea on the south of Eastern Europe representing unique and important ecosystem in the Black Sea catchment. It is bounded in the north and west by Ukraine and in the east by Russia, and connected with the Black Sea through the Kerch Strait in the south.

The Don is one of the main tributaries, bringing major part of freshwater to the Azov Sea. The Upper Don River subcatchment (Fig. 1), chosen for study, plays significant role in the region, comprising more than 50% of the total Don Basin catchment area and generating the Tsimlyansk reservoir inflow, the largest freshwater body in the basin. The reservoir plays important role in securing navigation and freshwater provision in the region.

The area is dominantly comprised of rainfed crops and mosaic croplands, therefore it can be considered as typical agricultural watershed. Predominance of agricultural areas

and relatively high urbanization levels determine changes in surface runoff and water yields, generated in the sub-catchment.

The sub-basin is characterized by relatively high humidity and moderate precipitation rates. Rivers are mainly fed by snowmelt, which highly varies and determines high seasonal variability and increase of water level during the flood period in spring

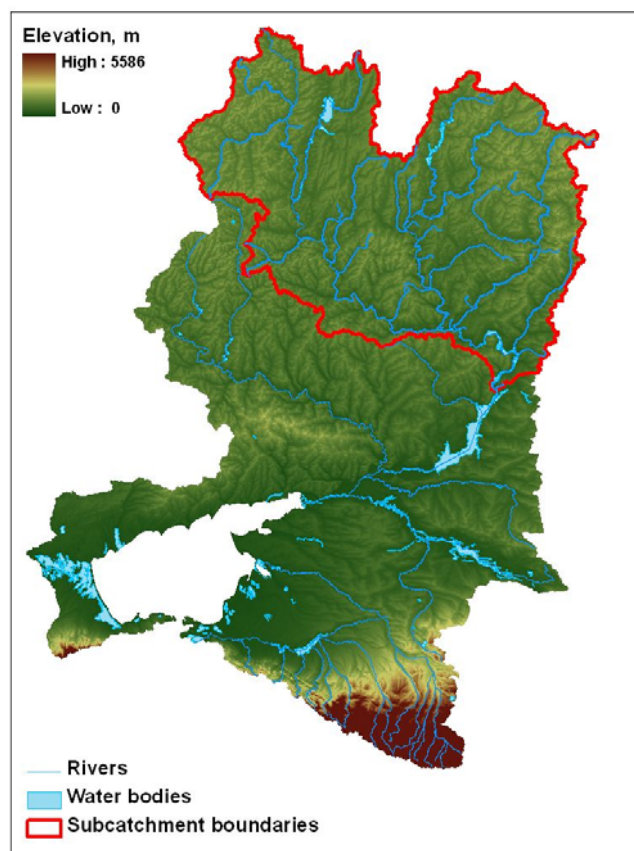


**Fig. 1.** Area of study (Gilfanova 2012)

## **2 The hydrological model description**

### **2.1 SWAT description**

SWAT was developed by the U.S. Department of Agriculture, Agricultural Research Service (Arnold and Fohrer 2005; Gassman *et al.* 2007). Gassman (2007) has made the comprehensive overview of the tool application.



Model simulates hydrological processes for watershed divided into subbasins or sub-catchments, represented by hydrologic response units (HRUs). These units are defined based on input data on land use, management, and soil parameters. Subbasins or sub-watersheds are spatially related to each other, though HRUs are not identified spatially, it only represents the percentage of the sub-watershed area.

The overall model continuously simulates daily water budget in each HRU, and can be calculated as following:

$$\Delta SW = P - Q - ET - DP - QR,$$

where

$\Delta SW$  - daily change in soil water content

P - precipitation

Q - surface runoff

ET – evapotranspiration

DP - vertical percolation,

QR - return flow to the stream channel.

## **2.2 Model set up**

For developing SWAT model CEU used ArcGIS-ArcView extension and graphical user input interface for SWAT ArcSWAT 2009.93.7b (Winchell et al. 2010) uploading different datasets in the format required by software.

The watershed has been delineated based on the data on elevation derived from the global dataset topography Shuttle Radar Topography Mission (SRTM) (Fig. 1). As a result, 37 subbasins with 37 outlets and 530 HRUs respectively have been defined for the watershed. The outlet adjacent to the entrance of the Don River to the Tsimlyansk reservoir has been chosen as a main outlet of the sub-catchment.

Unique hydrologic response units (HRU) have been determined based on combination of classes of land use, soil and slope.

Reclassified MODIS land cover datasets, developed by EnviroGRIDS project for Metronamica model have been used for land use data input. Global soil dataset FAO has been used for soil data input.

In order to simulate meteorological parameters in the model the data for the period 1998-2008 from 5 stations have been used.

The period of simulation for 7 years from 1 January 2001 to 31 December 2008 has been chosen. Two years of warm up period, which is required for better simulation



performance, have been set up. Default options with skewed normal distribution of rainfall and monthly printout setting have been selected. Finally, model simulation was run and simulation results were obtained through the Read SWAT output command.

### **2.3 Model calibration**

The SWAT-CUP application (Abbaspour 2011) has been used for model calibration and validation.

The SUFI2 method was chosen for calibration. In SUFI-2, uncertainty of input parameters are defined as unique distributions, while model output uncertainty is quantified by the 95% prediction uncertainty (95PPU) calculated at the 2.5% and 97.5% levels of the cumulative distribution of output variables obtained through Latin hypercube sampling.

SWAT-CUP program contains different input parameters of reaches, subbasins, that can be edited and optimized by user.

Observed monthly data on the water discharge for 9 outlets, covering period 2001-2008, was prepared in required format and loaded in the SWAT-CUP.

The parameters included in calibration are presented in Table 1. Streamflow was calibrated based on observed data from 9 gages until the Nash-Sutcliffe efficiency values reached from -0.6 to 0.3 on a monthly scale.

**Table 1.** Parameters used in calibration process

Alpha_Bf	Base flow Alpha factor (days)
Alpha_Bnk	Baseflow alpha factor for bank storage
Cn2	Initial SCS Curve Number II value
Esco	Soil evaporation compensation factor
Gw_Delay	Ground water delay (days)
Sftmp	Snow fall temperature (°C)
Snocovmx	Minimum snow water content that corresponds to 100% snow cover
Timp	Snow pack temperature lag factor



In order to improve calibration results it was decided to apply additional techniques to investigate hydrological parameters in the sub-catchment and develop products, which can be applied in further SWAT Model calibration and validation.

#### **2.4 Sensitivity analysis**

Within the SWAT model, the LH-OAT algorithm has been implemented (van Griensven et al.) with the aim to provide a ranking of the importance of the numerous parameters in SWAT. The algorithm has been adapted for this study so that it can analyze the sensitivities of parameters on the overall mass balance outputs, such as evapotranspiration estimates, averaged over the entire simulation time and river basin, having units of mm/year (as printed in the output.std file).

From the Table 3, it can be concluded that the main parameters affecting evapotranspiration are soil related parameters: ESCO (soil evaporation), sol\_awc, sol\_k, followed by the snow parameter “Timp” and the curve number (affecting infiltration).

The snow is affected by crop related parameters BLAI and CANMX followed by soil related parameters and Timp.



**Table 2:** Calibrated parameters

Parameters	Descriptions
Alpha_Bf	Base flow Alpha factor (days)
Biomix	Biological mixing efficiency
Blai	Maximum potential leaf area index
Canmx	Maximum canopy storage (mm)
Ch_K2	Channel effective hydraulic conductivity (mm/hr)
Ch_N2	Manning's 'n' value for main channel
Cn2	Initial SCS Curve Number II value
Epc0	Plant uptake compensation factor
Esco	Soil evaporation compensation factor
Gw_Delay	Ground water delay (days)
Gw_Revap	Ground water "revap" co-efficient
Gwqmn	Threshold water depth in the shallow aquifer for flow (mm)
Revapmn	Threshold water depth in the shallow aquifer for "revap" (mm)
Sftmp	Snow fall temperature (°C)
Slope	Average slope steepness (m/m)
Ssubbsn	Average slope length (m)
Smfmn	Melt factor for snow on December 21 (mm H <sub>2</sub> O/°C-day)
Smfmx	Melt factor for snow on June 21 (mm H <sub>2</sub> O/°C-day)
Smtmp	Snow melt base temperature (°C)
Sol_Al0	Moist soil Albedo
Sol_Awc	Available water capacity (mm H <sub>2</sub> O/mm soil)
Sol_K	Saturated hydraulic conductivity (mm/hr)
Sol_Z	Soil depth (mm)
Surlag	Surface runoff lag time (days)
Timp	Snow pack temperature lag factor
Tlaps	Temperature lapse rate ((°C/km)



**Table 3:** Results of the sensitivity analysis

	Obj F.= MSE	SNOW	SURFACE RUNOFF Q	LATERAL SOIL Q	GROUNDWATER (SHAL AQ) Q	TOTAL WATER YLD	ET
Alpha_Bf	4	27	27	27	17	17	27
Biomix	20	7	11	11	14	14	10
Blai	10	2	7	6	9	9	7
Canmx	11	1	9	5	8	8	6
Ch_K2	7	27	27	27	27	27	27
Ch_N2	13	27	27	27	27	27	27
Cn2	1	8	1	8	3	4	5
Epco	18	9	14	12	18	18	12
Esco	2	6	3	9	2	1	1
Gw_Delay	16	27	27	27	13	15	27
Gw_Revap	19	27	27	27	10	12	27
Gwqmn	6	27	27	27	1	3	27
Revapmn	14	27	27	27	7	6	27
Sftmp	27	27	27	27	27	27	27
Slope	17	27	12	3	16	10	9
Ssubbsn	22	27	27	27	20	27	27
Smfmn	27	27	27	27	27	27	27
Smfmx	27	27	27	27	27	27	27
Smtmp	12	27	10	10	12	16	11
Sol_Alb	21	27	13	13	19	19	13
Sol_Awc	5	5	4	1	5	2	2
Sol_K	15	27	6	4	15	11	8
Sol_Z	9	4	5	7	4	5	3
Surlag	8	27	8	27	11	13	27
Timp	3	3	2	2	6	7	4
Tlaps	27	27	27	27	27	27	27



### **3 Remote sensing analysis**

While some hydrologic information has been found to form very important information if watershed hydrology is to be better understood, the practicality of obtaining this information through field measurement has been a great challenge. Despite the ability to obtain field measurements in some cases, determination of the spatial variation still remains a challenge where the cost of carrying out field measurements and the time required has mainly been the challenge. It's against this background that the technology of obtaining this information without direct contact came into application and has over the years received a lot of recognition and application. The technology has been widely referred to as remote sensing.

Some other advantages that comes with the technology can be summarized as; no interference between data acquisition devices and the process being measured; spatially distributed measurements instead of point measurements; high spatial and temporal resolution; data available in digital form therefore easy use; information can be retrieved for remotely located and inaccessible areas (De Troch et al., 1996). With this technology being utilized within the field of hydrologic sciences, massive benefits have been ripped with the principal benefit being better understanding of hydrologic processes thereby supporting better simulation in models. Some very good example of products coming out of remote sensing are the highly dynamic land surface hydrologic parameters such as soil moisture, evapotranspiration, NDVI, LAI and the seasonally varying land surface features such as vegetation structure or hydrodynamic roughness. In these study the focus was on ET, LAI and snow cover. ET and snow cover are hydrologic components that play a big role in the hydrologic cycle therefore generating these products and understanding dynamics within them would greatly support better understanding the sub-basin. This would contribute subsequently support better modeling of the hydrology of the sub-basin.

#### **3.1 Evapotranspiration**

##### **3.1.1 Surface Energy Balance System (SEBS)**

The SEBS algorithm of estimation of atmospheric turbulent fluxes from satellite earth observation imagery as proposed by Su (2002) comes with sub-tools aimed at estimation of some key land surface parameters from sensor obtained radiance and reflectance. These parameters include among others; land surface temperature, surface albedo, emissivity, NDVI, vegetation fractions. It must however be noted that estimation of all these parameters and especially accurately contributes to the accuracy of the ultimate results to be obtained. In the event that some parameters cannot easily be



obtained, SEBS has been designed to roughly estimate those missing parameters using empirical equations. Other important information obtained from satellite data that are much needed in the SEBS algorithm are the solar/sensor zenith and azimuth angles. Other than the satellite estimated land surface parameters, the SEBS algorithm also requires ground data that are mostly measured from meteorological stations. These include data like air temperature, air pressure, humidity, wind speed and sunshine hours. Measurements of downward radiations are also very important for the algorithm.

The surface energy balance equation that the SEBS algorithm uses is represented as;

$$R_n = G_o + H + \lambda E$$

Where;

$R_n$  = Net radiation

$G_o$  = Soil Heat flux

$H$  = Turbulent sensible heat flux

$\lambda E$  = Turbulent latent heat flux ( $\lambda$  is the latent heat of vaporization and  $E$  is the actual evapotranspiration)

Within the surface energy balance equation, the Net radiation is solved using the equation;

$$R_n = (1 - \alpha) \cdot R_{swd} + \varepsilon \cdot R_{lwd} - \varepsilon \cdot \sigma \cdot T_o^4$$

Where;

$R_n$  = Net radiation

$\alpha$  = Albedo

$R_{swd}$  = Downward solar radiation

$\varepsilon$  = Emissivity

$R_{lwd}$  = Downward long wave radiation

$\sigma$  = Stefan-Bolzman constant

$T_o$  = Surface radiative temperature

In turn the soil heat flux ( $G_o$ ) is determined using the equation;

$$G_o = R_n \cdot [\Gamma_c + (1 - f_c) \cdot (\Gamma_s - \Gamma_c)]$$

Where;

$\Gamma$  = ratio of soil heat flux to Net radiation ( $\Gamma_c = 0.05$  for full vegetation canopy and  $\Gamma_s = 0.315$  for bare soil)

$f_c$  = Fractional canopy coverage

Determination of the evaporative fraction is then estimated by consideration the existence of two core limiting cases, the dry and wet limits. The dry limit in this case represents the point where the soil is believed to be totally dry therefore the latent heat is zero, meaning no evaporation occurs. This translates to the sensible heat flux being at its maximum. Therefore this scenario modifies the surface energy balance equation to;

$$\lambda E_{dry} = R_n - G_0 - H_{dry} \equiv 0 \quad \text{or} \quad H_{dry} = R_n - G_0$$

The wet limit on the other hand represents the point when evapo-transpiration occurs at its maximum, which is at the potential rate. At this point the sensible heat flux is at its minimum. This scenario modifies the surface energy balance equation to;

$$\lambda E_{wet} = R_n - G_0 - H_{wet} \quad \text{or} \quad H_{wet} = R_n - G_0 - \lambda E_{wet}$$

With the above limits being established, the relative evaporation is then evaluated using the relation;

$$\Lambda_r = \frac{\lambda E}{\lambda E_{wet}} = 1 - \frac{H - H_{wet}}{H_{dry} - H_{wet}}$$

Substitution of the other already obtained equations into this equation leads to the equation;

$$\Lambda_r = 1 - \frac{H - H_{wet}}{H_{dry} - H_{wet}}$$

This ultimately leads to the evaporative fraction which is represented as;

$$\Lambda = \frac{\lambda E}{H + \lambda E} = \frac{\lambda E}{R_n - G} = \frac{\Lambda_r \cdot \lambda E_{wet}}{R_n - G}$$

The evaporative fraction is may also be referred to as the crop coefficient especially when SEBS is applied in an agricultural context.

Finally the sensible heat flux (H) in the surface energy balance equation is determined by solving a series of non-linear equations but applying the similarity theory. Determination of the sensible heat flux (H) is carried out while fully making use of the dry and wet limits that have already been established.

### 3.1.2 Download of remote sensing imagery

In this study, imagery products from the Moderate Resolution Imaging Spectroradiometer (MODIS) instrument aboard the Terra satellite were selected and downloaded after an analysis of spatial/temporal resolution and wide area coverage advantages and disadvantages. A trade-off was made between resolution and efficiency of use in generation of products. MODIS products don't come with very good spatial resolution especially when compared to other products like Landsat, Spot and Aster however they have the great advantage of temporal resolution along with wide area coverage that in this case best suited the study area. The advantage of temporal



resolution is however sometimes reduced by the existence of cloud cover that greatly inhibits the use of the products in a study. This was especially the case for this study where getting cloud-free imagery covering the entire study area was almost impossible. Partly cloud-free images were therefore also utilized in the study by masking out the cloud-covered areas and later developing an interpolation technique to fill up the masked out regions. To minimize the likely errors obtained from the interpolation techniques, images with at most 15% cloud cover were utilized.

### **3.1.3 Preparation of MODIS data**

Prior to the making use of the MODIS products to generate the required products, the raw images had to be processed. Processing of the raw data was preceded by an exercise that entailed browsing and viewing the files that were archived in HDF format. The Hierarchical Data Format (HDF) is a file formats designed to store and organize large amounts of numerical data. The role of the browsing and viewing exercise was to acquire important information that would be needed during MODIS data processing. This was possible by making use of the HDFView tool, a java based tool developed by the HDF group. The relevant information obtained using this tool were mainly the calibration scale and offset coefficients for the different bands. This information was needed when transforming the raw bands into radiance or reflectance.

Processing of the raw MODIS data was also preceded by re-projection of the raw data from the swath (orbit based) projection to a universally accepted projection system that would also enable effective and efficient use of the data within almost all GIS software. In the study, Universal Transverse Mercator (UTM) was selected as the projection system of use. Re-projection was therefore implemented using the Modis Reprojection Tool Swath (mrtswath), a java based tool obtained from the Land Processes Distributed Active Archive Center (LP DAAC) website. It's also during re-projection of the raw data that conversion was also carried out from HDF format to TIFF/GeoTIFF format.

### **3.1.4 Processing of MODIS data**

In this study ILWIS 3.8 was selected as the main GIS software due to the presence of many inbuilt tools relevant for this study thereby greatly reducing the time spent to produce ET results. However, the firm appreciation of the fact that other GIS software also possesses other forms of advantages over ILWIS that were needed in this study, not all GIS operations were limited to ILWIS but where necessary the other GIS software were utilized.



Therefore the already re-projected and converted MODIS data were imported into ILWIS. It's within ILWIS that conversion of raw MODIS data (simplified integer number) to radiance and reflectance was carried out for the individual bands relevant to this study.

### **3.1.5 Atmospheric Correction of MODIS processed data**

The already re-projected and converted MODIS data couldn't be utilized unless correction for atmospheric defects was carried out. Atmospheric effect was therefore carried out by following the simplified method of atmospheric correction (SMAC), an algorithm developed by Rahman et al (1994). This correction algorithm required making use of information on sensor coefficients, Aerosol optical depth (AOD), ozone content, water vapor content, surface pressure along with solar/sensor zenith and azimuth. All these information were obtained from various sources ranging from websites to processing of MODIS of raw data.

### **3.1.6 Generation of preliminary ET input data**

With the atmospheric effect corrected MODIS data ready, input products to carry out evapotranspiration were then generated. These were surface Albedo, Normalized Difference Vegetation Index (NDVI), Emissivity, Emissivity difference, Vegetation fraction and land surface temperature.

To generate surface albedo, a formula developed by Liang et al (2003) was utilized which required making use the atmospherically corrected surface reflectance from bands 1, 2, 3, 4, 5 and 7.

NDVI was generated using the traditional formula;

$$NDVI = \frac{(B_{ntr} - B_{rsd})}{(B_{rsd} + B_{ntr})}$$

Vegetation fraction/proportion was then also generated by making use of the NDVI products in the formula;

Vegetation fraction



=

Next the land surface emissivity was generated by making use of the formula developed by Sobrino et al (2003). The formula made use of visible and near infrared reflectance bands and the surface albedo.

Finally the land surface temperature was generated by making use of the split window method that was also developed by Sobrino et al (2003). The method required input from brightness temperature information obtained from the radiances of bands 31 and 32, water vapor, land surface emissivity and surface emissivity difference.

### **3.1.7 Meteorological data**

Evapotranspiration estimation from remote sensing cannot be effectively and successfully achieved without making use of ground based meteorological data. Therefore in this study, data within the study area was collected and put into use. The meteorological data available and utilized in this case were specific to the days of clear sky satellite overpass of the MODIS instrument.

In this study, Meteorological data from Gotnja meteorological station was collected and prepared for use in the analysis. Here the primary weather aspects needed for the study were;

- Wind speed at 2 meter reference height (m/s)
- Relative Humidity (%)
- Sunshine duration (hours)
- Air temperature (°C)
- Mean daily air temperature (°C)
- Specific humidity (kg/kg)



**Table 4:** Meteorological data for the clear sky days in 2002

	<b>Dates</b>						
	<b>4/20/2002</b>	<b>5/8/2002</b>	<b>7/6/2002</b>	<b>7/18/2002</b>	<b>7/19/2002</b>	<b>7/20/2002</b>	<b>7/30/2002</b>
Julian dates	111	129	188	200	201	202	212
Wind speed (m/s)	1	2	2	2	1	3	3
Relative Humidity (%)	62	51	67	48	44	43	56
Sunshine duration (hours)	9	12	12	14	14	14	10
Air temperature (°C)	7.8	15	22.8	22.3	22.4	23.8	24.37
Mean daily air temperature (°C)	10.65	12.6	22.95	21	20.7	22.2	24.45
Specific humidity (kg/kg)	0.0041	0.0055	0.0117	0.0081	0.0075	0.0082	0.0108
	<b>Dates</b>						
	<b>7/31/2002</b>	<b>8/11/2002</b>	<b>8/20/2002</b>	<b>9/13/2002</b>	<b>9/29/2002</b>	<b>11/18/2002</b>	
Julian dates	213	224	233	257	273	323	
Wind speed (m/s)	2	1	2	2	1	2	
Relative Humidity (%)	86	39	60	75	83	91	
Sunshine duration (hours)	15	7	11	11	9	8	
Air temperature (°C)	18.8	20.2	18.5	10.1	5.4	3.2	
Mean daily air temperature (°C)	24.65	18.55	20	9.55	7.8	7.45	
Specific humidity (kg/kg)	0.0169	0.0053	0.0081	0.0054	0.0047	0.0044	



**Table 5:** Meteorological data for the clear sky days in 2002

	Dates						
	4/16/2003	4/17/2003	5/26/2003	5/27/2003	8/29/2003	9/23/2003	9/30/2003
Julian dates	107	108	147	148	242	267	274
Wind speed (m/s)	4	3	3	2	4	3	2
Relative Humidity (%)	55	44	49	45	60	72	63
Sunshine duration (hours)	7	12	14	16	12	10	8
Air temperature (°C)	5.3	3.6	20.6	22	18.2	13	13.8
Mean daily air temperature (°C)	5.85	5.25	21	20.65	20.65	15.8	15.3
Specific humidity (kg/kg)	0.0031	0.0022	0.0075	0.0075	0.0078	0.0068	0.0062

### 3.1.8 Evapotranspiration results

The results achieved from the analysis to determine ET for different dates of the years 2002 and 2003 are hereby summarized in the table below. Actual ET maps for the different days are presented in the appendix.



**Table 6:** Remote sensing evapotranspiration results

<b>2002</b>	<b>Dates</b>						
	<b>4/20/2002</b>	<b>5/8/2002</b>	<b>7/6/2002</b>	<b>7/18/2002</b>	<b>7/19/2002</b>	<b>7/20/2002</b>	<b>7/30/2002</b>
Julian dates	111	129	188	200	201	202	212
Reference ET (mm/day)	2.3	2.9	3.7	5.0	3.9	3.9	3.7
	<b>Dates</b>						
	<b>7/31/2002</b>	<b>8/11/2002</b>	<b>9/13/2002</b>	<b>9/29/2002</b>			
Julian dates	213	224	257	273			
Reference ET (mm/day)	3.8	4.2	2	1.3			
<b>2003</b>	<b>Dates</b>						
	<b>4/16/2003</b>	<b>4/17/2003</b>	<b>5/26/2003</b>	<b>5/27/2003</b>	<b>8/29/2003</b>	<b>9/23/2003</b>	<b>9/30/2003</b>
Julian dates	107	108	147	148	242	267	274
Reference ET (mm/day)	2.0	2.5	3.9	4.3	3.0	2.1	1.9

### 3.1.9 Estimation of reference ET (ET<sub>o</sub>)

To support better evaluation and interpolation of the generated ET products from remote sensing, reference ET was estimated using data from the available meteorological stations. This estimation was implemented using FAO ET<sub>o</sub> calculator which made it possible to generate time series results of ET<sub>o</sub> for the years 2002 and 2003. Below are the time series results generated for the two years under consideration in this study.

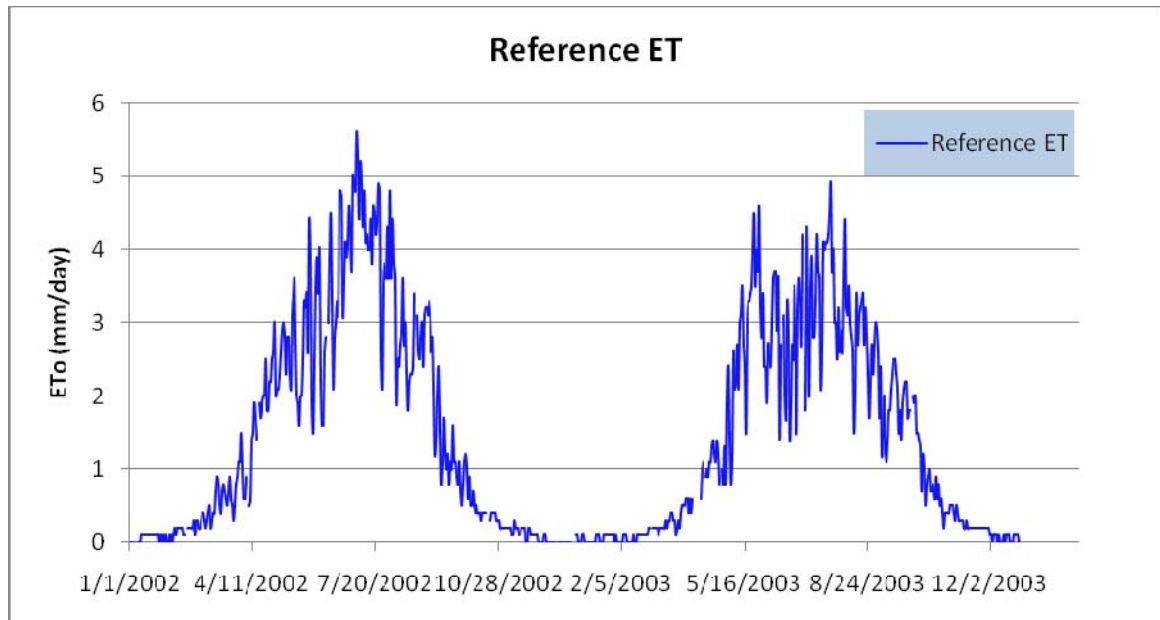


Fig. 2: Time series results of reference Evapotranspiration

Reference ET results for the dates when remote sensing analysis of ET was carried are also presented in the tables below.



**Table 7:** Reference evapotranspiration results for the clear sky days

<b>2002</b>	<b>Dates</b>						
	<b>4/20/2002</b>	<b>5/8/2002</b>	<b>7/6/2002</b>	<b>7/18/2002</b>	<b>7/19/2002</b>	<b>7/20/2002</b>	<b>7/30/2002</b>
Julian dates	111	129	188	200	201	202	212
Reference ET (mm/day)	2.0	2.8	4.4	4.5	4.2	4.4	3.6
	<b>Dates</b>						
	<b>7/31/2002</b>	<b>8/11/2002</b>	<b>9/13/2002</b>	<b>9/29/2002</b>			
Julian dates	213	224	257	273			
Reference ET (mm/day)	4.8	2.7	1.7	1.1			
<b>2003</b>	<b>Dates</b>						
	<b>4/16/2003</b>	<b>4/17/2003</b>	<b>5/26/2003</b>	<b>5/27/2003</b>	<b>8/29/2003</b>	<b>9/23/2003</b>	<b>9/30/2003</b>
Julian dates	107	108	147	148	242	267	274
Reference ET (mm/day)	0.9	1.1	3.7	4.6	3.0	2.2	1.9

**SWAT model ET products**

**Table 8:** SWAT evapotranspiration results for the clear sky days

<b>2002</b>	<b>Dates</b>						
	<b>4/20/2002</b>	<b>5/8/2002</b>	<b>7/6/2002</b>	<b>7/18/2002</b>	<b>7/19/2002</b>	<b>7/20/2002</b>	<b>7/30/2002</b>
Julian dates	111	129	188	200	201	202	212
Reference ET (mm/day)	1.43	1.36	3.39	2.22	2.48	1.71	1.56
	<b>Dates</b>						
	<b>7/31/2002</b>	<b>8/11/2002</b>	<b>8/20/2002</b>	<b>9/13/2002</b>	<b>9/29/2002</b>		
Julian dates	213	224	233	257	273		
Reference ET (mm/day)	1.06	0.78	0.5	1.01	0.84		
<b>2003</b>	<b>Dates</b>						
	<b>4/16/2003</b>	<b>4/17/2003</b>	<b>5/26/2003</b>	<b>5/27/2003</b>	<b>8/29/2003</b>	<b>9/23/2003</b>	<b>9/30/2003</b>
Julian dates	107	108	147	148	242	267	274
Reference ET (mm/day)	0.8	1.3	2.22	2.25	0.78	0.64	0.73

### 3.1.1 3.1.11 Comparison of Reference ET, SWAT ET and Remote sensing ET results

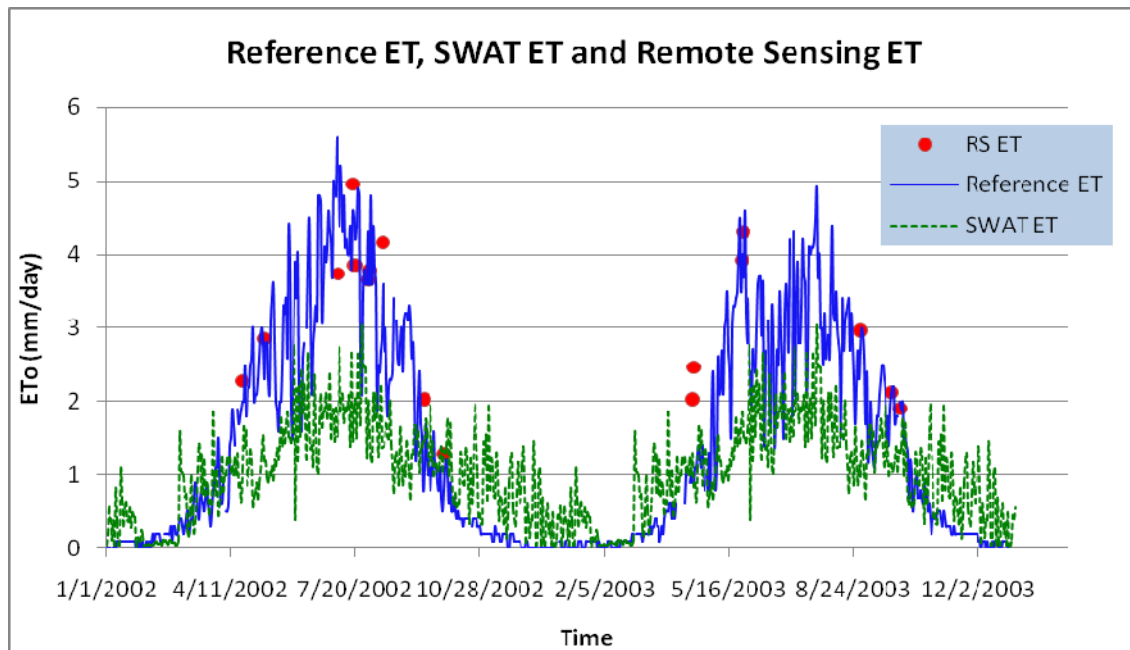


Fig. 3: Comparison of Reference ET, SWAT ET and Remote sensing ET results

## 3.2 Snow cover and Snow melt

### 3.2.1 MODIS Snow products interpretation

Despite the prevailing challenge of continuous cloud covers over the skies of Europe, the MODIS snow products were able to show that continuous snow cover during the winter period at the Don basin was experienced as from somewhere around November 14<sup>th</sup> 2001. The spatial percentage coverage of snow cover was impossible to determine also due to the cloud cover limitations. Cases of random snow fall may have been experienced before this date like in the first week of November 2001 however the snow cover seemed to have melted away almost immediately as shown by images of the second week of November 2001.

A further analysis of the snow cover products showed that the continuous snow cover from mid November 2001 ran through to somewhere around the second week of



February 2002 when snow melt started. This analysis is backed by records of increased river flows from around this period. Snow melt continued through the second week of April 2002 as also shown by the MODIS snow cover of the Don basin.

Later in the year 2002 during the winter season, continuous snow cover was experienced as from the first week of December. This was however not full snow cover of the entire Don basin but in the weeks that followed, partial or full snow cover was experienced. This partial or full snow cover continued to the first week of April when all the snow had melted away. Melting however started towards the last week of March 2003 when patches of snow free land could be spotted in the MODIS snow cover products. This was also backed but an increased river flow around this time which was highly likely to have been contributed by snow melt.

Finally towards the end year 2003 during the winter period, snow cover was first experience from mid-November. This may have been partial snow cover however continuous winter snow cover was experienced until the end march when snow melt started as seen in the MODIS snow products along with increased river flows.

### 3.2.2 Comparison of SWAT snowfall/snowmelt against Remote sensing snowcover/snowmelt

Presented below are plots where the SWAT model snow fall and snow melt results are compared to snow cover and snow melt products for remote sensing.

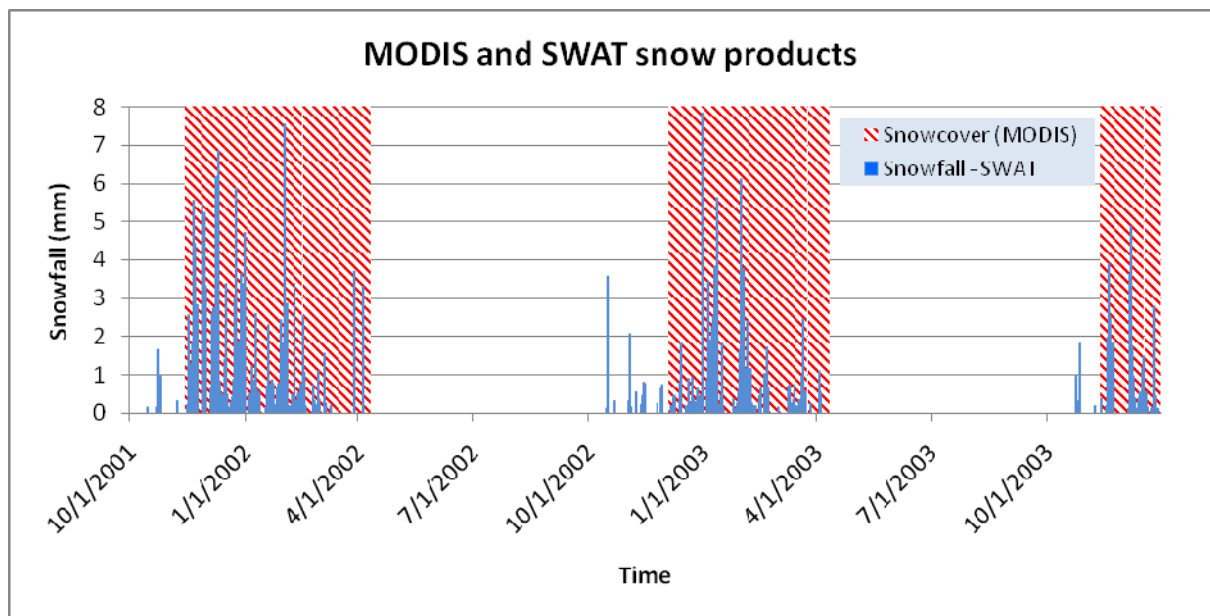


Fig. 4: Comparison of MODIS snow cover against SWAT snowfall

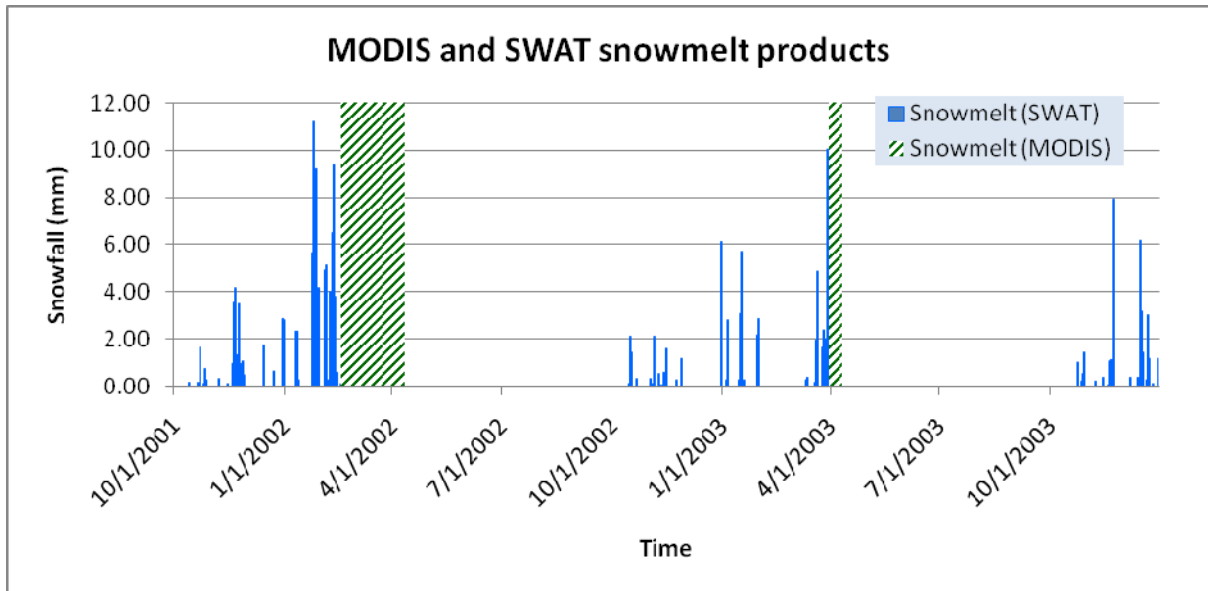


Fig. 5: Comparison of MODIS snowmelt against SWAT snowmelt

It was interesting to observe that the very high flows recorded in the year 2003 came as a result of snowmelt within the entire catchment melting in just about ten (10) days unlike in the year where snowmelt occurred over a period of almost two (2) months.

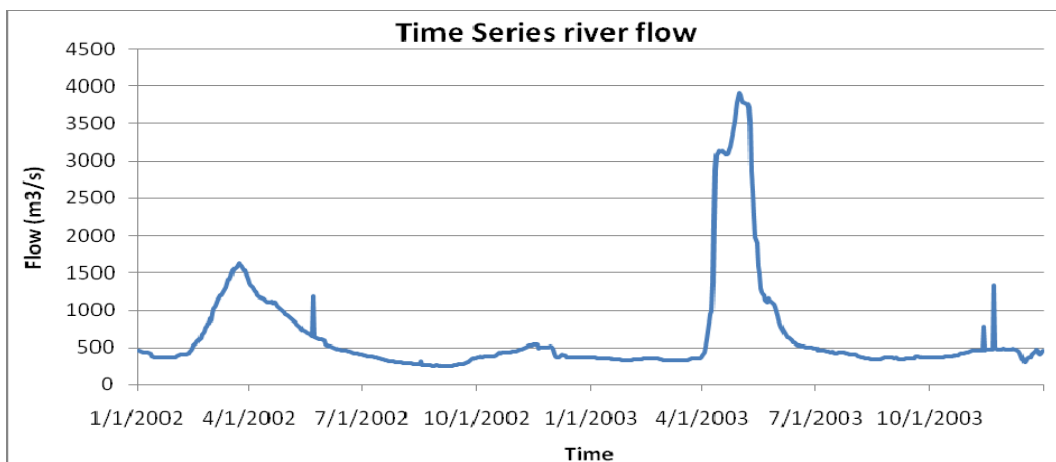


Fig. 6: Time series river flow results



### **3.3 Understanding the hydrology of the Don Basin from Remote sensing products**

Interpretation and analysis of remote sensing data can provide valuable information aimed at understanding the dynamics of some key hydrologic components. It must however be appreciated that an integrated approach of hydrologic analysis of field hydrologic experiments, modeling and remote sensing analysis through data assimilation is of utmost importance in better understanding of the hydrology of a catchment. In this study the vital role of remote sensing is explored especially when carrying out hydrologic modeling.

From the results presented above, it can be pointed out that the Don basin possesses a unique characteristic of low reference Evapo-transpiration. The estimated average actual ET therefore almost matches the reference ET thereby providing annual ET values estimated at approximately 75% of the annual precipitation. With the entire Don basin having annual average precipitation of about 600 mm, we therefore expect annual ET values in the orders of 450 mm. This leaves about 150 mm to contribute to surface runoff, lateral flow, return flow and deep aquifer recharge.

An analysis of river flows provided estimates of water yields to be approximately 107 mm therefore leaving 43 mm to deep aquifer recharge. This overall water balance estimates are vital during model calibration. Daily ET maps from remote sensing are also important to evaluate the performance of the models as presented in the maps provided in the appendix. This also applies to the model snow outputs that need to be checked against snow cover products from remote sensing.

### **3.4 Remote sensing study limitations**

In an effort to achieve the core objective of this study, which was to use remote sensing technology to estimate some core hydrologic water balance components, some limitations were however experienced in the process. The limitations were therefore expected to create uncertainty on the accuracy of the results obtained. Of utmost importance though was that the results could be trusted and relied upon to provide an idea especially as far as orders of magnitude are concerned.

The limitations of this study are therefore presented as;

- Lack of ground measurements to help validate the results and therefore estimate the error margins. Ideally measurements of ET from an instrument such as a lysimeter are often utilized during studies of this nature.
- The MODIS data utilized in this study came with a spatial resolution of one (1) kilometer. This in essence means that an area of one square kilometer that is in effect expected to have varying land use classes' thereby different ET values, is



- reduced to one single ET value obtained from the dominant land use class. This was therefore another source of error.
- With the study area being quite vast, way over 200,000 hectares, data from numerous meteorological stations within the study area should be made into use. This was however not possible due to lack of access to these data.
  - It's also possible that errors existed on the available meteorological data due to human or equipment errors.
  - During determination of ET, seasonal land use changes were not comprehensively taken into consideration thereby causing some level of inaccuracy of the land use surface parameters used in the analysis.
  - The ET estimation algorithm of SEBS also came with its own issues of application that mainly revolved around parameters such as determination of Aerodynamic roughness height.



---

## Case Study 2

### Vit Basin, Bulgaria

#### The use of satellite images for evaluating a SWAT model

---

**Anastassi Stefanova<sup>1,2</sup>, Ann van Griensven<sup>2,3</sup>, Shreedhar Maskey<sup>2</sup>, Silviya Stoyanova<sup>4</sup>, Karin Allenbach<sup>5</sup>**

<sup>1</sup>*Potsdam Institute for Climate Impact Research, Potsdam, Germany*  
(stefanova@pik-potsdam.de)

<sup>2</sup>*Department of Water Science and Engineering, UNESCO-IHE Institute for Water Education, Delft, The Netherlands*

<sup>3</sup>*Department of Hydrology and Hydraulic Engineering, Vrije Universiteit Brussel, Brussel, Belgium*

<sup>4</sup>*National Institute for Meteorology and Hydrology, Sofia, Bulgaria*

<sup>5</sup>*Section of Earth and Environmental Sciences, University of Geneva, Switzerland*

### 1. Introduction

Along with the increase of computational power the performance of hydrologic models has improved significantly and simulation outputs have become an essential part in watershed management. Remote sensing (RS) provides temporally dynamic and spatially explicit information on land surface characteristics [Zhang et al. 2011]. Thus the implementation of such data in physically-based models can be of great benefit, especially for river basins with poor data availability. Most studies use RS products to define the geometry, drainage network and land use of a watershed. Some parameterize hydrological variables such as leaf area index [Boegh et al., 2004] or soil moisture [Houser et al., 1998] applying satellite images. The use of remote sensing to calibrate or evaluate a hydrological model has been studied by several researchers (e.g. [Immerzeel and Droogers, 2007], [Campo et al. 2006], [Parajka and Blöschl, 2008]) but still can be further developed.

Within the scope of the EU funded 'EnviroGRIDS@BlackSeaBasin' project, which among others, aims to provide analyzed, processed and visualized information about the freshwater resources of the Black Sea Basin to decision makers and the public, the watershed scale model SWAT (Soil and Water Assessment Tool) was applied to the Vit



River, which is located in the northern part of Bulgaria and which is a direct tributary to the Danube. Calculations in SWAT are performed on a high level of spatial discretization, which allows plotting the results in detailed maps covering the entire basin. Satellite images can be then used for a visual comparison of specific outputs at different points in time. This approach enables the evaluation of the model for various parameters on a large scale rather than at single control points. It is therefore very useful for recognizing weaknesses and providing solutions at the same time.

The purpose of this paper is to show the preliminary results of the evaluation of SWAT in simulating evapotranspiration and leaf area index in watersheds with limited data availability, with the intention of providing useful information to researchers concerning model optimization.

## **2. The Vit Basin**

The river Vit is located in northern Bulgaria. The basin stretches out from the Balkan Mountains northwards through the hilly Danubian Plane down to the Danube River itself. The total length of the Vit is around 159 km and the average channel slope is about 1.2%. The catchment area is 3200 km<sup>2</sup>, while the average width is only 20.5 km. The mean annual discharge at the mouth is 19.18 m<sup>3</sup>/s. The distribution of annual runoff is dominated by the seasonal characteristics of the moderate continental climatic conditions. Typically winter months come along with snowfall in the mountainous areas. Precipitation occurs during spring, early summer and autumn. In summer however the rain events are of short duration and high intensity. The maximum discharge of the river can be observed during spring. The precipitation rates in the watershed vary from 500mm in the south to more than 1100mm in the north. The highest values are measured in June (55–75 mm), while February and March are the driest months. The total mean annual precipitation in the basin is 780 mm/a. The average annual temperature is 12°C, which reaches a maximum of 25°C in summer (June to August) and a minimum of about 0°C in winter months (December to February). Areas used for agricultural purposes have the greatest share (ca. 60%) in the watershed. Around 30% of the basin is covered by forest (deciduous broadleaf forest 22%, mixed forest 6% and evergreen needle forest 1%). The remaining area is shared by shrubland, grassland, wetlands, industry and urban areas. The main soil types in the basin are Chernozems, Luvisols, Planosols and Kastanozems.



### **3. Methods and Materials**

#### **3.1. Theoretical description of SWAT**

The Soil and Water Assessment Tool – SWAT [Arnold et al., 1998] is an open source watershed scale, semi-distributed hydrological model developed by Agricultural Research Service (ARS) of USDAS in the early 1990s. It uses physically-based input such as topography, soil properties, land cover and weather data to simulate the impacts of land management practices on water quantity and quality. The model can predict water flow, sediment transport, nutrient cycling and crop growth on a daily to hourly time-step for continuous long-term simulations in large and complex watersheds [Neitsch, et al., 2001]. SWAT has a graphical user input interface (ArcSWAT) for the definition and storage of hydrologic features, as well as the organization and manipulation of the related spatial and tabular data. SWAT subdivides a watershed into subbasins which are then further discretized into hydrological response units (HRUs). A HRU has a unique combination of land use, soil type and land slope. Calculations concerning surface runoff, plant growth and water quality are performed at the lowest level of aggregation and afterwards summed up for each subbasin. The simulated water flow, nutrients and sediment loading are then routed through the river using the Muskingum method. Climate data is assigned to each subbasin using the information from the station nearest to the centroid of the same.

The terms evapotranspiration and leaf area index are closely interrelated in SWAT. Actual evapotranspiration is calculated after potential evapotranspiration has been determined. The components of actual evapotranspiration; evaporation of intercepted rainfall, transpiration, sublimation and evaporation from the soil are computed separately. Potential evapotranspiration can be modeled using the Penman-Monteith (Monteith, 1965), Priestley-Taylor (Priestley and Taylor, 1972) or Hargreaves method according to data availability. For this study the Penman-Monteith method was selected. Leaf area index is calculated as a function of Potential Heat Units (PHUs). The Heat Unit (HU) theory postulates that plants are accumulating as many heat units as the average daily temperature (heat) lies above the minimum base temperature (i.e. 5°C) required for a certain plant to grow until they reach maturity and get harvested.

#### **3.2. Model application**

Using ArcSWAT the Vit basin was delineated and subdivided into 20 subbasins and 1538 HRUs. Weather data was derived from daily records of four climatic stations (min/max temperature, wind speed and relative humidity) and nine rainfall gauges available over a period of 10 years (2000-2009). Solar radiation was estimated using the weather generator (WGN) and a dataset provided by the enviroGRIDS project.

The WGN applies different statistical approaches to simulate missing data from a core set of basic properties such as monthly averages, standard deviations and others.

As proposed by Neitsch et al. (2002) the first two years of the simulation (2000-2001) were used as “warm-up” in order to stabilize the model and estimate correctly initial conditions such as soil moisture, groundwater level, nutrient content and others. Calibration was carried out for the period between 2002 and 2005, while validation was performed for 2006-2009. Daily records from five control gauges were available for model optimization, however due to data quality special attention was paid to only two of them (hms21650 and hms21750). Three different quantitative statistics were used to assess the goodness of the simulation; the Nash – Sutcliffe efficiency (NSE), the percent bias (PBIAS) and the coefficient of determination ( $R^2$ ). The statistics showed good results for monthly (NSE of 0.83 and 0.82) as well as daily (NSE of 0.66 and 0.54) stream flow predictions during calibration. The validation period was less satisfactory for simulations on a daily time step (NSE of 0.30 to 0.39) but monthly averages were still adequate (NSE of 0.66 and 0.72). A great share of model failure was attributed to insufficient data quality and availability.

The outputs for evapotranspiration and leaf area index were extracted from the database and attributed to the hydrological response units. The shape files were then converted to raster images with 1 km resolution and aggregated into classes in order to enable a better comparison with the satellite images (compare fig. 1).

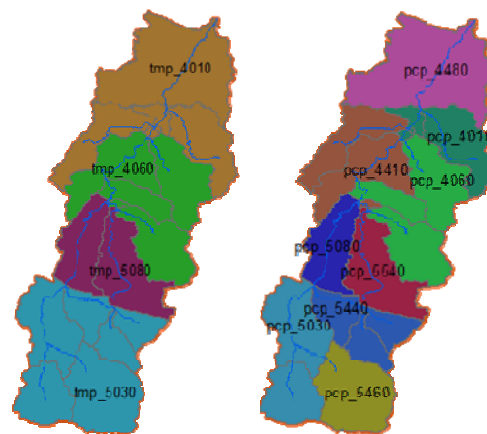


**Fig. 7:** Illustration of process applied to prepare HRU results for the comparison with satellite images



### **3.3. Remotely sensed data**

The ET images used in this study (MOD16A2) are products derived through Moderate Resolution Imaging Spectroradiometer (MODIS). They represent all transpiration by vegetation and evaporation from canopy and soil surfaces, expressed in 1-dimensional vertical mm/day units. The algorithm used to estimate evapotranspiration from remotely sensed data can be viewed in Mu et al. (2011). In simple terms, ET is computed globally every 8 days at 1km scale, using MODIS landcover, FPAR/LAI data and global surface meteorology from the Global Modelling and Assimilation Office. The LAI images (MOD15A) are Version-5 MODIS/Terra products composited every 8 days at 1-kilometer resolution on a Sinusoidal grid. To preserve information content of input data, LAI is retrieved directly from MODIS channel data. The images have been validated at stage 2, meaning that the accuracy has been assessed over a widely distributed set of locations and time periods via several ground-truth and validation efforts. According to the Center for Earth Resources Observation and Science (EROS) these data are ready for use in scientific publications.

### **4. Results and Discussions**

It should be noted that the model was not calibrated on plant growth and leaf area index. Moreover potential evapotranspiration was determined using solar radiation which was statistically estimated and not actually observed. The plots and satellite images used for evaluation can be viewed in the appendix.

The results for ET and LAI were assessed for two different years: a considerably wet year (1301 mm) and an average year (757 mm). The outputs during the year with average climatic conditions (2006) were visibly closer to the remotely sensed estimates for both parameters. The model is capable for representing the temporal distribution of the predictions pretty well, e.g. low values in winter, which increase during spring and summer and decrease towards autumn and winter. However in 2005, the model failed in simulating the seasonal variability of LAI. Moreover a remarkable difference in spatial distribution was observed for both years and parameters. While remotely sensed ET and LAI were clearly following the land use pattern of the basin, the visual assessment of the simulated outputs showed a very distinct clustering of the results into areas with values of the same range.

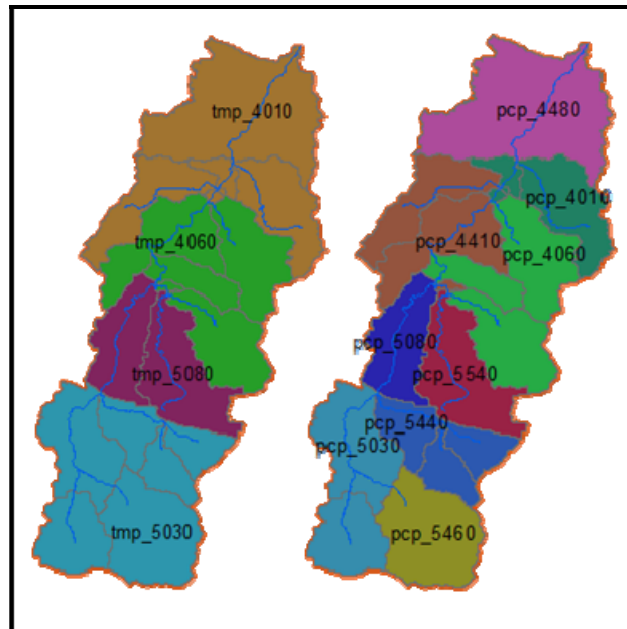


Figure 8: Segmentation of the catchment based on temperature stations (left) and precipitation gauges (right)

Those areas were not based on the land use type but on climatic conditions which follow the subbasin borders as climate data in SWAT are uniform within a subbasin. On the basis of the SWAT results the basin could be subdivided into mainly four different zones resulting from the four available weather stations for temperature (min/max), wind speed and relative humidity. In some cases the effect appeared as a composite of the above mentioned and the zones resulting from the nine rainfall gauges located in the basin (compare fig. 2).

Evapotranspiration is a SWAT component that has had limited testing [Arnold et al., 2008] so far and so does leaf area index. Daily predictions for ET and LAI were compared against average daily ET and LAI estimates derived through remote sensing. Please note that SWAT results were not necessarily compared to real values.

The simulated and remotely sensed rates for evapotranspiration were mostly in the same range, even if in particular areas the model over or underestimating the values. In general ET was very low during winter (0 to 1 mm) as a result of low temperatures and restraint vegetation and elevated during spring with averages between 1.5 mm to 3 mm. Maximum values were observed during summer reaching on average 5 mm to 7 mm. On average SWAT performed relatively well in simulating evapotranspiration during cold periods, while it overpredicted the rates in springtime and underestimated



the values in summer and autumn. In 2006 the overall comparison with remote sensing estimates showed a slightly better match than in 2005, although the zoning of the basin into areas with similar evapotranspiration rates occurred more significantly.

The segmentation effect of LAI estimates was less distinct (compare figure 4) but nevertheless noticeable and even enhanced during the year of extreme events (2005). The overall predictions however were not as good. In 2005 the model did not show any changes in LAI predictions from June until October, while the remote sensing images indicated a clear decrease. This phenomenon may be contributed to the precipitation rates, which were above average in the year 2005. Optimal plant growth depends mostly on adequate water, nutrient supply and a favorable climate [Neitsch et al. 2001]. Higher water availability during summer could have improved the conditions under which biomass is produced and extended the growing season. If the time when a plant reaches maturity is postponed and the harvested date come later there will be no decrease in biomass and LAI. The sum of the average recorded precipitation for June, July, August and September in 2005 was 667 mm, while the average sum of all ten years of records for the same period was only 348 mm. In 2006 the model performed better in predicting LAI and moreover in simulating seasonal variability. The LAI varied between 0-1.5 in winter and spring, while in early summer it was between 1.5 and 2.5. Maximum values were observed during August (2.5 and 3.5). Towards autumn the values decreased to 1.5-2 and in December they reached again a minimum of 0-1. On the whole SWAT overpredicted the leaf area index by a relative value of 1.5

Remote sensing estimates strongly correlate with the landuse pattern of the study area, which itself is a RS product. Evapotranspiration and leaf area index predictions didn't indicate such pattern (see fig 3).

The leaf area index appears to be less dependent on climatic condition than ET, however only during periods with dense vegetation (i.e. growing season). In fact, as LAI is a function of plant heat units it is plausible that the landuse type has a greater influence on leaf area index during the growing season than in times when no crops are cultivated. For instance, during summer (June 2006) SWAT estimates values close to the ones obtained through remote sensing in the agricultural part of the watershed but it underpredicts the leaf area index in the forested area located in the South of the catchment. This can be explained by the fact that the model doesn't assume a fully developed tree canopy, while the satellite image indicates the contrary. It should be recalled that 21% of the catchment area (mainly in the upper part) are covered with a deciduous broadleaf forest, which is known to fully develop its canopy during spring and summer and begin to lose leaves in autumn.

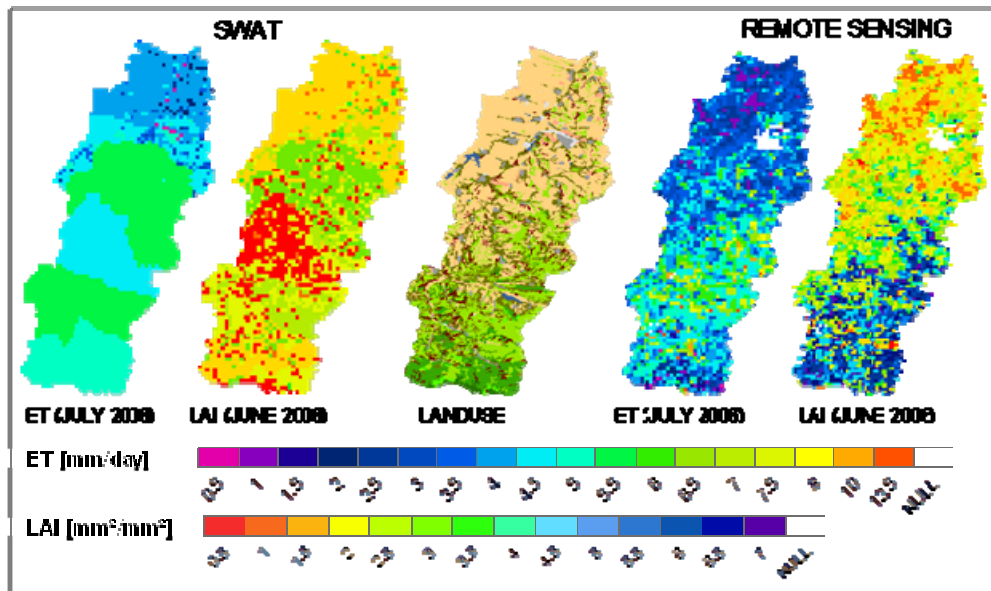


Fig. 9: Comparison of simulated and remotely sensed ET and LAI with the landuse pattern of the catchment

## 5. Conclusions and Recommendations

Given the complexity of a hydrological system as well as the limited data availability the SWAT model performed reasonably well in predicting daily and average monthly discharges, however a need for improvement was identified for evapotranspiration and leaf area index simulation. In summary the following findings can be concluded:

- ET and LAI estimates were strongly correlated to climatic zones, while RS images showed a clear relationship with the land use pattern of the watershed
- Climate had a considerably greater impact on evapotranspiration and leaf area index simulation rather than different landuses or vegetation types
- The model performed better in simulating LAI and ET for an year with average climatic condition than for an year with increased total precipitation rates
- On average the evapotranspiration rates tend to be slightly underestimated, while leaf area indices were clearly overpredicted compared to the corresponding values estimated from remote sensing
- During summer (growing season) the model predicted reasonable LAI values for the agricultural areas but strongly underestimated the leaf area index for the forested areas
- The visual comparison of SWAT outputs with satellite images is a relatively simple yet effective way of evaluating the performance of the model on specific parameters



---

Note that the results of this study are exclusively valid for the model of Vit Basin developed using the described methods and materials. Other watersheds, with different characteristics and greater data availability may give different results.

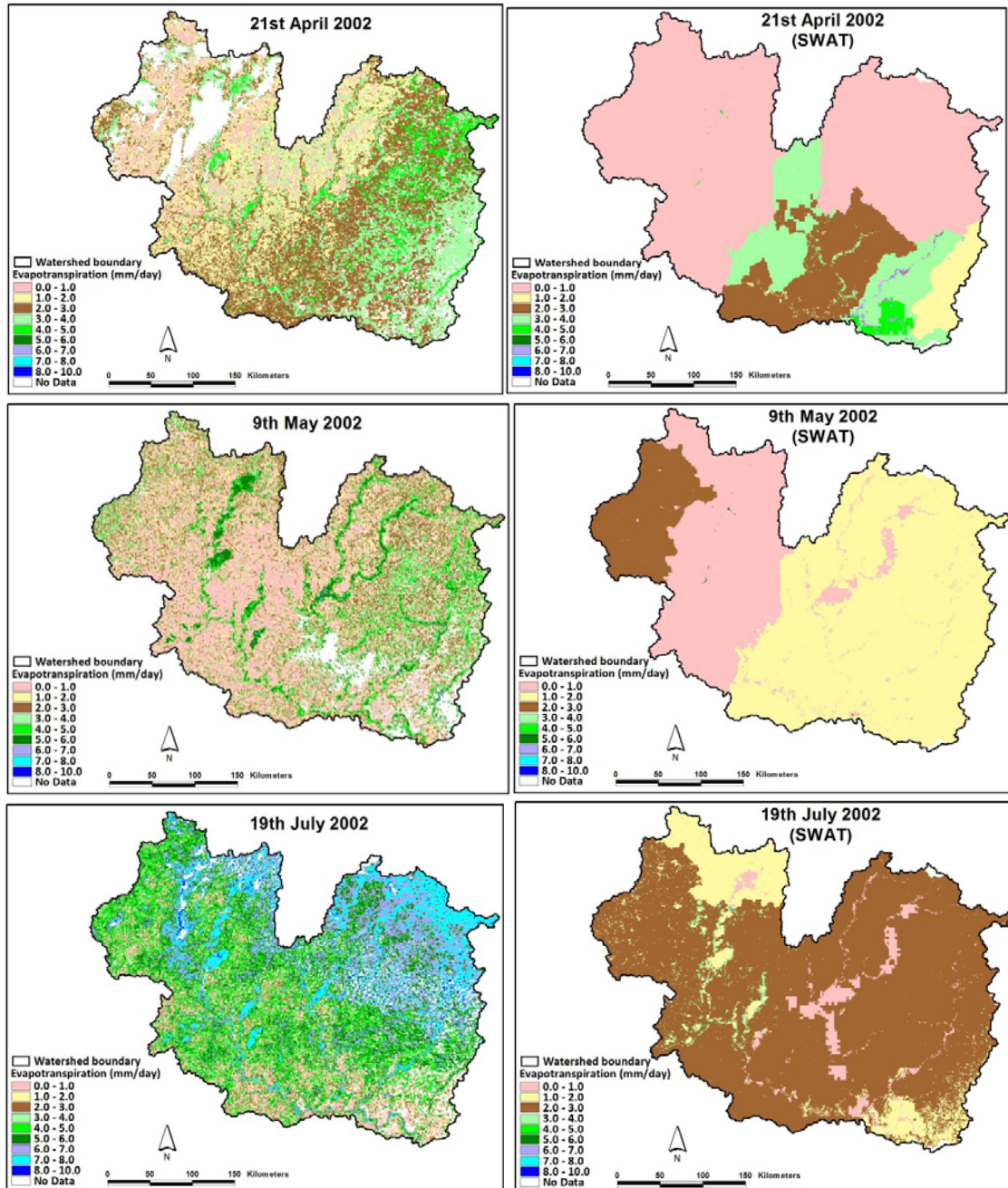
The effect of insufficient data, especially climatic information is enhanced by the approach used in SWAT to simulate weather conditions. Instead of assigning data from the station nearest to the centroid of a subbasin, it could be more practical to apply some basic interpolation method between the available stations including elevation.

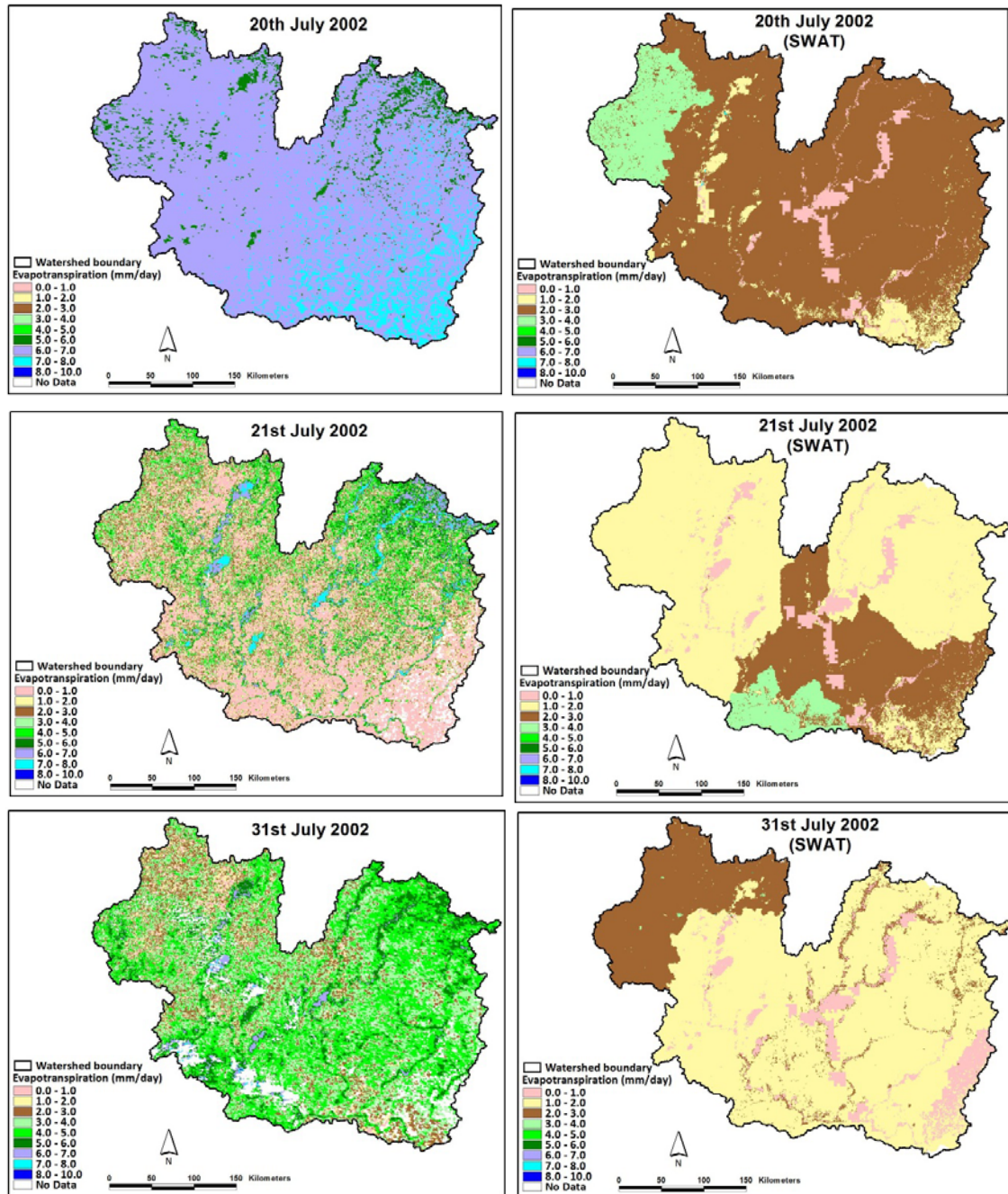
The adjustment of specific parameters related to the assessed outputs was beyond the scope of this study. However a calibration on the evaluated output is recommended for future undertakings with similar aims. The crop database could be revised by implementing information from local farmers and field measurements/observations.

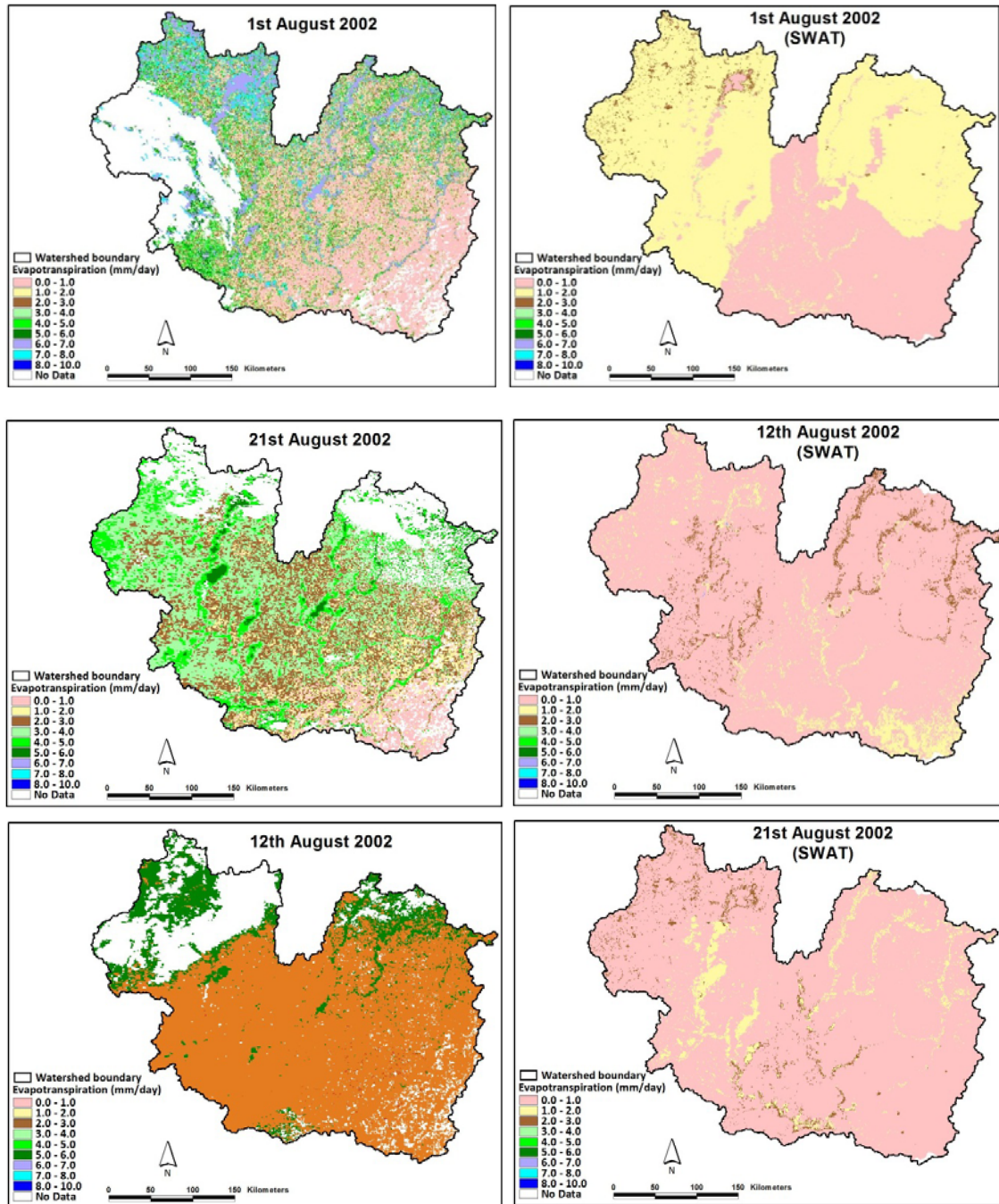
The implementation of remote sensing images can also be used to calibrate hydrological models of watersheds with limited data. Besides evapotranspiration and leaf area index, remote sensing products for soil moisture, snow cover and primary productivity (to name a few) are available and can be applied.

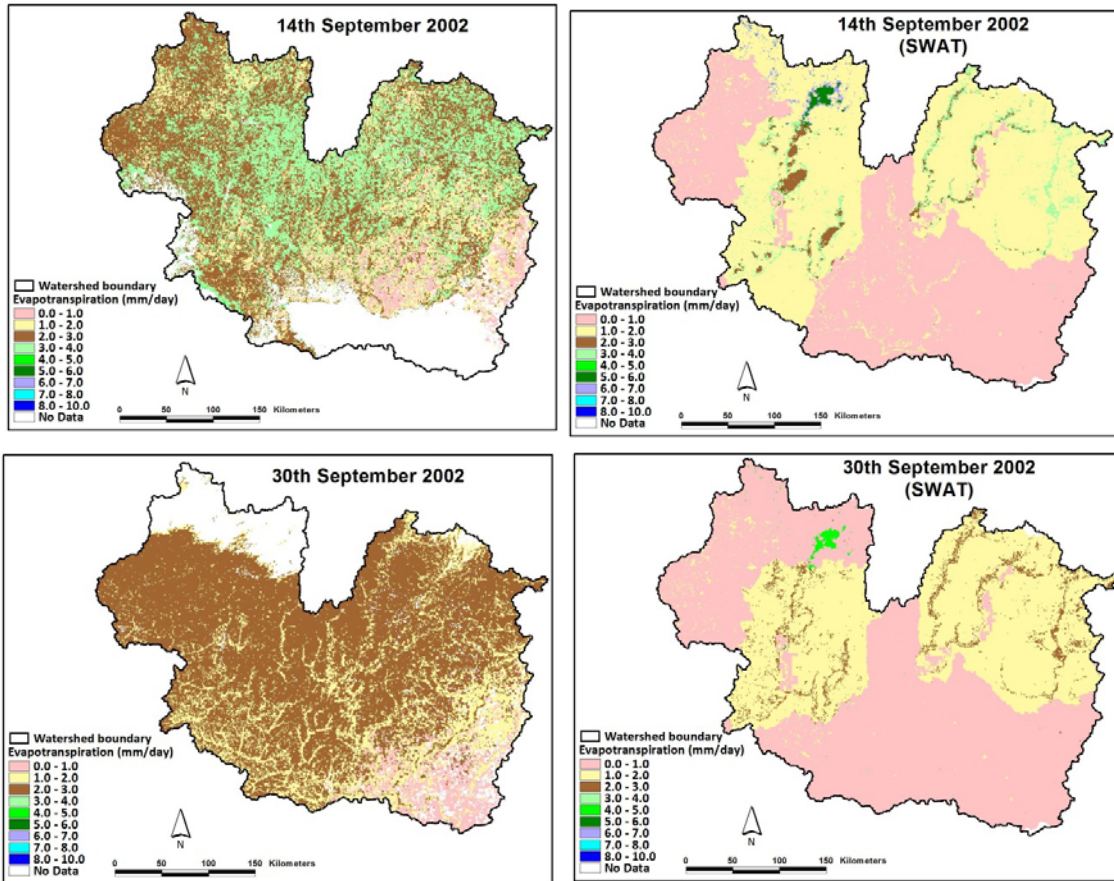
## 7. Appendices

### Comparison of RS and SWAT 2002 Evapotranspiration products

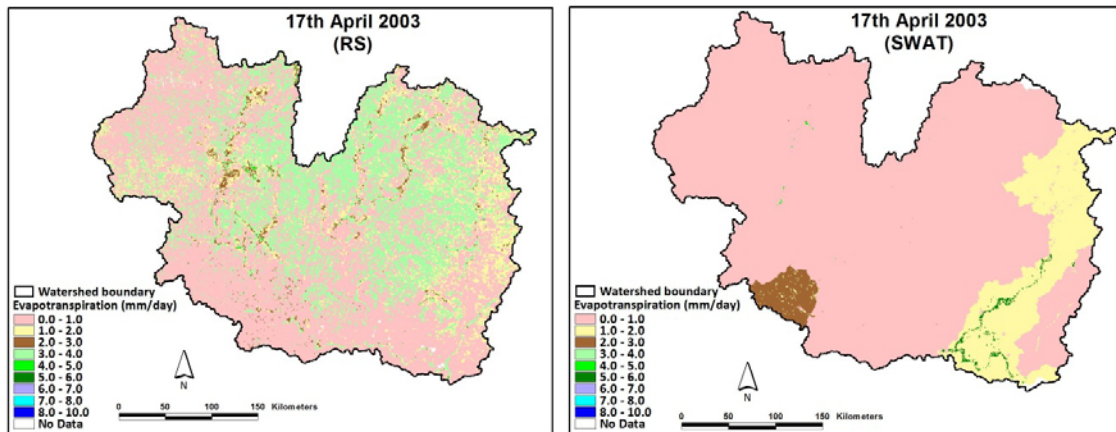


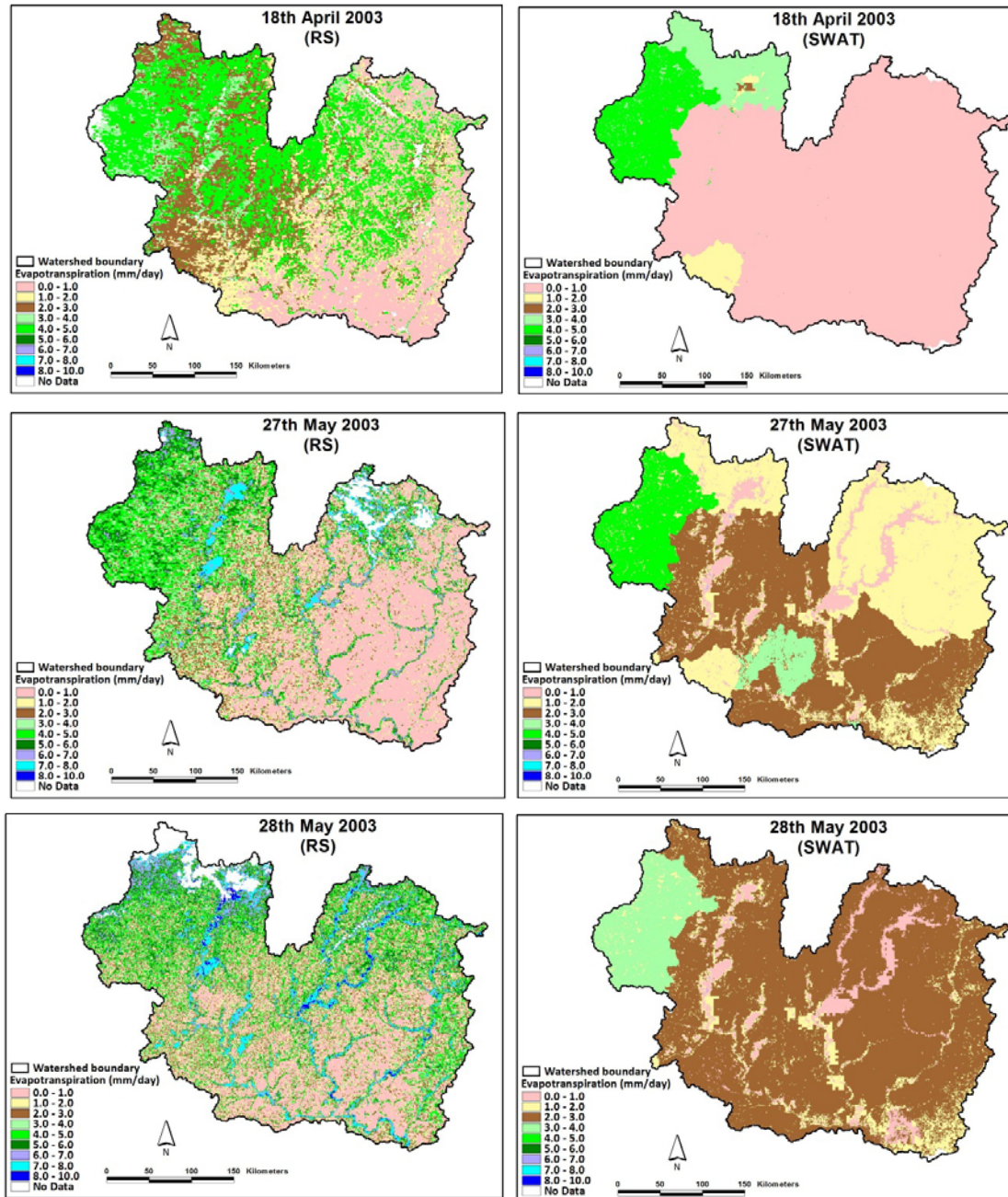


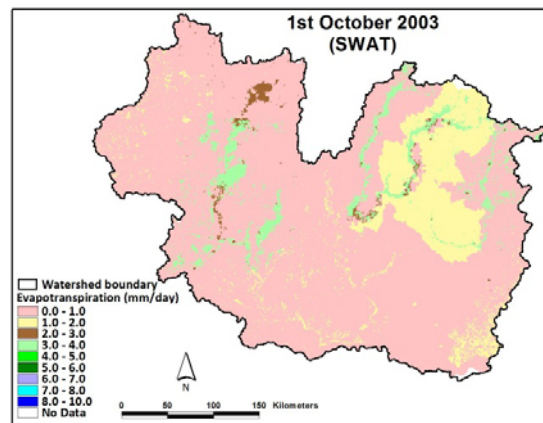
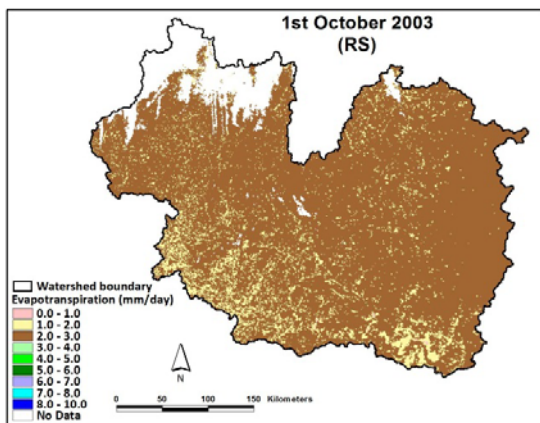
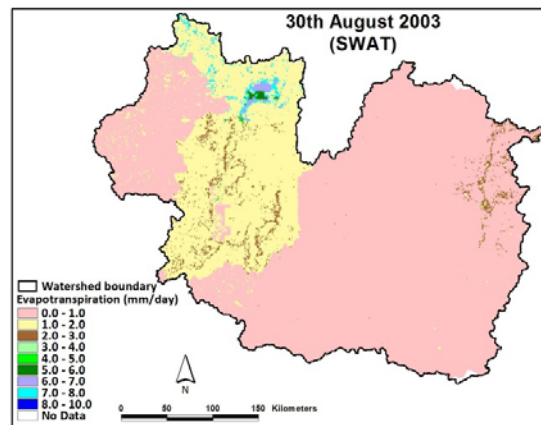
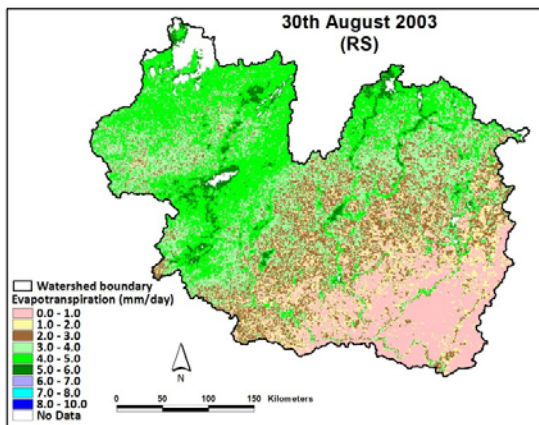
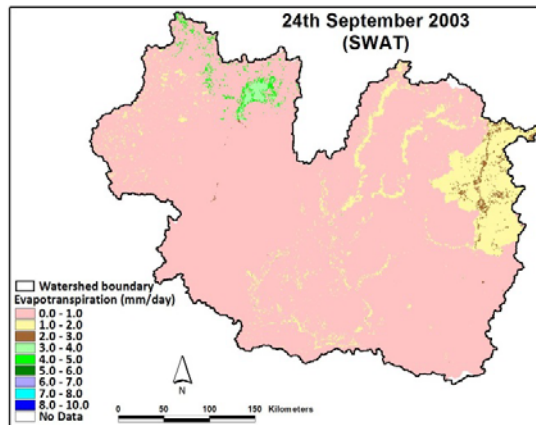
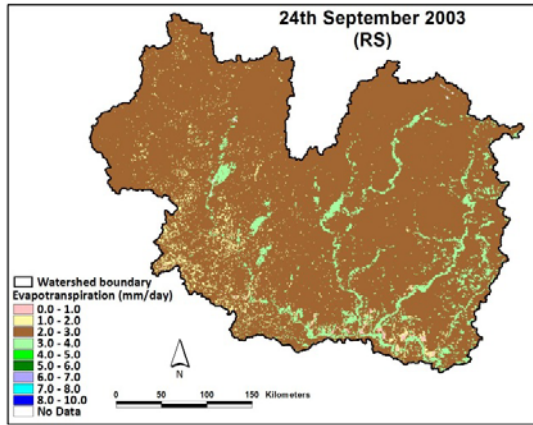




**Comparison of RS and SWAT 2003 Evapotranspiration products**









---

## **Case Study 3**

### **Azov Sea Basin, Don River Basin**

Assessment of stream flow change

---

#### **Aims and objectives**

The aim of the research was to assess the changes of water inflow into the Tsimlyansk reservoir, the largest freshwater body in the Azov Sea Basin, using the ArcSWAT modeling tool. The reservoir plays crucial role in securing freshwater ecosystem goods and services provision in the region.

The following objectives have been formulated in order to achieve the goal:

- Gather, process, and bring to the ArcGIS format the data required for running the Soil Water Assessment Tool (SWAT);
- Develop the SWAT model of water spatial distribution in the Upper Don River sub-catchment;
- Calibrate the developed model based on historical meteorological and hydrological data;
- Based on the input by other EnviroGRIDS Work Packages formulate and analyse scenarios of land use and climate change using the developed model.

#### **Study area**

The Upper Don River catchment is defined upstream the Don River's confluence with the Tsimlyansk reservoir (Fig. 10). Due to climatic conditions the water influx generated in this catchment is the key factor defining water balance of the Tsimlyansk reservoir.

The Upper Don River watershed comprises more than 50% of the total Don River catchment area. It includes 15 gorsovet, 162 rayons within 8 administrative regions of Russia. Two large highly developed industrial cities with population more than 1.3 million people each are located in this area.

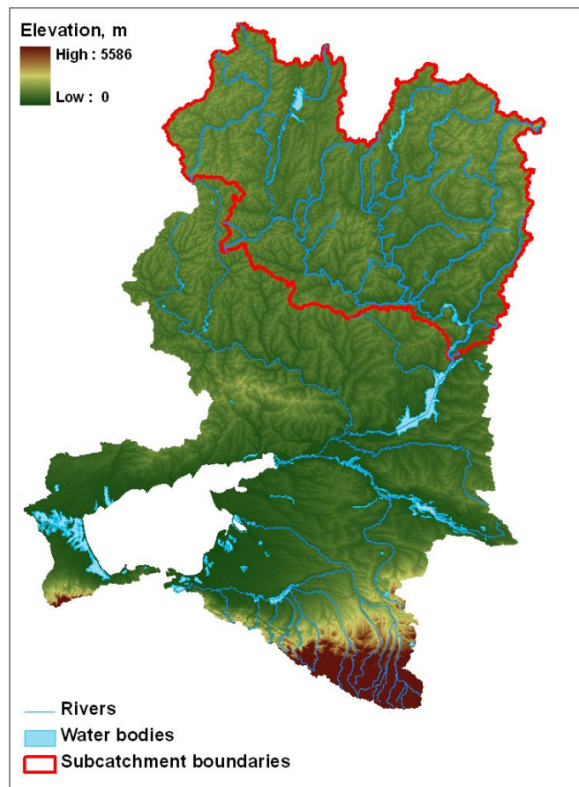
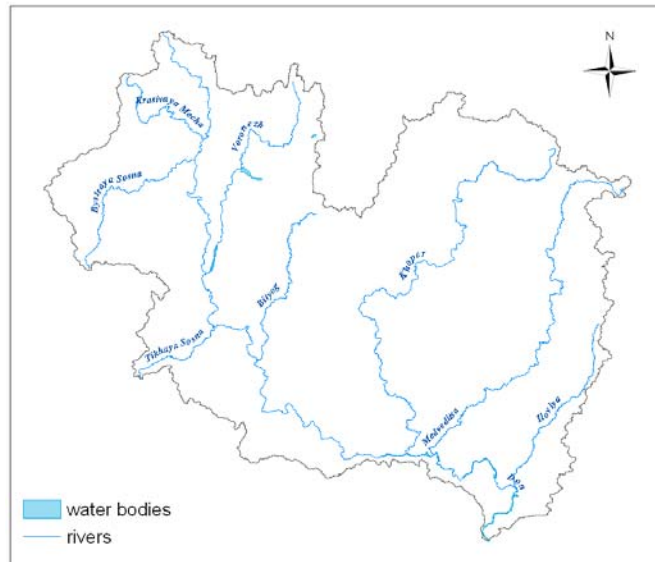


Fig. 10. Upper Don River catchment

The river network can be divided into the 8 main river streams and contains no large reservoirs. Rivers are mainly fed by snowmelt causing significant annual fluctuations in water flow and uneven ecosystem services annual distribution.



**Figure 11. Rivers and water bodies in the sub-catchment**

Correspondingly, the water influx to the reservoir and its water level considerably increases during the spring flood period **Error! Reference source not found.** The average annual inflow in the Tsimlyansk reservoir is 590 m<sup>3</sup>/sec.

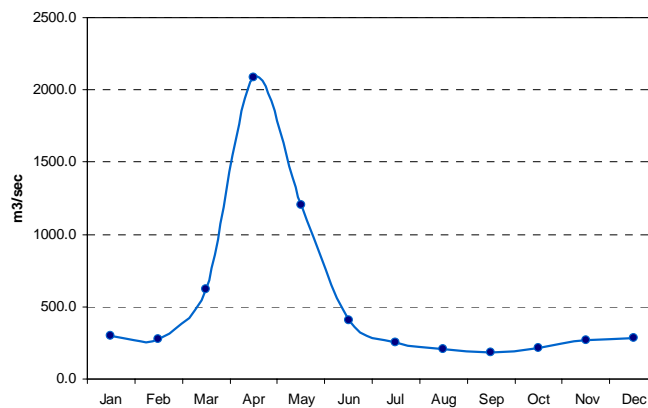


**Fig. 12. The average monthly inflow in the Tsimlyansk reservoir (2000-2010) (Based on CRWISWT 2012)**

Rainfed crops and mosaic croplands comprise the major part of the basin (47.9% and 39.8% respectively). Other less presented land use types are mosaic vegetation (5.81%), different types of forest (3.45%) and urban areas (0.3%) (Fig. 13).

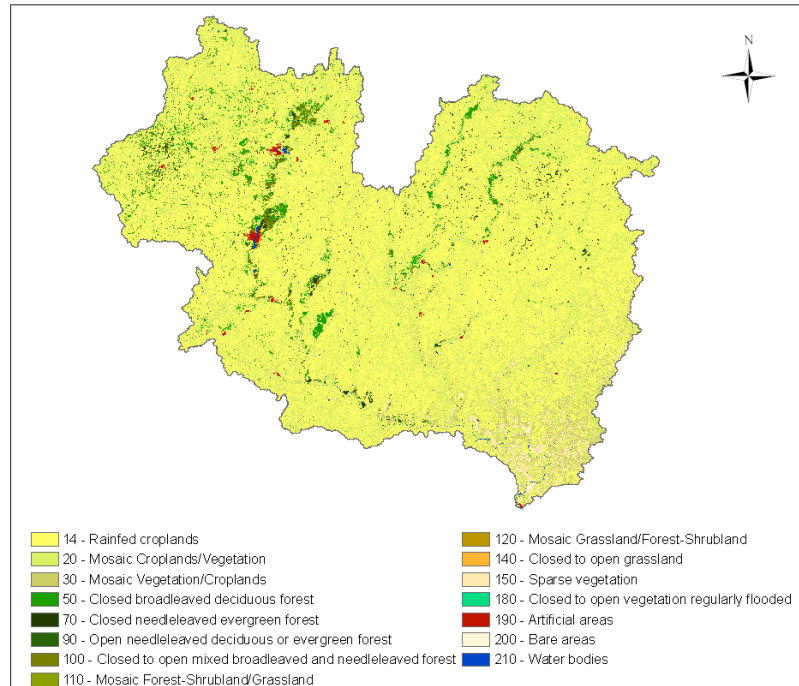


**Fig. 13.** Land use patterns in the area of study (Based on ESA 2009)

Abundance of agricultural areas and relatively high urbanization level has determined historical changes in surface runoff and water yields generation in the sub-catchment.

The Upper Don River catchment can be defined as a typical agricultural watershed, for which effectiveness of ArcSWAT application for hydrological modelling has been proved by different studies (e.g.: Van Liew 2003, Vigerstol and Aukema 2011).



**SWAT model setup**

Elevation data have been obtained from the global dataset topography Shuttle Radar Topography Mission (SRTM) (Farr *et al.* 2007).

The entrance of the Don River to the Tsimlyansk reservoir has been chosen as the main outlet to delineate watershed boundaries. As a result of ArcSWAT analysis 37 subbasins with 37 outlets comprising 530 Hydrological Response Units (HRUs) have been defined for this watershed.

The hydrologic response units (HRUs) have been defined based on land use categories, soil types as and slope characteristics derived from SRTM DEM input data.

The MODIS land cover dataset (2008) has been used as the land cover layer model input. However, in order to support further SWAT analysis of scenarios developed by EnviroGRIDS project for Metronamica land use model (

Fig. 14) have been used to reclassify this dataset.

	<b>MODIS Land use classes</b>		<b>Metronamica land use classes</b>
<b>0</b>	Water	<b>9</b>	Water
<b>1</b>	Evergreen needleleaf forest	<b>3</b>	Forest
<b>2</b>	Evergreen broadleaf forest		
<b>3</b>	Deciduous needleleaf forest		
<b>4</b>	Deciduous broadleaf forest		
<b>5</b>	Mixed Forests		
<b>6</b>	Closed Shrubland	<b>1</b>	Shrubland
<b>7</b>	Open Shrubland		
<b>8</b>	Woody Savannas		
<b>9</b>	Savannas		
<b>10</b>	Grasslands	<b>4</b>	Grassland
<b>11</b>	Permanent wetlands	<b>7</b>	Permanent wetlands
<b>12</b>	Croplands	<b>5</b>	Croplands
<b>13</b>	Urban and built-up	<b>6</b>	Urban and built-up
<b>14</b>	Crops/natural vegetation	<b>0</b>	Crop/ Natural Vegetation
<b>15</b>	Snow and ice	<b>8</b>	Snow and Ice
<b>16</b>	Barren or sparsely vegetated	<b>2</b>	Barren or sparsely vegetated

**Fig. 14.** MODIS land use classes and new classes created to fit the Metronamica land use model (Mancosu *et al.* 2012)

Global soil dataset FAO has been used as the model soil layer input (FAO and IIASA 2012).

Thresholds were set to zero for multiple HRUs on Land Use, Soil and Slope in order to make accurate comparison of land use scenarios.

Finally, weather data have been derived from the Climate Data Online dataset (National Climate Data Center) and Russian National Service "Russia's Weather" developed by the Space Monitoring Information Support Laboratory of Space Research Institute of Russian Academy of Science (SMIS IKI RAN). Some meteorological stations with data missing for several years have been updated by the dataset "Daily surface air temperature and precipitation series for 20th-century" provided by the European Climate Assessment (ECA) (Klein Tank *et al.* 2002).

The observations for the following 5 meteorological stations for the period 1998-2008 have been chosen as weather data input: Urjupinsk, Elec, Frolovo, Voronej and Kamyshin (Figure 6).

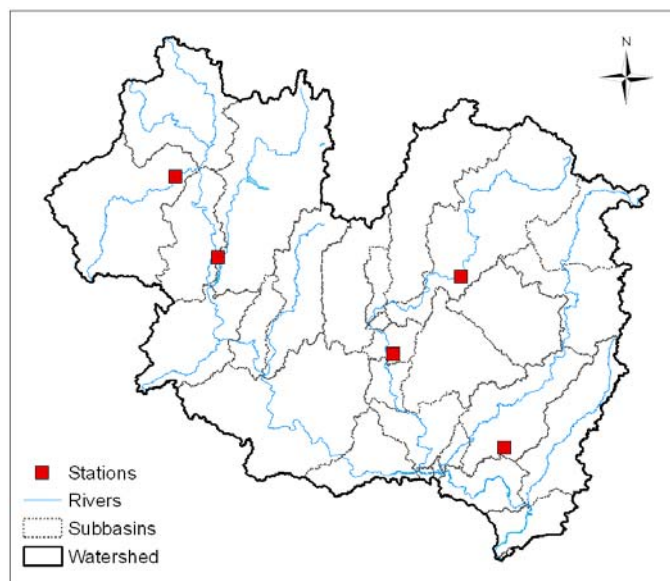


**Figure 15.** The Upper Don River watershed and meteorological stations delineated using SRTM DEM data

The 10 years simulation period from 1 January 1998 to 31 December 2008 has been specified with two years of warm up period. The default options with skewed normal distribution of rainfall and monthly printout setting have been used. Finally, the model was run and simulation results were obtained through the Read SWAT output.



### **SWAT model calibration**

The model was calibrated using SWAT-CUP software (Abbaspour 2011) applying SUFI2 method. In this method uncertainty of input parameters is depicted as uniform distributions, while model output uncertainty is quantified by the 95% prediction uncertainty (95PPU) calculated at the 2.5% and 97.5% levels of cumulative distribution of output variables obtained through Latin hypercube sampling. Uncertainty here includes different driving variables (e.g., rainfall), conceptual model, parameters, and measured data.

The SWAT-CUP interface allows combine input/output of calibration program itself with the ArcSWAT model. It contains different input parameters of reaches, subbasins that can be edited and optimized by user.

3 watershed outlets have been set in matching the existing hydrological gages with historical monthly discharge observations for 2001-2008. The datasets have been reformatted appropriately and loaded to the SWAT-CUP.

10 parameters have been included in calibration (

Table 9). Calibration was performed for monthly streamflow and satisfactory Nash-Sutcliffe efficiency (0.3 to 0.4 on a monthly scale) has been achieved.

**Table 9.** Calibrated parameters

<b>Alpha_Bf</b>	Base flow Alpha factor (days)
<b>Gw_Delay</b>	Ground water delay (days)
<b>Cn2</b>	Initial SCS Curve Number II value
<b>Esco</b>	Soil evaporation compensation factor
<b>Sftmp</b>	Snow fall temperature (OC)
<b>Timp</b>	Snow pack temperature lag factor
<b>Snocovmx</b>	Minimum snow water content that corresponds to 100% snow cover
<b>Alpha_Bnk</b>	Baseflow alpha factor for bank storage
<b>Sol_Awc</b>	Available water capacity (mm H2O/mm soil)
<b>Sol_K</b>	Saturated hydraulic conductivity (mm/hr)

Calibration results were considered as sufficient since the main purpose of study was to analyse the changes in annual streamflows into the Tsimlyansk reservoir.



### Scenario analysis

The scenarios on land use and climate change till 2050 have been formulated using the outcome of the EnviroGRIDS Work Package 3 (WP3). The following four alternative land use scenarios were constructed for the study area: BS HOT, BS ALONE, BS COOP and BS COOL.

The storylines of these scenarios are based on emissions forecasts proposed by IPCC-SRES (Nakicenovic et al. 2000) depending on different ways of global socio-economic development. Additionally, a number of studies on global and European change scenarios have been used. More information can be found in the WP3 deliverables “D3.8 The enviroGRIDS scenarios” (Mancosu et al. 2012).

Time-series of climatic conditions corresponding to land use change scenarios were generated using the stochastic weather generator Long Ashton Research Station Weather Generator (LARS-WG) (Racsko et al. 1991; Semenov and Barrow 1997). The generator simulates time-series of daily weather at a single site. One of the main purposes of this tool is generating long time-series for assessing agricultural and hydrological risks and producing daily site-specific climate scenarios for climate change impact assessment. This tool has been applied successfully in previous SWAT studies (e.g Obuobie 2008) showing satisfactory level of weather simulation.

Table 10 shows the scenarios of climate change used for weather data generation in correspondence to EnviroGRIDS land use change scenarios. Green areas indicate correspondence between land use scenarios proposed by EnviroGRIDS and emission scenarios used for generating weather time-series.

**Table 10.** Correspondence of LARS-WG climate scenarios to EnviroGRIDS land use change scenarios

	BS HOT	BS COOL	BS COOP	BS ALONE
SRA1B				
SRA2				
SRB1				

The LARS-WG model version 5.0 does not generate weather data on SRB2 scenario, therefore it was assumed that data on SRB1 scenario will be relevant as it also implies low environmental pressure and relatively low economic and population growth (Semenov and Stratonovitch 2010).



The temperature and precipitation time-series for 5 meteorological stations have been generated and used for the baseline model.

The main hydrological parameters at the primary watershed outlet specified at the inflow of the Don River into the Tsimlyansk reservoir are presented in Table 3. The column 1 (“baseline”) shows average annual values obtained from the calibrated SWAT model for the period 2001-2008. The last row (“streamflow”) presents annual average inflow into the Tsimlyansk reservoir (cubic meters per second).

**Table 11.** Baseline (2001-2008) and projected (2050) annual average hydrological parameters for the Upper Don River

	BASELINE	BS HOT	BS COOP	BS ALONE	BS COOL
Water yield	177.64 mm	139.78 mm	141.07 mm	143.04 mm	140.36 mm
Precipitation	546.2 mm	550.13 mm	535.39 mm	541.19 mm	535.39 mm
Surface runoff	136.25 mm	119.21 mm	117.81 mm	120.11 mm	118.25 mm
Evapotranspiration	368.5 mm	383.68 mm	390.70 mm	390.79 mm	393.90 mm
Streamflow	1254.91 cms	879.22 cms	799.27 cms	892.20 cms	799.27 cms

**BS HOT.** In this scenario the water yield decreases almost by 22% what is greater than in all other scenarios with highest decrease of precipitation. The baseflow decreases as well while evapotranspiration and potential evapotranspiration increases by 4% and 6% correspondingly. As a result the average annual inflow into the Tsimlyansk reservoir will decrease by 30% in 2050.

**BS COOL.** Under this scenario the water yield will decrease by 20%, however baseflow will not decrease as much as under other scenarios. Surface runoff will decrease by 13%, less than in BS HOT that can be explained by increase in forests and shrublands area according to the land use change scenario. Nevertheless, higher ET rates and relatively lower precipitation rates will lead to decrease in the average annual inflow into the Tsimlyansk reservoir by 36% in 2050.

**BS ALONE.** Under this scenario runoff will decrease, but less than under other scenarios (12%). This can be explained not only by relatively high precipitation rates, but also by increase of barren and sparsely vegetation according to the land use change scenario. As a result the average annual inflow into the reservoir will decrease by 28% in 2050, smallest decrease among all scenarios.



**BS COOP.** Under this scenario runoff will increase that can be explained by increase of barren and sparsely vegetation. However baseflow will decrease less than in other scenarios that can be explained by increase of forests and shrublands in 2050 according to the land use change scenario. In this case water content in soil may increase, while surface runoff will decrease (14%). As a result the average annual inflow into the Tsimlyansk reservoir will decrease by 36% in 2050.

### **Conclusions**

The analysis of land use and climate changes according to the proposed scenarios reveals substantial decrease in water flow generated in the Upper Don River watershed and corresponding decrease of water inflow into the Tsimlyansk reservoir.

It was found that the inflow into the Tsimlyansk reservoir from the Upper Don River catchment will decrease by 28 -36% depending on a scenario.

The Tsimlyansk reservoir plays a crucial role in the regional water distribution scheme and possible changes in water availability should be taken into account in the regional policy-making process in order to secure sustainable water resources management.

The developed SWAT model can be used for further analysis of water management and regional planning within the Azov Sea Basin. The Don River Watershed GIS database developed to support SWAT model can also be used for studying this area by means of alternative methods and techniques.



## **Case Study 4**

### **Seversky Donets River in Ukraine**

#### **The main outcomes of USRIEP team activities on WP4 “Hydrological catchment models”**

---

Through the WP4 duration USRIEP team has performed activities on learning and mastering the SWAT programme. An investigation area placed at Ukrainian part of Seversky Donets River which is significant source of drinking water and water for industrial, agriculture and household needs. The main goal of current research is testing the simulation of hydrological and hydrochemical characteristics using SWAT modeling with regard to the river basin of the Black Sea Catchment with large area. Investigated area is thickly populated, has high levels of industry and agriculture.

The full range of work includes the activities from data collection to obtaining the final numerical results.

The river basin is divided on 66 sub-basins and corresponding main watercourses. The catchment areas were classified by type of land use, soil types and level of surface slope defining the hydrologically homogeneous units. Point contamination sources were grouped according to sub-basins. If the number of this sources is more than one in sub-basin, they are grouped to one effective source with aggregated data and recorded on a digital map.

The table which includes wastewater discharge and load of the parameters required for the simulation was composed.

Volume of run-off and distribution of contaminants in water were simulated. Based on water supply needs and the presence of environmental problems, the modeling of the following non-conservative substances content was performed: phosphorus mineral  $P_{min}$ , nitrate nitrogen  $NO_3$ , ammonia nitrogen  $NH_4$ , readily soluble organics  $BOD_5$  and as non-conservative substances - total iron, chromium  $Cr^6$  and zinc. Heavy metals are typical for the compound of run-off waters in main part of point sources. The model calculations were carried out for the period of 2009-2010, the following parameters were calculated: monthly and annual river water discharge and concentration of pollutants. Three monitoring stations in the middle of the basing were chosen for model calibration.

Model calibration was realized using SWAT-CUP2 programme and PARASOL method. During the calibration process except indicators, proposed for optimization by default, some additional parameters were included in the list of optimized parameters. These



parameters define snowmelt and precipitation of organic matter processes, phosphorus transition from organic to inorganic forms and transformation of nitrogen compounds. Carrying out the calibration on BOD<sub>5</sub>, additional parameters characterizing the processes of biological oxygen demand and reaeration were added to the list of optimized parameters.

Verification was carried out by comparing the results with the field observations data concerning river water quality and water discharge in the closing range of the Ukrainian part of the river on the border with Russia. Comparison of the water river discharge, ammonia nitrogen, nitrate nitrogen, phosphorus and mineral BOD<sub>5</sub> were performed for both the average annual and for the average monthly parameters. Comparing of heavy metals was performed for average annual parameters. This is due to the fact that annual dynamics of conservative substances concentration caused by the dynamic of incoming substances with return waters from the point sources. To compare observed and calculated concentrations of conservative metals, some monitoring points used for calibration were chosen, besides the closing monitoring point.

Comparison of the modeling results with field observations data has shown a quite good correspondence between calculated and observed values of the simulated parameters.

The relative error of annual values of the investigated parameters is following: - 2,1% - river water discharge, 2,4% - ammonia nitrogen, 10,3% - phosphorus mineral, 15,8% - nitrate nitrogen, 14% - BOD<sub>5</sub>. Comparison of the monthly calculated and observed parameters showed a qualitative correspondence of the simulated and observed seasonal dynamics. Average relative error of the calculated annual concentrations of conservative metals are: 5.3% - for total iron content , 5,0%- hexavalent chromium, 7% - zinc .

Thus, on the basis of the performed activities, we can conclude about the possibility of SWAT-modeling using for predictions of the river water quality and water discharge in the whole basin or part of the big river basin in European part of the Black Sea basin, taking into account various loadings of contaminants from point sources and various weather conditions, including changes related to climate change.

The results of performed activities were reported to three international conferences.



---

## **Case Study 5**

### **Seversky Donets River, Ukraine**

#### **Impact of non-point source pollution on drinking water**

---

Through the WP4 duration USRIEP team has performed activities on learning and mastering the SWAT programme. An investigation area placed at Ukrainian part of Seversky Donets River which is significant source of drinking water and water for industrial, agriculture and household needs.

The main goal of current research is testing the simulation of hydrological and hydrochemical characteristics using SWAT modeling with regard to the river basin of the Black Sea Catchment with large area. The full range of work includes the activities from data collection to obtaining the final numerical results.

Work methodology was tested using the Severskiy Donets river basin case (within Ukrainian territory). Through the reporting period the following stages were carried out:

1. Watershed Delineation;
2. Mapping of the point sources and composing the table with data on water run-off waters discharge and its compound;
3. HRU-analysis – segregation of the hydrologically homogeneous units in catchment areas;
4. Adding the weather conditions data to monitoring stations map; composing the table with average values of meteorological parameters;
5. The model calculations of the average annual river water discharge and annual mass of contaminants in rivers control points;
6. Composing the table of actual river water discharge and concentrations of contaminants in monitoring stations;
7. Model calibration and verification for estimation of the average annual values of non-conservative substances concentrations and their mass flow rate (ammonia nitrogen, BOD<sub>5</sub>, phosphorus mineral and nitrate nitrogen) in transboundary outlet of Severskiy Donets river;
8. Composing the table of actual extremes of daily air temperature and daily precipitation;



9. model calculations of the average monthly river water discharge and monthly mass of contaminants discharge in rivers control points;
10. Model calibration and verification for estimation of monthly concentrations and mass flow rates of non-conservative substances (ammonia nitrogen, BOD<sub>5</sub>, phosphorus mineral and nitrate nitrogen) in transboundary outlet of Severskiy Donets river;
11. Model calibration and verification for estimation of monthly concentrations and mass flow rates of non-conservative substances (total iron, hexavalent chromium and zinc) in different monitoring stations placed within Severskiy Donets river.

#### 1. Watershed Delineation

For the «Watershed Delineation» stage, digital elevation map (DEM) of Ukraine with 90 m resolution was applied. In order to facilitate implementation of this stage, visual analysis of DEM was applied in order to delineate borders of Severskiy Donets river basin within DEM. Further, stream definition was made only within the borders of this polygon.

At the beginning of work, automatic stream and sub-basin delineation feature, based on DEM analysis, was applied. As a result of application of this method, the contours of Severskiy Donets river basin were delineated, sub-basins and major streams within the basin were highlighted (Fig 1). As can be seen from the map, located on Fig. 1, part of the territories inside delineated Severskiy Donets river basin were not attributed to any of the sub-basins (shown red on the map). It may be explained by the fact, that in our case the DEM does not provide enough detail to allow accurate prediction of the location of the stream network.

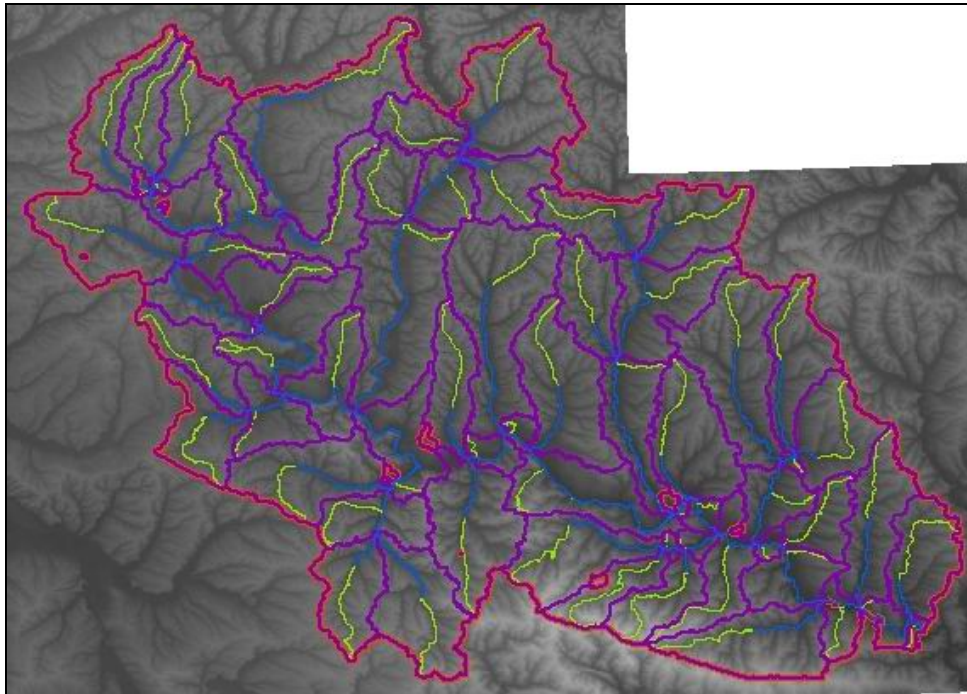


**Fig. 1.** Results of automatic catchment delineation based on DEM. (Red line – border of Severskiy Donets river basin, lilac lines – sub-basin borders, blue lines – reaches, yellow lines - longpasses).

So that, Pre-defined method for streams and sub-basins delineation was applied. In order to do that, automatically delineated sub-basins and streams were adjusted using ArcGIS in such a way, that correspondence between each territory inside the river basin and a certain sub-basin was established. After application of Pre-defined method of stream and sub-basin delineation, 66 sub-basins and 66 corresponding major streams were established (Fig. 2).

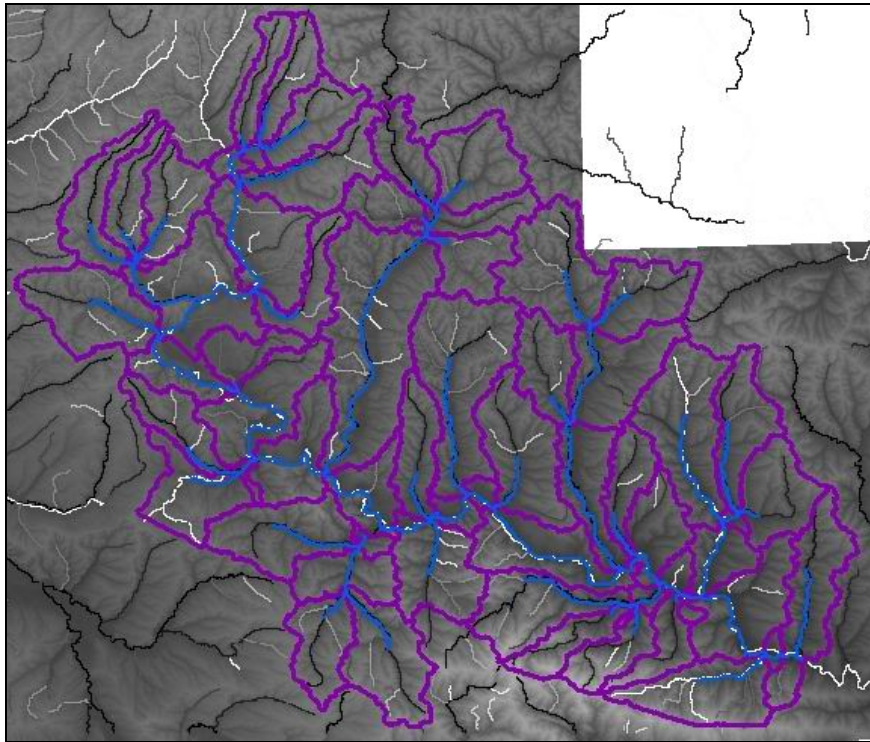


**Fig. 2.** Results of sub-basins and reaches border delineation (lilac lines – catchment borders, blue lines – sub-basins (reaches)).

Required parameters were calculated for all selected watersheds: catchment area, average/minimum/maximum heights, average incline, coordinates and other characteristics.

## 2. Point sources

Because Pre-defined method of streams and sub-basins delineation was applied, at the second stage of performed activities additional Outlets and draining watershed inlets were not added, yet point sources were added manually. For this purpose annual reporting forms concerning water discharge of more than 400 enterprises were analyzed within the Kharkiv, Donetsk and Lugansk regions. All investigated enterprises discharge waste waters into Severskiy Donets Basin. 23 point sources having a major impact on river water quality formation were selected within Ukrainian part of Severskiy Donets river basin.



In the process of point sources selection, 2 major indicators were considered:

1. Generalized discharge by water quality indicator, developed by our institute.
2. Total volume of waste waters.

Apart from that, location of discharge points relative to administrative units (oblasts), constituting the basin territory, was taken into account.

SWAT-modeling programme assumes that each sub-basin attributes with not more than one point source of contamination. Therefore, all point sources located within one sub-basin were replaced by one effective source of contamination. Waste water discharge for effective source of contamination was assumed to be the sum of waste water discharge of all point sources of contamination located within sub-basin. It was also assumed that annual mass of each above mentioned pollutants equaled the total annual mass of the substance discharge contained in waste waters of all point sources within sub-basin. Location of the effective source of contamination was established on the main water stream of respective sub-basin. 13 effective sources of contamination were researched through the SWAT modeling process (Fig. 3).

Based on the data on all selected point sources, the table, including waste water discharges and pollutant loads, necessary for modeling, was organized. Data in the table were presented as constant daily loadings.

As the SWAT modeling provides an evaluation of 3 conservative substances, to perform the calculations we have chosen Total Fe, Chromium (6+) and Zinc as three indicators, characterizing metals content in return waters, because these metals are typical for return waters of most point sources within Severskiy Donets river basin.

Results of analysis showed that total Fe is present in significant amounts in wastewater of 394 enterprises; Chromium (6+) – in wastewater of 45-enterprises; zinc – in waste water of 66 enterprises. Total annual mass of iron discharged with waste water was 121.664 kg, total annual mass of hexavalent chromium – 2284 kg and the total annual mass of zinc – 4153 kg.

Besides metal entering to surface water with waste waters, we have considered metal entering in consequence of transboundary transport of contaminants in river water. For these purposes, the data on river water quality observing in the some areas of cross-border monitoring points were analyzed:

1. Oskol river, Topoli village;
2. Severskiy Donets river, Ogurtsovo village;
3. Volchia river, Zemlianki village;
4. Kharkiv river, Strelechia smt;

5. Lopan' river, Kazachia Lopan' smt;

6. Udy river, Okop village.

All transboundary ranges located on the border with Russia. Observation data on river water discharge on hydrological stations, close to transboundary monitoring stations was used in order to estimate the transboundary transport of contaminant substances with river waters. Location of transboundary monitoring points and the nearest hydrological stations is shown on Fig. 3.

Transboundary transport has to be considered due to high concentrations of contaminants in transboundary ranges. The concentration of metals in transboundary rivers for 2009 year is shown in Table 1.

**Table 1.** Concentration of metals in transboundary river ranges in Kharkiv region for 2009

№	Monitoring station	Average concentration, mg/dm <sup>3</sup>			Maximal concentration, mg/dm <sup>3</sup>			Minimal concentration, mg/dm <sup>3</sup>		
		Fe	Cr <sup>6+</sup>	Zn	Fe	Cr <sup>6+</sup>	Zn	Fe	Cr <sup>6+</sup>	Zn
1.	Oskol river, Topoli village	0.115	0.002	0.012	0.05	0.002	0.01	0.15	0.002	0.013
2.	Severskiy Donets river, Ogurtsovo village	0.11	0.002	0.008	0.05	0.001	0.003	0.15	0.003	0.014
3.	Volchia river, Zemlianki village,	0.12	0.0018	0.007	0.06	0.001	0.003	0.16	0.002	0.01
4.	Kharkiv river, Strelechia smt	0.16	0.003	0.012	0.15	0.002	0.008	0.19	0.004	0.014
5.	Lopan' river, Kazachia Lopan' smt	0.20	0.0027	0.010	0.16	0.002	0.006	0.28	0.003	0.012
6.	Udy river, Okop village	0.29	0.0027	0.006	0.23	0.002	0	0.38	0.003	0.009

As we can see from Table 1, annual concentration of total Fe exceed the Fisheries standards used in Ukraine (MAC=0.1 mg/dm<sup>3</sup>) in all transboundary monitoring stations. The largest exceeding (almost 3 MACs) was observed in transboundary range in Udy River.

In transboundary ranges of Kharkiv, Lopan and Udy rivers even minimum annual total iron concentrations exceeded fishery MACs. The maximum single exceeding of fishery

regulations (3.8 MAC) was also observed in the Udy River. Annual Chromium (6+) concentrations also exceeded fisheries standards (MAC = 0.001 mg/dm<sup>3</sup>) in all areas of transboundary monitoring stations. The highest exceeding (3 MAC) was observed in transboundary range in Kharkiv River. Minimum concentration of hexavalent chromium in the transboundary ranges of Volchia and Severskiy Donets rivers was at the level of fishery MACs. But in transboundary river ranges in Oskol, Kharkiv, Uda and Lopan' rivers concentration of Chromium (6+) exceeded MPC more than 2 times. Maximum single exceeding of fishery regulations (4 MAC) was observed in Kharkiv River.

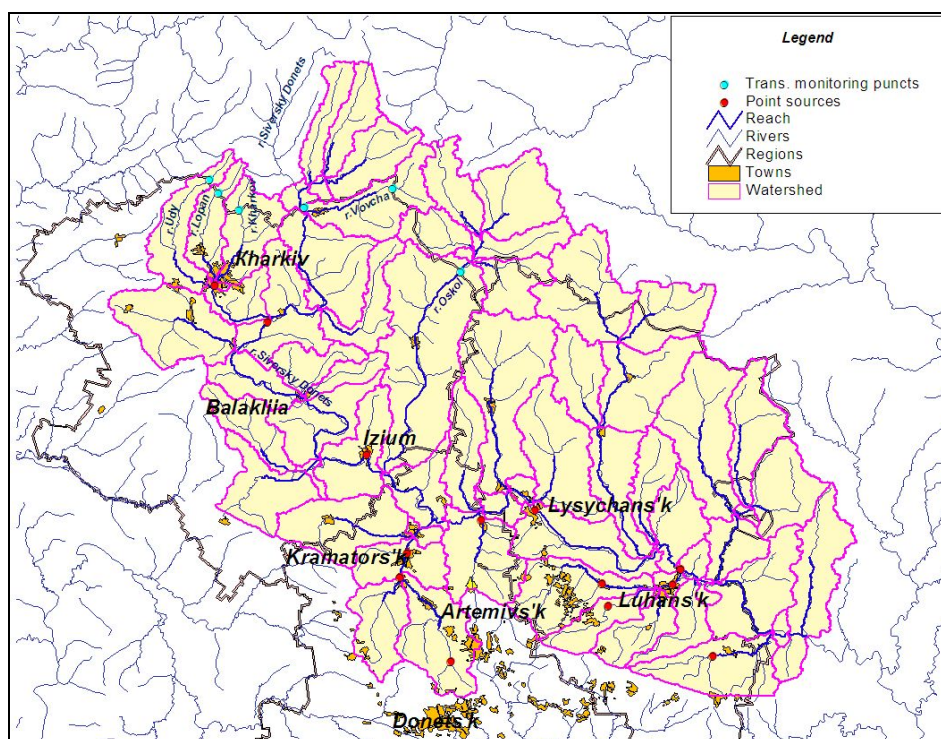


**Fig. 3.** Localization of point sources and transboundary monitoring stations

Annual average Zinc concentrations are slightly exceeded the fisheries regulations (1.2 MAC) in transboundary ranges of 2 rivers: Oskol and Kharkiv. In other rivers the concentrations were within MAC limits. Minimal zinc concentration in Oskol River was at MAC level, but in other rivers - low than MPC. The maximum annual concentration of zinc in Oskol, Severskiy Donets, Kharkov and Lopan' rivers slightly exceeded fisheries

regulations (1.2-1.4 MAC), and in Volchoa and Udy rivers the concentrations were within MAC limits.

### 3. HRU analysis

This stage of activities (HRU analysis) included the following sub-stages:

1. Classification of catchment areas by type of land use;
2. Classification of catchment areas by soil type;
3. Defining the areas with different levels of incline;
4. Defining the hydrologically homogeneous units (HRU-units).

At the *first sub-stage of HRU analysis*, 12 types of land usage were defined (Fig. 4). All classes were identified using the correspondence table. The CROP table of a database SWAT2009\_Europe.mdb was applied. The following types of land usage were predominant at the Severskiy Donets river basin territory: CRIR (IRRIGATED CROPLAND AND PASTURE) – 71.1%, CRGR (CROPLAND/GRASSLAND MOSAIC) – 15.8%, CRDY (DRYLAND CROPLAND AND PASTURE) – 4.8%, CRWO (CROPLAND/WOODLAND MOSAIC) – 4.2%, FOEN (EVERGREEN NEEDLELEAF FOREST) – 1.53% and FOMI (MIXED FOREST) – 1.48%. Each of the other 6 types of land usage occupies less than 1% of a territory.

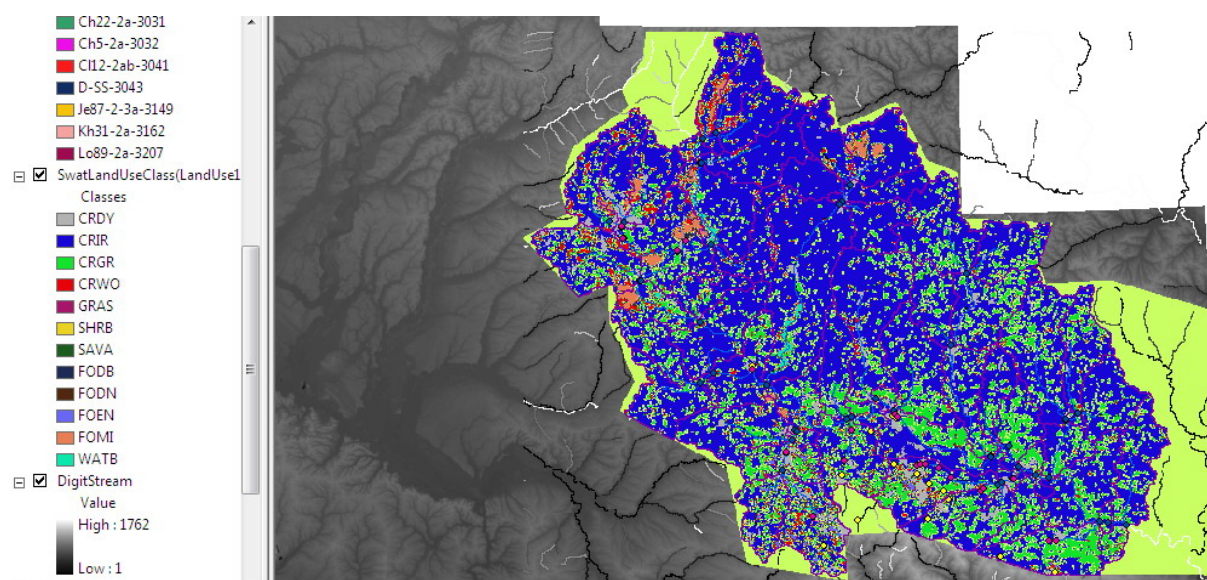


**Fig. 4.** Distribution of land use types over the territory of Severskiy Donets River basin

At the *second sub-stage of HRU-analysis* 7 soil classes were identified. All classes were also identified using the correspondence table (Fig. 5). The table USERSOIL, belonging to a database SWAT2009\_Europe.mdb. was used for identification. All selected soil classes corresponded to more than 3% of a total area. The most widespread soil class was Ch22-2a-3031 (59,2%). Soils, belonging to class Je87-2-3a-3149 occupied (13,0%). Soils of other classes occupied less than 10% of the total area.

At the *third sub-stage* 2 slope levels were selected: 1) up to 2% and 2) more than 2%. Part of the Severskiy Donets river basin territory showing selected slope levels is depicted at Fig 6. Further, super-positioning of selected land use types, soil classes and slope levels was conducted, and, as a result, hydrologically uniform units (HRU-units) were defined.

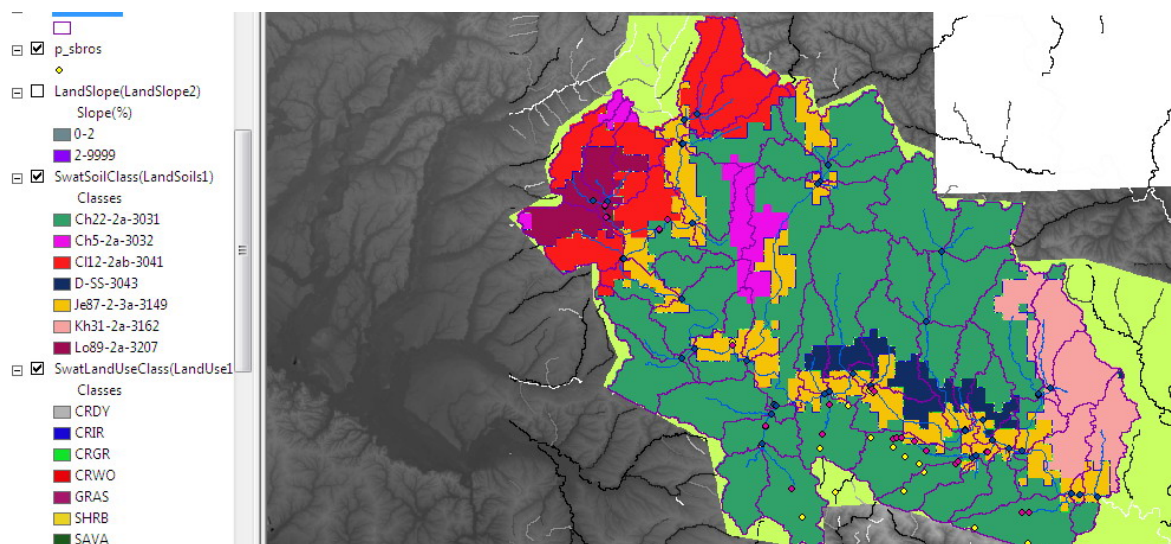


**Fig. 5.** Distribution of soil classes over the territory of Severskiy Donets River basin

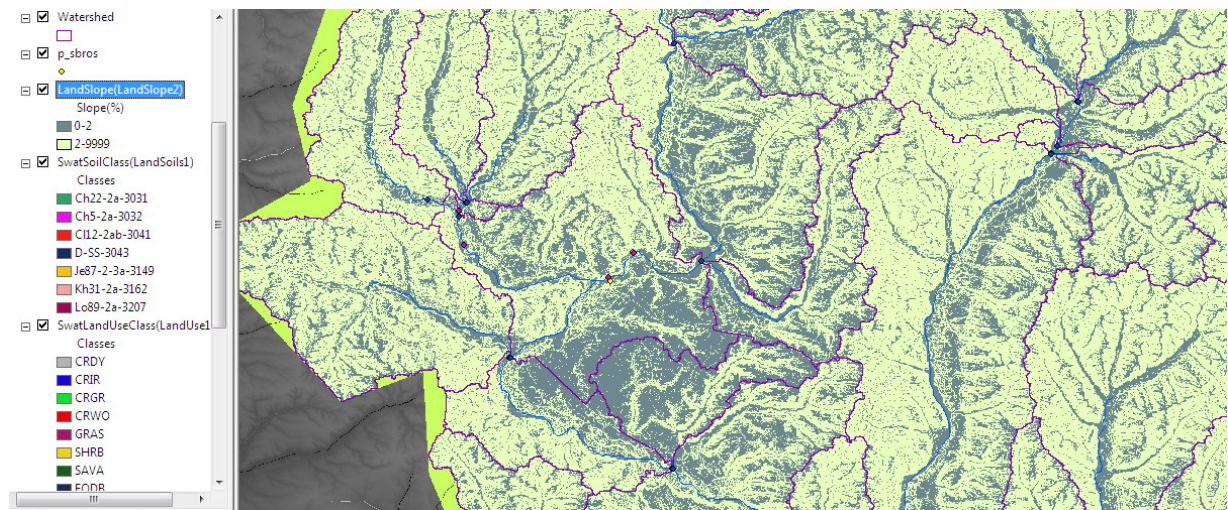


**Fig. 6.** Distribution of slope levels over the territory of Severskiy Donets River basin

#### 4. Meteorological data

At the *fourth sub-stage of HRU analysis* 4 weather monitoring stations were selected within Severskiy Donets river basin: Kharkov, Izjum, Artemovsk and Lugansk. For each station, tables of statistical characteristics, necessary for modeling of meteorological parameters were created. It is not possible to find the info on dewpoint temperatures in open statistical sources. Yet the data on relative humidity are available. So that, average dewpoint temperatures were calculated based on correlation between the relative humidity and the dewpoint. Based on gathered meteorological data, table USERWGN was created, which became a part of the SWAT2009\_Europe.mdb database.

#### 5. Monthly and annual average river water discharge assessment

Further, Swat modeling (SWAT Simulation) was conducted. At the *fifth sub-stage* the following simulation period was applied: Starting Date – 1.1.1991 and Ending Date – 12.31.1992. Such choice of simulation period can be explained by the fact, that we only



had data on discharges and river water quality for the period of 1991 – 1992. The type of Rainfall Distribution was set as Skewed normal.

The timeframe of one month (monthly frequency) was selected for the delivery of modeling results. Such a timeframe can be explained by the fact, that water quality observations at the monitoring stations are conducted once per month.

## **6. Actual river water discharge data and concentration of contaminants in monitoring stations**

Performing the sixth sub-stage, data on 16 monitoring points on Severskiy Donets river basin, 5 points on Lugan' river, 4 points on Udy river, 3 points on each of the Bakhmut and Kazeniy Torets rivers and 2 points on Lopan', Belen'kaya and Oskol rivers and 1 point on Krivoy Torets, Sukhoi Torets, Volchia, Kharkov, Krasnaya and Mokraya Plotva. Apart from that, data on 2 monitoring points on Krasnooskol'ske reservoir and 1 point on Pechenez'ke reservoir were prepared.

## **7. Model calibration**

Model calibration was conducted at the seventh sub-stage of HRU-analysis using the program SWAT-CUP2. ParaSol method was applied. In the process of calibration optimization of 10 model parameters was conducted. 10-parameter optimization is a default feature of ParaSol program. The maximal number of trials before optimization is terminated was set to 200. Calibration by only one parameter – river discharge and only for one monitoring station (Severskiy Donets, near Izjum smt.) was conducted.

## **8. Validation**

Validation was conducted as the next step. In order to conduct Validation, observation data from the monitoring station, located on Severskiy Donets River at the Ukrainian border (Kruzshilovka village) were used. Location of sub-basins, selected for calibration and validation, is shown on a Fig. 7.

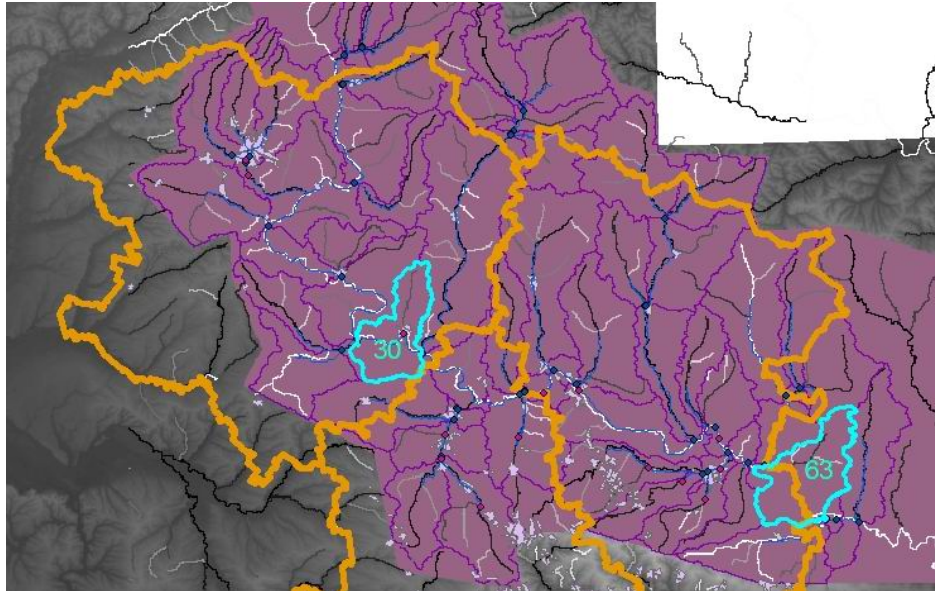


**Fig. 7.** Distribution of sub-basins, selected for calibration (30) and validation (63): borders of selected sub-basins are highlighted by thick blue lines; orange lines define oblast borders

As a result of calibration procedure, the best parameter set was defined. Optimal values of corresponding parameters were entered with the help of Edit SWAT Input into the database of SWAT program. After that, the new modeling run was conducted.

Validation results for “Severskiy Donets river monitoring station, below Kruzshilovka village” (for 1992) are shown on Fig. 8.

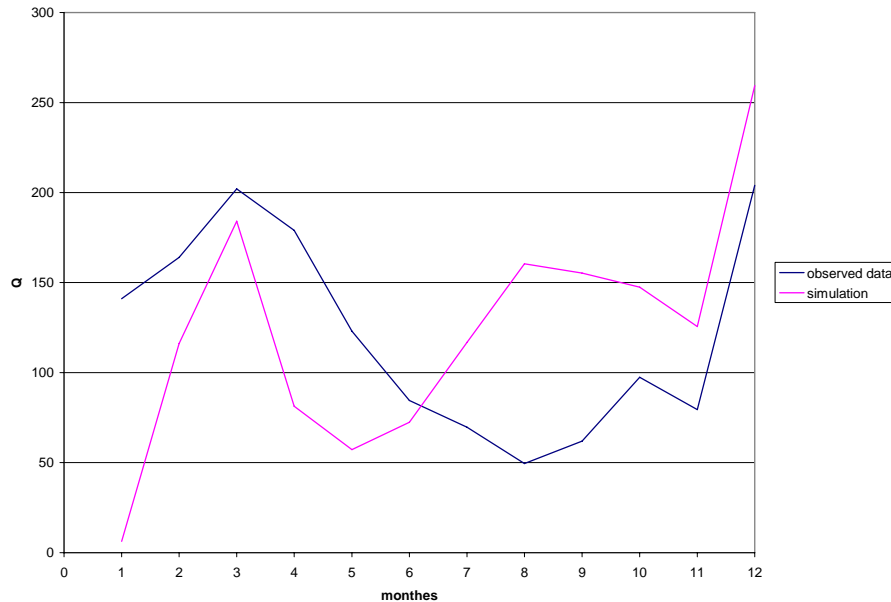


Fig. 8. Results of Validation for monitoring station “Kruzshilovka smt.”

As presented above, calculated and actual average monthly flow values differ significantly. The most significant differences are for January, August and September. At the same time, the forecasted average annual flow volume  $Q_{sim} = 123,5 \text{ m}^3/\text{s}$  is quite close to the observed value  $Q_{obs} = 110,8 \text{ m}^3/\text{s}$ .

The forecasted values for pollutant masses (BOD-5, ammonia nitrogen, nitrate nitrogen and mineral phosphorus), contributed annually from the Severskiy Donets river basin, at the Ukraine – Russia border (sub-basin 63 outlet), and average annual concentrations of these ingredients were calculated for a given river station.

Comparison of forecasted and observed values demonstrated the necessity of additional calibration based on BOD-5 parameter. At the same time optimization of RK1 parameter (carbonaceous biological oxygen demand deoxygenation rate coefficient in the reach at  $20^\circ\text{C}$  [ $\text{day}^{-1}$ ]) was carried out. This parameter controls the speed of water self-purification from a given non-conservative pollutant, for current conditions its value is  $RK1=1.71$ .

Figures 9-10 show comparison diagrams between calculated masses (or average annual concentrations) and observation data on Severskiy Donets river monitoring Station, below Kruzshilovka village.

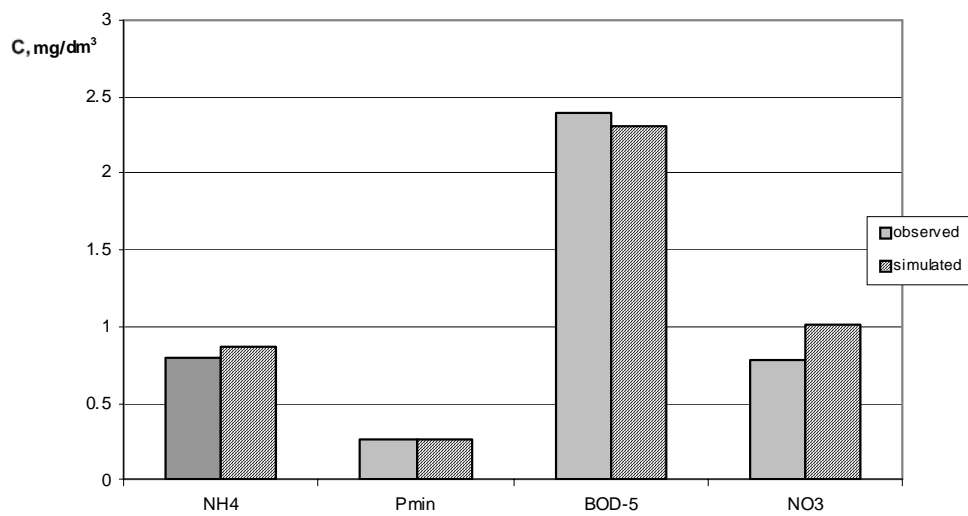
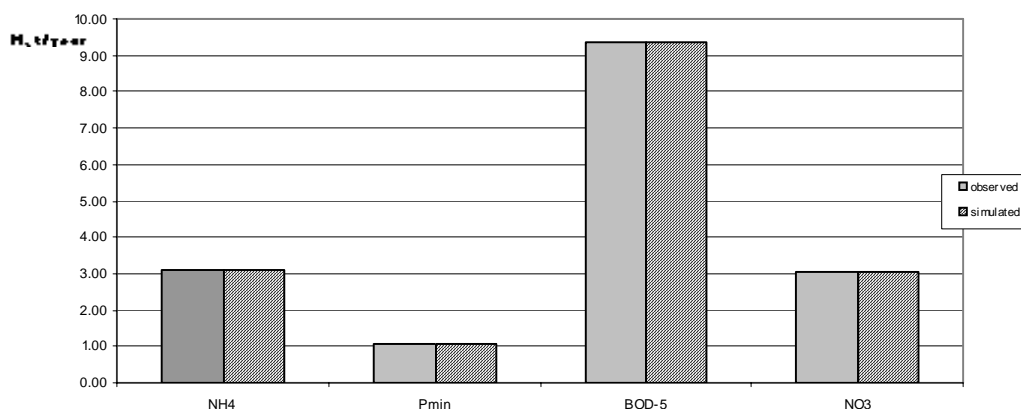


*Fig. 9. Masses of substances, carried out from the territory of Severskiy Donets River basin (within Ukrainian borders) at the border with Russia*



10. Average concentrations of substances, carried out from the territory of Severskiy Donets river basin (within Ukrainian borders), at the border with Russia (Kruzshilovka smt.)

As it presented at diagrams, the lowest assessment error is for the annual average phosphorus mineral. The error magnitudes for calculated Severskiy Donets river water discharge in Kruzshilovka smt. and annual masses of substances are listed in Table 2.

**Table 2.** Assessment errors for the annual river water discharge and masses of substances, annually carried out from the Severskiy Donets river basin territory (within Ukrainian borders).

Substance	River discharge (Q), m <sup>3</sup> /s	Masses of substances, T/year			
		NH4	Pmin	BOD-5	NO3
observed	123.5	3.12	1.05	9.35	3.05
simulated	110.8	3.04	0.94	8.04	3.53
Assessment error %	10.3	2.4	10.3	14.0	15.78

Thus, on the basis of the performed activities, we can conclude about the possibility of SWAT-modeling using for predictions of the river water quality and water discharge in the whole basin or part of the big river basin in European part of the Black Sea basin,



taking into account various loadings of contaminants from point sources and various weather conditions

Conducted calculations have shown that the use of averaged values - monthly or less frequent as input data in predicting monthly averages, has led to significant discrepancies between the calculated and observed data.

It was assumed that such discrepancies are caused by significant deviation of actual meteorological parameters from average parameters. Therefore, the most significant meteorological parameters (daily precipitation and daily temperature extremes) were considered in SWAT modeling process.

For these purposes at the *eighth sub-stage of HRU-analysis (composing the tables with data on actual river water discharge and contaminants concentrations in other monitoring stations)* two tables were composed. One table includes data on daily precipitation for 2009 year, the other one – data on daily temperature extremes for 2009 year. Data on precipitation and temperatures data were prepared for two meteorological stations – Izjum and Lugansk.

## **9. SWAT modeling**

At the *ninth sub-stage* SWAT modeling for the period of 1.01.2009 -31.12.2009 was performed. Daily precipitation and temperature data was used for the SWAT modeling process. Other meteorological parameters included average data from the following meteorological stations: Kharkiv, Izjum, Artemivsk and Lugansk. As a result of performed activities, average monthly river water discharge values for outfall ranges of all sub-basins were calculated.

At the *tenth sub-stage* the model calibration and validation were conducted. Model calibration was conducted using the SWAT-CUP2 program. ParaSol method was applied. At the first stage of calibration, optimization of 10 modeling parameters (default option) was performed. Calibration was conducted based on the “river flow” parameter. Data on actual monthly river water discharge for the monitoring station placed at Severskiy Donets river, below Izjum smt were used for calibration. The maximal number of iterations (trials allowed before optimization is terminated) was set to 2500.

In spite of the large number of iterations, it was not possible to achieve proper correlation between calculated and observed data for the first months of the year.

Therefore, re-calibration was performed, in the process of which, in addition to the default parameters, the 6 parameters, describing snowmelt processes were included:

1. SMTMP – snow melt base temperature,

2. SMFMX – melt factor for snow on June 21,
3. SMFMN – melt factor for snow on December 21,
4. TIMP – snow pack temperature lag factor,
5. SNOWCOVMX – minimum snow water content that corresponds to 100% snow cover;
6. SNO50COV – fraction of snow volume represented by SNOWCOVMX that corresponds to 50% snow cover.

Calibration results for the Seversky Donets monitoring station, below the city of Izjum, with optimization of 16 model parameters are shown at the figure 11.

Validation was carried out for the Ukrainian part of the Seversky Donets river basin, below the Kruzshilovka village, at the border with Russia. Validation results are given below (Figure 12).

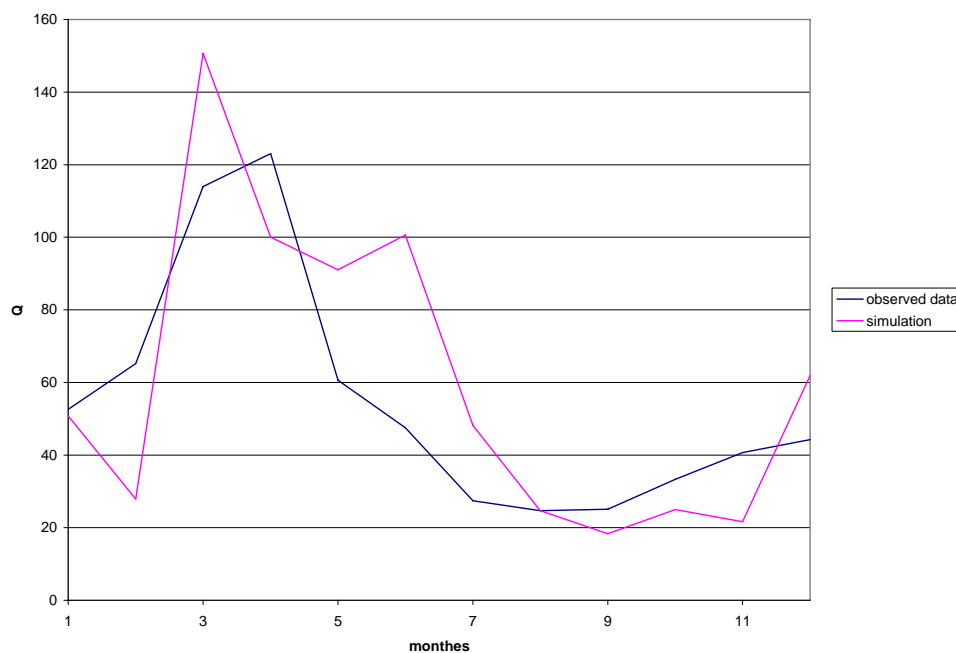


**Fig. 11.** Observed and estimated average monthly river water discharge for the monitoring stations on Seversky Donets river, below Izjum smt. (the results of model calibration)

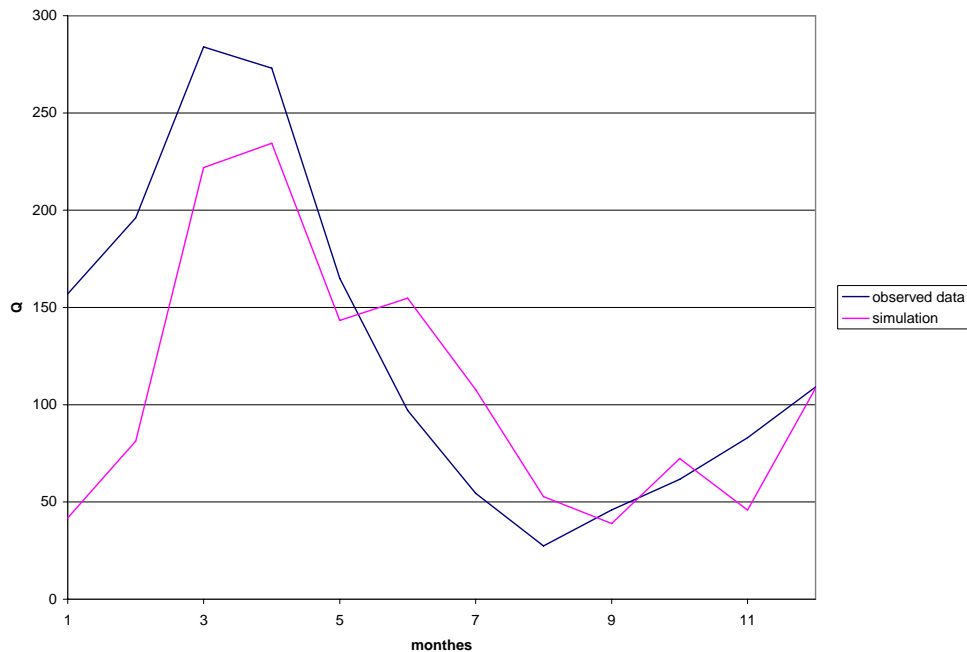


**Fig. 12.** Observed and estimated average monthly river water discharge for the monitoring stations on Seversky Donets river, below Kruznilovka smt, border with Russia (the results of model validation)

After the river water discharge calibration, the calibration for phosphorus mineral, ammonia nitrogen and BOD<sub>5</sub> was carried out. For the phosphorus mineral calibration, the following model parameters were optimized:

1. RS2 – benthic (sediment) source rate for dissolved in the reach at 20°C;
2. RS5 – organic phosphorus setting rate in the reach at 20°C;
3. BC4 – rate constant for mineralization of organic phosphorus to dissolved phosphorus in the reach at 20°C.

For the ammonia nitrogen calibration, the following model parameters were optimized:

1. BC1 – rate constant of biological oxidation of NH<sub>4</sub> to NO<sub>2</sub> in the reach at 20°C in well-aerated conditions;
2. BC2 – rate constant of biological oxidation of NO<sub>2</sub> to NO<sub>3</sub> in the reach at 20°C.

For the BOD<sub>5</sub> calibration, the following model parameters were optimized:

1. RK1 – carbonaceous biological oxygen demand deoxygenation rate coefficient in the reach at 20°C;
2. RK2 – oxygen reaeration rate in the reach at 20°C;
3. RK3 – rate of loss of carbonaceous biological oxygen demand due to the setting in the reach at 20°C;
4. RK4 – benthic oxygen demand rate in the reach at 20°C;
5. RS1 – local algal setting rate in the reach at 20°C.

Results of water quality data for 2009 were used for calibration and validation process. Validation results on non-conservative water quality parameters for outfall range placed at Ukrainian part of Severskiy Donets River, Popovka smt. (border with Russia) are shown in Fig. 13-15.

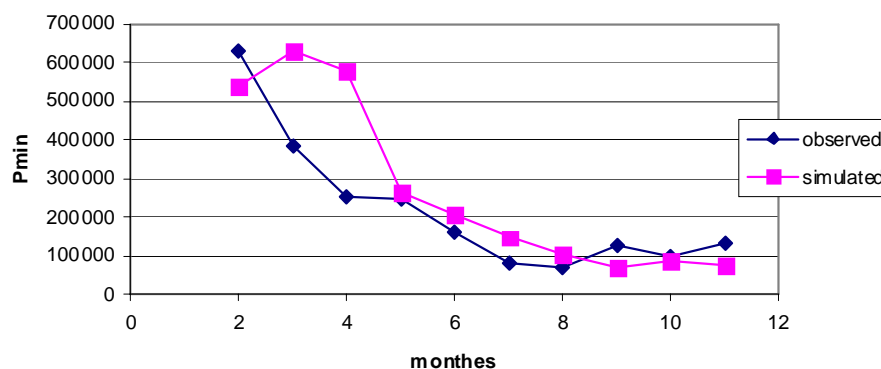


**Fig. 13.** Observed and estimated average monthly loadings of phosphorus mineral (kg/month) for the monitoring station placed at Severskiy Donets River, Popovka smt, border with Russia

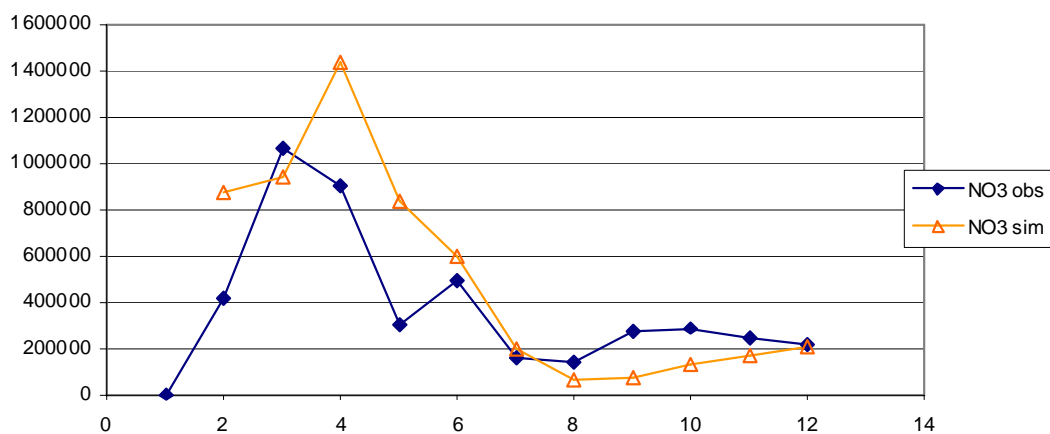


**Fig. 14.** Observed and estimated average monthly loadings of ammonia nitrogen mineral (kg/month) for the monitoring station placed at Severskiy Donets River, Popovka smt., border with Russia

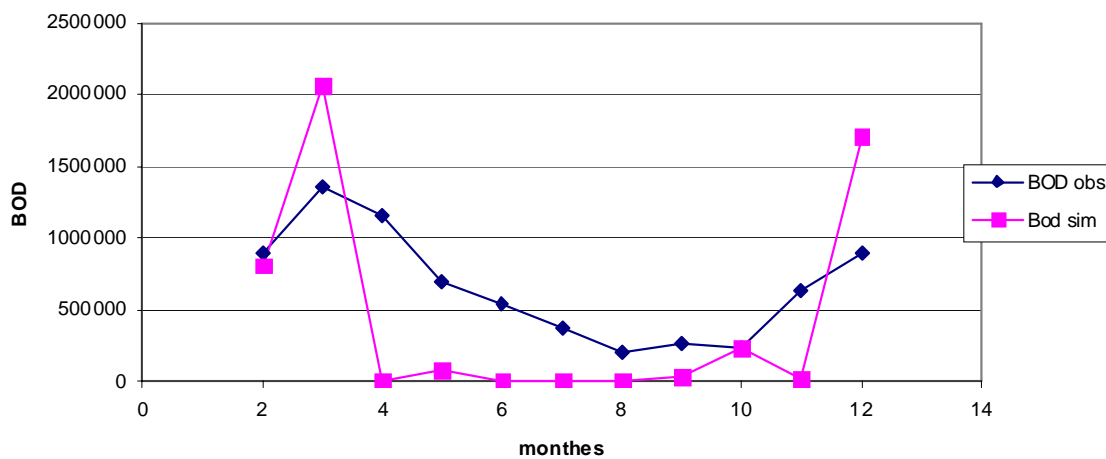


**Fig. 15.** Observed and estimated average monthly loadings BOD<sub>5</sub> mineral (kg/month) for the monitoring station placed at Severskiy Donets River, Popovka smt., border with Russia



Performed activities showed a good correlation between simulated and observed data on annual average river water discharge and contaminant loadings of BOD-5, ammonia nitrogen, phosphorus mineral and nitrogen nitrate.

At the final stage of the work the model calculations, calibration and verification for the annual average concentrations of metals were carried out.

### **10. Final modeling calculations**

The modeling was performed only for the average annual values because dynamics of concentrations in the river waters is caused mainly by changes in inflow from the point sources (wastewater discharge from enterprises). Statistical reporting data of investigated enterprises used for modeling. Such data includes average annual masses of contaminants (T/year).

The model calculations of the total iron concentrations, hexavalent chromium, and zinc were performed for 4 monitoring stations located on the Severskiy Donets River:

1. Zmijiv town (below the town);
2. Krasna Gusarovka smt. (below Balakleya town);
3. Sinichnoe smt. (below Izjum town);
4. Popovka smt. (border with Russia).

The first 3 points of monitoring are located within the Kharkiv region, 4th monitoring point - in the Luhansk region. In monitoring stations placed at towns Zmijiv and Izjum there are hydrological stations for river water discharge measurements.

Location of the hydrological stations for water quality monitoring is shown Fig. 16.

After performing the model calculations, the model calibration was carried out. Calibration process considered only one parameter – river water quality discharge ( $Q_{simi}$ ).

This parameter was compared with the observed values of the of river water discharge ( $Q_{obsi}$ ,  $i = 1-4$  - the serial number of the hydrological station) in 4 hydrological stations (see Fig. 2). The average monthly river water discharge data for the period 2009-2010 are presented in Tables 3-4.

Model calibration was conducted using the program SWAT-CUP2. ParaSol method was applied. In the process of calibration optimization of 16 model parameters was conducted. 10-parameter optimization is a default feature of ParaSol program and 6 parameters describe snow melt process:

- SMTMP – snow melt base temperature;
- SMFMX – melt factor for snow on June 21;
- SMFMN – melt factor for snow on December 21;
- TIMP – snow pack temperature lag factor;
- SNOWCOVMX – minimum snow water content that corresponds to 100% snow cover;
- SNO50COV – fraction of snow volume represented by SNOWCOVMX that corresponds to 50% snow cover.

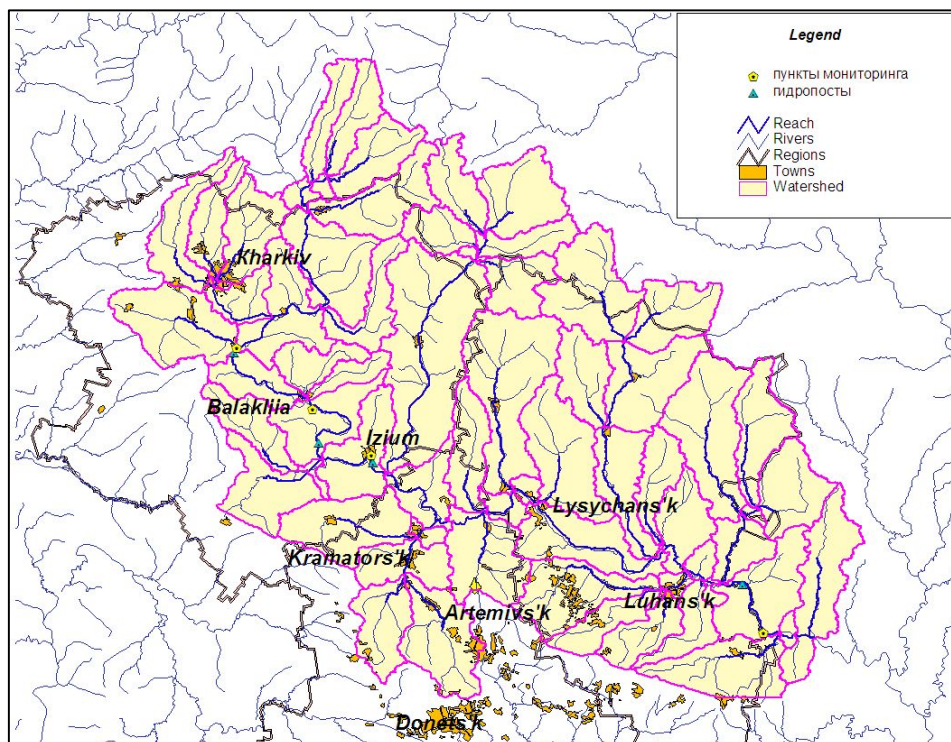


Fig. 16. Location of hydrological stations, monitoring stations for weather conditions measurements and monitoring stations for water quality control

The maximal number of trials before optimization is terminated was set to 500.

The results of comparing the calculated river water discharge values (after model calibration process) and water discharge values observed at hydrological stations are shown in the Fig. 17 and in Table 6.

As it is shown in the Figure 3, water discharge values increase from Zmijiv smt. To Kruzhilovka smt. Table 5 shows that maximum relative error of river water discharge value (22.1%) was observed for hydrological station in Kruzhilovka smt. For other hydrological stations the relative error varied from 2.7-5.3%.

**Table 3.** Average monthly river water discharge data for 2009 used for model calibration

Hydrological stations	Average monthly river water discharge, m <sup>3</sup> /sec											
	1	2	3	4	5	6	7	8	9	10	11	12
Zmijiv town	26.0	39.8	46.5	34.1	29.0	21.5	19.0	20.7	24.3	27.3	26.1	27.5
Protopopova smt.	41.0	40.2	92.3	104	42.6	27.3	23.7	22.0	20.9	34.9	37.9	41.4
Izjum town	52.6	65.2	114	123	60.6	47.5	27.4	24.7	25.1	33.3	40.7	44.3
Kruzhilovka smt.	157	196	284	273	165	97.1	54.5	27.4	45.9	61.6	83.0	109

**Table 4.** Average monthly river water discharge data for 2010 used for model calibration

Hydrological stations	Average monthly river water discharge, m <sup>3</sup> /sec											
	1	2	3	4	5	6	7	8	9	10	11	12
Zmijiv town	38.5	36.7	99.1	87.6	31.4	22.7	21.2	18.8	21.4	32.5	33.7	42.7
Protopopova smt.	35.3	42.3	47.4	41.2	31.0	22.9	18.1	18.9	21.7	25.6	31.5	34.4
Izjum town	39.9	53.1	61.3	51.2	38.2	30.1	24.2	19.1	20.9	26.6	32.2	32.5
Kruzhilovka smt.	107	127	157	146	92.9	72.5	47.8	40.3	47.4	55.8	69.3	89.9



It should be noted that in 2009 the river water discharge was about 1.5 times lower than the average long-term values of these parameters, and in 2010, approximately equal to long-term average values (Table 5).

Validation process was performed for 3 parameters: total iron, chrome hexavalent chromium and zinc. Concentrations of investigated metals in monitoring stations are given in Table 7.

**Table 5.** Average annual river water discharge near monitoring stations used for model calibration

Hydrological stations	Average annual river water discharge, m <sup>3</sup> /sec		
	2009	2010	Average long-term
Zmijiv town	28.5	40.5	46.4
Protopopova smt.	30.9	44.0	48,7
Izjum town	35.8	54.9	54,2
Kruzhilovka smt.	87.7	129.5	137

**Table 6.** Estimated and observed values of river water discharge for 2010

Parameter	Hydrological stations			
	Zmiiv 22	Protopopovka 27	Izum 30	Krujilovka 63
Qobs, m <sup>3</sup> /s	40.5	44.0	54.9	129.5
Qsim, m <sup>3</sup> /s	38.36	45.24	53.39	100.9
Relative error, %	5.3	2.8	2.7	22.1

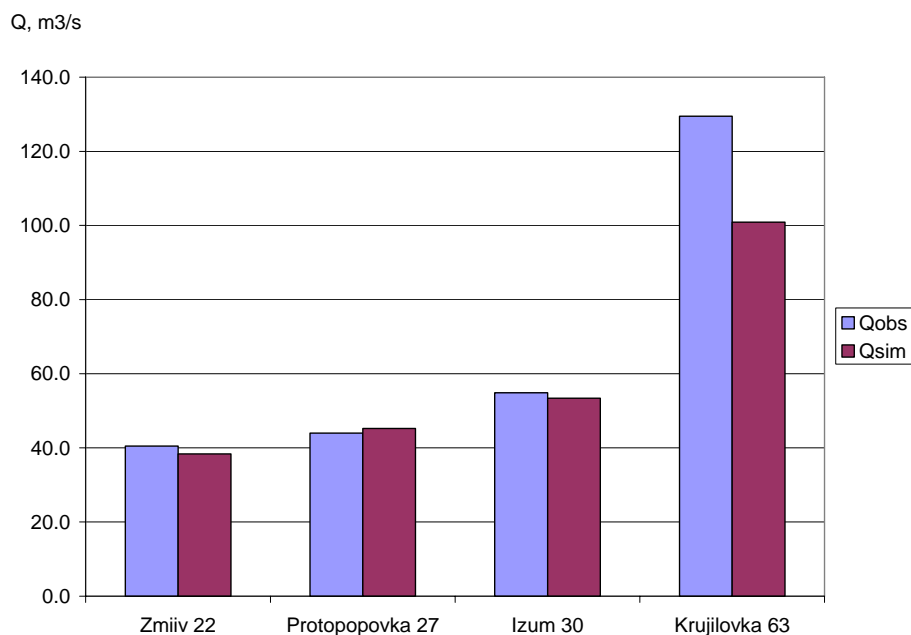


**Fig.17.** Estimated and observed values of river water discharge for 2010 (numbers of sub-basins are written with smt. names)

**Table 7.** Concentration of metals in monitoring stations placed at Severskiy Donets River for 2010

№	Monitoring station	Average concentration, mg/dm <sup>3</sup>			Minimal concentration, mg/dm <sup>3</sup>			Maximal concentration, mg/dm <sup>3</sup>		
		Fe	Cr <sup>6+</sup>	Zn	Fe	Cr <sup>6+</sup>	Zn	Fe	Cr <sup>6+</sup>	Zn
1.	Zmijiv smt.	0,113	0,0043	0,0125	0,1	0,004	0,012	0,12	0,005	0,013
2.	Krasnaya Gusarovka smt. (below Balakleya smt.)	0,103	0,0025	0,0128	0,09	0,002	0,011	0,12	0,003	0,015
3.	Sinic hnoe smt. (below Izjum smt.)	0,075	0,0023	0,01	0,05	0,002	0,009	0,09	0,003	0,011
4.	Popovka smt. (border with Russia)	0,111	0,0019	0,0044	0,1	0,001	0,004	0,16	0,005	0,005

Obtained data show that concentration of metals decrease from Zmijiv smt. to Sinichnoe smt. (below Izjum smt.). Decrease of concentrations is caused by dilution of polluted water by river water. In the first 2 monitoring stations the concentration of all metals exceed fishery regulations. In monitoring station placed at Sinichnoe smt. (below Izjum smt.) average annual iron concentration is below fisheries MACs, and the zinc concentration reaches the level of MAC.

In Popovka smt. (border with the Russian Federation), the concentration of iron increases again, due to the arrival run-off water from point sources located at Donetsk and Lugansk regions in river water. The annual average concentration of iron in this monitoring station exceeds the MAC, and the maximal concentration even exceeds the concentration in monitoring station placed at Zmijiv smt. The concentration of hexavalent chromium and zinc in the monitoring station placed at Popovka smt. (border with Russia) continues to decrease, average annual concentration of zinc is lower than fisheries MACs, but the concentration of hexavalent chromium continues to exceed the MPC.

The results of comparing the calculated annual average concentrations of metals with the observed average annual data are shown in Figures 18-20.

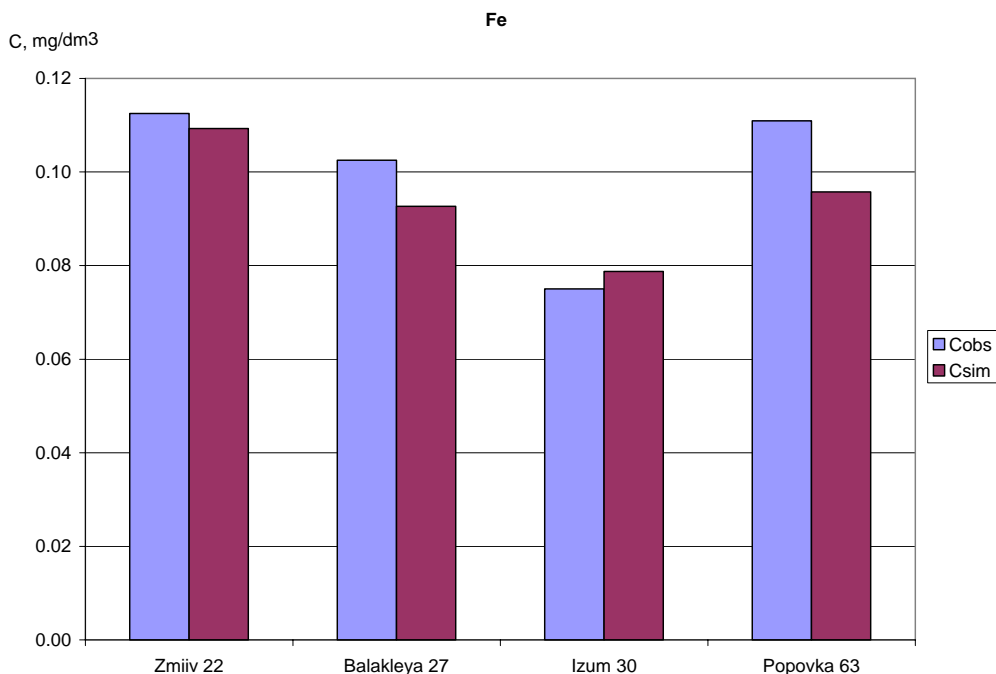


**Fig. 18.** Estimated and observed average annual iron concentrations in monitoring stations placed at Severskiy Donets River

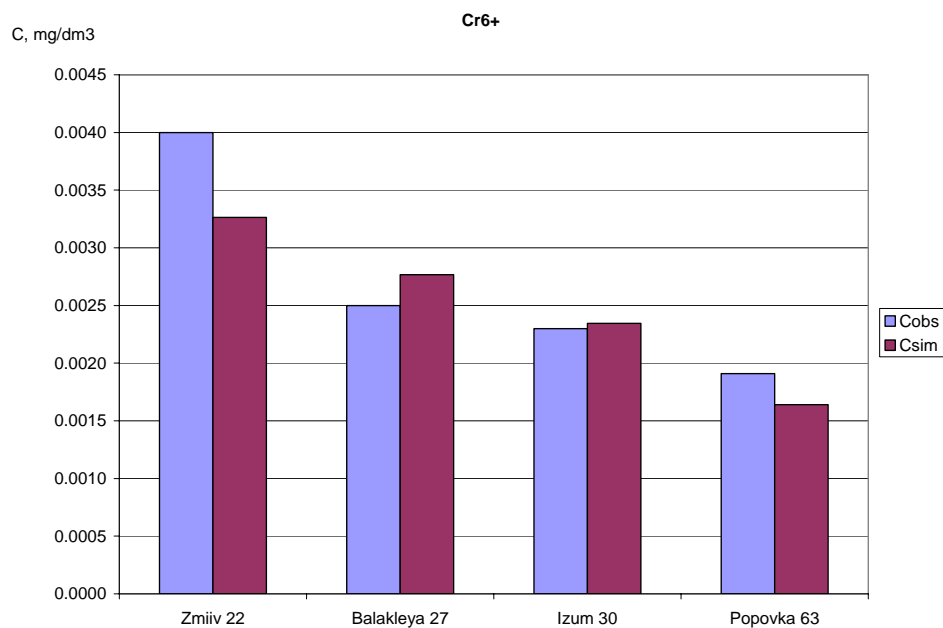


**Fig. 19.** Estimated and observed average annual chromium concentrations in monitoring stations placed at Severskiy Donets River

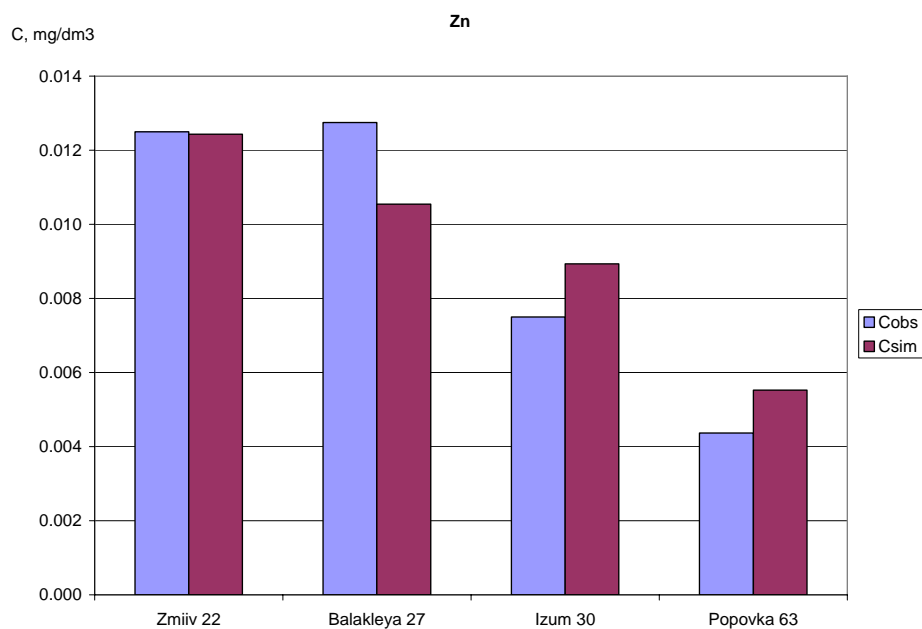


**Fig. 20.** Estimated and observed average annual zinc concentrations in monitoring stations placed at Severskiy Donets Rive



btained diagrams (Figures 18-20) show good agreement between calculated and observed annual average concentrations of metals in 4 investigated monitoring stations. Dynamics of the spatial variation of estimated concentrations for all metals coincides with the dynamics of the spatial variation of observed concentrations. The relative error of metal concentrations are shown in Tables 8-10.

**Table 8.** The relative error of total iron concentration in monitoring stations placed at Severskiy Donets River

	Monitoring stations/sub-basins			
	Zmiiv /22	Balakleya /27	Izum /30	Popovka /63
Observed concentration, mg/dm <sup>3</sup>	0.11	0.10	0.08	0.11
Estimated concentration, mg/dm <sup>3</sup>	0.11	0.09	0.08	0.10
Relative error, %	<3	9.6	<5	13.7

**Table 9.** The relative error of chromium concentration in monitoring stations placed at Severskiy Donets River

	Monitoring stations/sub-basins			
	Zmiiv /22	Balakleya /27	Izum /30	Popovka /63
Observed concentration, mg/dm <sup>3</sup>	0.0040	0.0025	0.0023	0.0019
Estimated concentration, mg/dm <sup>3</sup>	0.0033	0.0028	0.0023	0.0016
Relative error, %	18.4	10.7	<2	14.1



**Table 10.** The relative error of zinc concentration in monitoring stations placed at Severskiy Donets River

	Monitoring stations/sub-basins			
	Zmiiv /22	Balakleya /27	Izum /30	Popovka /63
Observed concentration, mg/dm <sup>3</sup>	0.0125	0.0128	0.0075	0.0044
Estimated concentration, mg/dm <sup>3</sup>	0.0124	0.0105	0.0089	0.0055
Relative error, %	0.5	17.3	19.1	26.6

The maximal relative error for all metals was observed in the monitoring point placed at Popovka smt. (border with the Russian Federation). This is probably caused by the highest error of wastewater discharge estimation.

The highest relative error value is for zinc. Average relative errors for monitoring stations are: for total iron - (-5.3%), hexavalent chromium - (-5%) and zinc - 7%.

Thus, on the basis of the performed activities for the Ukrainian part of Severskiy Donets River basin we can conclude the possibility of using SWAT-model for prediction of water discharge and water quality, considering the variable contaminant loadings from point sources; meteorological conditions, including climate change.



## REFERENCES

- Abbaspour, K. C. 2011. User manual for SWAT-CUP, SWAT calibration and uncertainty analysis programs, 93 pp., Eawag: Swiss Fed. Inst. of Aquat. Sci. and Technol., Dübendorf, Switzerland. (Available at <http://www.eawag.ch/organisation/abteilungen/siam/software/swat/index> EN)
- Abbaspour, K.C., Faramarzi, M., Ghasemi, S.S., Yang, H., 2009. Assessing the impact of climate change on water resources in Iran, *Water Resour. Res.*, 45, W10434, doi:10.1029/2008WR007615.
- Abbaspour, K.C., Yang, J., Maximov, I., Siber, R., Bogner, K., Mieleitner, J., Zobrist, J., Srinivasan, R., 2007. Modelling hydrology and water quality in the pre alpine/alpine Thur watershed using SWAT. *Journal of Hydrology* 333, 413-430.
- Abbaspour, K.C., Johnson, A., van Genuchten, M.Th, 2004. Estimating uncertain flow and transport parameters using a sequential uncertainty fitting procedure. *Vadose Zone Journal* 3(4), 1340-1352.
- Arnold, J. G. and Fohrer, N. 2005. SWAT2000: current capabilities and research opportunities in applied watershed modelling. *Hydrological Processes* 19 (3): 563-572.
- Arnold, J.G., Srinivasan, R., Muttiah, R.S., Williams, J.R., 1998. Large area hydrologic modeling and assessment - Part 1: Model development. *Journal of the American Water Res. Association* 34(1), 73-89.
- Arnold, J.G., Allen, P.M., 1996. Estimating hydrologic budgets for three Illinois watersheds. *Journal of Hydrology* 176, 57-77.
- Beven, K., Binley, A., 1992. The future of distributed models - model calibration and uncertainty prediction. *Hydrol. Process* 6(3), 279-298.
- Bloesch J., 2003. Flood plain conservation in the Danube River, the link between hydrology and limnology, summard report on the 34th IAD-conference, August 27-30, in Tulcea (Romania) and thw 21st IHP-UNESCO hydrological conference in Bucharest (Romania) 14/3-4: 347-362.
- BSEI, Black Sea Investment Facility. 2005: 'Review of the Black Sea Environmental Protection Activities. General review', Black Sea Investment Facility.
- Boegh, E., Thorsen, M., Butts, M.B., Hansen, S., Christiansen, J.S., Abrahamsen, P., Hasager, C.B., Jensen, N., Van der Keur, P., Refsgaard, J.C., Schelde, K., Soegaard, H., Thomsen, A., 2004. *Incorporating remote sensing data in physically based distributed agro-hydrological modeling*. *Journal of Hydrology* 287, 279-299.



- Campo, L., Caparrini, F., Castelli, F., 2006. *Use of multi-platform, multi-temporal remote-sensing data for calibration of a distributed hydrological model: an application in the Arno basin, Italy*. *Hydrological Processes* 20, 2693–2712.
- CEC., 2000. Directive 2000/60/EC of the European Parliament and of the Council Establishing a Framework for the Community Action in the Field of Water Policy. Page 327.
- Duan, Q., 2003. Global Optimization for Watershed Model Calibration, in *Calibration of Watershed Models*, edited by Duan, Q., Gupta, H.V., Sorooshian, S., Rousseau, A. N., Turcotte, R., pp. 89-104, AGU, Washington, DC.
- Eckhardt, K., Ulbrich, U., 2003. Potential impacts of climate change on groundwater recharge and streamflow in a central European low mountain range, *J. Hydrol.* 284, 244–252.
- European Space Agency (ESA). GlobCover Land Cover version 2.2. Online database. URL: <http://ionia1.esrin.esa.int/index.asp> [consulted 15 December 2012]
- FAO (Food and Agricultural Organization), 1995. The digital soil map of the world and derived soil properties. CD-ROM, Version 3.5, Rome.
- Faramarzi, M, Yang H., Schulin R., Abbaspour K.C. 2010. Modeling wheat yield and crop water productivity in Iran: Implications of agricultural water management for wheat production. *Agricultural Water Management*. 97: 1861-1875.
- Faramarzi, M., K.C. Abbaspour, R. Schulin, and H. Yang. 2009. Modeling blue and green water availability in Iran. *Hydrological Processes*. 23(3): 486-501.
- Farr, T. G., Rosen, P. A., Caro, E., Crippen, R., Duren, R., Hensley, S., Kobrick, M., Paller, M., Rodriguez, E., Roth, L., Seal, D., Shaffer, S., Shimada, J., Umland, J., Werner, M., Oskin, M., Burbank, D. and Alsdorf, D. 2007. The Shuttle Radar Topography Mission. *Reviews of geophysics* 45 (2): 934–948
- Fernandez-Quiruelas, V., Fernandez, J., Cofino, A. S., Fita, L., Gutierrez, J. M., 2011. Benefits and requirements of grid computing for climate applications. An example with the community atmospheric model. *Environmental Modelling and Software*, 26, 1057-1069.
- Fontaine, T.A., Klassen, J.F., Cruickshank, T.S., Hotchkiss, R.H., 2001. Hydrological response to climate change in the Black Hills of South Dakota, USA, *Hydrol. Sci. J.* 46, 27– 40.
- Food and Agriculture Organization and International Institute for Applied Systems Analysis (FAO-IIASA). Harmonized World Soil Database. Version 1.2. FAO, Rome, Italy and IIASA, Laxenburg, Austria. URL:



<http://www.iiasa.ac.at/Research/LUC/External-World-soil-database/HTML/>  
[consulted 10 July 2012]

- Gassman, P. W., Reyes, M. R., Green, C. H. and Arnold, J. G. 2007. The soil and water assessment tool: historical development, applications, and future research directions. *Transactions of the ASABE* 50 (4): 1211-1250.
- Gilfanova, I.R.. 2012. *Application of SWAT modeling for assessment of ecosystem goods and services in the Azov Sea basin*. Master of Science thesis, Central European University, Budapest.
- Gorgan D., Bacu V., Mihon D., Rodila D. Abbaspour K.C., Rouholahnejad E. 2012. Grid based calibration of SWAT hydrological models. *Nat. Hazards Earth Syst. Sci.*, 12, 2411–2423.
- Gupta, H.V., Sorooshian, S., Yapo, P.O., 1998. Toward improved calibration of hydrologic models: multiple and non-commensurable measures of information, *Water. Resour. Res.* 34,751-763.
- Hall, D.K., A.B. Tait, G.A. Riggs, V.V. Salomonson, with contributions from J.Y.L. Chien, A.G. Klein, October 7, 1998. Algorithm Theoretical Basis Document (ATBD) for the MODIS Snow, Lake Ice and Sea Ice Mapping Algorithms. Version 4.0
- Hargreaves, G. L., G. H. Hargreaves, and J. P. Riley. 1985. Agricultural benefits for Senegal River Basin. *J. Irrig. and Drain. Engr.* 111( 2): 113- 124.
- Houstis, C.; Kapidakis, S., Markatos, E. P., Gelenbe, E., 1997. Execution of computer-intensive applications into parallel machines. *Information Sciences*, 97, 83-124.
- Immerzeel, W.W., Droogers, P., 2007. *Calibration of a distributed hydrological model based on satellite evapotranspiration*. *Journal of Hydrology* 349, 411-424.
- ICPDR 2005. The Danube River Basin District. River basin characteristics, impact of human activities and economic analysis required under article 5, Annex II and III and inventory of protected areas. (Roof Report 2004) Vienna, Austria.
- IPCC, 2007a. Climate Change 2007 - Impacts, Adaptation and Vulnerability - Contribution of Working Group II to the Fourth Assessment Report of the IPCC.
- IPCC, 2007b. Climate Change 2007 - Mitigation of Climate Change - Contribution of Working Group III to the Fourth Assessment Report of the IPCC.
- IPCC, 2007c. Climate Change 2007 - The Physical Science Basis - Contribution of Working Group I to the Fourth Assessment Report of the IPCC.



- Jarvis, A., H.I. Reuter, A. Nelson, E. Guevara, 2008, Hole-filled SRTM for the globe Version 4, available from the CGIAR-CSI SRTM 90m Database (<http://srtm.csi.cgiar.org>)
- Kalyanapu, A. J., Shankar, S., Pardyjak, E. R., Judi, D. R., Burian, S. J., 2011. Assessment of GPU computational enhancement to a 2D flood model. *Environmental Modelling and Software*, 26, 1009-1016.
- Kennedy, J., Eberhart, R., 1995. IEEE International Conference on Neural Networks (ICNN 95), Nov 27-Dec 01, 1995 UNIV W Australia, Perth, Australia, Source: 1995 IEEE International Conference on Neural Networks Proceedings 1-6, 1942-1948.
- Klein Tank, A. M. G., Wijngaard, J. B., Können, G. P., Böhm, R., Demarée, G., Gocheva, A., Mileta, M., Pashiardis, S., Hejkrlik, L., Kern-Hansen, C., Heino, R., Bessemoulin, P., Müller-Westermeier, G., Tzanakou, M., Szalai, S., Pálsdóttir, T., Fitzgerald, D., Rubin, S. and Capaldo, M., Maugeri, M., Leitass, A., Bukantis, A., Aberfeld, R., van Engelen, A. F. V., Forland, E., Miletus, M., Coelho, F., Mares, C., Razuvaev, V., Nieplova, E., Cegnar, T., Antonio López, J., Dahlström, B., Moberg, A., Kirchhofer, W., Ceylan, A., Pachaliuk, O., Alexander, L. V., Petrovic, P. 2002. Daily dataset of 20th-century surface air temperature and precipitation series for the European Climate Assessment. *International Journal of Climatology* 22 (12): 1441–1453.
- Kuczera, G., Parent, E., 1998. Monte Carlo assessment of parameter uncertainty in conceptual catchment models: the Metropolis algorithm. *Journal of Hydrology*, 211(1-4), 69-85.
- Lecca, G., Petitdidier, M., Hluchy, L., Ivanovic, M., Kussul, N., Ray, N., Thieron, V., 2011. Grid computing technology for hydrological applications. *Journal of Hydrology*, 403, 186-199.
- Li, T., Wang, G., Chen, J., Wang, H. 2011. Dynamic parallelization of hydrological model simulation. *Environmental Modelling and Software*, 26, 1736-1746.
- Liu, J.G., Zehnder, A.J.B., Yang, H. 2008. Drops for crops: modeling crop water productivity on a global scale. *Global NEST Journal*. 10(3): 295-300.
- Mancosu, E., Gago da Silva, A. and De Bono, A. 2012. D3.7. Proposed land use scenario analysis, model input parameters and allocation rules. <http://www.envirogrids.net> [consulted 10 January 2013]
- Marshall, L., Nott, D., Sharma, A., 2004. A comparative study of Markov chain Monte Carlo methods for conceptual rainfall-runoff modeling. *Water Resour. Res.*, 40, W02501, doi:10.1029/2003WR002378.



- Mateos, C., Zunino, A., Campo, M., 2010. On the evaluation of gridification effort and runtime aspects of JGRIM applications. *Future Generation Computer Systems*, 26, 797-819.
- Masuoka E., A. Fleig, Robert E. Wolfe and F. Patt, July 1998, Key Characteristics of MODIS Data Products", *IEE Transactions on Geoscience and Remote Sensing*, Vol 36(4), 1313-1323
- McKay, M.D., Beckman, R.J., Conover, W.J., 1979. A comparison of three methods for selecting values of input variables in the analysis of output from a computer code. *Technometrics* 21, 239-245.
- Miller, M., 2009. Cloud computing pros and cons for end users. Article on Internet. <http://www.informit.com/articles/article.aspx?p=1324280>.
- Mitchell and Jones, 2005. An improved method of constructing a database of monthly climate observations and associated high-resolution grids. *Int. J. Climatology*, 25, 693-712, Doi: 10.1002/joc.1181. version TS3.0, (<http://www.cru.uea.ac.uk/cru/data/hrg/>).
- Monfreda, C., Ramankutty, N., Foley, J. A., 2008. "Farming the planet: 2. Geographic distribution of crop areas, yields, physiological types, and net primary production in the year 2000", *Global Biogeochemical Cycles*, Vol.22, GB1022, doi:10.1029/2007GB002947.
- Mu, Q., Zhao, M., Running, S.W., 2011. *Improvements to a MODIS global terrestrial evapotranspiration algorithm*. *Remote Sensing of Environment* 115, 1781-1800
- Nakicenovic, N., Alcamo, J., Davis, G., de Vries, B., Fenhann, J., Gaffin, S., Gregory, K., Grübler, A., Jung, T. Y. and Kram, T., La Rovere, E., Michaelis, L., Mori, S., Morita, T., Pepper, W., Pitcher, H., Price, L., Riahi, K., Roehrl, A., Rogner, H.H., Sankovski, A., Schlesinger, M., Shukla, P., Smith, S., Swart, R., van Rooyen, S., Victor, N. and Dadi, Z. 2000. *Special Report on emissions scenarios*. Cambridge: Cambridge University Press.
- Neal, J. C., Fewtrell, T. J., Bates, P. D., Wright, N. G. 2010. A comparison of three parallelization methods for 2D flood inundation models. *Environmental Modelling and Software*, 25, 398-411.
- Neitsch, S.L., Arnold, J.G., Kiniry, J.R., Williams, J.R., 2001. *Soil and Water Assessment Tool theoretical documentation version 2000*. Available at: <ftp://ftp.brc.tamus.edu/pub/swat/doc/swat2000theory.pdf>. Accessed 27 June 2011.



- Obuobie, E. 2008. Estimation of groundwater recharge in the context of future climate change in the White Volta River Basin, West Africa. Ecology and Development Series University of Bonn.
- Olivera F, Valenzuela M, Srinivasan R, Choi J, Cho HD, Koka S, Agrawal A. 2006. ArcGIS-SWAT: A geodata model and GIS interface for SWAT. Journal of the American Water Resources Association **42**: 295–309.
- Palearli S., Heinonen P., Rautalahti-Miettinen E., Daler D. 2005. Trans-boundary waters in the Black Sea-Danube region; legal and financial implications. University of Kalmar, Sweden.
- Parajka, J., Blöschl, G., 2008. *The value of MODIS snow cover data in validating and calibrating conceptual hydrologic models*. Journal of Hydraulics 358, 240-258.
- PCU, 1999.  
[http://www.envirogrids.net/index.php?option=com\\_content&view=article&id=5&Itemid=16](http://www.envirogrids.net/index.php?option=com_content&view=article&id=5&Itemid=16).
- Portmann, F. T., Siebert, S., Döll, P., 2010. MIRCA2000—Global monthly irrigated and rainfed crop areas around the year 2000: A new high-resolution data set for agricultural and hydrological modeling. GLOBAL BIOGEOCHEMICAL CYCLES, VOL. 24, GB1011, doi:10.1029/2008GB003435.
- Racsko, P., Szeidl, L. and Semenov, M. A. 1991. A serial approach to local stochastic weather models. *Ecological Modelling* 57: 27-41.
- Rahman, H. and G. Dedieu, 1994. SMAC : A simplified method for the atmospheric correction of satellite measurements in the solar spectrum, International Journal of Remote Sensing, 1994, vol.15, no.1, 123-143.
- Ritchie, J. T. 1972. A model for predicting evaporation from a row crop with incomplete cover. Water Resour. Res. 8: 1204- 1213.
- Rouholahnejad E., K.C. Abbaspour, R. Srinivasan, V. Bacu, A. Lehmann. 2013. Water resources status of the Black Sea Catchment: Building and calibrating a high-resolution integrated SWAT model. Water Resources Research. Submitted.
- Rouholahnejad E, Abbaspour KC, Vejdani M, Srinivasan R, Schulin R, Lehmann A. 2012. Parallelization framework for calibration of hydrological models, Environmental Modelling Software, 31: 28-36.
- Schuol, J., Abbaspour, K.C., Sarinivasan, R., Yang, H., 2008a. Estimation of freshwater availability in the West African Sub-continent using the SWAT hydrologic model.



- Schuol, J., Abbaspour, K.C., Srinivasan, R., Yang, H., 2008b. Modelling Blue and Green Water Availability in Africa at monthly intervals and subbasin level. *Water Resources Research*. 44, W07406, doi:10.1029/2007WR006609.
- Semenov, M. A. and Stratonovitch, P. 2010. The use of multi-model ensembles from global climate models for impact assessments of climate change. *Climate Research* 41: 1-14
- Semenov, M. A. and Barrow, E. M. 1997. Use of a stochastic weather generator in the development of climate change scenarios. *Climatic Change* 35: 397-414.
- Sharpley, AN., and JR. Williams. 1990. EPIC-Erosion Productivity Impact Calculator: 1. model documentation. U.S. Department of Agriculture, Agricultural Research Service, Tech. Bull. 1768.
- Singh, B., Pardyjak, E. R., Norgren, A., Willemsen, P., 2011. Accelerating urban fast response Lagrangian dispersion simulation using inexpensive graphics processor parallelism. *Environmental Modelling and Software*, 26, 739-750.
- Sobrino, J.A. and N. Raissoini ,2003. Surface temperature and water vapour retrieval from MODIS data, *International Journal of Remote Sensing* ,VOL. 24, NO. 24, 5161-5182.
- Stanners, D. & P.Boudreau, 1995. Europe's environment: the Dobris assessment. European Environment Agency Task force. Newsletter 5, ISBN 92-826-5409-5; ECU: 55.Luxembourg: Office for official publication of the EC.
- Su, Z, 2002. The Surface Energy Balance System (SEBS) for estimation of turbulent heat fluxes, *Hydrology and Earth System Sciences*, 6(1), 85-99.
- Su, Z., 2005. Estimation of the surface energy balance. In: *Encyclopedia of hydrological sciences : 5 Volumes*. edited by M.G. Anderson and J.J. McDonnell. Wiley & Sons, 2005. 3145 p. ISBN: 0-471-49103-9. Vol. 2 pp. 731-752.
- Sundaram, K., 2010. Cloud Computing vs. Grid Computing. Article on Internet.  
<http://www.brighthub.com/environment/green-computing/articles/68785.aspx>
- Taylor, S.J.E., Popescu, G.V., Pullen, J.M., Turner, S.J. 2004. Panel on distributed simulation and the grid. *Proceeding of 8th IEEE International Symposium on Distributed Simulation and Real-Time Applications (DS-RT 2004)*, Budapest, Hungary October 21-23, 2004. IEEE Comp Soc Tech Comm Parallel Process; IEEE Comp Soc Tech Comm Simulat; IEEE Comp Soc Tech Comm Comp Architecture; Pages: 144-149 DOI: 10.1109/DS-RT.2004.14.
- Tockner, K., U. Uehlinger., and C. T. Robinson. 2009. *Rivers of Europe.*, ISBN: 978-0-12-369449-2.



- UNEP, 2005. Eutrophication in the Black Sea Region: impact assessment and causal chain analysis. University of Kalmar, Sweden.
- Van Griensven, A., Meixner, T., 2006. Methods to quantify and identify the sources of uncertainty for river basin water quality models. *Water Sci. Technol.* 53(1), 51-59.
- Van Liew, M. W., J. G. Arnold, and J. D. Garbrecht. 2003. Hydrologic simulation on agricultural watersheds: choosing between two models. *Transactions of the ASAE* 46 (6): 1539-1551.
- Vassilios, P., 2008. Computing, virtualization, configuration management. Article on Internet. <http://it.toolbox.com/people/outervillage/>
- Vigerstol, K. L. and Aukema, J. E. 2011. A comparison of tools for modeling freshwater ecosystem services. *Journal of Environmental Management* 92 (10): 2403-2409
- Vrugt, J.A., Gupta, H.V., Bouten, W., Sorooshian, S., 2003. A Shuffled Complex Evolution Metropolis algorithm for optimization and uncertainty assessment of hydrologic model parameters. *Water Resour. Res.* 39(8), 1201.
- Weedon, G. P., S. Gomes, P. Viterbo, W. J. Shuttleworth, E. Blyth, H. Österlie, J. C. Adam, N. Bellouin, O. Boucher AND M. Best, 2011. Creation of the WATCH Forcing Data and Its Use to Assess Global and Regional Reference Crop Evaporation over Land during the Twentieth Century. *Water and Global change (WATCH), SPECIAL COLLECTION*: 823-848.
- Winchell, M., Srinivasan, R., Di Luzio, M., Arnold, J. 2010. ArcSWAT interface for SWAT2009, User's Guid. Blackland Research and Extension Center Texas AgriLife Research. Temple, Texas 76502. pp.495.
- Wolfe, R.E., D.P. Roy, E. Vermote, November 1997, MODIS land data storage, gridding and compositing methodology: level 2 grid. Submitted to IEEE TGARS
- Yang, J., Reichert, P., Abbaspour, K.C., Yang, H., 2007. Hydrological modelling of the Chaohe basin in China: Statistical model formulation and Bayesian inference. *Journal of Hydrology* 340, 167–182.
- Zhang, Y., Viney, N., Chiew, F., van Dijk, A. Liu, Y., 2011. *Improving hydrological and vegetation modelling using regional model calibration schemes together with remote sensing data*. Modelling and Simulation Society of Australia and New Zealand, MSSANZ 2001 Perth.
- Zessner, M. and Lindtner, S, 2005. Estimations of municipal point source pollution in the context of river basin management. *Water Science & Technology* Vol 52 No 9 pp 175–182.